

✓ D65-78 T
NAT

RADIATION CHARACTERISTICS OF CERTAIN DIELECTRIC LOADED MICROWAVE ANTENNAS

A THESIS
Submitted to the
UNIVERSITY OF ROORKEE
for the award of the degree
of
DOCTOR OF PHILOSOPHY
in
ELECTRONICS & COMMUNICATION ENGINEERING

by
R. APPUKUTTAN NAIR



1978

DEPARTMENT OF ELECTRONICS AND COMMUNICATION ENGINEERING
UNIVERSITY OF ROORKEE
ROORKEE (INDIA)

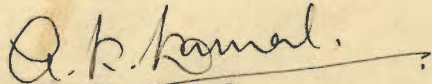
C E R T I F I C A T E

Certified that the thesis entitled "Radiation Characteristics of Certain Dielectric Loaded Microwave Antennas" which is being submitted by Mr. R. Appukuttan Nair in fulfilment of the requirements for the award of the Degree of Doctor of Philosophy in Electronics and Communication Engineering of the University of Roorkee is a record of the student's own work carried out by him under the joint supervision and guidance of the undersigned and Dr.S.C.Gupta from September 1975 to August 1977 and under my guidance and supervision from August 1977 to February 1978. The matter embodied in this thesis has not been submitted for the award of any other degree.

This is further to certify that he has worked for a period of two years and five months, from September 1975 to February 1978, at this university for preparing this thesis.

Roorkee

February 2 , 1978


Dr. A. K. Kamal,
Professor and Head,
Department of Electronics and
Communication Engineering,
University of Roorkee,
Roorkee (INDIA).

A C K N O W L E D G E M E N T

The author is deeply indebted to his thesis adviser Dr. A.K. Kamal, Professor and Head of the Department for his valuable guidance and substantial encouragement during the entire Ph.D. curriculum. Words would fail to record the invaluable help which the author was privileged to receive from him on many an occasion. This work would scarcely have been completed but for his active guidance and understanding co-operation.

The author wishes to express his immense gratitude to Dr. S.C. Gupta, presently visiting professor at the Mosul University, Iraq, for the valuable guidance and encouragement he gave from September 1975 till August 1977.

Thanks are also due to the author's colleagues Mr. J.S. Bedi, Mr. Shamim Ahammad, Mr. S. Swaminathan and Dr. John Mathew for extending necessary help.

Special thanks are due to the author's wife, Latha, for reading the manuscript and for her patience throughout its preparation.

The author is, further, thankful to all those who have extended their help, directly or indirectly,

in carrying out this work.

Thanks are also due to Mr. Darshan Lal Jaggi for his efficient typing of the thesis.

Finally, this work was made possible through the support of the Technical Education Department, Government of Kerala by deputing him under the Quality Improvement Programme at the University of Roorkee, and the grant of a research fellowship by the Ministry of Education and Social Welfare, Government of India, during the period of the research work and this assistance is gratefully acknowledged.

TABLE OF CONTENTS

Chapter	Page
ABSTRACT	x
I INTRODUCTION AND STATEMENT OF THE PROBLEM	1
1.1 Introduction	1
1.2 Statement of the Problem	4
1.3 Organisation of the Thesis	6
II REVIEW AND GENERAL CONSIDERATION	9
2.1 Introduction	9
2.2 Historical Review of Microwave Horn Antennas	10
2.2.1 Studies on Pyramidal and Sectoral Horns	10
2.2.2 Performance of Conical Horns	11
2.2.3 Studies on Reflector Antennas	12
2.3 Review of Improved Feed Horns	12
2.3.1 Modified Horn Feeds	13
2.3.2 Corrugated Horn Feeds	14
2.3.3 Investigations on Multimode Horns	15
2.3.4 Studies on Dielectric Loaded Horns	17
2.3.5 Dielectric Sphere Loading as a Means of Pattern Shaping	18
2.3.6 Studies on Surfacewave Horns	19
2.4 General Considerations	19
2.4.1 Vector Potential Approach	19
2.4.2 Aperture Field Method based on Vector Diffraction Formula	20
III RADIATION PROPERTIES OF DIELECTRIC LOADED CONICAL HORNS	23
3.1 Introduction	23
3.2 A Wide Angle Conical Horn with a Homogeneous Dielectric Sphere in front of its Aperture	24

Chapter	Page
3.2.1 Geometry of the System	24
3.2.2 Analysis of the Fields	25
3.2.3 Radiation from the Sphere Loaded Conical Horn	30
3.2.4 Forward Directivity of the System	32
3.2.5 Experimental Observations and Comparison with Theory	34
3.3 Dielectric Coated Conical Horn	39
3.3.1 Modal Analysis	39
3.3.2 Computation of Radiation Fields	45
3.3.3 The Axial Gain	47
3.3.4 Experimental Results	48
3.4 Dielectric Sphere Loaded Dielectric Coated Conical Horn	49
3.4.1 Analytical Formulation	50
3.4.2 Experimental Observations	52
3.5 Dielectric Sphere Loaded Conical Helix Horn	56
3.5.1 Modal Fields in a Conical Horn with Helical Boundary	58
3.5.2 Radiation from Conical Horn with Helical Boundary	62
3.5.3 The Axial Gain of the Conical Helix Horn	65
3.5.4 Conical Helix Horn with Dielectric Sphere in front of its Aperture	66
3.5.5 Experimental Observations	67
3.6 Conclusion	73
IV DIELECTRIC LOADED BICONICAL HORN	75
4.1 Introduction	75
4.2 Geometry of the Horn	76
4.3 Analysis of the Fields	76
4.4 Radiation from Dielectric Coated Biconical Horn	83

Chapter	Page
4.5 Power Gain of Dielectric Coated Biconical Horn	86
4.6 Experimental Results and Comparison with Theory	87
4.7 Conclusion	93
V DIELECTRIC SPHERE-LOADED CORRUGATED HORNS	94
5.1 Introduction	94
5.2 A Corrugated E -plane Sectoral Horn with Dielectric Sphere in front of its Aperture	95
5.2.1 Analytical Treatment	96
5.2.2 Design Aspects of the Corrugated E-plane Sectoral Horn	101
5.2.3 Experimental Results	103
5.3 A Corrugated Conical Horn with a Dielectric Sphere in front of its Aperture	107
5.3.1 Theoretical Formulation	108
5.3.2 Axial Gain of the System	114
5.3.3 Experimental Results	115
5.4 Conclusion	119
VI DIELECTRIC LOADED SECTORAL HORNS	121
6.1 Introduction	121
6.2 Dielectric Loaded E -plane Sectoral Horn	122
6.2.1 Theory of Operation	123
6.2.2 Radiation from the Dielectric Loaded Horn	128
6.2.3 The Axial Gain of the Horn	131
6.2.4 Dielectric Sphere Mounted Dielectric Coated E-plane Sectoral Horn	133
6.2.5 Experimental Results and Comparison with Theory	135
6.3 Dielectric Loaded H-plane Sectoral Horn with Cylindrical Aperture	137
6.3.1 Modal Fields in Dielectric Loaded Small Flare Angle H-plane Sectoral Horn	140

Chapter	Page
6.3.2 Radiation Field	145
6.3.3 Axial Gain of the Horn	147
6.3.4 Radiation from a Wide Flare Angle Dielectric Loaded H-plane Sectoral Horn	149
6.3.5 Experimental Results and Verification with Theory	154
6.4 Conclusion	156
VII DIELECTRIC LOADED MULTIMODE HORNS	158
7.1 Introduction	158
7.2 Multimode Dielectric Loaded Rectangular Horn Antenna	159
7.2.1 Analysis of Modal Fields	160
7.2.2 Radiation from Multimode Dielectric Loaded Horn	166
7.2.3 On-axis Gain of the Multimode Dielectric Loaded Horn	169
7.2.4 Design Considerations of the Double- Flare Multimode Dielectric Loaded Horn	171
7.2.5 Experimental Results	174
7.3 Beam Shaping Hybrid Mode Dielectric Loaded Horn	181
7.3.1 Hybrid Mode Horn with Symmetrical Dielectric Loading on the H-plane walls of the Horn	182
7.3.2 Hybrid Mode Horn with Symmetrical Dielectric Loading on E -plane walls of the Horn.	191
7.3.3 Evaluation of Modal Amplitudes of Hybrid Mode Dielectric Loaded Horn by Modal Expansion of Fields	195
7.3.4 Computed Results	197
7.3.5 Experimental Results and Comparison with Theory	199
7.4 Conclusion	203

Chapter	Page
VIII SUMMARY OF RESULTS AND CONCLUSIONS	205
8.1 Summary of Results	205
8.2 Suggestions for Future Work	209
TABLE - 1	213
LIST OF PUBLICATIONS	214
BIBLIOGRAPHY	216
APPENDIX A Equations for Dielectric Sphere Mounted Conical Horn	228
APPENDIX B Equations for Dielectric Coated Conical Horn	237
APPENDIX C Equations for Conical Horn with Helical Boundary	245
APPENDIX D Equations for Dielectric Loaded Biconical Horn	258
APPENDIX E Evaluation of the Scattered Field for Dielectric Sphere Loaded Corrugated E-plane Sectoral Horn	271
APPENDIX F Derivation of Expressions for Dielectric Loaded Corrugated Conical Horn	272
APPENDIX G Equations for Dielectric Coated E -plane Sectoral Horn	280
APPENDIX H Deriving Expressions for Dielectric Loaded H -plane Sectoral Horn with Cylindrical Aperture	291
APPENDIX I Deriving Equation for Multimode Dielectric Loaded Rectangular Horn	304
APPENDIX J Deriving Equations for Hybrid Mode Dielectric Loaded Horns	319.

A B S T R A C T

(R. Appukuttan Nair, 'Radiation Characteristics of Certain Dielectric Loaded Microwave Antennas', Ph.D. Thesis, Department of Electronics and Communication Engineering, University of Roorkee, February 1978.

Guides and Supervisors : Dr. A.K. Kamal, Professor and Head, September 1975 to February 1978, and Dr. S.C. Gupta, Professor, September 1975 to August 1977).

The widespread application of paraboloidal reflector antennas in microwave communication, radar and radio astronomy has stimulated considerable interest in the development of physically small improved feed systems which will have high directivity, low sidelobes and a multiple beam facility. This work comprises of a detailed theoretical and experimental investigations into the radiation characteristics of some improved primary feeds, with greater directivity, increased on-axis gain and low sidelobes, for reflector antennas. The development of these new feed systems are based on the property of dielectric materials in improving the performance of conventional microwave antennas.

The radiation behaviour of a wide angle conical horn with a homogeneous dielectric sphere in front of its aperture

has been investigated on the basis of the Scattering super - position technique. Results show that the system will have patterns with greater directivity and low sidelobes as compared with conventional conical horns of the same dimensions. Analysis of the fields in the dielectric coated conical horn is presented using spherical hybrid modes. Dielectric coating is seen to increase the pattern directivity at the cost of sidelobe level. Dielectric sphere loading in front of the radiating coated conical horn aperture is established to contribute greater directivity, higher on-axis gain and low sidelobes in addition to a variable beamwidth facility. A conical horn with a helical boundary is analysed using spherical hybrid modes and is shown to have desirable radiation characteristics to offer itself for applications in satellite communications. The technique of dielectric sphere loading is successfully applied to improve the helical horn pattern directivity with higher gain and low sidelobes. Dielectric coating on the Biconical horn walls has been treated to improve its pattern with a significant increase in its vertical pattern directivity.

The effect of placing dielectric spheres in the vicinity of radiating corrugated E -plane sectoral horn and corrugated conical horn has been investigated on the basis of scattering theory approach. Sphere loading is seen to narrow

the - 3 dB beamwidths. The sphere-loaded systems also possess greater on axis gain, low sidelobes and a multiple beam facility.

Dielectric loaded E -plane sectoral horn is analysed and is shown to have increased directivity at the cost of slight deterioration in sidelobe levels. Dielectric spheres off-set in front of the radiating dielectric loaded E- plane sectoral horn aperture is found to be a variable beam feed system with greater on-axis gain, narrow beamwidth and low sidelobes. A dielectric loaded H -plane sectoral horn with a cylindrical aperture has been discussed to prove its ability to be an efficient reflector feed for greater directivity and low sidelobes.

A multimode dielectric loaded rectangular horn operating in two orthogonal $TE_{10}+TE/TM_{12}$ and $TE_{01}+TE/TM_{21}$ mode sets to generate a circularly polarised elliptical beam is analysed. The antenna is seen to have fairly good directivity, on-axis gain and low sidelobes, with a nearly unity polarization axial ratio, over a wide frequency range. A technique of pattern shaping for monopulse radar antennas, by combining a controlled amount of higher order modes in dielectric loaded rectangular horn is also developed from a known throat excitation.

Finally, some suggestions are made for further work in this field.

CHAPTER I

INTRODUCTION AND STATEMENT OF THE PROBLEM

1.1 INTRODUCTION

The choice of microwave frequencies, on account of their increased bandwidth and ability to use high gain directive antennas, in communications, radar, astronomy and other fields has stimulated considerable interest in the development of efficient microwave antennas. Many different forms of microwave antennas are in practice, the most commonly used type being the horn antennas.

Electromagnetic horns in general are characterised by their ability to effect a transition from a medium supporting a small number of propagating modes, such as a waveguide, to one supporting a large or infinite number of modes, such as free space. They represent another means of approximating the ideal wavefront needed for good directivity, with the additional advantage of being able to accommodate an exceptionally broad band of frequencies.

The main characteristics of horn antennas are : radiation pattern directivity, gain, polarization and bandwidth.

High directivity can be obtained from horn radiators only if the horn is very long or if some means of correcting

the phase error due to spherical wave in the horn aperture is provided. An alternative to a lens [27],[38] for this purpose is the use of a reflecting surface - the most widely used reflecting surface being parabolic - whose focal point lies at the apex of the horn. Reflector antennas [57],[90] now form the largest class of antennas used in microwave communications, radar and radio astronomy.

Pencil beams are most widely used in point to point communications since this pattern yields the highest axial gain. In terrestrial applications the beam is usually fixed whereas in satellite communication applications the up-link beam may require to be steered. Antennas for spacecraft, radar and broadcast may require shaped beams which transmit substantial power over a wide angle and in the first case the need for multiple spot beams is also being considered. In general, for antennas meant for use in ground stations for space communication purposes the usual requirements, on account of very low signal level, are very high gain and low antenna noise. Of the several factors responsible for the contribution of antenna noise is the feed pattern through spill-over radiation from ground. An excellent method of achieving high gain with much reduced effect of feed pattern is to use the cassegrain antenna [34],[35],[116],[140], system which, however, has

a disadvantage of causing aperture blockage due to sub-reflector. This disadvantage of aperture blockage due to sub-reflector of a cassegrain system can be eliminated by using off-set feed techniques [55],[114],[117],[118]. The cassegrain type despite the aperture blockage appears to be widely accepted for current and future space applications because of its further advantage of providing large bandwidth with scanning facility. Paraboloid [39],[53],[62],[123] is the most commonly used reflector type because this produces high gain pencil beam with quite low sidelobes when fed efficiently from the focal point.

Another important characteristic of horn radiators for most applications is sidelobe level. It is important in antenna range, and standard gain applications because of multiple path considerations. In reflector illuminator applications it is important because of main beam efficiency and spurious wideangle radiation effects. For the latter application, electric - and magnetic-plane phase centre coincidence is also of importance. For many applications [3] equality of principal plane beamwidths is an important third consideration.

Thus the ideal feed horn for paraboloidal reflectors for many space applications is one which combines high

gain, low spill-over, nearly uniform aperture illumination, equal E- and H -plane patterns, wide frequency bandwidth as well as providing a well defined center of phase. Hence, with the advent of cassegrain antenna systems incorporating large paraboloidal reflectors for many space applications, it has become inevitable to develop improved primary feeds that will have greater directivity, high gain, low sidelobes as well as a variable beamwidth facility in addition to the polarization and phase centre requirements.

1.2 STATEMENT OF THE PROBLEM

This dissertation is concerned with the development of some new improved feed systems that will have increased directivity, greater on-axis gain and reduced sidelobe levels, for large paraboloidal reflectors for many applications. The possibility of providing a variable beamwidth facility for the improved feed systems is also considered. The improvement of axial directivity and on-axis gain is aimed at by the technique of dielectric loading, particularly on the horn walls. The reduction of sidelobe levels as well as a facility for variable beamwidth is investigated by dielectric sphere mounting over the horn aperture at an off-set position. Specifically the problems in this thesis can be stated as follows.

- i) To increase the directivity of conventional horns by the use of dielectric materials. Conical horn, biconical horn, E -plane sectoral horn, and H -plane sectoral horn with a cylindrical aperture are investigated with appropriate dielectric loading on the horn walls ; and the radiation pattern characteristics are compared with experimental results.
- ii) To study the effect of dielectric sphere mounting over a radiating horn aperture at an off-set position [85] The possibility of sidelobe reduction, gain enhancement and a variable beam facility with dielectric sphere loading is investigated in empty conical horn, a conical horn with a helical boundary, dielectric coated conical horn and dielectric loaded E -plane sectoral horn, corrugated conical horn and corrugated E -plane sectoral horn.
- iii) To investigate the development of some new feed systems that will provide shaped beam facility with relatively low sidelobes by combining the technique of multimode operation [108],[51] for low sidelobes, and dielectric loading [17],[50]for greater directivity at the cost of slightly raised sidelobes.

1.3 ORGANISATION OF THE THESIS

The work embodied in this thesis has been arranged in the following way

The critical review of the existing literature in the field of microwave antennas has been included in the second chapter. This chapter also contains the general considerations that have been utilized in the analysis of the performance of the various antenna systems discussed.

In chapter III, the effect of dielectric loading on the performance of horns with conical boundaries has been investigated. The radiation characteristics of a conical horn with a dielectric sphere in front of its aperture have been first studied. The radiation characteristics of dielectric coated conical horn are analysed, and the observations of its performance are repeated with dielectric spheres in front of the aperture of the radiating dielectric coated cone. The effect of dielectric sphere loading on the radiation behaviour of a conical horn with a helical boundary has also been investigated.

The radiation behaviour of a dielectric coated biconical horn is investigated in chapter IV, for the control of its pattern directivity in the vertical plane.

Chapter V deals with the investigation reports of the radiation characteristics of corrugated horns- conical horn and E -plane sectoral horn - in the presence of dielectric spheres in front of their aperture when they are radiating.

The radiation and propagation behaviour of dielectric loaded E -plane sectoral horn, and dielectric loaded H -plane sectoral horn with a cylindrical boundary are reported in chapter VI. In both cases the theoretical and experimental results are compared; and a brief account of their inference is included.

The behaviour of the multimode horn with dielectric loaded walls are dealt with in chapter VII. A double flare multimode horn with dielectric loading on E -plane walls has been studied analytically and experimentally. The radiation patterns have greater directivity with slightly increased sidelobe levels. To reduce the sidelobe level the technique of dielectric sphere mounting is employed. A dielectric loaded hybrid mode horn has also been considered in this chapter. The possibility of pattern shaping with higher order mode contents present in such a horn has been illustrated both experimentally and theoretically.

A summary of the work together with the conclusions

drawn therein has been given in chapter VIII. A brief account of the guidelines for further work which would lead to the development of some fruitful antenna systems has been included in this chapter.

CHAPTER II

REVIEW AND GENERAL CONSIDERATIONS

2.1 INTRODUCTION

The use of microwave frequencies for communication systems has initiated the development of efficient microwave antennas for the transformation of the applied energy of high frequency into energy of electromagnetic radiation establishing a definite directional pattern. The advent of large low noise cassegrain [34],[35],[116] antenna for space communication has focussed additional attention on the importance of horn antenna design and performance. Moreover, the wide spread application of paraboloidal reflectors[39],[53] with high cost-per-unit area in satellite communication and radio astronomy, and the need for multiple or adaptive beam [107] parabolic antennas in spacecraft have stimulated considerable interest in the design and development of physically small antenna feeds which will have high directivity, greater gain and low sidelobes with a variable beamwidth facility. Several investigations have been carried out, and new techniques have been developed towards this goal . A critical survey of the work done in the field of

microwave antennas is embodied in this Chapter.

2.2 HISTORICAL REVIEW OF MICROWAVE HORN ANTENNAS

The more frequently used horn configurations are (i) pyramidal (ii) sectoral (iii) conical.

2.2.1 STUDIES ON PYRAMIDAL AND SECTORAL HORNS

Pyramidal horns [63],[64],[121], have been used for many years at UHF and microwave frequencies for applications requiring a simple type of antenna with medium gain (10 - 30 dB), and are popular as antenna range illuminators, gain standards and reflector illuminators.

Extensive studies on the propagation and radiation behaviour of sectoral horns have been carried out [13],[18],[24],[54], [110], and was established that they can be used to obtain 'fan-shaped' beams of specified sharpness in the plane containing the flare. The pattern is very broad in the other plane and is essentially the same as that of an open ended waveguide. A correction to the available radiation formula for the E -plane sectoral horn was made by Narasimhan and Rao [100], and Jull [66] has made a new proposal for the evaluation of the exact on-axis gain of the E -plane sectoral horn yielding perfect agreement

with the experimental results.

2.2.2 PERFORMANCE OF CONICAL HORNS

It was made well known that conical horn [47],[76], [97],[105],[123], operating in the dominant TE_{11} mode has effectively a tapered aperture distribution in the E -plane and this results in nearly equal beamwidths in the electric and magnetic planes. By virtue of this pattern symmetry, it can handle any polarization of the dominant TE_{11} mode - a valuable feature for polarization diversity applications. Moreover, as a result of the tapered E -field distribution, the conical horns have more favourable sidelobe structure than with the rectangular aperture horn. A simpler approach for the evaluation of the performance of conical horn has been suggested by Narasimhan and Rao[96] ; and conical horn antennas have assumed considerable importance in recent years for polarization diversity applications [3].

The propagation and radiation behaviour of biconical horn that produces an omni-directional pattern in the horizontal plane and a directional pattern in the vertical plane was discussed in detail by Barrow and Chu [12]. A biconical horn which radiates circular polarization was designed[87] and used successfully with radar transponder beacon responding to a ship's standard S -band navigational radar.

2.2.3 STUDIES ON REFLECTOR ANTENNAS

A method of obtaining high directivity from a short horn is by the use of reflecting surfaces whose focal points lie at the apex of the horn. The performance characteristics of horn reflector antennas suitable for space communications [36], [75], were investigated and established successfully. Paraboloidal [39], [53], [124] is the most practical form of the reflector as this results in a high gain pencil beam with low sidelobes. Slight shaping of the reflector's surface leads to substantial gain enhancement [140], and these techniques have been widely used in earth station antennas. Other reflector surfaces have also been used to produce shaped beams for special purpose antennas. For example the spherical reflector antenna [82], [106], [122] has been investigated for small earth-station applications because the beam can be efficiently scanned by the movement of the feed system. Rusch [116] has studied the performance of a hyperboloid reflector in a cassegrannian feed system.

2.3 REVIEW OF IMPROVED FEED HORNS

The almost optimum solution for high aperture efficiency and low spill-over of a paraboloidal reflector antenna is a sector shaped feed pattern of a horn that will

have nearly equal E - and H -plane patterns, a well defined phase center, wider frequency bandwidths and zero cross-polarization. A broad band feed horn which when mounted at the focal point of a parabolic dish yielded equal E -and H -plane patterns was introduced by Shimizu [124] . Techniques for optimising paraboloidal reflector antennas have been developed and successfully experimented [53],[86],[137],[138] . Optimum horn feeds for reflector antennas were also investigated [113],[137],[138].

2.3.1 MODIFIED HORN FEEDS

A horn antenna with modified horn walls for low sidelobes, a well defined phase center at its apex, and nearly identical E- and H -plane patterns over a wide frequency band was suggested by Lawrie and Peters [78]. Rumsey [115] has shown that a linearly polarized horn that has the same power pattern in the planes through the axes can be made from a synthetic material for which the boundary conditions on E and H are the same. The concept of an open-ended cylindrical corrugated feed in which hybrid modes propagate was successfully demonstrated by Minnett and MacA [89] for axially symmetric patterns, zero cross-polarization, low-noise and high efficiency. Practically high gain, narrow beam horns are very long and bulky because of the flare angle limitations. Even though

good phase correction for flare angles by mounting appropriate lens in the horn aperture [27],[38] was possible, a lens-less method of phase correction for wideflare angle sectoral horns was achieved by Ancona [4] by supplying the narrow walls of the horn with a leaky wave interface corresponding to a fast phase velocity. For such antennas low sidelobes were obtained due to the tapered distribution linked with leaky wave attenuation constant. A H -plane sectoral horn with a cylindrical aperture [133] was found to possess more directivity and low sidelobes than identical horns with a rectangular aperture.

2.3.2 CORRUGATED HORN FEEDS

Antenna research in the early 1960's was inspired by the need for improved feed systems for large radio astronomy and satellite tracking dishes requiring horn feeds that would reduce spill-over and cross-polarization losses, and increase aperture efficiency. Simmon and Kay [126] developed a 'Scalar feed' with appropriate grooved corrugations in horn wall. This corrugated structure eliminated edge diffractions to result in equal E - and H -plane beamwidths. At about this time, the propagation and radiation behaviour of corrugated horns were also studied by Minnett and Thomas [91] in Australia. Following

these, a lot of work has been done on corrugated surfaces and corrugated horn structures of different geometry [20],[21],[28],[41],[59],[83],[88],[139]. An extensive analytical treatment of the corrugated E -plane sectoral horn that has desirable radiation patterns with low sidelobes has been made by Narasimhan and Rao [99],[101] . The properties of corrugated conical horns as reflector feeds have been investigated [25],[26],[58],[83],[94], and the importance of corrugated conical horns as low noise feeds for large reflector antennas has been discussed [60],[61],[92],[95],[98] . Ring loading [130],[131] and dielectric loading [2],[99] techniques have been found to be effective in broadening the useful frequency bandwidths of corrugated horns when used as reflector antenna primary feeds. The improvement of corrugated conical horn performance has also been made effective by lens correction [27].

2.3.3 INVESTIGATIONS ON MULTIMODE HORNS

Pattern shaping by combining orthogonal TE_{10} and TE_{01} modes in a radiating horn was made possible [80] and the horn was found to possess patterns with equal E - and H -plane beamwidths and suppressed E -plane sidelobes. These properties were achieved only at the expense of pairs of cross-polarized lobes into intercardinal planes that render it unsuitable for applications in which high

degree of polarization purity is required. But the original concept of using both dominant and higher order modes (multimodes) in a radiating horn for pattern shaping was due to Potter [108] who utilised the technique of superposition of dominant and higher order modes in a dual mode conical horn. The technique simultaneously resulted in complete beamwidth equalisation in all planes, complete phase center coincidence and at least 30 dB sidelobe suppression in the E -plane. Beam shaping by higher order modes in a conical horn also has been discussed by Potter and Ludwig [109]. Based on these investigations much work on multimode horns as desirable primary feeds were successfully carried out [42],[136]. The technique of mode conversion has also been studied by many [93],[132] for the generation of the wanted higher order modes. A multimode rectangular horn antenna generating circularly polarised elliptical beam was studied by Han and Wickert [51]. They used a square step discontinuity in an oversized waveguide for the generation of the wanted higher order (TE/TM_{12} and TE/TM_{21}) modes to operate the antenna in two orthogonal mode sets ($TE_{10} + TE/TM_{12}$ and $TE_{01} + TE/TM_{21}$). The horn was found to possess equal beamwidths in E - and H - planes, low sidelobes and low off-axis polarization axial ratio.

2.3.4 STUDIES ON DIELECTRIC LOADED HORN

The use of the dielectric materials for improving the axial directivity of aperture antennas has been well established [10],[17],[49],[50] . A new technique called 'Dielguide' for providing highly efficient low noise antenna feeds has been developed by Bartlett and Moseley [14] , by placing dielectric guiding structures (Dielguides) between primary feed and reflector or subreflector. These guiding structures utilise the phenomenon of total internal reflection (TIR), which is a property of the boundary between dielectric media, to reduce spill-over and provide more uniform reflector illumination. The enhancement of horn aperture efficiency was verified by Tsandanlas and Fitzgerald[134] by the use of dielectric wedges inside the horn walls. Satoh[119] could develop a wideband dual mode horn which has a rotationally symmetric beam and lowsidelobe levels by loading a dielectric band inside the horn antenna. Ajioka and Harry [1] devised a dielectric loaded horn for a satellite- born shaped beam antenna, with a dielectric cap or tube at the horn aperture.

The possibility of developing dielectric antennas of different geometry has been explored [19],[31],[56], and has been applied [29],[30] as effective feeds for cassegrain antenna systems.

2.3.5 DIELECTRIC SPHERE ^ALOADING AS A MEANS OF PATTERN SHAPING

In 1972 Chatterjee and Crosswell [23] introduced a method of producing multiple beam or variable beamwidth feeds for a paraboloidal reflector, and minimising aperture blockage by dielectric spheres placed at the aperture of radiating circular and rectangular horns. In a related study Neelakantaswamy and Banerjee have shown that circular waveguide excited dielectric sphere backed by a metallic hemisphere [103] ; and circular waveguide excited dielectric sphere with matched sphere-air boundary [102] produce patterns with low sidelobe levels, increased on-axis gain and reduced - 3dB beamwidths. Similar results were obtained by Martin and Oxtoby [85] with dielectric spheres placed in front of, but displaced from, the aperture of a circular waveguide; and by Neelkantaswamy and Banerjee [104] with off-set placed dielectric spheres in front of the corrugated pipe aperture. Recently Crosswell et al [37] have made a thorough investigation into the effects of placing a homogeneous dielectric sphere over the aperture of circular waveguide, and have established that such dielectric sphere-mounted antennas have directivities in excess of that obtained by a uniformly illuminated aperture of the same cross-section.

2.3.6 STUDIES ON SURFACE WAVE HORNS

The surface wave phenomenon [11] of propagation of electromagnetic energy without radiation along an interface between two different media are verified [8],[5] to result in a greater on-axis gain due to high concentration of energy in the neighbourhood of the interface. It has been shown [33,Pt.2] that surface wave propagation can be effected in a reactive surface bounded between high side walls. The possibility of developing a surface wave horn by a wedge shaped bounded reactive surface was suggested by Arora [6] and this idea was put into practice [67] to show that a surface wave H -plane sectoral horn antenna possesses on-axis gain in excess of conventional horns of the same dimensions.

2.4 GENERAL CONSIDERATIONS

The main considerations that have been used for the analysis of the antennas discussed in the thesis are mentioned below.

2.4.1 VECTOR POTENTIAL APPROACH

In view of the divergenceless character of electric and magnetic field intensities, it is possible to express the field in terms of the magnetic vector potential \bar{A}

or in terms of an electric vector potential \bar{F} . The total field of a system can then be expressed by the superposition of the fields in terms of \bar{A} and \bar{F} . For source free regions \bar{A} and \bar{F} should satisfy the Helmholtz equations,

$$\begin{aligned}\nabla^2 \bar{A} + k_0^2 \bar{A} &= 0 \\ \nabla^2 \bar{F} + k_0^2 \bar{F} &= 0\end{aligned}\tag{2.1}$$

The electromagnetic field in terms of \bar{A} and \bar{F} , for the source free case, is given by,

$$\begin{aligned}\bar{E} &= -\nabla \times \bar{F} + \frac{1}{j\omega\epsilon_0} \nabla \times \nabla \times \bar{A} \\ \bar{H} &= \nabla \times \bar{A} + \frac{1}{j\omega\mu_0} \nabla \times \nabla \times \bar{F}\end{aligned}\tag{2.2}$$

Thus the concept of the vector potential has become an important tool for the analysis of modal fields inside an antenna system. The vector potential concept has been utilised for the analysis of the fields of the horn antennas embodied in this report.

2.4.2 THE APERTURE FIELD METHOD BASED ON THE VECTOR DIFFRACTION FORMULA

There are several methods [125] of computing accurately the radiation patterns of horn antennas. The aperture field method based on the vector diffraction

formula [44, Chap -3, pp.84-86] is the one frequently used now-a-days in respect of its simplicity. In the aperture field method, radiation fields are obtained from the field distribution (\bar{E}_t, \bar{H}_t) tangential to the horn aperture. By this method, the radiation field from a rectangular aperture is given by

$$E = \frac{jk_o}{4\pi} \frac{e^{-jk_o r}}{r} (1+\cos\theta) \iint_s \bar{E}_t \cdot e^{jk_o (x_s \sin\theta \cos\phi + y_s \sin\theta \sin\phi)} dx_s dy_s \quad (2.3)$$

It is noted that all points in the XZ -plane (H -plane) have spherical co-ordinates $\phi = 0$, while points in the YZ -plane (E-plane) have the co-ordinates $\phi = \pi/2$. Accordingly from Eq. (2.3) the H - and E -plane patterns are obtained respectively as

$$E_\phi = j \frac{k_o}{4\pi} \frac{e^{-jk_o r}}{r} (1+\cos\theta) \iint_s \bar{E}_t e^{jk_o x_s \sin\theta} dx_s dy_s$$

$$E_\theta = j \frac{k_o}{4\pi} \frac{e^{-jk_o r}}{r} (1+\cos\theta) \iint_s \bar{E}_t e^{jk_o y_s \sin\theta} dx_s dy_s \quad (2.4)$$

where \bar{E}_t is the transverse electric field over the horn aperture contour s .

To calculate E accurately from formula (2.4) it

is necessary to consider the dependence of \bar{E}_t on the co-ordinates x_s and y_s .

In the case of circular aperture, the respective radiation field components are given by

$$\begin{aligned}
 E_{\phi} &= j \frac{k_o}{4\pi} \frac{e^{-jk_o r}}{r} (1+\cos\theta) \iint_s \bar{E}_t e^{jk_o \rho_s \cos\phi_s \sin\theta} \rho_s d\rho_s d\phi_s \\
 E_{\theta} &= j \frac{k_o}{4\pi} \frac{e^{-jk_o r}}{r} (1+\cos\theta) \iint_s \bar{E}_t e^{jk_o \rho_s \sin\phi_s \sin\theta} \rho_s d\rho_s d\phi_s \quad (2.5)
 \end{aligned}$$

The basic relations given by Eqs. (2.4) and (2.5), formulated on the aperture field method based on the vector diffraction formula, have been conveniently used for the computation of the radiation characteristics of the antenna systems of different geometries considered in this thesis report.

CHAPTER III

RADIATION PROPERTIES OF DIELECTRIC LOADED CONICAL HORNS

3.1 INTRODUCTION

The conical horn antenna has assumed considerable importance in recent years because of its radiation patterns having low sidelobes and nearly equal beamwidths in the electric and magnetic planes - a valuable feature for polarization diversity applications[3] - due to the tapered aperture field distribution in the electric plane. Yet, plane conical horn is not often used in practice because of its relative incompatibility with rectangular aperture antennas. Corrugated conical horn[26],[94],[95] has been devised as a very useful primary feed for reflector antennas for satellite communication earth stations and radiotelescopes, as it has the property of symmetric radiation patterns having a broadband (1:1.5) and negligible sidelobes. But, the widespread application of paraboloidal reflector antennas in satellite communication and radio astronomy has stimulated considerable interest in the development of new improved feed systems which will have low sidelobes and high directivity for a given cross-sectional area. The present chapter accounts the results of the theoretical and experimental investigations in improving the radiation characteristics of conical horns by the technique of appropriate dielectric loading.

Dielectric coating on the horn walls[10],[48],[49],[50],[134] is used for the improvement of its axial directivity, and the technique of dielectric sphere mounting on the radiating horn aperture[37],[85],[103],[104] is utilised to improve the pattern with narrow beamwidth, greater on-axis gain and reduced sidelobe levels.

3.2 A WIDE ANGLE CONICAL HORN WITH A HOMOGENEOUS DIELECTRIC SPHERE IN FRONT OF ITS APERTURE [73]

In this section the effects of placing a homogeneous dielectric sphere in front of the aperture of a radiating wide angle conical horn have been investigated both theoretically and experimentally. The theoretical formulation of the radiation characteristics is made on the basis of scattering of electromagnetic waves by a dielectric sphere. Calculations based on this formulation are compared with experimental results of pattern and gain measurements.

3.2.1 GEOMETRY OF THE SYSTEM

The antenna system under consideration is shown in Fig. 3.1. The homogeneous dielectric sphere of radius 'b' and permittivity ϵ_1 is placed in front of the aperture of a wide angle conical horn of flare angle θ_0 . The regions exterior ($r > b$) and interior ($r < b$) to the sphere have propagation constants k_0 and k_1 respectively where

$$k_0 = \omega \sqrt{\mu_0 \epsilon_0} \quad (\text{region } r > b)$$

$$k_1 = \omega \sqrt{\mu_0 \epsilon_1} \quad (\text{region } r < b)$$

Here both the regions are assumed to have the same permeability μ_0

3.2.2 ANALYSIS OF THE FIELD

The dielectric material of the sphere is assumed to be lossless. For convenience in applying the boundary conditions, it is assumed that both E and H modes are present in the horn region. The components of the hybrid modes (HE_{mn} modes) may be derived from the vector potentials \bar{A} and \bar{F} , each having a single component only in the radial direction such that $\bar{A} = \bar{i}_r A_r$ and $\bar{F} = \bar{i}_r F_r$; and satisfying the equations

$$\begin{aligned} \frac{1}{r^2} \frac{\partial}{\partial r} \left(r^2 \frac{\partial A_r}{\partial r} \right) + \frac{1}{r^2 \sin^2 \theta} \frac{\partial}{\partial \theta} \left(\sin \theta \frac{\partial A_r}{\partial \theta} \right) + \\ \frac{1}{r^2 \sin^2 \theta} \frac{\partial^2 A_r}{\partial \phi^2} + k_0^2 A_r = 0 \end{aligned} \quad (3.1)$$

and

$$\begin{aligned} \frac{1}{r^2} \frac{\partial}{\partial r} \left(r^2 \frac{\partial F_r}{\partial r} \right) + \frac{1}{r^2 \sin^2 \theta} \frac{\partial}{\partial \theta} \left(\sin \theta \frac{\partial F_r}{\partial \theta} \right) + \\ \frac{1}{r^2 \sin^2 \theta} \frac{\partial^2 F_r}{\partial \phi^2} + k_0^2 F_r = 0 \end{aligned}$$

where \bar{i}_r = the unit vector.

Applying the method of separation of variables to

Eqs. (3.1), and also giving attention to the following boundary conditions :

- i) The field must be periodic in 2π on ϕ , and finite at $\theta = 0$.
- ii) Tangential E must be zero at $\theta = \theta_0$, the flare angle of the cone, A_r and F_r can be obtained as

$$A_r = a_{mn} P_n^m(\cos\theta) \hat{B}_n(k_0 r) e^{jm\phi} \quad (3.2)$$

$$F_r = b_{mn} P_n^m(\cos\theta) \hat{B}_n(k_0 r) e^{jm\phi}$$

where m is an integer, and for the given values of m the eigen values n are evaluated from the characteristic equations

$$\frac{d}{d\theta} P_n^m(\cos\theta) = 0 \quad \text{at } \theta = \theta_0 \quad \text{for TE modes}$$

and $P_n^m(\cos\theta) = 0 \quad \text{at } \theta = \theta_0 \quad \text{for TM modes}$

$P_n^m(\cos\theta)$ = Associated Legendre function of the first kind

$\hat{B}_n(k_0 r)$ = Solution to the modified Bessel's equation for the spherical functions.

Now the transverse electric field over the horn aperture becomes

$$\bar{E}_t = \bar{i}_\theta E_\theta + \bar{i}_\phi E_\phi \quad (3.3)$$

where \bar{i}_θ and \bar{i}_ϕ are the unit vectors, and the tangential field components E_θ and E_ϕ are given by

$$E_{\theta} = - \frac{1}{r \sin \theta} \frac{\partial F_r}{\partial \phi} + \frac{1}{j \omega \epsilon_0 r} \frac{\partial^2 A_r}{\partial r \partial \theta}$$

$$E_{\phi} = \frac{1}{r} \frac{\partial}{\partial \theta} F_r + \frac{1}{j \omega \epsilon_0 r \sin \theta} \frac{\partial^2 A_r}{\partial r \partial \phi}$$
(3.4)

Assuming balanced condition at the horn aperture, the transverse electric field \bar{E}_t over the horn aperture, under far-field approximation (i.e. $k_0 r \gg 1$, $\hat{B}_n(k_0 r) = j^{n+1} e^{-jk_0 r}$, $\hat{B}_n(k_0 r)/\hat{B}'_n(k_0 r) = -j$), is obtained by Eqs. (3.2), (3.3) and (3.4) as,

$$\bar{E}_t = -(j)^{n+1} \frac{e^{-jk_0 r}}{r} a_{mn} \sqrt{\mu_0/\epsilon_0} \left[\frac{P_n^m(\cos \theta)}{\sin \theta} + \frac{\partial}{\partial \theta} P_n^m(\cos \theta) \right] (\bar{i}_{\theta} + j \bar{i}_{\phi}) e^{jm\phi}$$
(3.5)

Under the assumption of minimal edge diffraction in wide flare angle cones, the horn aperture and radiation patterns should be similar when the far field approximation applies; and hence the field pattern at the sphere location may be taken as that at the horn aperture. Restricting the consideration to $m = 1$, the proper form of the electric and magnetic potential functions for the electromagnetic waves incident on the dielectric sphere placed in front of the horn aperture, on application of wave transformation [52] for spherical functions, can conveniently be expressed in the most general way as a summation over all possible values

of n ; and are given by

$$A_r^i = \sum_{n=1}^{\infty} a_n P_n^1(\cos\theta) \hat{B}_n(k_o r) \cos\phi \quad (3.6)$$

$$F_r^i = \eta_o \sum_{n=1}^{\infty} a_n P_n^1(\cos\theta) \hat{B}_n(k_o r) \sin\phi$$

where

$$a_n = j^{-n} \frac{(2n+1)}{n(n+1)}$$

$$\eta_o = \sqrt{\mu_o / \epsilon_o}$$

$\hat{B}_n(k_o r) = \hat{J}_n(k_o r)$, the n^{th} order modified spherical Bessel function of the first kind for the field in the near-zone defined by $r \leq b$.

$= \hat{H}_n^{(2)}(k_o r)$, the n^{th} order modified spherical Hankel function of second kind for the field in the far-zone defined by $r > b$

The assumption that $\hat{B}_n(x) = \hat{J}_n(x)$ for the near-zone and $\hat{B}_n(x) = \hat{H}_n^{(2)}(x)$ for the far-zone is made in order to facilitate the evaluation of the constants involved, on application of the boundary conditions.

This wave incident on the sphere induces secondary fields [129] having two components viz. (i) the scattered field external to the dielectric sphere and (ii) the transmitted field internal to the sphere. Taking outward

travelling waves (i.e. $\hat{H}_n^{(2)}(k_0 r)$) for the scattered fields, by Eq. (3.6) the proper forms of the magnetic and electric potential functions for the scattered field become

$$A_r^S = \cos\theta \sum_{n=1}^{\infty} b_n \hat{H}_n^{(2)}(k_0 r) P_n^1(\cos\theta) \quad (3.7)$$

$$F_r^S = \eta_0 \sin\theta \sum_{n=1}^{\infty} c_n \hat{H}_n^{(2)}(k_0 r) P_n^1(\cos\theta)$$

Likewise, the field internal to the sphere (transmitted field) would be developed by the potential functions,

$$A_r^t = \cos\theta \sum_{n=1}^{\infty} d_n \hat{J}_n(k_1 r) P_n^1(\cos\theta) \quad (3.8)$$

$$F_r^t = \eta_1 \sin\theta \sum_{n=1}^{\infty} e_n \hat{J}_n(k_1 r) P_n^1(\cos\theta)$$

Here b_n , c_n , d_n and e_n are constants of the scattered and transmitted field potentials to be determined from the boundary conditions, viz. the tangential components of E and H must be continuous at $r = b$ (radius of the sphere). The constants involved in the radiation behaviour are those of the scattered field potentials b_n and c_n only; and these constants of interest are derived in Appendix A -1 as,

$$b_n = \frac{-\sqrt{\epsilon_1} \hat{J}'_n(k_0 b) \hat{J}_n(k_1 b) + \sqrt{\epsilon_0} \hat{J}_n(k_0 b) \hat{J}'_n(k_1 b)}{\sqrt{\epsilon_1} \hat{H}_n^{(2)'}(k_0 b) \hat{J}_n(k_1 b) - \sqrt{\epsilon_0} \hat{H}_n^{(2)}(k_0 b) \hat{J}'_n(k_1 b)} \cdot a_n \quad (3.9)$$

$$c_n = \frac{-\sqrt{\epsilon_1} \hat{J}_n(k_0 b) \hat{J}'_n(k_1 b) + \sqrt{\epsilon_0} \hat{J}'_n(k_0 b) \hat{J}_n(k_1 b)}{\sqrt{\epsilon_1} \hat{H}_n^{(2)}(k_0 b) \hat{J}'_n(k_1 b) - \sqrt{\epsilon_0} \hat{H}_n^{(2)'}(k_0 b) \hat{J}_n(k_1 b)} \cdot a_n$$

where the prime denotes differentiation with respect to r . Knowing the constants, the incident and the scattered field components can be obtained by inserting the appropriate potential functions in Eqs. (3.4).

3.2.3 RADIATION FROM THE SPHERE LOADED CONICAL HORN

As the necessary potential functions have been established, the radiation from the device may be treated as a boundary value problem; and solutions can be obtained by the scattering superposition technique as presented in [37] for a case based on the Huygen's Source model. Accordingly, in this case, the total field outside the sphere becomes the sum of the incident and scattered fields; and hence from Eqs. (3.6) and (3.7) the potential functions at any point in the far-zone are given by,

$$A_r^+ = \cos\theta \sum_{n=1}^{\infty} \hat{H}_n^{(2)}(k_0 r) P_n^1(\cos\theta) (a_n + b_n) \quad (3.10)$$

$$F_r^+ = \eta_0 \sin\theta \sum_{n=1}^{\infty} \hat{H}_n^{(2)}(k_0 r) P_n^1(\cos\theta) (a_n + c_n)$$

Using the appropriate formula

$$E_{\theta}^{+} = E_{\theta}^{i} + E_{\theta}^{s} = -\frac{1}{r \sin\theta} \frac{\partial F_r^{+}}{\partial \theta} + \frac{1}{j\omega \epsilon_0 r} \frac{\partial^2 A_r^{+}}{\partial r \partial \theta}, \quad (3.11)$$

by Eq. (3.10), the θ -component of the radiated far field is obtained in Appendix A-2 as,

$$E_{\theta}^{+} = -\eta_0 \cos\theta \frac{\exp(-jk_0 r)}{r} \sum_{n=1}^{\infty} j^{n+1} \left[\frac{P_n^1(\cos\theta)}{\sin\theta} (a_n + c_n) + \frac{\partial}{\partial \theta} P_n^1(\cos\theta) (a_n + b_n) \right] \quad (3.12)$$

And substitution of A_r^{+} and F_r^{+} from Eq. (3.10) in the expression,

$$E_{\theta}^{+} = E_{\theta}^{i} + E_{\theta}^{s} = \frac{1}{r} \frac{\partial}{\partial \theta} F_r^{+} + \frac{1}{j\omega \epsilon_0 r \sin\theta} \frac{\partial^2 A_r^{+}}{\partial r \partial \theta} \quad (3.13)$$

the ϕ - component of the radiated far-field is derived as,

$$E_{\phi}^{+} = \eta_0 \sin\theta \frac{\exp(-jk_0 r)}{r} \sum_{n=1}^{\infty} j^{n+1} \left[\frac{\partial}{\partial \theta} P_n^1(\cos\theta) (a_n + c_n) + \frac{P_n^1(\cos\theta)}{\sin\theta} (a_n + b_n) \right] \quad (3.14)$$

The resultant expression for the far-zone field becomes,

$$E_R(r) = \bar{i}_{\theta} E_{\theta}^{+} + \bar{i}_{\phi} E_{\phi}^{+}, \quad (3.15)$$

and it is shown in Appendix A-2, that by using Eqs. (3.12) and (3.14) in Eq. (3.15) the resultant field is obtained as,

$$E_R(r) = -j \eta_0 \frac{\exp(-jk_0 r)}{r} \sum_{n=1}^{\infty} \frac{(2n+1)}{n(n+1)} (M_n \alpha_n + N_n \beta_n) \quad (3.16)$$

where

$$M_n = \frac{P_n^1(\cos\theta)}{\sin\theta} \cos\phi \bar{i}_\theta - \frac{\partial}{\partial\theta} P_n^1(\cos\theta) \sin\phi \bar{i}_\phi$$

$$N_n = \frac{\partial}{\partial\theta} P_n^1(\cos\theta) \cos\phi \bar{i}_\theta - \frac{P_n^1(\cos\theta)}{\sin\theta} \sin\phi \bar{i}_\phi$$

$$\alpha_n = 1 + \frac{c_n}{a_n}, \quad \beta_n = 1 + \frac{b_n}{a_n}$$

\bar{i}_θ and \bar{i}_ϕ are unit vectors. The radiation pattern based on Eq. (3.16) has been computed by evaluating α_n and β_n for typical values, and the results are presented in Fig. 3.2 a.

3.2.4 FORWARD DIRECTIVITY OF THE SYSTEM

The total power W_t radiated by the system may be determined by integrating the total power flow across an infinite sphere placed concentric with the diffracting dielectric sphere.

$$\text{Thus } W_t = \frac{1}{2} \text{Re} \left[\int_{\phi=0}^{2\pi} \int_{\theta=0}^{\pi} r^2 (E_R \times H_R^*) \sin\theta d\theta d\phi \right] \quad (3.17)$$

This integral can be evaluated with the help of the following orthogonality relationships [129, pp. 569]:

$$\int_0^\pi \left(\frac{d}{d\theta} P_n^m \frac{d}{d\theta} P_{n'}^m + \frac{m^2 P_n^m P_{n'}^m}{\sin^2 \theta} \right) \sin \theta d\theta = 0 \text{ where } n \neq n'$$

$$= \frac{2}{(2n+1)} \frac{(n+m)!}{(n-m)!} n(n+1) \text{ where } n = n'$$

$$\int_0^\pi \left(\frac{d}{d\theta} P_n^1 \frac{d}{d\theta} P_{n'}^1 + \frac{1}{\sin^2 \theta} P_n^1 P_{n'}^1 \right) \sin \theta d\theta = 0, \text{ if } n \neq n'$$

$$= \frac{2}{(2n+1)} \frac{(n+1)!}{(n-1)!} n(n+1), \text{ if } n=n'$$

and

$$\int_0^\pi \left(\frac{P_n^1}{\sin \theta} \frac{d}{d\theta} P_{n'}^1 + \frac{P_{n'}^1}{\sin \theta} \frac{d}{d\theta} P_n^1 \right) \sin \theta d\theta = 0.$$

Using the above orthogonality relationships W_t is derived (see Appendix A-3) as,

$$W_t = \eta_0 \pi \sum_{n=1}^{\infty} (2n+1) (|\alpha_n|^2 + |\beta_n|^2) \quad (3.18)$$

An expression for the directivity of the antenna device in the forward direction relative to an isotropic source may be obtained by setting $\theta = \pi$ in Eq. (3.16) and using the expression for W_t . (Forward directivity and the maximum power gain are the same in this case, since the dielectric sphere has been assumed lossless).

Thus the forward directivity D_0 becomes,

$$D_0 = \frac{\frac{1}{2} |E_R(r)|_{\theta=\pi}^2 \cdot 4\pi r^2}{\eta_0 W_t} \quad (3.19)$$

Making use of the relationships,

$$\frac{P_n^1(\cos\theta)}{\sin\theta} \xrightarrow{\theta \rightarrow \pi} \frac{(-1)^n}{2} n(n+1)$$

and $\sin\theta P_n^1(\cos\theta)$ (or $-\frac{\partial}{\partial\theta} P_n^1(\cos\theta)$) $\xrightarrow{\theta \rightarrow \pi} \frac{(-1)^n}{2} n(n+1)$,

in the expression for $E_R(r)$, the forward directivity is derived in Appendix A-3 as,

$$D_o = \frac{\left| \sum_{n=1}^{\infty} \frac{2n+1}{2} (-1)^n (\alpha_n + \beta_n) \right|^2}{\sum_{n=1}^{\infty} \frac{2n+1}{2} (|\alpha_n|^2 + |\beta_n|^2)} \quad (3.20)$$

The directivity is estimated using Eq. (3.20) for known values of b , ϵ_1 and the operating frequency f_0 ; and the results are plotted in Fig. 3.3.

3.2.5 EXPERIMENTAL OBSERVATIONS AND COMPARISON WITH THEORY

In order to test the validity of the equations derived, and to investigate the effectiveness of placing the dielectric sphere in front of the aperture of a radiating conical horn, an experimental horn of half flare angle (θ_0) 26° and aperture diameter 11.75 cm was fabricated. Experiments were performed with paraffin wax ($\epsilon_r = 2.25$) dielectric

spheres of diameter 9 cm, 6 cm and 4 cm placed in front of the cone aperture. The horn was excited by a TE_{11} mode in the input circular waveguide; and the gain and pattern measurements were carried out at the X-band frequency ($f_0 = 9.68$ GHz). The directivity of the antenna system was measured by the substitution method using a pyramidal horn of gain 17 dB as the reference antenna.

The E-plane radiation pattern of the system with 6 cm diameter sphere at a distance of 24 cm from the cone aperture is experimentally obtained and is compared with the theoretical results based on Eq. (3.16) in Fig. 3.2. There is good overall agreement between these results.

The experimental results of the directivity measurement and the theoretical values based on Eq. (3.20) are shown in Fig. 3.3 as a function of the sphere diameter in wavelengths. The theoretical results show overall agreement with the experimental directivity measurements. It is observed from Fig. 3.3 that the directivity of the horn increases with the diameter of the test sphere. Fig. 3.4 shows the directivity of the system with different sphere dimensions as a function of the distance of the spheres from the horn aperture. It is observed that the gain increases as the distance of the sphere from the horn aperture is reduced, and the maximum gain is reached at an optimum

distance from the cone aperture.

From the results, it can be concluded that the dielectric sphere mounted conical horns have directivities in excess of that obtained with conventional conical horns of the same dimensions. The system also possesses a variable beamwidth facility depending on the dimensions of the dielectric spheres. The increase in directivity is seen to depend on the sphere dimensions and its location from the horn aperture. For a typical sphere, there is an optimum position for maximum gain, and the improvement in gain is particular for spheres of diameter $b \leq 3\lambda_0$.

The effect of placing a dielectric sphere in front of, but displaced from, the aperture of the radiating horn in narrowing the -3 dB beamwidth, and in reducing the sidelobe levels is discussed in the cases of other antennas considered. The possibility of obtaining a variable beamwidth facility at a low input VSWR by appropriate sphere off-set positions in front of the horn aperture has also been discussed in those sections.

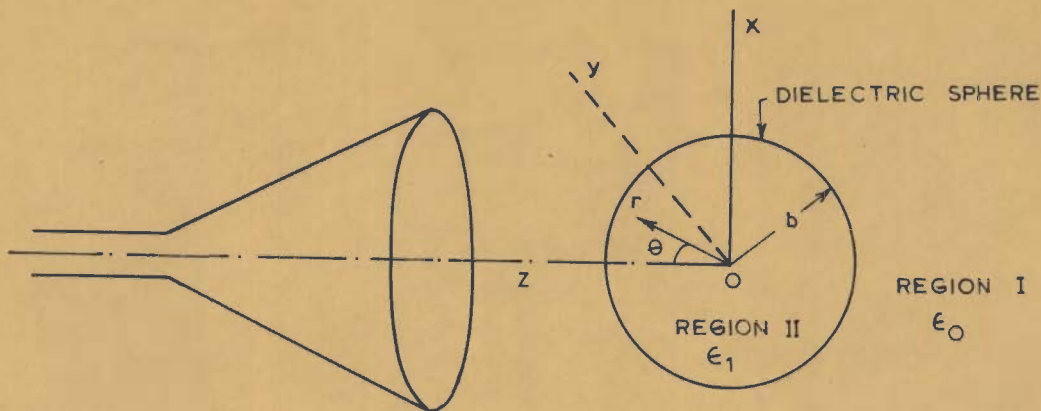


FIG. 3.1 - GEOMETRY OF THE ANTENNA SYSTEM
PARAFFINWAX SPHERE OF RADIUS 'b'
PLACED INFRONT OF THE CONE APERTURE

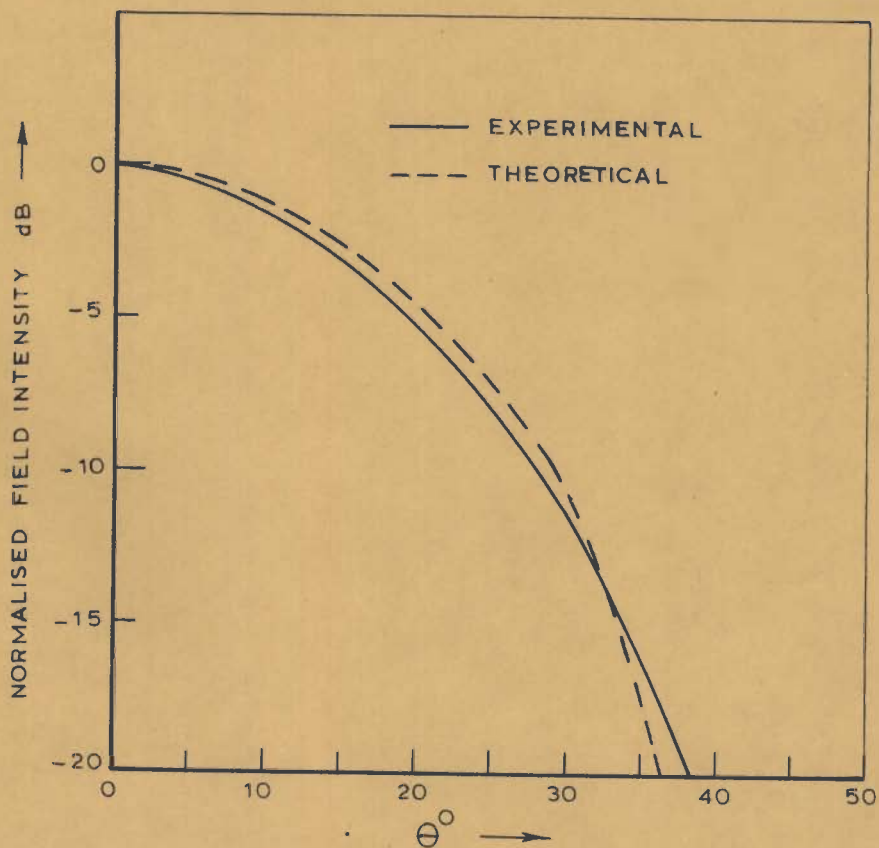


FIG. 3.2 - THEORETICAL & EXPERIMENTAL RADIATION
PATTERN FOR A CONE WITH A DIELECTRIC
SPHERE OF 6cm DIA. AT A DISTANCE OF
24cm INFRONT OF THE CONE APERTURE

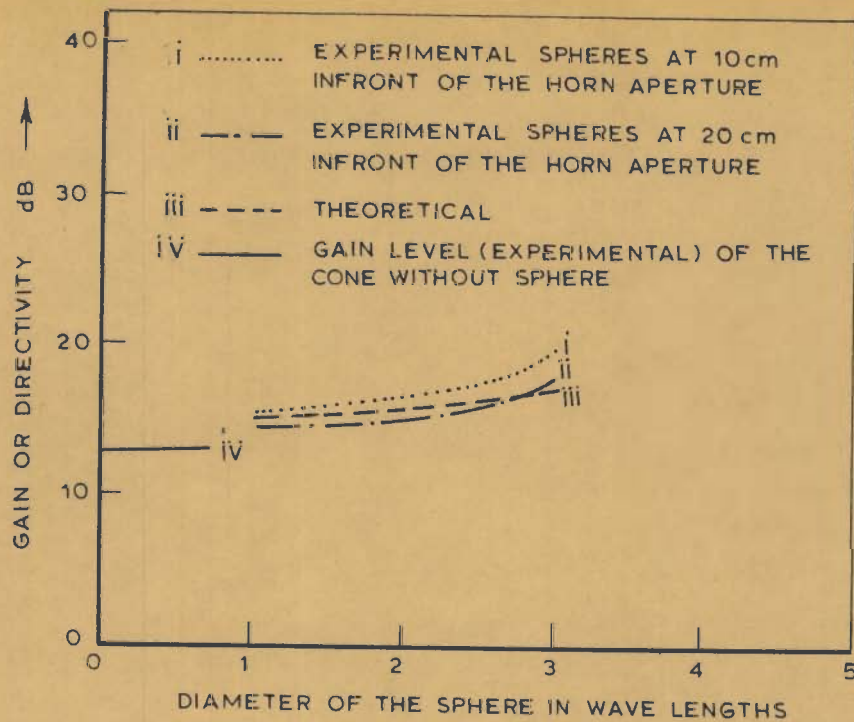


FIG. 3.3 - DIRECTIVITY (EXPERIMENTAL AND THEORETICAL) AS A FUNCTION OF SPHERE DIAMETER IN WAVE LENGTHS

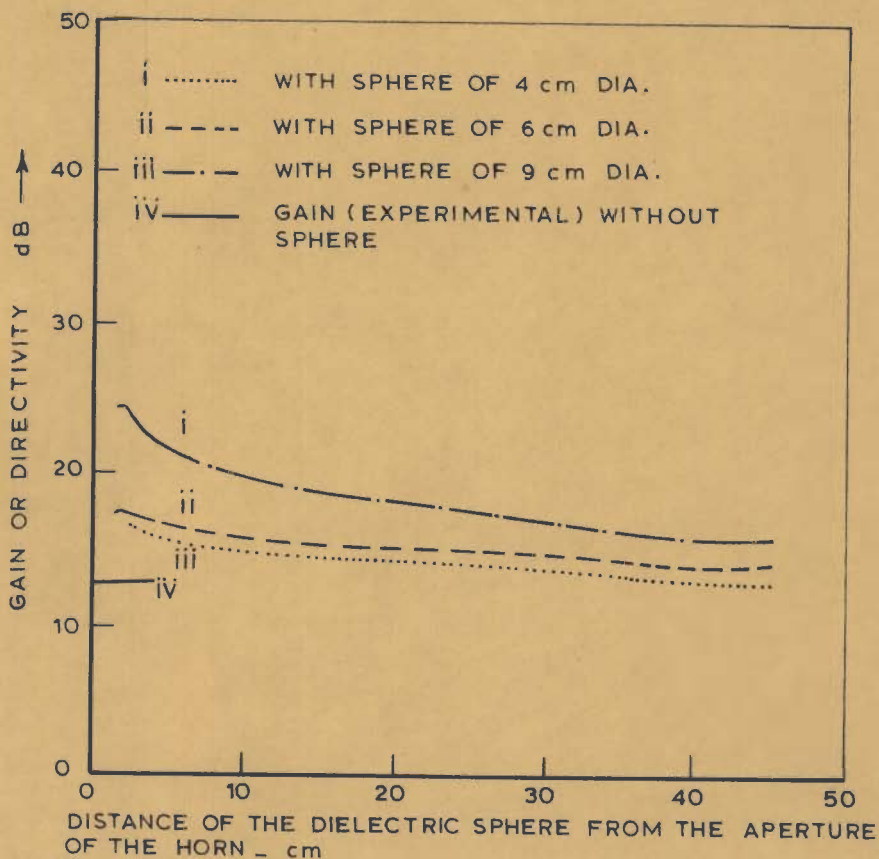


FIG. 3.4 - (EXPERIMENTAL) DIRECTIVITY WITH SPHERES OF DIFFERENT DIMENSIONS AS A FUNCTION OF THE DISTANCE OF THE SPHERE FROM THE CONE APERTURE

3.3 DIELECTRIC-COATED CONICAL HORN

Analytical and experimental results of the radiation properties of dielectric-coated conical horns with small flare angles are presented in this section. Hamid et al.[48] have computed the radiation characteristics of conical horn loaded with dielectric layer along the horn walls with the aid of Keller's ray theory. But, in the present section the radiation characteristics of the dielectric coated conical horn are derived in a much simpler form, using spherical hybrid modes on the basis of the vector diffraction formula. The characteristic equation for the eigen values is derived ; and the values computed for the HE_{11} mode is compared with those for conventional and corrugated conical horns. Analytical results of the radiation characteristics are established in good agreement with the theoretical results.

3.3.1 MODAL ANALYSIS

The inner walls of the conical horn of flare angle θ_0 is layered with a dielectric material of permittivity ϵ_1 as shown in Fig. 3.5 . (The flare angle of the coated cone is θ_1). The modal fields in a conical horn can be derived from the scalar potential functions A_r and F_r ; and giving attention to the outward travelling waves, Eqs.(3.2) can be written as,

$$A_r = a_{mn} \hat{H}_n^{(2)}(k_0 r) P_n^m(\cos\theta) e^{jm\phi} \quad (3.21)$$

$$F_r = b_{mn} \hat{H}_n^{(2)}(k_0 r) P_n^m(\cos\theta) e^{jm\phi}$$

where a_{mn} and b_{mn} are constants depending on the excitation of the modes, and are related by the equation

$$\frac{b_{mn}}{a_{mn}} = -j \eta_0 B_0 \quad \text{where } \eta_0 = \sqrt{\mu_0 / \epsilon_0}$$

and B_0 is a coefficient depending on the boundary conditions ($B_0 = \pm 1$ for balanced conditions).

In Eqs. (3.21) 'm' is an integer, and 'n' is real and positive corresponding to the ordinal number of the root of the characteristic equation (i.e. corresponding to the order of the wave in the horn). In order to obtain simpler solution for spherical hybrid modes in the dielectric coated conical horn, the θ - part of the Helmholtz equation in spherical coordinates, given by Eqs.(3.1), after separation of variables can be written as

$$\frac{1}{X(\theta) \sin\theta} \frac{\partial}{\partial\theta} \left(\sin\theta \frac{\partial X(\theta)}{\partial\theta} \right) + n(n+1) - \frac{m^2}{\sin^2\theta} = 0 \quad (3.22)$$

For small values of θ , replacing $\sin\theta$ by θ , the above Eq.(3.22) is modified as,

$$\frac{\partial^2 X(\theta)}{\partial\theta^2} + \frac{1}{\theta} \frac{\partial X(\theta)}{\partial\theta} + \left[n(n+1) - \frac{m^2}{\theta^2} \right] X(\theta) = 0 \quad (3.23)$$

Denoting $\sqrt{n(n+1)} = q$; and putting $v = q\theta$, Eq(3.23) is

modified as,

$$\frac{\partial^2 X(\theta)}{\partial v^2} + \frac{1}{v} \frac{\partial X(\theta)}{\partial v} + \left(1 - \frac{m^2}{v^2}\right) X(\theta) = 0 \quad (3.24)$$

Eq. (3.24) is the Bessel's differential equation which will have solution as

$$X(\theta) = D_m J_m(v) \quad (3.25)$$

where $J_m(v)$ is the Bessel function of the first kind ,

$$v = q\theta, \quad q = \sqrt{n(n+1)}$$

and D_m is an arbitrary constant.

Inserting this relation for the θ -part, Eqs. (3.21) can be written as,

$$\begin{aligned} A_r &= a_{mn} \hat{H}_n^{(2)}(k_o r) J_m(q\theta) \exp(jm\phi) \\ F_r &= b_{mn} \hat{H}_v^{(2)}(k_o r) J_m(q\theta) \exp(jm\phi) \end{aligned} \quad (3.26)$$

The time factor $e^{j\omega t}$ is implicit throughout.

Inside the dielectric layer there will be standing waves due to reflections from the interfaces, and hence by Eqs.(3.26) the proper form of the potential functions for fields in the dielectric coated region becomes,

$$\begin{aligned} A_r^d &= [c_{mn} J_m(q\theta) + d_{mn} y_m(q\theta)] \hat{H}_n^{(2)}(k_1 r) \exp(jm\phi) \\ F_r^d &= [e_{mn} J_m(q\theta) + f_{mn} y_m(q\theta)] \hat{H}_n^{(2)}(k_1 r) \exp(jm\phi) \end{aligned} \quad (3.27)$$

where $J_m(x)$ = Bessel function of the first kind

$y_m(x)$ = Bessel function of the second kind

$\hat{H}_n^{(2)}(x)$ = modified spherical Hankel function of the second kind

$$\text{and } k_1 = \omega \sqrt{\mu_0 \epsilon_1}$$

(The superscript 'd' in Λ_r and F_r denotes dielectric coated region).

The constants c_{mn} and e_{mn} ; d_{mn} and f_{mn} are related by the same way as a_{mn} and b_{mn}

$$\text{i.e. } e_{mn}/c_{mn} = -j\eta_1 B_0 \quad \text{and } f_{mn}/d_{mn} = -j\eta_1 B_0$$

The characteristic equation for the separation constant 'n' can be derived by matching the fields at $\theta = \theta_1$ and also by applying the appropriate boundary conditions. The characteristic equation for the hybrid (HE_{mn}) mode is obtained in Appendix B-1 as,

$$\begin{aligned} & \frac{qJ_m'(q\theta_1)}{J_m(q\theta_1)} + \frac{jH'(k_0 r)}{H(k_0 r)} \frac{mB_0}{\sin\theta_1} \\ & = \frac{\epsilon_1}{\epsilon_0} \left[q \frac{J_m'(q\theta_1) y_m(q\theta_0) - J_m(q\theta_0) y_m'(q\theta_1)}{J_m(q\theta_1) y_m(q\theta_0) - J_m(q\theta_0) y_m(q\theta_1)} + \right. \\ & \quad \left. + \frac{j}{\sin\theta_1} \frac{mB_0}{H(k_0 r)} \frac{H'(k_0 r)}{H(k_0 r)} \right] \end{aligned} \quad (3.28)$$

$$\text{where } H(x) = \hat{H}_n^{(2)}(x)$$

$$H'(x) = \frac{\partial}{\partial r} \hat{H}_n^{(2)}(x)$$

(The subscript 'n' in HE_{mn} denotes the ordinal number of the root of characteristic equation that designates the order of the wave in the horn). Under far-field approximation (i.e. $k_0 r \gg 1$, $\frac{H'}{H} = -j$) Eq. (3.28) becomes

$$q \cdot \frac{J'_m(q\theta_1)}{J_m(q\theta_1)} \sin\theta_1 + mB_0 = \frac{\epsilon_1}{\epsilon_0} \left[q \frac{J'_m(q\theta_1)y_m(q\theta_0) - J_m(q\theta_0)y'_m(q\theta_1)}{J_m(q\theta_1)y_m(q\theta_0) - J_m(q\theta_0)y_m(q\theta_1)} \right. \\ \left. \sin\theta_1 + mB_0 \right] \quad (3.29)$$

Now restricting the consideration to the case with $m = 1$, and the excitation coefficient $B_0 = +1$, the characteristic equation for the HE_{1n} mode becomes,

$$\sin\theta_1 \cdot q \frac{J'_1(q\theta_1)}{J_1(q\theta_1)} + 1 \\ = \frac{\epsilon_1}{\epsilon_0} \left[q \frac{J'_1(q\theta_1)y_1(q\theta_0) - J_1(q\theta_0)y'_1(q\theta_1)}{J_1(q\theta_1)y_1(q\theta_0) - J_1(q\theta_0)y_1(q\theta_1)} \sin\theta_1 + 1 \right] \quad (3.30)$$

This characteristic equation is solved graphically for a coating thickness of 2° with paraffin wax ($\epsilon_r = 2.25$). (The method of solution is illustrated in Fig. B - 1. The values of 'n' thus obtained for HE_{11} mode, by taking the

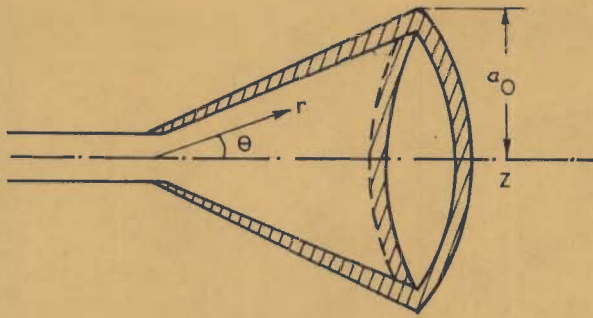


FIG. 3.5 - DIELECTRIC COATED CONICAL HORN

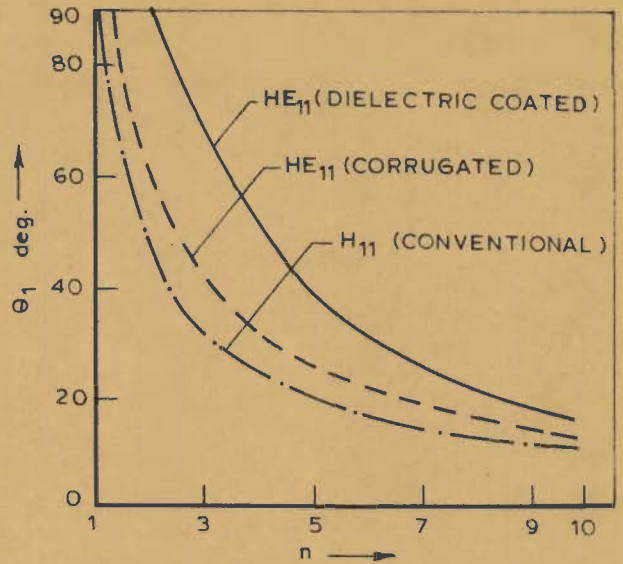


FIG. 3.6 - SEPARATION CONSTANT 'n' AS A FUNCTION OF θ_1

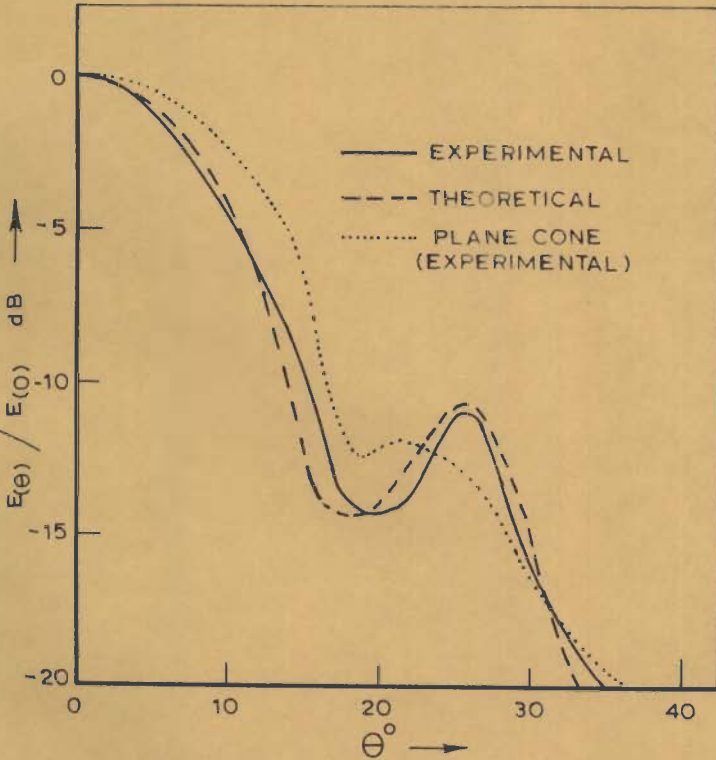


FIG. 3.7a - RADIATION PATTERN (E-PLANE) OF A DIELECTRIC COATED CONICAL HORN

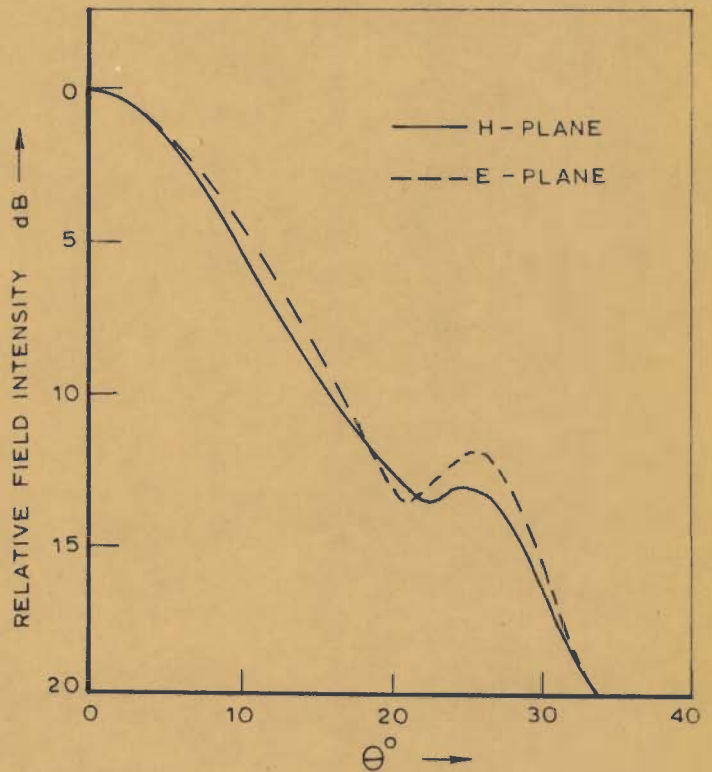


FIG. 3.7b - E-PLANE & H-PLANE PATTERNS OF DIELECTRIC COATED CONE

first root of Eq. (3.30) for different values of coated cone flare angle θ_1 are shown in Fig. 3.6 together with those for conventional and corrugated conical horns.

Substitution of A_r and F_r given by Eqs.(3.26) in the appropriate field relations [52] (Eqs.(3.4)) yields the interior horn fields. Accordingly for the HE_{11} mode, under far-field approximation, the interior horn field components are obtained as,

$$E_{\theta} = -j^{n+1} a_{11} \eta_0 \frac{e^{-jk_0 r}}{r} \left[\frac{J_1(q\theta)}{\sin\theta} + qJ_1'(q\theta) \right] \exp(j\phi) \quad (3.31)$$

and

$$E_{\phi} = -j^{n+1} j \eta_0 a_{11} \frac{e^{-jk_0 r}}{r} \left[\frac{J_1(q\theta)}{\sin\theta} + qJ_1'(q\theta) \right] \exp(j\phi) \quad (3.32)$$

The value of q in the above equations for E_{θ} and E_{ϕ} corresponds to that for the HE_{11} mode i.e. corresponding to the first root of the characteristic equation.

3.3.2 COMPUTATION OF RADIATION FIELDS

The transverse electric field \bar{E}_t over the horn aperture, under far-field approximation, for the HE_{11} mode is obtained from the values of E_{θ} and E_{ϕ} ; and becomes

$$\bar{E}_t = \bar{i}_{\theta} E_{\theta} + \bar{i}_{\phi} E_{\phi}$$

$$\bar{E}_t = -(j)^{n+1} a_{11} \eta_0 \frac{e^{-jk_0 r}}{r} \left[\frac{J_1(q\theta)}{\sin\theta} + qJ_1'(q\theta) \right] (\bar{i}_\theta + j\bar{i}_\phi) \exp(j\phi) \quad (3.33)$$

Using the following recurrence formula for Bessel functions

$$J_n'(x) + \frac{n}{x} J_n(x) = J_{n-1}(x) ;$$

and with the assumption of $\sin\theta \approx \theta$ for small values of θ , the above equation for \bar{E}_t becomes simpler as

$$E_t = -(j)^{n+1} a_{11} \eta_0 \frac{e^{-jk_0 r}}{r} q \cdot J_0(q\theta) (\bar{i}_\theta + j\bar{i}_\phi) \exp(j\phi) \quad (3.34)$$

The simpler expression for \bar{E}_t given by Eq. (3.34) facilitates an easy evaluation of the diffracted far-field on the basis of the vector diffraction formula [120]. Thus the diffracted far-field, under the assumption of no phase variation of \bar{E}_t over the aperture, is obtained (Appendix B-2) as,

$$E_R(r, \theta, \phi) = B_{11} (1 + \cos\theta) j \frac{e^{-jk_0 r}}{r} \cdot \frac{J_0\left(\frac{2\pi}{\lambda_0} a_0 \sin\theta\right)}{(q\theta_0)^2 - \frac{4\pi^2 a_0^2}{\lambda_0^2} \sin^2\theta} (i_\theta + j i_\phi) \exp(j\phi) \quad (3.35)$$

where a_0 = the radius of the conical horn aperture

and B_{11} is a constant independent of (r, θ, ϕ) as defined in Appendix B-2.

The validity of the assumption of no phase variation of \bar{E}_t over the horn aperture is true only for a maximum phase error [125] of $\pi/4$; and this is possible with $\theta_1 \leq 20^\circ$. The radiation pattern based on Eq.(3.35) has been computed and is given in Fig. 3.7a.

3.3.3 THE AXIAL GAIN

The total power radiated from the horn may be obtained by considering the conical horn as a spherical cap of radius 'L'. (L is the axial length of the horn). Thus the total power P_t crossing the spherical cap of radius 'L' in the cone region is given by,

$$P_t = \frac{1}{2} \text{Re} \left[\iint_S (\mathbf{E}_t \times \mathbf{H}_t^*) ds \right]$$

It is shown in Appendix B-3 that by using Eq.(3.34), P_t is obtained as

$$P_t = \frac{1}{2} \pi \eta_0 a_{11}^2 q^2 \theta_1^2 [J_0^2(q\theta_1) + J_1^2(q\theta_1)] \quad (3.36)$$

Now the axial gain is defined as

$$G = \frac{4\pi P(0,0)}{P_t} \quad (3.37)$$

$$\text{where } P(0,0) = \frac{1}{2 \eta_0} r^2 |E_R|_{\max}^2$$

Using Eqs.(3.35) and (3.36), the axial gain is derived in Appendix B-3 as,

$$G = 16\pi^2 \left(\frac{a_0}{\lambda_0} \right)^2 \cdot \frac{J_1^2(q\theta_0)}{(q\theta_1)^2 [J_0^2(q\theta_1) + J_1^2(q\theta_1)]} \quad (3.38)$$

The substitution of the typical values of a_0 , θ_1 , q and λ_0 in Eqs.(3.38) will give the gain of the dielectric coated conical horn for HE_{11} mode excitation. For typical values of the experimental horn (see Sec. 3.3.5) at $f_0 = 8.86$ GHz, the gain based on Eq. (3.38) was found to be approximately 17.2 dB. The range of validity of the radiation pattern and gain formulae given by Eqs.(3.34) and (3.37) depends on both θ_0 and a_0 . These formulae are accurate only for $\theta_1 \leq 20^\circ$.

3.3.4 EXPERIMENTAL RESULTS

The radiation behaviour of the dielectric coated conical horn was investigated with a cone of $\theta_0 = 20^\circ$ and aperture diameter 11.75 cm coated with paraffin wax ($\epsilon_r = 2.25$) for a thickness of 2° . The horn was excited by TE_{11} mode in a circular input waveguide at a frequency of 8.86 GHz. In Fig. 3.7 a the experimental E -plane pattern is compared with the theoretical results based on Eq. (3.35). There is good overall agreement between the two results. The pattern for the cone without dielectric coating is also included for comparison. The E-plane and H -plane patterns of the coated conical horn are depicted in Fig. 3.7b. The gain

of the cone with and without dielectric coating was observed and was found to be 17.75 dB and 14.5 dB respectively. The gain based on Eq. (3.38) for the typical values was found to be approximately 17.2 dB and is in good agreement with the experimental value.

From the results, it is concluded that dielectric coated conical horns have increased axial directivity and on-axis gain; and reduced -3 dB beamwidth at the expense of a minor deterioration in the sidelobe levels.

3.4 DIELECTRIC SPHERE LOADED DIELECTRIC COATED CONICAL HORN

In an effort to attain improved radiation pattern with increased directivity as well as low sidelobe levels from dielectric coated conical horns, investigations have been carried out with dielectric spheres placed in front of, but displaced from, the aperture of the coated cone. The analytical expression for the radiated far - field components of the system with dielectric spheres are derived by treating the device as a microwave lens illuminated by an aperture source. Theoretical results thus obtained are found in good overall agreement with experimental results. The test feed system has improved radiation characteristics with low sidelobe levels and obvious increased directivity.

3.4.1 ANALYTICAL FORMULATION

The radiation behaviour of the system is analysed by treating it as a dielectric lens illuminated by an aperture source. The feed system under study is shown in Fig. 3.8 a , and its optical equivalent in Fig. 3.8b . The homogeneous dielectric sphere (spherical lens) is illuminated by the dielectric coated conical horn (aperture source). Following the method due to Bakefi and Farnel[9] the amplitudes of the field distributions in the vertical and horizontal planes respectively at an equivalent circular aperture at BB through the centre of the sphere are given by

$$u_i^\theta(\sigma) = \alpha \left[P_\theta(\psi) TE_1 TE_2 \frac{\sin\psi}{\sigma} \frac{d\psi}{d\sigma} \right]^{1/2} \quad (3.39)$$

$$u_i^\phi(\sigma) = \alpha \left[P_\phi(\psi) TE_1 TE_2 \frac{\sin\psi}{\sigma} \frac{d\psi}{d\sigma} \right]^{1/2}$$

where TE_1 and TE_2 are the effective transmission coefficients at the two refracting boundaries of the sphere, α is a normalisation constant, and $P_\theta(\psi)$ and $P_\phi(\psi)$ denote the field patterns (power) in the two principal planes (vertical and horizontal) at an arbitrary position. For the dielectric coated cone, edge diffraction will be minimum and hence, under far field approximation, the patterns at the location of the off-set placed sphere at a small distance from the horn aperture will be the same as those at the horn aperture



Accordingly the magnitudes of the fields in the two principal planes at the location of the off-set sphere can be taken as those given by \bar{E}_t in Eq. (3.34). As the field distribution at the sphere location has been assumed the approximate expressions for the far field components, with an assumed azimuthal symmetry [9] can be obtained as,

$$\begin{aligned} \mathbb{L}_\theta(\theta) &= j(k_0 b)^2 \frac{e^{-jk_0 r}}{k_0 r} \int_0^{\sigma_m} u_i^\theta(\sigma) J_0(k_0 b \sigma \sin\theta) \cdot \\ &\quad e^{-jk_0 v(\sigma)} \sigma d\sigma \\ &\quad \text{(vertical plane)} \quad (3.40) \\ \mathbb{L}_\phi(\theta) &= j(k_0 b)^2 \frac{e^{-jk_0 r}}{k_0 r} \int_0^{\sigma_m} u_i^\phi(\sigma) J_0(k_0 b \sigma \sin\theta) \cdot \\ &\quad e^{-jk_0 v(\sigma)} \sigma d\sigma \\ &\quad \text{(Horizontal plane)} \end{aligned}$$

where σ_m denotes the radius of the equivalent circular aperture over which the amplitude $u_i(\sigma)$ and the phase distribution $k_0 v(\sigma)$ are known, and b is the radius of the sphere.

Using the values of $u_i(\sigma)$ computed from Eqs. (3.34) and (3.39), the integrals in Eqs. (3.40) have been evaluated by numerical method (Simpson's rule) and the results are plotted in Fig. 3.9b.

3.4.2 EXPERIMENTAL OBSERVATIONS

To investigate the radiation properties of the test feed system, experiments were carried out with the same conical horn of $\theta_0 = 20^\circ$ and aperture diameter 11.75 cm coated with paraffin wax ($\epsilon_r = 2.25$) for a thickness of 2° discussed in Sec. 3.3.5. The horn was excited by a TE_{11} mode in the input circular waveguide at $f_0 = 8.64$ GHz, and measurements were made with paraffin wax spheres of diameter 9 cm, 6 cm and 4 cm kept displaced in front of the horn aperture. The sphere displaced positions from the horn aperture were determined experimentally for minimum input VSWR performance [85]. Experimental results of the radiation pattern for the feed system are presented in Fig. 3.9a together with those for dielectric coated and conventional conical horns. Theoretical patterns obtained for the feed system by the present method using Eqs. (3.40) for paraffin wax spheres of diameter 6 cm and 4 cm are depicted in Fig. 3.9b together with experimental patterns, showing a good overall agreement. The gain (experimental) of the system as a function of the sphere diameter in wavelength is shown in Fig. 3.10. Decrease in -3 dB beamwidth as a function of off-set dielectric sphere diameter is depicted in Fig. 3.10a.

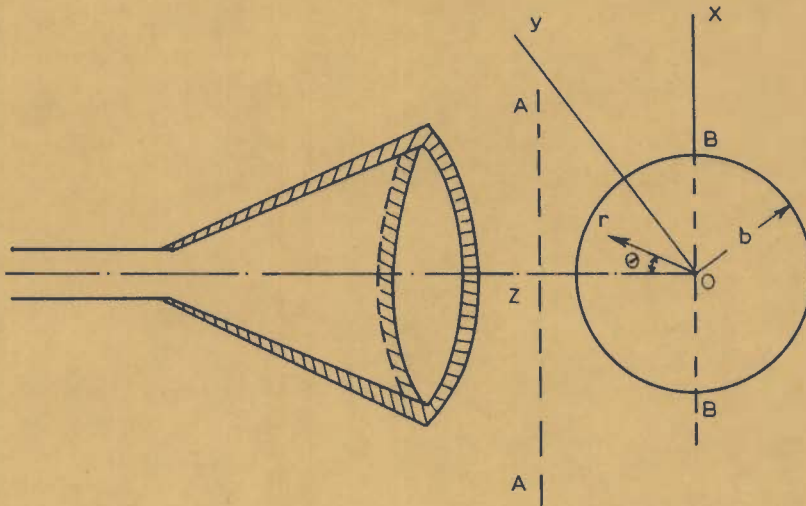
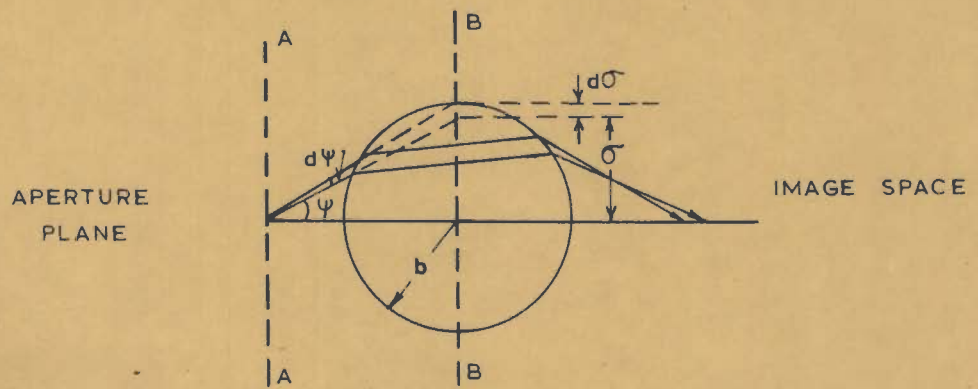


FIG. 3.8 a - GEOMETRY OF THE DIELECTRIC SPHERE LOADED DIELECTRIC COATED CONICAL HORN



AA - APERTURE PLANE

BB - THE EQUIVALENT CIRCULAR APERTURE THROUGH THE CENTRE OF THE SPHERE

FIG. 3.8b - OPTICAL SYSTEM FOR THE GEOMETRY OF FIG. 3.8 a

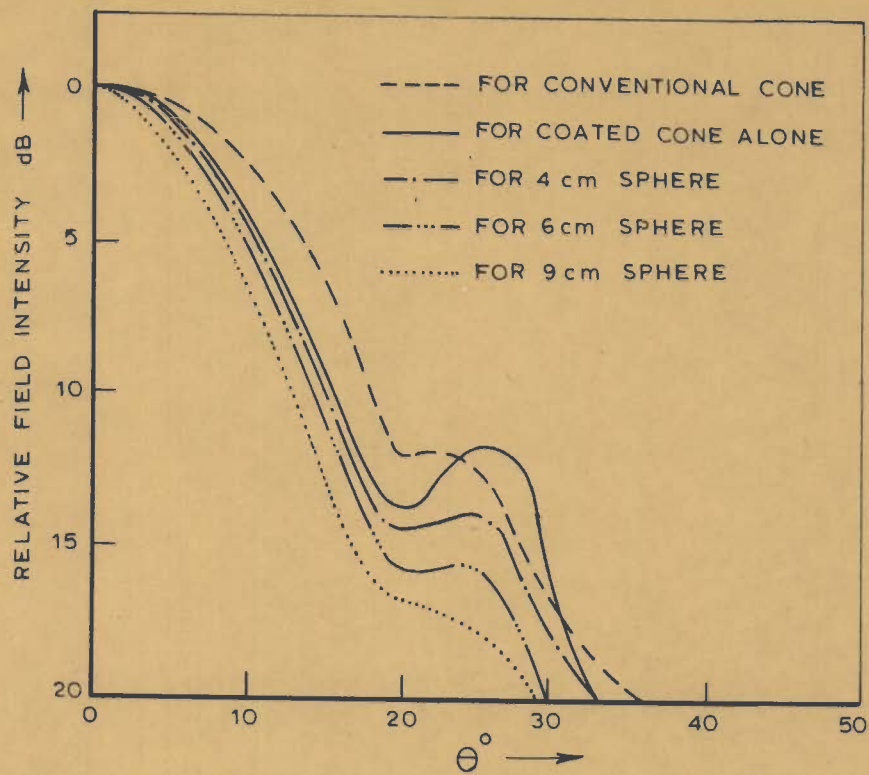


FIG. 3.9a - EXPERIMENTAL PATTERN (E-PLANE) OF SPHERE LOADED DIELECTRIC COATED CONICAL HORN

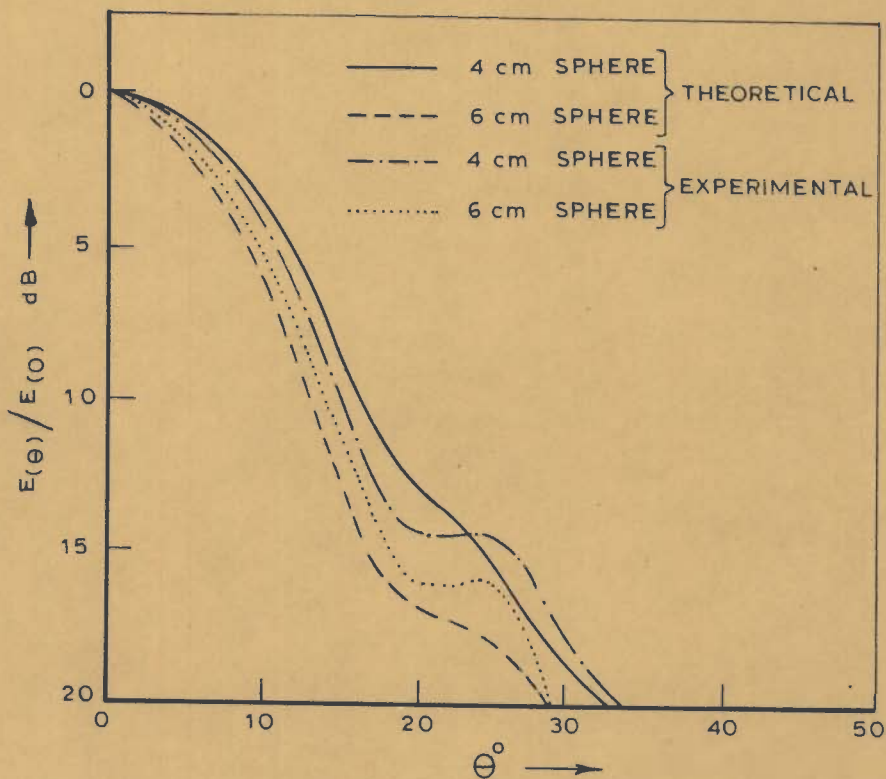


FIG. 3.9b - RADIATION PATTERN (E-PLANE) OF SPHERE LOADED DIELECTRIC COATED CONICAL HORN

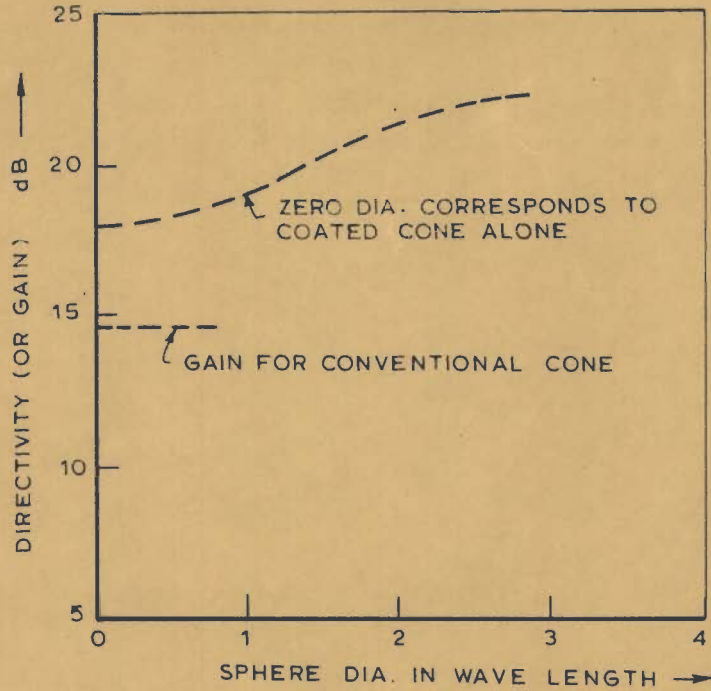


FIG. 3.10_ GAIN OF SPHERE LOADED DIELECTRIC COATED CONICAL HORN

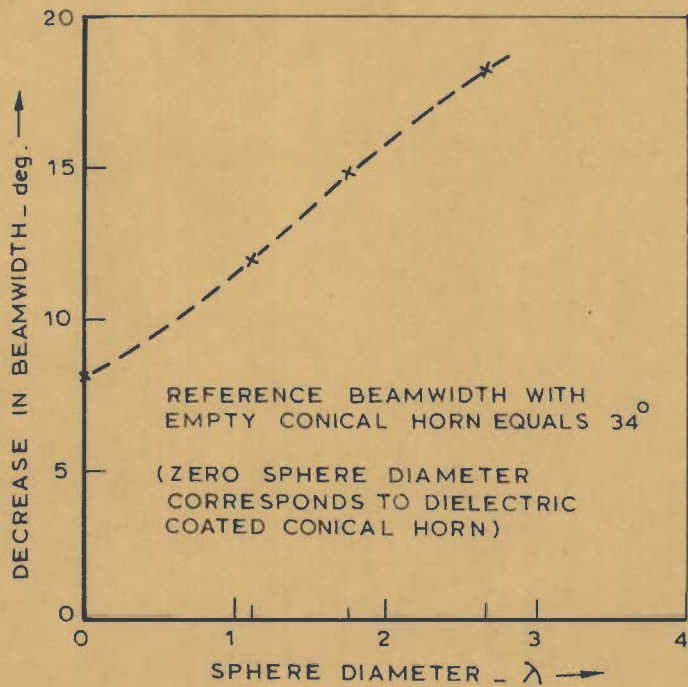


FIG. 3.10^a-DECREASE IN BEAM WIDTH VS SPHERE DIA. FOR DIELECTRIC SPHERE LOADED DIELECTRIC COATED CONICAL HORN

From the results presented it can be concluded that dielectric sphere loading improves the radiation characteristics of the dielectric-coated conical horns with reduced sidelobe levels, and increased directivity and on-axis gain. The feed system also provides a variable beamwidth facility with minimum input VSWR for optimal sphere displaced positions in front of the horn aperture. Hence the dielectric sphere loaded dielectric coated conical horn may be used as an effective reflector antenna feed system having improved performance with greater directivity, higher axial gain and low sidelobes together with a variable beamwidth facility.

3.5 DIELECTRIC SPHERE LOADED CONICAL HELIX HORN [74]

A new type of hybrid mode feed system for applications in satellite communication is considered in this section. The feed system consists of a dielectric sphere placed at a displaced position in front of the aperture of a conical horn with a helical boundary. The conical horn formed by a helical conductor with close spacings allows only circumferential

currents to flow. It has been proved that a suitably designed helix will have axial radiation[22],[77] with relatively wideband characteristics. A.W. Ashton [7] has analysed a spiral horn antenna by assuming the fields associated with it to be the same as those in a cylindrical waveguide, and has established that it has desirable radiation characteristics to be used as a satellite antenna. In this section the analysis of the fields in a conical horn with helical boundary is presented using spherical hybrid modes; and the far-field radiation characteristics of the horn are derived on the basis of the vector diffraction formula with the assumption of a quadratic phase variation of the field over the horn aperture . In order to improve the radiation characteristics of this conical helix horn, with increased directivity and reduced sidelobe levels, investigations have been carried out with dielectric sphere loading in front of the horn aperture. The analytical treatment of the system with dielectric sphere in front of the horn

aperture is made by treating the system as a microwave lens illuminated by an aperture source. Analytical results are established in good agreement with experimental results.

3.5.1 MODAL FIELDS IN A CONICAL HORN WITH HELICAL BOUNDARY

The feed system under study is shown in Fig. 3.11a. The helical cone of flare angle θ_0 consists of a closely wound wire helix that allows only circumferential currents to flow. Because of the way the horn is excited with a fast wave, the fields contained in the horn are also fast waves; and hence this horn differs from the antenna devised by Kraus [77(a)] which supports slow waves.

Analysis of the horn fields is made by using spherical hybrid modes. In order to satisfy the boundary conditions both TE and TM modes need to exist. For small flare angle cones, by Eqs. (3.26), modal fields inside the horn region can be obtained from the potential functions given by,

$$\begin{aligned} \bar{A}_r &= A_n \hat{J}_n(k_0 r) J_m(q\theta) e^{jm\phi} \\ \bar{F}_r &= B_n \hat{J}_n(k_0 r) J_m(q\theta) e^{jm\phi} \end{aligned} \tag{3.40a}$$

and the potential functions for hybrid modes outside the horn are given by

$$\begin{aligned}
 A_r^o &= C_n \hat{H}_n^{(2)}(k_o r) J_m(q\theta) e^{jm\phi} \\
 F_r^o &= D_n \hat{H}_n^{(2)}(k_o r) J_m(q\theta) e^{jm\phi}
 \end{aligned}
 \tag{3.41}$$

where $q = \sqrt{n(n+1)}$, m is an integer and ' n ' is real and positive. A_n , B_n , C_n and D_n are constants that depend on the excitation of the horn; and can be determined by applying appropriate boundary conditions. The superscripts - and o in A_r and F_r denote the corresponding potential functions for the regions inside and outside the horn respectively. Here the functions $\hat{J}_n(k_o r)$ and $\hat{H}_n^{(2)}(k_o r)$ are chosen respectively for inside and outside the horn regions since at $r = 0$ the field is finite, and at $r = \infty$ the field is infinite.

The characteristic equation for the eigen values may be formed by using the following boundary conditions

- i) $E_r(\text{inside}) = E_r(\text{outside})$
- ii) $H_r(\text{inside}) = \vec{H}_r(\text{outside})$ at the horn boundary
i.e. at $\theta = \theta_o, r = a_o$
- iii) $E_\theta = E_\phi = 0$
- iv) The field is finite at the horn radius = 0, and is infinite at the radius = ∞ .

It is seen in Appendix C-1 that the characteristic equation for the hybrid mode is obtained as,

$$\frac{\hat{J}'_n(k_0 a_0) J'_m(q\theta_0)}{\hat{J}_n(k_0 a_0) J'_m(q\theta_0)} = \frac{q^2}{m^2} \sin^2 \theta_0 \frac{\hat{H}_n^{(2)'}(k_0 a_0) J'_m(q\theta_0)}{\hat{H}_n^{(2)}(k_0 a_0) J'_m(q\theta_0)} \quad (3.42)$$

where a_0 is the radius of the conical helix horn and θ_0 is its flare angle. The primes indicate differentiation with respect to the argument.

Restricting the consideration to $m = 1$, Eq.(3.42) becomes,

$$\frac{\hat{J}'_n(k_0 a_0) J'_1(q\theta_0)}{\hat{J}_n(k_0 a_0) J'_1(q\theta_0)} = q^2 \sin^2 \theta_0 \frac{\hat{H}_n^{(2)'}(k_0 a_0) J'_1(q\theta_0)}{\hat{H}_n^{(2)}(k_0 a_0) J'_1(q\theta_0)} \quad (3.43)$$

This characteristic equation can be solved for the eigen values 'n' for any wave number corresponding to ordinal number of the root of this equation. Thus, for typical values of $a_0 = 3.5$ cm, $f_0 = 9.58$ GHz, the eigen values 'n' for HE_{11} mode corresponding to the first root of the characteristic equation are obtained for horns of various flare angles θ_0 , and are plotted in Fig. 3.12 as a function of θ_0 .

With the eigen value 'n' known for the particular horn of flare angle θ_0 , the E-fields associated with the horn for the HE_{11} mode become (see Appendix C-1),

inside the horn

$$E_r = \frac{\Lambda_1}{j\omega\epsilon_0} \frac{n(n+1)}{r^2} \hat{J}_n(k_0 r) J_1(q\theta) e^{j\phi}$$

$$E_\theta = \frac{j\Lambda_1 k_0 q}{\omega\epsilon_0 r} \hat{J}'_n(k_0 a_0) J'_1(q\theta_0) \cdot$$

$$\left[\frac{\hat{J}_n(k_0 r) J_1(q\theta)}{\hat{J}_n(k_0 a_0) J_1(q\theta_0)} \frac{\sin\theta_0}{\sin\theta} - \frac{\hat{J}'_n(k_0 r) J'_1(q\theta)}{\hat{J}'_n(k_0 a_0) J'_1(q\theta_0)} \right] e^{j\phi}$$

(3.44)

$$E_\phi = \frac{\Lambda_1 k_0}{\omega\epsilon_0 r} \hat{J}'_n(k_0 a_0) J'_1(q\theta_0) \cdot$$

$$\left[\frac{-q^2 \hat{J}_n(k_0 r) J'_1(q\theta)}{\hat{J}_n(k_0 a_0) J_1(q\theta_0)} \sin\theta_0 + \frac{\hat{J}'_n(k_0 r) J_1(q\theta)}{\hat{J}'_n(k_0 a_0) J'_1(q\theta_0)} \frac{1}{\sin\theta} \right] e^{j\phi}$$

outside the horn

$$E_r = \frac{\Lambda_1}{j\omega\epsilon_0} \frac{n(n+1)}{r^2} \frac{\hat{H}_n^{(2)}(k_0 r)}{\hat{H}_n^{(2)}(k_0 a_0)} \hat{J}_n(k_0 a_0) J_1(q\theta)$$

$$E_\theta = \frac{j\Lambda_1 k_0 q}{\omega\epsilon_0 r} \hat{J}_n(k_0 a_0) \frac{\hat{H}_n^{(2)'}(k_0 a_0)}{\hat{H}_n^{(2)}(k_0 a_0)} J'_1(q\theta_0) \cdot$$

$$\left[\frac{\hat{H}_n^{(2)}(k_0 r) J_1(q\theta)}{\hat{H}_n^{(2)}(k_0 a_0) J_1(q\theta_0)} \frac{\sin\theta_0}{\sin\theta} - \frac{\hat{H}_n^{(2)'}(k_0 r) J'_1(q\theta)}{\hat{H}_n^{(2)'}(k_0 a_0) J'_1(q\theta_0)} \right] e^{j\phi}$$

(3.45)

$$E_{\phi} = \frac{A_1 k_0 \hat{J}_n(k_0 a_0)}{\omega \epsilon_0 r \hat{H}_n^{(2)}(k_0 a_0)} \hat{H}_n^{(2)'}(k_0 a_0) J_1'(q\theta_0).$$

$$\left[-q^2 \sin\theta_0 \frac{\hat{H}_n^{(2)}(k_0 r) J_1'(q\theta)}{\hat{H}_n^{(2)}(k_0 a_0) J_1(q\theta_0)} + \frac{\hat{H}_n^{(2)'}(k_0 r) J_1(q\theta)}{\hat{H}_n^{(2)'}(k_0 a) J_1'(q\theta_0)} \frac{1}{\sin\theta} \right] e^{j\phi}$$

In Eqs. (3.34) and (3.35), 'n' is the eigen value for HE_{11} mode, ($q = \sqrt{n(n+1)}$ corresponds to HE_{11} mode), and A_1 is the mode coefficient for HE_{11} mode of excitation.

3.5.2 RADIATION FROM CONICAL HORN WITH HELICAL BOUNDARY

The far-field radiation from the horn may be computed by the aperture field method based on the vector diffraction formula for a circular aperture. The transverse electric field over the horn aperture for HE_{11} mode, is obtained as,

$$\bar{E}_t = \bar{i}_{\theta} E_{\theta} + \bar{i}_{\phi} E_{\phi}$$

where, from Eqs. (3.4) and (3.41), under far-field approximation (i.e. $H'/H = -j$)

$$E_{\theta} = D_1 \frac{e^{-jk_0 r}}{r} j^n \left[\frac{J_1(q\theta)}{\sin\theta} - jq \eta_0 \frac{C_1}{D_1} J_1'(q\theta) \right] e^{j\phi} \quad (3.46)$$

and

$$E_{\theta} = D_1 \frac{e^{-jk_0 r}}{r} j^{n+1} \left[qJ_1'(q\theta) - \frac{C_1}{D_1} \eta_0 j \frac{J_1(q\theta)}{\sin\theta} \right] e^{j\theta} \quad (3.47)$$

Inserting the values of E_{θ} and E_{ϕ} from Eqs. (3.46) and (3.47) \bar{E}_t becomes,

$$\bar{E}_t = D_1 \frac{e^{-jk_0 r}}{r} j^n \left\{ \left[\frac{J_1(q\theta)}{\sin\theta} - jq \eta_0 \frac{C_1}{D_1} J_1'(q\theta) \right] \bar{i}_{\theta} + \left[qJ_1'(q\theta) - \frac{C_1}{D_1} \eta_0 j \frac{J_1(q\theta)}{\sin\theta} \right] j \bar{i}_{\phi} \right\} e^{j\theta} \quad (3.48)$$

A much simpler expression for \bar{E}_t can be obtained by assuming balanced condition at the horn aperture. (Under balanced condition E and H are related by the free space characteristic impedance η_0).

Thus $\frac{D_1}{C_1} = -j\eta_0$. Inserting this relation in Eq. (3.48), \bar{E}_t becomes,

$$\bar{E}_t = D_1 \frac{e^{-jk_0 r}}{r} j^n \left[\frac{J_1(q\theta)}{\sin\theta} + q_1 J_1'(q\theta) \right] (i_{\theta} + j i_{\phi}) e^{j\theta} \quad (3.49)$$

Using recurrence formula for Bessel functions, and $\sin\theta \approx \theta$ for small values of θ , \bar{E}_t becomes simpler as,

$$\bar{E}_t = j^n D_1 \frac{e^{-jk_0 r}}{r} q J_0(q\theta) (i_{\theta} + j i_{\phi}) e^{j\theta} \quad (3.50)$$

where D_1 = a constant depending on the excitation for HE_{11} mode.

This simpler expression for E_t enables the evaluation of the radiated far-field by applying the diffraction formula for a circular opening. Here, in the case of conical horn with helical boundary, because of the fields outside the horn even for a very narrow flare angle cone the phase variation of the field over the horn aperture must be taken into consideration. Assuming a quadratic phase variation of the field over the circular horn aperture as [44, p.134]

$$\psi_\rho = e^{-j \frac{\pi}{\lambda_0} \frac{\rho^2}{L}}, \quad \text{the diffracted far-field [44]}$$

for the HE_{11} mode of excitation in the H-plane ($\phi = 0$) (see Appendix C-2) becomes,

$$E_\phi(r, \theta) = \frac{D_1 \lambda_0 q}{2\pi L \sin^2 \theta} S_k J_0(q\theta) \cos^2 \frac{\theta}{2} \left(\frac{e^{-jk_0 r'}}{r} \right) \cdot e^{-j \frac{\pi a_0^2}{\lambda_0 L}} \left(\sum_{n=1}^{\infty} \frac{\pi a_0^2}{\lambda_0 L} \right)^{n-1} \frac{j^{2n}}{n!} \wedge_n(\xi) \quad (3.51)$$

where $S_k = \pi a_0^2$, the area of the horn aperture

$\xi = k_0 a_0 \sin \theta$, a_0 being the aperture radius

$r' = r + r_0$, with r_0 as the horn flare length

L = axial length of the helical horn

and $\wedge_n(x) = \frac{n!}{(x/2)^n} J_n(x)$, is the Lamda function.

The radiation pattern for the HE_{11} mode is evaluated on the basis of Eq. (3.51), and the results are shown in Fig. 3.13.

3.5.3 THE AXIAL GAIN OF THE CONICAL HELIX HORN

The total power P_t crossing the horn aperture can be evaluated by considering the cone region as a spherical cap of radius L .

Thus the total power crossing the spherical cap of radius L in the cone region is given by

$$P_t = \frac{1}{2} \operatorname{Re} \left[\iint_S (\bar{E}_t \times \bar{H}_t^*) ds \right]$$

Inserting \bar{E}_t from Eq. (3.50) and remembering that $\bar{H}_t = \bar{E}_t / \eta_0$, it is seen in Appendix C-3 that P_t , with the assumption of $\sin\theta \approx \theta$ for small angle cone, is obtained as,

$$P_t = D_1^2 q^2 \frac{\pi \theta_0^2}{2 \eta_0} \left[J_0^2(q\theta_0) + J_1^2(q\theta_0) \right] \quad (3.52)$$

The on-axis gain is given by

$$G(0,0) = \frac{\frac{1}{2} \left| \bar{E}_\phi \right|_{\max}^2 4\pi r^2}{\eta_0 P_t} \quad (3.53)$$

It is shown in Appendix C-3, that

$$r^2 \left| E_{\theta} \right|_{\max}^2 = 4L_1^2 q^2 \sin^2 \frac{\pi a_o^2}{2 \lambda_o L}, \text{ and thus the gain becomes,}$$

$$G(0,0) = \frac{16 \sin^2 \frac{\pi a_o^2}{2 \lambda_o L}}{\theta_o^2 [J_o^2(q\theta_o) + J_1^2(q\theta_o)]} \quad (3.54)$$

since $\theta_o \approx \frac{a_o}{L}$

$$G(0,0) = \frac{16 \left(\frac{L}{a_o} \right)^2 \sin^2 \frac{\pi a_o^2}{2 \lambda_o L}}{J_o^2(q\theta_o) + J_1^2(q\theta_o)} \quad (3.55)$$

The axial gain of the conical helix horn based on Eq.(3.55) is obtained for the typical values of θ_o, L, a_o and f_o ; and the result is shown in Fig.3.17 .

3.5.4. CONICAL HELIX HORN WITH DIELECTRIC SPHERE IN FRONT OF ITS APERTURE

The technique of dielectric sphere mounting discussed in Sec.3.4, to improve the radiation patterns with better directivity and low sidelobe levels, is applied to the conical horn with helical boundary also. The test feed system with dielectric sphere placed in front of the horn aperture is shown in Fig.3.11a and its equivalent optical system for theoretical treatment by considering the system

as an aperture source illuminated microwave lens is shown in Fig.3.11 b .

As in Sec. 3.4.1 , following the method due to Bakefi and Farnel [9] , the radiated far field is obtained as

$$U(\theta) = j(k_0 b)^2 \left(e^{-jk_0 r} \right) \int_0^{\sigma_m} u_i(\sigma) J_0(k_0 \sigma \sin\theta) e^{-jk_0 v(\sigma)} \sigma d\sigma \quad (3.56)$$

with $u_i(\sigma) = \alpha \left[P(\psi) TE_1 TE_2 \frac{\sin\psi}{\sigma} \frac{d\psi}{d\sigma} \right]^{\frac{1}{2}}$

where $P(\psi)$ denotes the field pattern (power) at the sphere off-set position. In the case of conical horn with helical boundary, because of the fields outside the horn, the aperture field \bar{E}_t given by Eq. (3.50) can be taken with good accuracy as the field at the sphere placed near the horn aperture. All the other quantities are as specified in Sec. 3.4.1 . The radiation patterns are computed by evaluating the integral in Eq. (3.56) by Simpson's rule inserting the value of $u_i(\sigma)$; and computed results are plotted in Fig. 3.14

3.5.5 EXPERIMENTAL OBSERVATIONS

Experiments were carried out at $f_0 = 8.64$ GHz with a conical horn of radius $a_0 = 3.7$ cm, $L = 10.5$ cm and half flare angle $\theta_0 = 11^\circ$, having a helical boundary formed by winding 14 SWG (2.23 mm dia) copper wire on an expanded

polyethylene conical base. The conical base was only a thin shell of polyethylene supporting the wire, in order to have no effect on the performance of the horn. In Fig. 3.13 the theoretical results based on Eq. (3.51) is plotted together with the experimental results of E- and H -plane pattern measurements. The reasonably good agreement noticed between the theoretical and experimental results of the H -plane pattern shows the validity of the assumptions made in the derivation of Eq. (3.51).

The E -plane pattern of the horn with helical boundary is seen broader than the H-plane pattern due to the fields outside the horn. A 'flat topped' effect to the pattern is also noticed which, even though not desirable for maximising the gain, is useful for giving constant illumination over a specified area. The sidelobe level remains similar to that of a plain horn.

As the conical horn with helical boundary has a broader E -plane pattern than H -plane, which is opposite to that of a conventional conical horn, it was considered that a combination of these horns may have equal E- and H -plane patterns. Accordingly the helical horn of the above specifications has been excited by starting the helical horn from the inside of a conventional conical horn supporting TE_{11} mode at 8.64 GHz. The radiation patterns of

such a horn are shown in Fig. 3.14.

Experiments were repeated with paraffin was ($\epsilon_r = 2.25$) spheres of diameter 9 cm, 6 cm and 4 cm placed off-set at the minimum input VSWR position [74] in front of this horn (with equal E-and H -plane beam widths) aperture. The radiation patterns are shown in Fig. 3.15. In Fig. 3.16 the theoretical pattern based on Eq. (3.56) is compared with experimental pattern for 6 cm diameter sphere with reasonable agreement. The gain variation of the system as a function of the dielectric sphere diameter in wavelengths is depicted in Fig. 3.17 .

From the results, it is seen that the conical horn with helical boundary excited by a flared out plane horn has desirable radiation characteristics, with flat tops, to be used either as a satellite antenna for giving constant illumination to a section of the earth or as a feed for a reflector antenna. (The phase center of the helical horn differed in the E-and H -planes. This was because the E -plane had an effectively larger aperture than H -Plane. However, the difference between the two centers was generally small. The VSWR of the conical helix horn was small being 1.10. The conical helix horn that can be used for circular polarisation is relatively wideband and light weight. The radiation characteristics of this horn may be improved considerably with reduced -3 dB beamwidth, higher

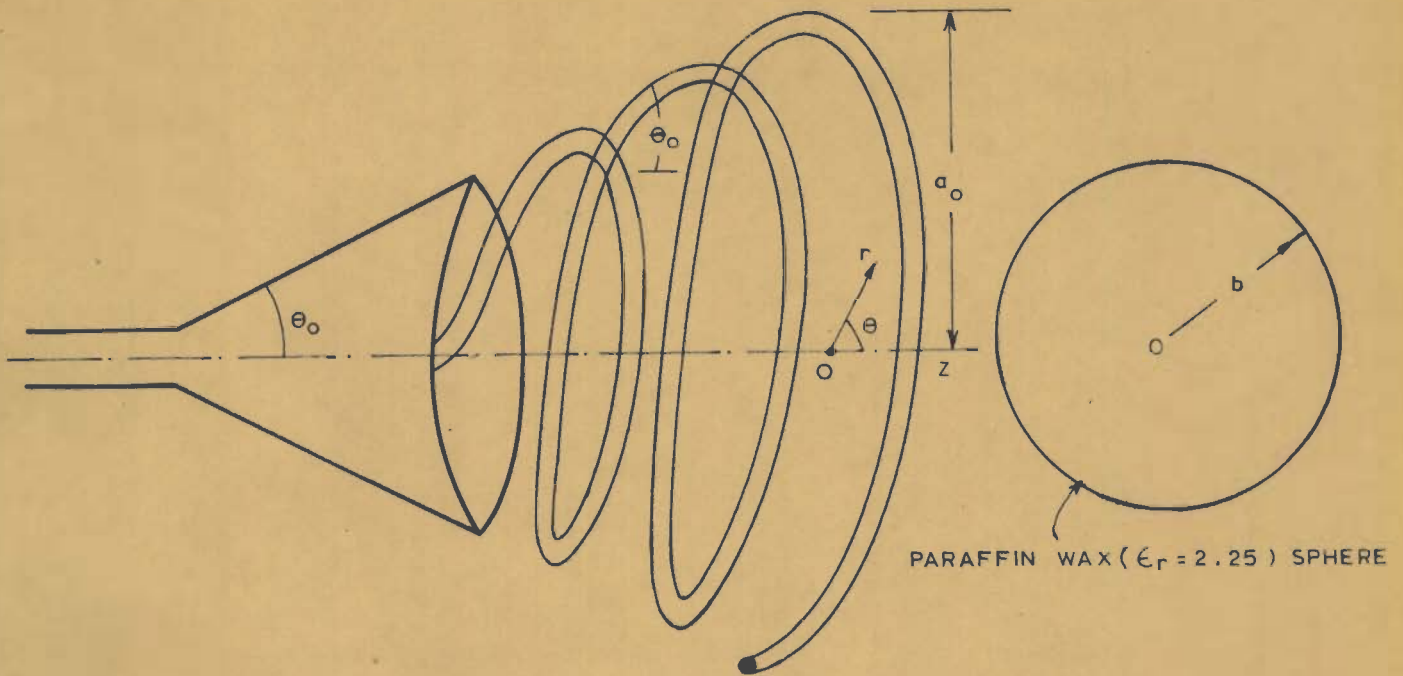
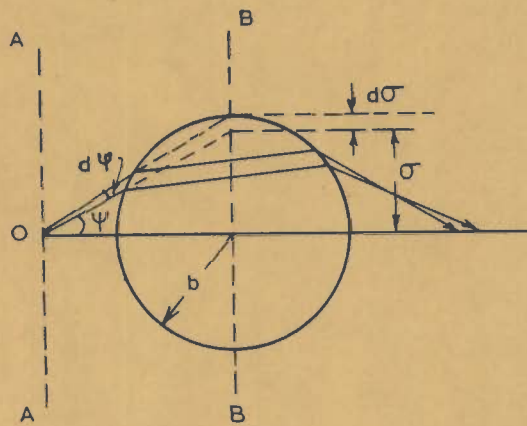


FIG.3.11a - DIELECTRIC SPHERE LOADED HELIX-
CONICAL HORN



AA - APERTURE PLANE

BB - THE EQUIVALENT CIRCULAR
APERTURE THROUGH THE CENTRE
OF THE SPHERE

FIG. 3.11b - OPTICAL SYSTEM FOR THE GEOMETRY
OF FIG. 3.11a

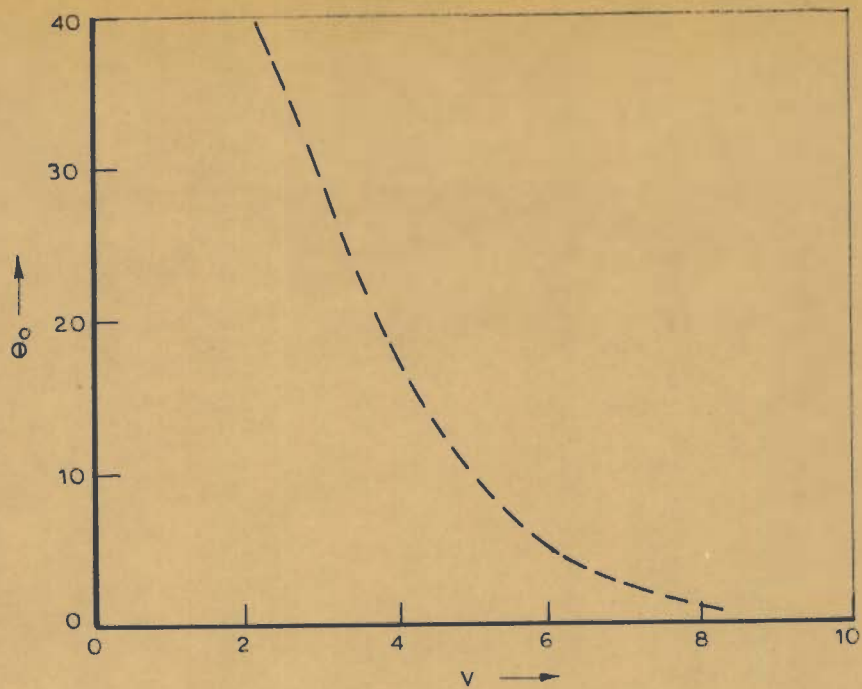


FIG.3.12 _SEPARATION CONSTANT VS θ_0

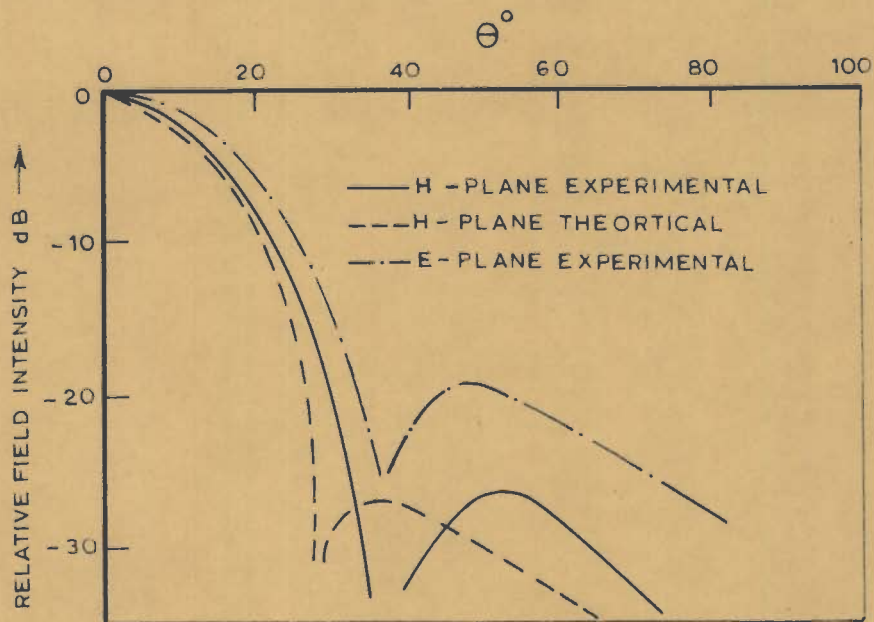


FIG.3.13 _RADIATION PATTERNS OF THE HELICAL HORN ALONE

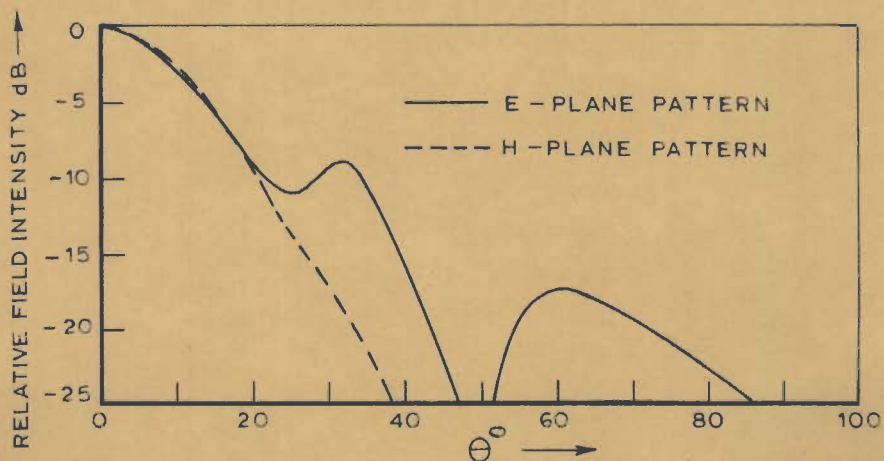


FIG.3.14 _E - PLANE AND H - PLANE PATTERN OF HELIX - CONICAL HORH

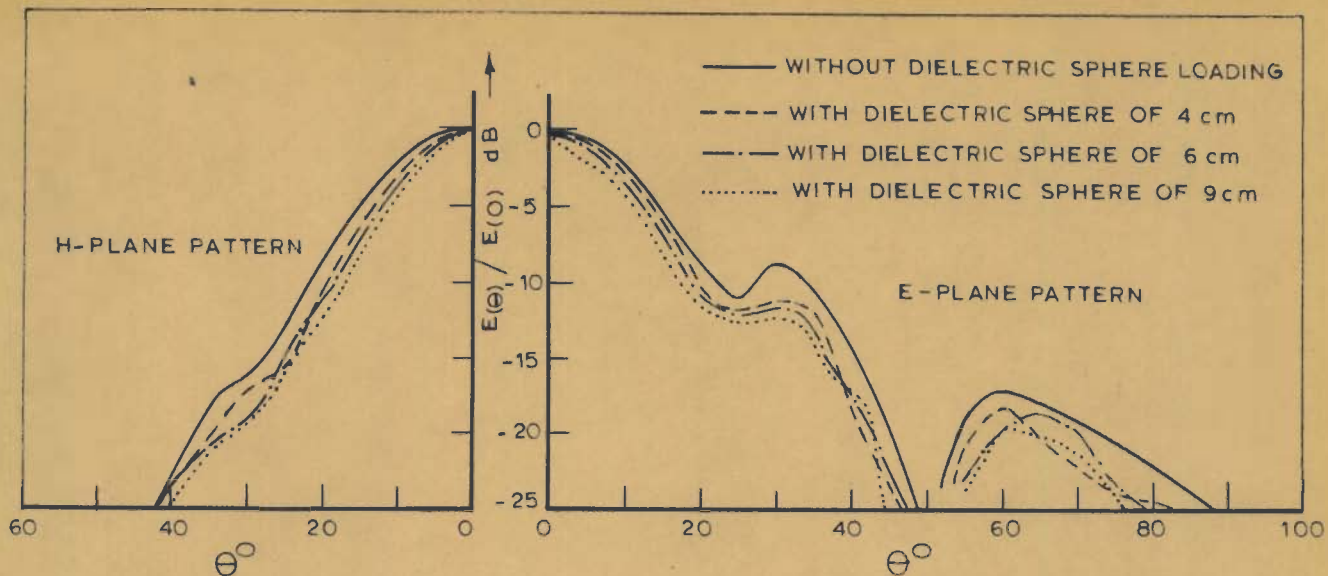


FIG.3.15 _ RADIATION PATTERNS OF DIELECTRIC SPHERE LOADED HELIX CONICAL HORN

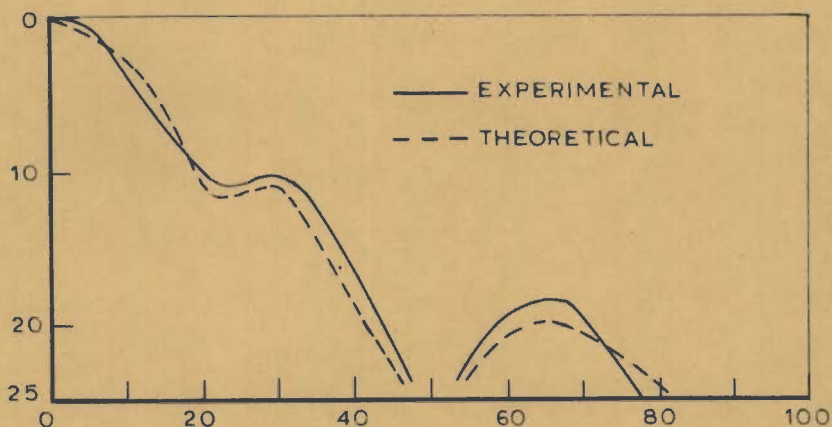


FIG.3.16 _ E-PLANE PATTERNS FOR 6 cm SPHERE LOADED HORN

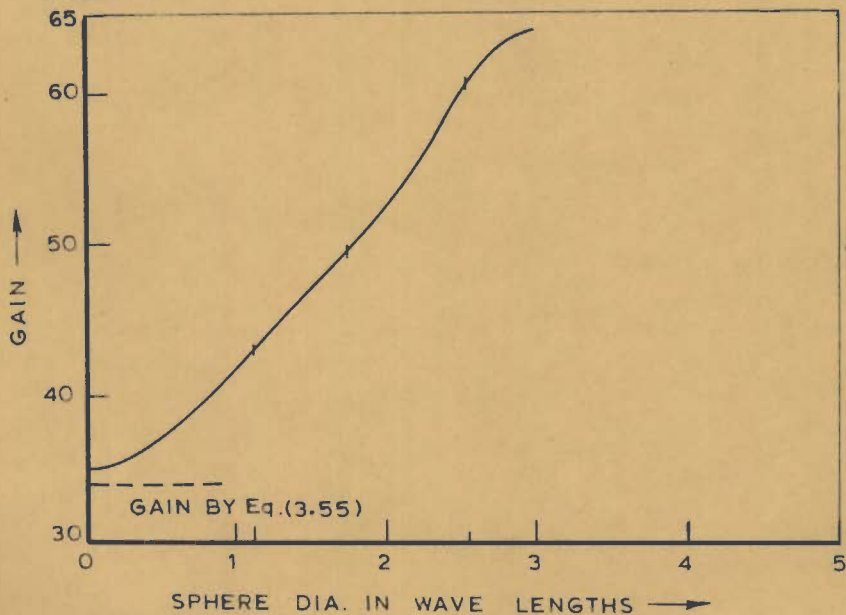


FIG.3.17 _ GAIN OF DIELECTRIC SPHERE LOADED HELIX - HORN

gain and low sidelobes by dielectric spheres mounted at the horn aperture.

3.6. CONCLUSION

The radiation properties of dielectric loaded conical horns have been investigated. A plane conical horn with dielectric sphere mounted at its aperture is found to possess greater forward directivity. The effect of dielectric coating on the horn wall has been investigated to establish that dielectric coating helps in narrowing the radiation pattern and increasing the gain at the cost of slight deterioration in the sidelobe levels. The technique of dielectric sphere loading in front of the radiating horn aperture is effectively utilized to improve the radiation patterns of the dielectric coated conical horn with reduced sidelobe levels and further increase in directivity and gain. The radiation characteristics of a conical helix horn have been analysed using spherical hybrid modes. A 'flat topped effect' to its pattern which is useful for giving a constant illumination over a specified area has been noticed. The conical helix horn excited by a flared out plane horn is seen to have desirable radiation characteristics with approximately equal E-and H -plane beamwidths to be used either as a satellite antenna or as feed for reflector antenna. The horn is seen to possess

increased directivity and axial gain with reduced sidelobes in the presence of dielectric spheres in front of its aperture. The dielectric sphere mounting at the conical horn aperture contributes a variable beamwidth facility to the system.

CHAPTER IV

DIELECTRIC LOADED BICONICAL HORN

4.1 INTRODUCTION

Barrow et al.[12] have done some significant work on biconical horns which have omnidirectional horizontal radiation patterns and controllable vertical radiation patterns. These biconical horns find frequent use in the VHF - UHF band for broadcast purposes. Recently the importance of biconical horns which radiate circular polarization has been discussed [87] for use with radar transponder beacons. Eventhough the use of dielectric materials for improving the directivity of some aperture antennas has been well established [48],[50],[134], no substantial work has been done on dielectric loaded biconical horns for improved radiation characteristics.

In this section the analytical and experimental results of the radiation behaviour of a dielectric loaded biconical horn which radiates circular polarization are presented. Theoretical results of radiation pattern and power gain are derived from an electric vector potential by the aperture field method. The characteristic equation

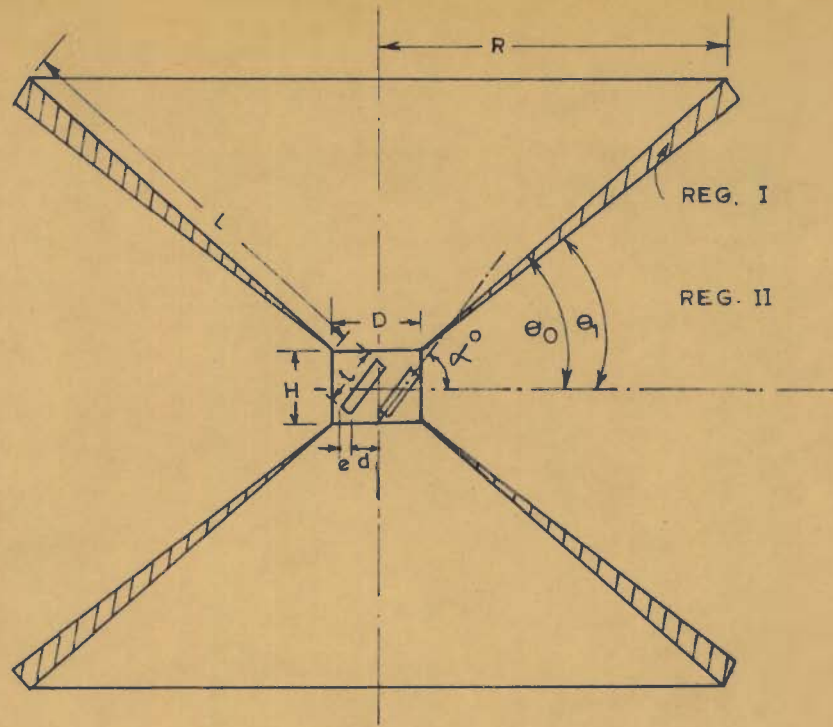
for the separation constant has also been derived. The calculated results of radiation pattern and gain of the dielectric coated biconical horn have been experimentally established using a test horn designed to radiate circular polarization [37] in the X-band. It is concluded that the pattern directivity of the biconical horn in the vertical plane is significantly increased due to the dielectric coating, and a desired beamwidth in the vertical plane may be obtained by a suitable dielectric coating.

4.2 GEOMETRY OF THE HORN

The geometry of the dielectric coated biconical horn is shown in Fig.4.1. The principal axis of the horn coincides with the y -axis, and the sides of the cones if extended to their apexes would meet at the origin of the spherical co-ordinate system (r, θ, ϕ) . The exciting means may be situated at or near the origin which is a singular point in the analysis. The conducting symmetrical biconical horn of apex angle $2\theta_0$ is coated with a dielectric material of permittivity ϵ_1 so that the apex angle of the coated horn is $2\theta_1$.

4.3 ANALYSIS OF THE FIELDS

Waves are excited near the origin of the system



- | | |
|-------------------------|---------------------------|
| $R = 17.5 \text{ cm}$ | $H = 2.5 \text{ cm}$ |
| $L = 17 \text{ cm}$ | $D = 3.2 \text{ cm}$ |
| $\theta_0 = 17.5^\circ$ | $e = 3 \text{ mm}$ |
| $\theta_1 = 15^\circ$ | $L = 1.9 \text{ cm}$ |
| | $d = 2.14 \text{ cm}$ |
| | $\alpha^\circ = 45^\circ$ |

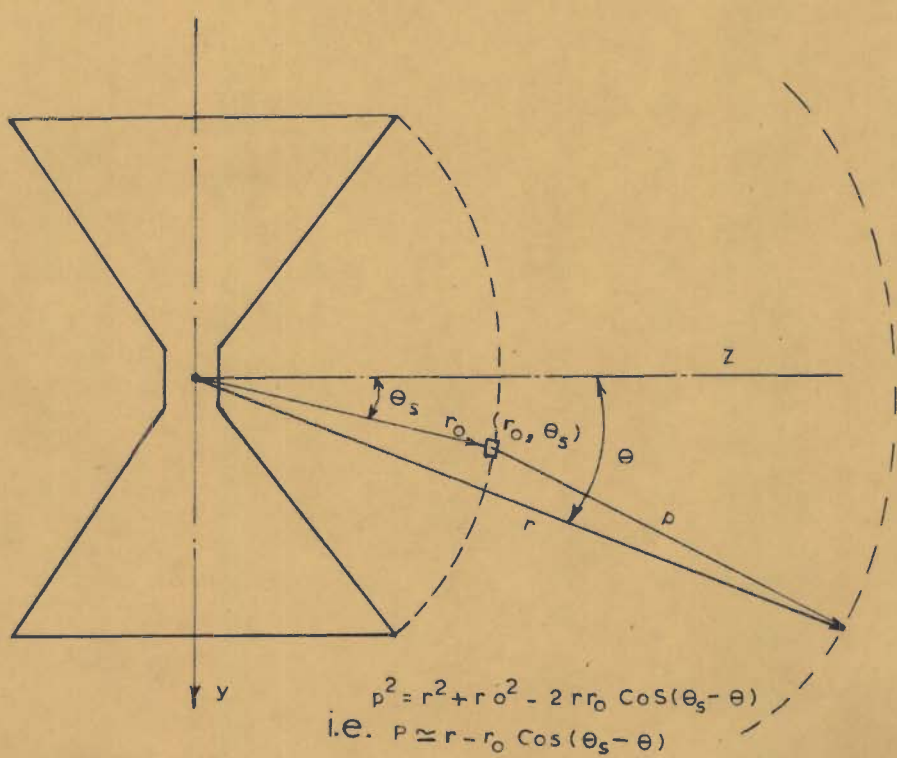


FIG. 4.1 _ GEOMETRY OF DIELECTRIC LOADED BICONICAL HORN FOR CIRCULAR POLARISATION

and propagate outward in the space between the cones. The transmission properties of these waves within the horn region (between cones) may be obtained by making approximate solution of the Helmholtz's wave equation in spherical co-ordinates satisfying the boundary conditions. In order to satisfy the boundary conditions hybrid modes (HE_{mn} modes) having both E_r and H_r components (r is the direction of propagation) are to exist. Horn waves of the transverse electric type (TE modes) having both E_r and H_r components may be obtained from an electric vector potential \bar{F} that has a single component in the θ direction only such that $\bar{F} = \bar{i}_\theta \psi$ and satisfying the wave equation [52],[129]

$$\frac{1}{r^2} \frac{\partial}{\partial r} \left(r^2 \frac{\partial \psi}{\partial r} \right) + \frac{1}{r^2 \sin \theta} \frac{\partial}{\partial \theta} \left(\sin \theta \frac{\partial \psi}{\partial \theta} \right) + \frac{1}{r^2 \sin^2 \theta} \frac{\partial^2 \psi}{\partial \phi^2} + k^2 \psi = 0 \quad (4.1)$$

Applying the method of separation of variables to Eq. (4.1) the potential function ψ can be obtained as

$$\psi = \hat{B}_n(kr) L_n^m(\cos \theta) e^{jm\phi} \quad (4.2)$$

where $\hat{B}_n(kr)$ = modified spherical Bessel function

$L_n^m(\cos \theta)$ = Associated Legendre functions

m = an integer, and n is positive and real corresponding to the order of the wave in the horn designated by the ordinal number of the root of the characteristic equation.

But it is to be noted that Ψ will be different for the two regions, viz. the dielectric coated region (Reg.I) and the horn apex angle region (Reg.II). The proper forms of Ψ for these two regions can be taken from the following reasoning.

In the dielectric loaded region there will be standing waves due to reflections from the air-dielectric and metal - dielectric interfaces. Since $\hat{J}_n(kr)$ and $\hat{Y}_n(kr)$ (i.e. modified spherical Bessel functions of the first kind and second kind respectively) exhibit oscillatory behaviour for k real, these functions represent standing waves; but only $\hat{J}_n(kr)$ is finite at $r = 0$. Hence for the dielectric coated region (Reg.I) the proper form of $\hat{B}_n(kr) = \hat{J}_n(k_1 r)$.

$$\text{where } k_1 = \omega \sqrt{\mu_0 \epsilon_1}$$

$$\text{In general } L_n^m(\cos\theta) = C_n P_n^m(\cos\theta) + D_n Q_n^m(\cos\theta)$$

where, $P_n^m(\cos\theta)$ = Associated Legendre function of the first kind.

$Q_n^m(\cos\theta)$ = Associated Legendre function of the second kind.

and C_n and D_n are constants.

For the dielectric coated region, since $\theta = 0$ and $\theta = \pi$ are excluded, the general form of

$$L_n^m(\cos\theta) = C_n P_n^m(\cos\theta) + D_n Q_n^m(\cos\theta)$$

is to be taken.

For the horn apex angle region (Reg.II) , i.e. the region of horn apex angle $2\theta_1$ $\hat{B}_n(kr)$ should be replaced by $\hat{H}_n^{(2)}(k_0 r)$ to represent outward travelling waves. (Here $k_0 = \omega \sqrt{\mu_0 \epsilon_0}$). Similarly for this region since $\theta = 0$ and $\theta = \pi$ are included, and $Q_n^m(\cos\theta) = 0$ for $\theta = 0$ and $\theta = \pi$, $L_n^m(\cos\theta)$ becomes only $P_n^m(\cos\theta)$. Thus the proper forms of the potential function Ψ for the dielectric loaded and the horn apex angle regions respectively become

$$\Psi_d = \hat{J}_n(k_1 r) \left[C_n P_n^m(\cos\theta) + D_n Q_n^m(\cos\theta) \right] e^{jm\phi} \quad (4.3)$$

$$\Psi_o = F_n \hat{H}_v^{(2)}(k_0 r) P_n^m(\cos\theta) e^{jm\phi}$$

where $k_0 = \omega \sqrt{\mu_0 \epsilon_0}$ and $k_1 = \omega \sqrt{\mu_0 \epsilon_1}$. The subscripts

'd' and 'o' denote the dielectric coated and the horn apex angle regions respectively.

Using Eqs.(4.3) in the appropriate field relations [5.2] it is seen in Appendix D-1 that the different field components in the two regions are obtained as,

In the dielectric coated region

$$E_{rd} = \frac{j m}{r \sin \theta} \hat{J}_n(k_1 r) L_n^m(\cos \theta) e^{j m \phi}$$

$$E_{\phi d} = - \left[\frac{\hat{J}_n(k_1 r)}{r} + k_1 \hat{J}'_n(k_1 r) \right] L_n^m(\cos \theta) e^{j m \phi}$$

$$E_{\theta d} = 0$$

$$H_{rd} = \frac{1}{j \omega \mu_0} \left[k_1 \hat{J}'_n(k_1 r) \frac{\partial}{\partial \theta} L_n^m(\cos \theta) + \frac{1}{r} \hat{J}_n(k_1 r) \frac{\partial}{\partial \theta} L_n^m(\cos \theta) \right] e^{j m \phi} \quad (4.4)$$

$$H_{\phi d} = \frac{m}{\omega \mu_0 r \sin \theta} \hat{J}_n(k_1 r) \frac{\partial}{\partial \theta} L_n^m(\cos \theta) e^{j m \phi}$$

$$H_{\theta d} = \frac{1}{j \omega \mu_0} k_1^2 \hat{J}_n(k_1 r) L_n^m(\cos \theta) e^{j m \phi}$$

where $L_n^m(\cos \theta) = C_n P_n^m(\cos \theta) + D_n Q_n^m(\cos \theta)$

and the prime indicates differentiation with respect to r .

In the horn apex angle region

$$E_{r_0} = \frac{j^m F_n}{r \sin \theta} \hat{H}_n^{(2)}(k_0 r) P_n^m(\cos \theta) e^{jm\phi}$$

$$E_{\phi_0} = - \left[\frac{\hat{H}_n^{(2)}(k_0 r)}{r} + k_0 \hat{H}_n^{(2)'}(k_0 r) \right] F_n P_n^m(\cos \theta) e^{jm\phi}$$

$$E_{\theta_0} = 0 \quad (4.5)$$

$$H_{r_0} = \frac{F_n}{j \omega \mu_0} \left[k_0 \hat{H}_n^{(2)}(k_0 r) \frac{\partial}{\partial \theta} P_n^m(\cos \theta) + \right.$$

$$\left. \frac{1}{r} \hat{H}_n^{(2)}(k_0 r) \frac{\partial}{\partial \theta} P_n^m(\cos \theta) \right] e^{jm\phi}$$

$$H_{\phi_0} = \frac{m F_n}{\omega \mu_0 r \sin \theta} \hat{H}_n^{(2)}(k_0 r) \frac{\partial}{\partial \theta} P_n^m(\cos \theta) e^{jm\phi}$$

$$H_{\theta_0} = \frac{F_n k_0^2}{j \omega \mu_0} \hat{H}_n^{(2)}(k_0 r) P_n^m(\cos \theta) e^{jm\phi}$$

The value of the separation constant n can be obtained from the characteristic equation that can be derived by applying the appropriate boundary condition and by matching the fields at the air-dielectric interface i.e. at $\theta = \theta_1$.

It is shown in Appendix D-2 that the characteristic

equation for the HE_{1n} mode ($m=1$) is obtained as,

$$\frac{[P_n^1(\cos\theta_0) Q_n^1(\cos\theta_1) - P_n^1(\cos\theta_1) Q_n^1(\cos\theta_0)] \frac{\partial}{\partial \theta} P_n^1(\cos\theta_1)}{[P_n^1(\cos\theta_0) \frac{\partial}{\partial \theta} Q_n^1(\cos\theta_1) - Q_n^1(\cos\theta_0) \frac{\partial}{\partial \theta} P_n^1(\cos\theta_1)] P_n^1(\cos\theta_1)} = \frac{1 + (k_1 r) \frac{\hat{J}_n'(k_1 r)}{\hat{J}_n(k_1 r)}}{1 + (k_0 r) \frac{\hat{H}_n^{(2)'}(k_0 r)}{\hat{J}_n^{(2)}(k_0 r)}} \quad (4.6)$$

The above characteristic equation is valid for any value of $r \leq L$ where L is the flare length of the horn. This equation can be solved graphically for typical values of θ_0 , θ_1 , ϵ_1 and f_0 ; and the value of n for HE_{11} mode can be determined by taking the first root of the above characteristic equation and was found $n = 0.5$ for the typical values used.

4.4 RADIATION FROM DIELECTRIC COATED BICONICAL HORN

The radiation properties of the dielectric loaded

biconical horn may be calculated by the vector diffraction formula using the general procedures [12],[13]. The assumption is made that the field distribution between the edges of cones is that which would exist were the horn not finite in length. (The magnitude of the electric intensity in space over a sphere of radius great compared to both λ_0 and the dimensions of the horn comprises the radiation pattern). Thus using the vector diffraction formula[12] the radiation pattern in the vertical plane (E -plane with $\phi = \pi/2$) for HE_{11} mode is given by

$$E_{\theta}(\theta) = jk_0 \frac{e^{-jk_0 r}}{4\pi r} (1+\cos\theta) \iint_S \bar{E}_t e^{jk_0 r_0 \cos(\theta_s - \theta)} ds \quad (4.7)$$

where \bar{E}_t = the transverse E -field in the horn apex angle region and is given by

$$\bar{E}_t = \bar{i}_{\theta} E_{\theta_0} + \bar{i}_{\phi} E_{\phi_0} \Big|_{r=r_0} = \bar{i}_{\phi} E_{\phi_0} \Big|_{r=r_0} \quad (\text{since } E_{\theta_0} = 0)$$

and $r_0 \approx$ the horn axial length.

It is seen in Appendix D-3 that an approximate expression for the vertical pattern may be obtained as,

$$E_{\theta}(\theta) = -jE_1 \pi \frac{e^{-jk_0 r}}{2\lambda_0 r} (1 + \cos\theta) r_0^2 \sqrt{\frac{v}{\pi} \frac{\lambda_0}{2r_0}} \cdot$$

$$\left[M \left\{ C(u_1) - C(u_2) - j [S(u_1) - S(u_2)] \right\} + \right. \\ \left. N \left\{ C(v_1) - C(v_2) - j [S(v_1) - S(v_2)] \right\} \right] \quad (4.8)$$

where $E_1 = E_0 \left(k_0 \hat{H}_v^{(2)'}(k_0 r_0) + \frac{\hat{H}_v^{(2)}(k_0 r_0)}{r_0} \right) e^{jk_0 r_0}$

with E_0 as a constant depending on the horn excitation

$$M = e^{j \frac{\lambda_0}{4r_0} \frac{(v+1)^2}{\pi}} e^{j(v+1)\theta}$$

$$N = e^{j \frac{\lambda_0}{4r_0} \frac{v^2}{\pi}} e^{-j(v\theta + \frac{\pi}{2})}$$

$$u_1 = \left[\theta_1 - \theta - \frac{\lambda_0}{2r_0} \frac{(v+1)}{\pi} \right] \sqrt{\frac{2r_0}{\lambda_0}}$$

$$u_2 = \left[-\theta_1 - \theta - \frac{\lambda_0}{2r_0} \frac{(v+1)}{\pi} \right] \sqrt{\frac{2r_0}{\lambda_0}}$$

$$v_1 = \left[\theta_1 - \theta + \frac{\lambda_0}{2r_0} \frac{v}{\pi} \right] \sqrt{\frac{2r_0}{\lambda_0}}$$

$$v_2 = \left[-\theta_1 - \theta + \frac{\lambda_0}{2r_0} \frac{v}{\pi} \right] \sqrt{\frac{2r_0}{\lambda_0}}$$

(In the above expressions v denotes the value of the separation constant for the HE_{11} mode)

The radiation pattern based on Eqs. (4.8) has been computed for typical test values and the pattern thus obtained is compared with the experimental pattern in Fig. 4.4

4.5 POWER GAIN OF DIELECTRIC COATED BICONICAL HORN

The total power P_t transmitted through the horn may be calculated by integrating the power density flowing in the radial direction over a closed surface of $r = r_o$, a constant, between the two cones. Accordingly it is shown in Appendix D-4 that P_t for the HE_{11} mode can be derived as,

$$P_t = \frac{4|E_1|^2 \nu r_o^2 \theta_1}{\eta_o} \quad (4.9)$$

$$\text{where } |E_1| = E_o \left(k_o \hat{H}_v^{(2)}(k_o r_o) + \frac{\hat{H}_v^{(2)}(k_o r_o)}{r_o} \right)$$

The gain of the dielectric coated biconical horn is given by

$$G = \frac{4\pi r^2 |E_\theta|_{\max}^2}{\eta_o P_t} \quad (4.10)$$

By using Eqs. (4.8) and (4.9) in Eqs. (4.10), the gain is obtained as,

$$G = \frac{\pi^2 r_o}{2 \lambda_o \theta_1} \left[\sqrt{[C(u_{o1}) - C(u_{o2})]^2 + [S(u_{o1}) - S(u_{o2})]^2} + \sqrt{[C(v_{o1}) - C(v_{o2})]^2 + [S(v_{o1}) - S(v_{o2})]^2} \right]^2 \quad (4.11)$$

where

$$\begin{pmatrix} u_{o1} \\ u_{o2} \end{pmatrix} = \left[-\frac{\lambda_o}{2r_o} \frac{(v+1)}{\pi} \pm \theta_1 \right] \sqrt{\frac{2r_o}{\lambda_o}}$$

$$\begin{pmatrix} v_{o1} \\ v_{o2} \end{pmatrix} = \left[\frac{\lambda_o}{2r_o} \frac{v}{\pi} \pm \theta_1 \right] \sqrt{\frac{2r_o}{\lambda_o}}$$

The gain based on Eq.(4.11) has been computed for typical values and is found in agreement with experimental results.

4.6 EXPERIMENTAL RESULTS AND COMPARISON WITH THEORY

In order to investigate the radiation properties of the dielectric coated biconical horn, and to examine the validity of the expressions derived, a biconical horn for circular polarization [87] was designed for the specifications detailed in Fig. 4.1. The biconical horn was coated with paraffin wax ($\epsilon_r = 2.25$) for an angular thickness of 2.5° , and measurements were made for HE_{11}

mode excitation of the horn at a frequency of 8.86 GHz. In Fig.4.2 the H -plane pattern of the dielectric coated biconical horn together with that for the empty horn is depicted. In both cases, the H -plane pattern is fairly circular, the maximum variation from uniformity is ± 2.3 dB which is of no practical consequence, as far greater variations are introduced by terrain, buildings etc. It is to be noted that the variations from uniformity is less for the dielectric coated case. The E -plane patterns of the biconical horn with and without dielectric coating are shown in Fig. 4.3 . The increase in the vertical pattern directivity, at the cost of slightly raised secondary lobes, due to dielectric coating is evident. The E -plane beamwidth of the biconical horn is considerably reduced as compared to that of the empty biconical horn. The reduced beamwidth that indicates a stronger concentration of energy in the equatorial plane will result in an increased power gain. In Fig.4.4 the E -plane pattern of the dielectric coated biconical horn based on Eq.(4.8) is compared with the experimental results. The fairly good agreement between these two patterns upholds the validity of the assumptions and approximation made in the derivation of the E -plane pattern. Theoretical value based on Eq.(4.11) and the experimental value of the power gain are found almost

the same, being 21.5 and 22.7 respectively, thereby establishing the validity of Eq.(4.11). The power gain (experimental) of the empty biconical horn was found to be 12. Thus, the power gain increases approximately by 2.7 dB due to dielectric loading.

From the results presented, it may be concluded that

- i) the vertical pattern directivity of the biconical horn can be increased significantly, at the cost of slightly raised secondary lobes, due to appropriate dielectric coating.
- ii) the E -plane pattern beamwidth of the dielectric coated biconical horn is considerably reduced and the power gain is increased as compared to the respective quantities of empty horn.
- iii) the horizontal pattern of the dielectric coated biconical horn is fairly circular with less variation from uniformity as compared with that for empty horn; and
- iv) the circularly polarised dielectric coated biconical horn can be used to give an omnidirectional pattern in its H -plane orientation to serve the useful purpose of telemetry and command during the launch and orbital phases of a spacecraft's (or satellites)

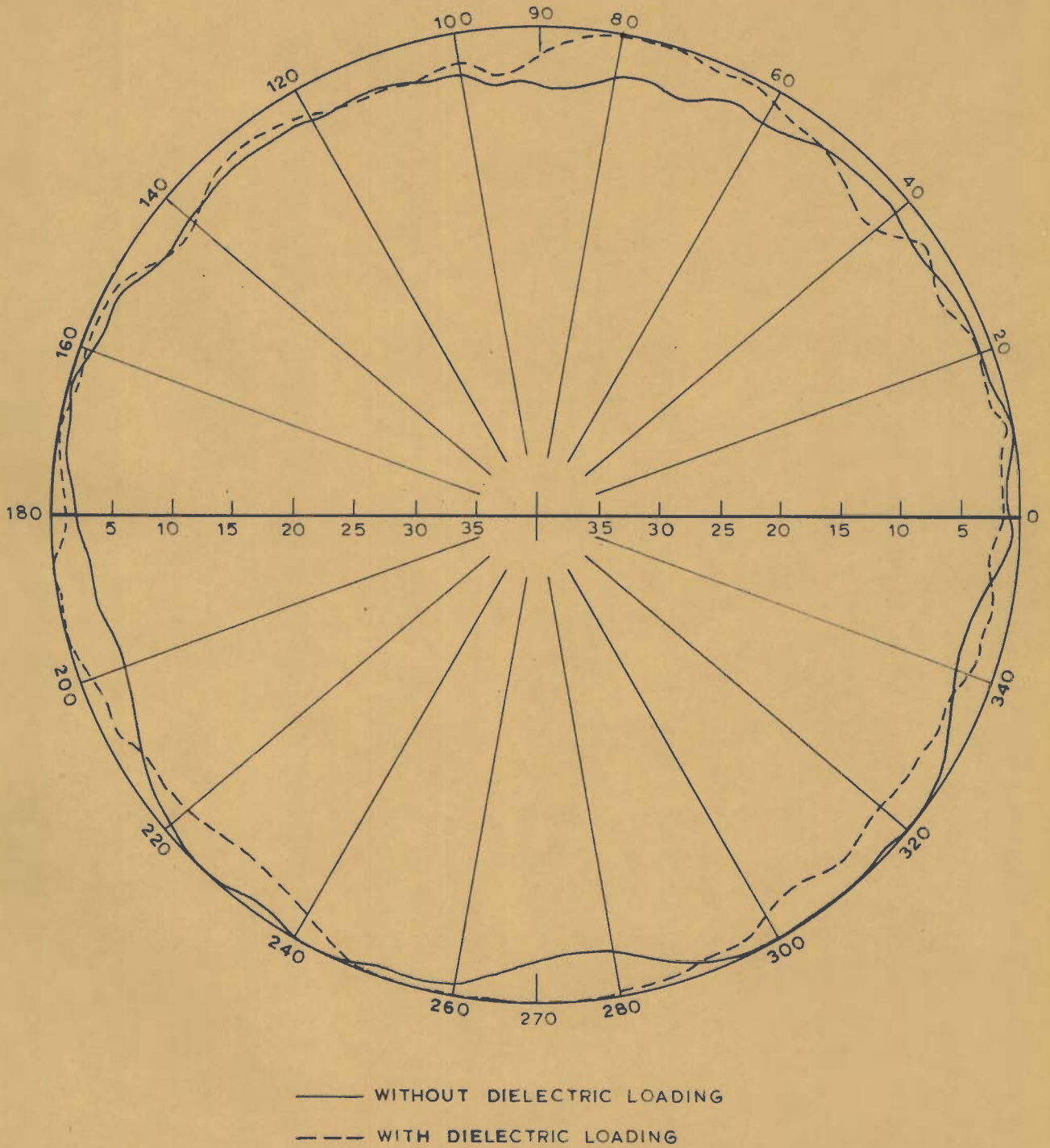


FIG. 4.2_H - PLANE PATTERNS OF BICONICAL HORN

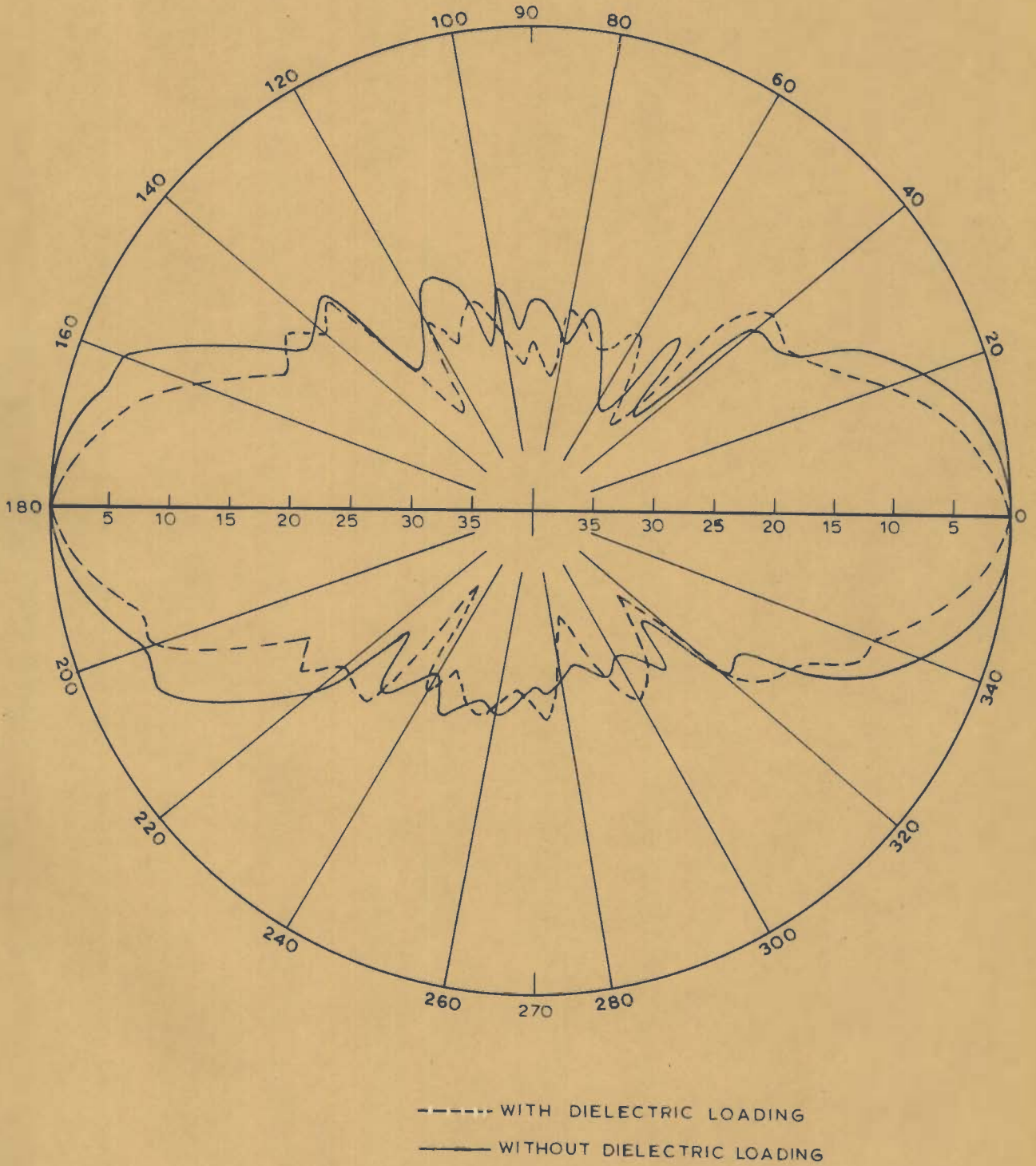


FIG.4.3 _E-PLANE PATTERNS OF BICONICAL HORN

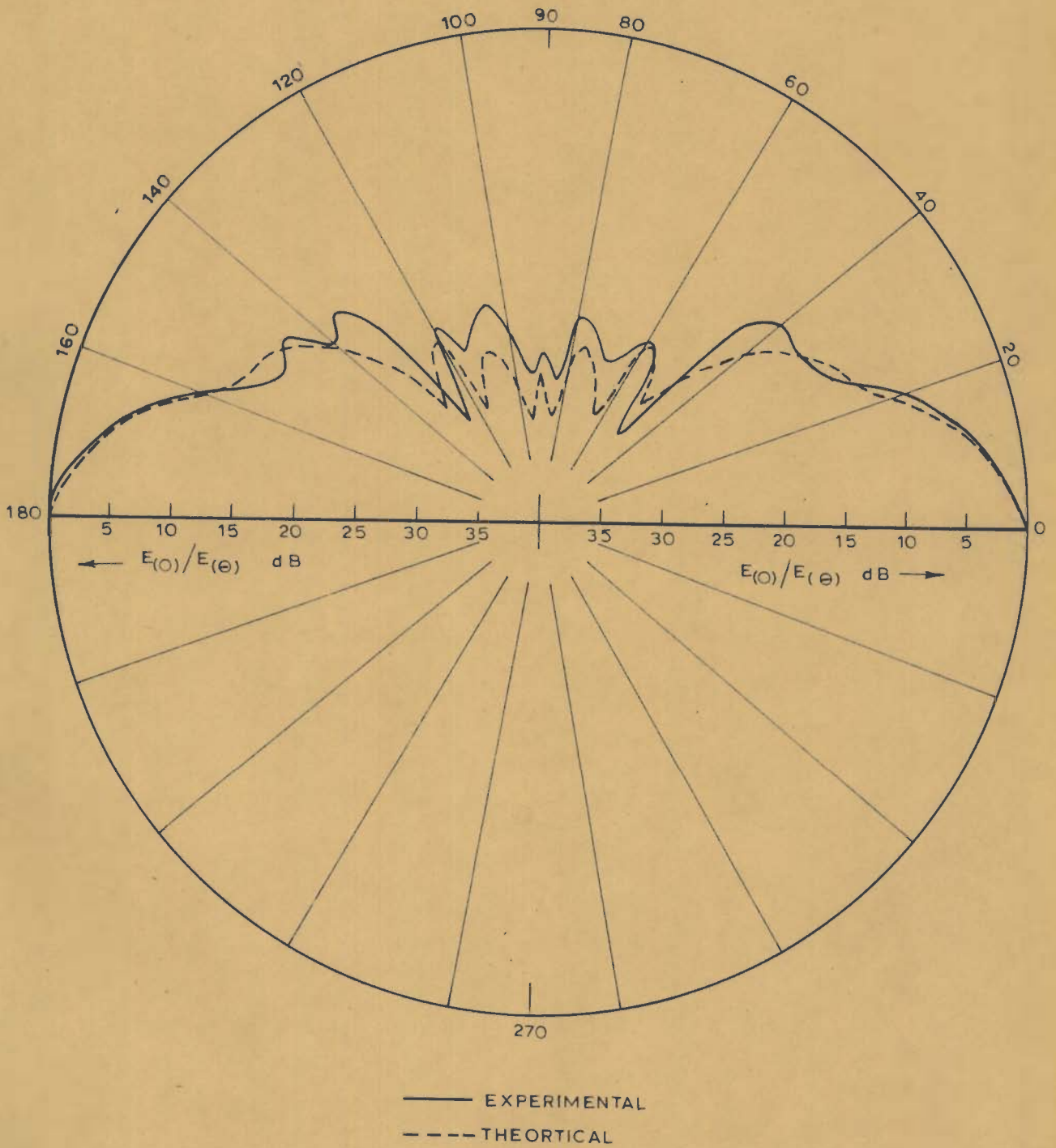


FIG. 4.4 _RADIATION PATTERNS OF DIELECTRIC LOADED BICONICAL HORN

life, and once the spacecraft (or satellite) becomes stabilised correctly, the same horn with its E -plane orientation can be used for concentration of energy toward the surface of the earth . This antenna which radiates circular polarization can also be used conveniently with a radar transponder beacon responding to a ship's navigational radar.

4.7 CONCLUSION

The technique of dielectric loading in improving directivity of aperture antennas has been applied to biconical horns. Theoretical results of radiation pattern and gain are derived from an electric vector potential by the aperture field method, and are established in excellent agreement with their experimental values. Dielectric loading is found to modify the E -plane pattern of biconical horn with reduced -3 dB beamwidth at the cost of slightly raised secondary lobes. Thus desired beamwidth in the vertical plane may be obtained by a suitable dielectric loading. The H -plane pattern which is fairly circular is improved in the sense that the variation from uniformity is less with dielectric loaded biconical horns.

CHAPTER V

DIELECTRIC SPHERE-LOADED CORRUGATED HORN

5.1 INTRODUCTION

The corrugated horns are very useful as primary radiators for reflector antennas for satellite communication earth stations and radio telescopes because they have patterns with rotationally symmetrical main beam and low sidelobes. The importance of corrugated conical horns as low noise feeds for reflector antennas has been stressed by several authors [25], [95], [98]. Analytical and experimental studies made on the radiation properties of corrugated E-plane sectoral horn [99], [101] have established its desirable features to be used as an improved feed system for paraboloidal reflectors in satellite communication and radio astronomy. In this section, results of the investigations carried out into the radiation properties of corrugated horns for producing multiple beam or variable beamwidth feeds for paraboloidal reflectors are accounted. Two of the most commonly used hybrid mode reflector antenna feeds are considered with dielectric spheres mounted in front of their apertures. First the analytical and experimental studies of the radiation behaviour of dielectric sphere mounted corrugated E-plane sectoral horn

are made; and the results established that dielectric sphere loading has increased the axial gain of the horn with the radiation patterns having reduced -3 dB beamwidths and sidelobes. A variable beamwidth facility was available at low input VSWR performance with spheres of different dimensions placed at the optimal position in front of the radiating horn aperture. Then the same technique of dielectric sphere loading is applied to corrugated conical horn also for improving its performance. In both the cases the theoretical formulation is made on the basis of the scattering theory approach. Experimental data show reasonable agreement with theoretical results.

5.2. A CORRUGATED E -PLANE SECTORAL HORN WITH A DIELECTRIC SPHERE IN FRONT OF ITS APERTURE [68]

The results of radiation characteristics of a dielectric sphere in front of an excited corrugated E-plane sectoral horn together with the design aspects of the horn are described. Theoretical formulation of the radiation behaviour is based on the scattering theory approach. Experiments were carried out with the test antenna system consisting of paraffin wax spheres kept off-set at the minimum input VSWR position in front of the aperture of the horn excited in the balanced HE_{11} mode. The test results have shown that such a feed system

has promising radiation pattern with low sidelobes and greater directivity together with a variable beamwidth facility to be used as a feed for paraboloidal reflector antennas for possible applications in satellite communication and radio astronomy.

5.2.1 ANALYTICAL TREATMENT

Geometry of the test feed system is shown in Fig.5.1. Dielectric sphere of radius 'b' is placed in front of the radiating corrugated E -plane sectoral horn aperture. As the effect of placing a dielectric sphere in the vicinity of the radiating horn is expected to modify its radiation pattern, the system can be treated as a scattering problem and can be analysed on the basis of scattering theory approach.

In the case of a dielectric scatterer , the total electric field vector E at any point can be related to the incident field E^i by the expression

$$E(r, \theta, \phi) = E^i + \frac{j\omega}{4\pi} \nabla_x \nabla_x \int_{S'} [\epsilon_r(r-r') - 1] \cdot \frac{E^i \cdot e^{-jk(r-r')}}{|r-r'|} ds' \quad (5.1)$$

where r = position vector at the point of observation

r' = position vector of a typical point on the scatterer

ϵ_r = relative permittivity of the scatterer

s' = the surface area of the scatterer.

Since we are interested only in the far-field pattern, Eq. (5.1) can be written for a homogeneous spherical scatterer of radius 'b' [15] as,

$$E_{\theta}(\theta, \phi) = E_{\theta}^i(\theta, \phi) + \frac{k_o^2 (\epsilon_r - 1)}{4\pi} \int_0^{2\pi} \int_0^{\pi} E^i(b, \theta', \phi') e^{jk_o r' [\{\cos\theta\cos\theta' + \sin\theta\sin\theta'\} \cos(\phi - \phi')]} \frac{1}{b^2} d\phi' \sin\theta' d\theta' \quad (5.2)$$

after the vector operations and the usual far-field approximations have been carried out on the factor

$$\frac{e^{-jk_o (r-r')}}{|r-r'|}$$

Here $E^i(\theta, \phi)$ = the radiation field of the open ended E-plane sectoral horn (without the presence of dielectric sphere) and the integral term represents the scattered field $E_{\theta}^s(\theta, \phi)$.

To facilitate an easy evaluation of the factor with integral representing the scattered field component $E^s(\theta, \phi)$, the co-ordinates of a typical point on the spherical scatterer is taken as $(b, \pi/2, \phi')$. Thus Eq.(5.2) can

be written as

$$E(\theta, \phi) = E^i(\theta, \phi) + \frac{k_o^2 (\epsilon_r - 1)}{4\pi} \int_0^{2\pi} \int_0^\pi E^i(b, \theta', \phi') e^{jk_o b \sin\theta \cos(\phi - \phi')} \cdot b^2 d\phi' \sin\theta' d\theta' \quad (5.3)$$

Now it is assumed that the effective field incident on dielectric sphere kept in the vicinity of the feed horn is the same as the radiation field of the isolated feed horn. This assumption is particularly true for wide flare angle horns as edge diffraction will be minimal in such cases.

Narasimhan and Rao [101] have discussed the radiation properties of a wide flare ($10^\circ < \alpha_o < 70^\circ$) corrugated E-plane sectoral horn, and have shown that for such a horn supporting balanced HE_{11} mode, far-field pattern in the E-plane can be given in terms of a spectrum of cylindrical waves [52] as,

$$E_\theta(\theta) = \frac{e^{-jk_o r}}{\pi r} \frac{2aA'}{q\pi^2} \sum_{n=-\infty}^{\infty} j^n \exp(jn\theta) \frac{\cos na_o}{(1 - \frac{n}{q})^2} \cdot \frac{1}{H_n^{(2)'}(k_o r_o)} \quad (5.4)$$

where

$$q = \frac{\pi}{2\alpha_0}$$

$$A' = k_r E_1 \frac{H_{\pi}^{(2)'}}{2\alpha_0} (k_r r_0)$$

a = the width of the corrugated E-plane

α_0 = the half flare angle of the horn

r_0 = the horn flare length

k_r = the propagation constant.

E_1 = modal amplitude depending on the horn excitation.

In fact to get the near field from this radiation field, the near-field far-field transformation technique suggested by Ludwig [81] can be used. But from the nature of radiation pattern given by Eq. (5.4), as it has $e^{jn\theta}$ variation, it is suggested that the same form of the field can be taken for the near-field also.

Thus expression for the scattered field E^S becomes,

$$E^S = \frac{k_0^2 (\epsilon_r - 1)}{4\pi} \int_0^{2\pi} \int_0^{\pi} A_0 e^{jn\theta'} e^{jk_0 b \sin\theta \cos(\theta - \theta')} \cdot b^2 \cdot d\theta \sin\theta' \, d\theta' \quad (5.5)$$

where

$$A_0 = \frac{e^{-jk_0 r}}{\pi r} \frac{2aA'}{q\pi^2} \sum_{n=-\infty}^{\infty} (j)^n \frac{\cos n\alpha_0}{(1 - \frac{n}{q})^2} \frac{1}{H_n^{(2)'}(k_0 r_0)}$$

It is seen in Appendix E that the integral is evaluated to get the scattered field as,

$$E_{\theta}^s = \frac{k_o^2 (\epsilon_r - 1)}{4\pi} A_o b^2 2\pi J_o(k_o b \sin\theta) \frac{1 + \cos n\pi}{(1 - n^2)} \quad (5.6)$$

and inserting the value of A_o , scattered field becomes,

$$E_{\theta}^s = \frac{k_o^2 (\epsilon_r - 1)}{2} \frac{e^{-jk_o r}}{\pi r} \frac{2aA'}{q\pi^2} b^2 J_o(k_o b \sin\theta) \sum_{n=-\infty}^{\infty} j^n \frac{\cos n\alpha_o}{(1 - \frac{n}{q})^2} \frac{1}{H_n^{(2)'}(k r_o)} \frac{(1 + \cos n\pi)}{(1 - n^2)} \quad (5.7)$$

It is seen that the scattered field has non-zero value only for even values of n ($n=0, 2, 4, \dots$) including $n = 0$. From Eqs. (5.2), (5.4) and (5.7), the E-plane pattern of the corrugated E-plane sectoral horn excited in balanced HE_{11} mode in the presence of a dielectric sphere of radius 'b' in front of its aperture is obtained as,

$$E_{\theta}(\theta) = E_{\theta}^i(\theta) + E_{\theta}^s(\theta) = \frac{e^{-jk_o r}}{\pi r} \frac{2aA'}{q\pi^2} \sum_{n=-\infty}^{\infty} \frac{j^n \cos n\alpha_o}{(1 - \frac{n}{q})^2 H_n^{(2)'}(k_o r_o)} \cdot [e^{jn\theta} + k_o^2 \left(\frac{\epsilon_r - 1}{2} \right) b^2 J_o(k_o b \sin\theta) \frac{(1 + \cos n\pi)}{(1 - n^2)}] \quad (5.8)$$

and taking the real part of $e^{jn\theta}$, the $E_\theta(\theta)$ finally becomes,

$$E_\theta(\theta) = \frac{e^{-jk_0 r}}{\pi r} \frac{2aA'}{q\pi^2} \sum_{n=-\infty}^{\infty} j^n \frac{\cos n\alpha_0}{(1-\frac{n}{q})^2} \frac{1}{H_n^{(2)'}(k_0 r_0)} \cdot$$

$$\left[\cos n\theta + \frac{k_0^2 (\epsilon_r - 1)}{2} b^2 J_0(k_0 b \sin\theta) \frac{(1 + \cos n\pi)}{(1 - n^2)} \right]$$

(5.9)

Thus the scattering theory approach, under the appropriately mentioned assumptions, yields results without any complexity of mathematical operations. The radiation pattern has been computed by substituting typical test values of α_0 , r_0 , b and ϵ_r in Eq. (5.9), and the results are shown in Fig. 5.2.

5.2.2 DESIGN ASPECTS OF THE CORRUGATED E-PLANE SECTORAL HORN

Assuming that a balanced HE_{11} hybrid mode exists inside the horn, the corrugation depth to support such a HE_{11} mode is given by,

$$h = \frac{\frac{\pi}{2}}{\sqrt{k_0^2 - \left(\frac{\pi}{a}\right)^2}} \quad (5.10)$$

where $k_0 = \frac{2\pi}{\lambda_0}$

and a = the E - plane width of the corrugated horn.

When the input X-band waveguide feeding the horn (with $a = 0.9$ inch) supports the dominant TE_{10} mode at an operating frequency $f_0 = 8.8$ GHz, the value of corrugation depth is found to be

$$h = 1.3 \text{ cm}$$

For the realization of an impedance boundary from a corrugated surface, which is essential for the analysis of fields in the axial region of the horn, the corrugations are to be infinitely thin and sufficiently closely spaced. This conditions is listed as,

$$\frac{\lambda_0}{w+t} \geq 10 \quad (5.11)$$

where,

t = the corrugation thickness

and w = the corrugation width.

For the typical sectoral horn, it is taken

$t = w = 0.15$ cm so that

$$\frac{\lambda_0}{w+t} = \frac{3.5}{0.3} > 10 \quad (5.12)$$

For the phase error over sectoral horn aperture to be minimum (maximum allowable phase error is 45°) the H -plane aperture dimension of the horn b_0 has to keep the relation with λ_0 as,

$$\frac{b_0}{\lambda_0} \leq 2.7 \quad (4.13)$$

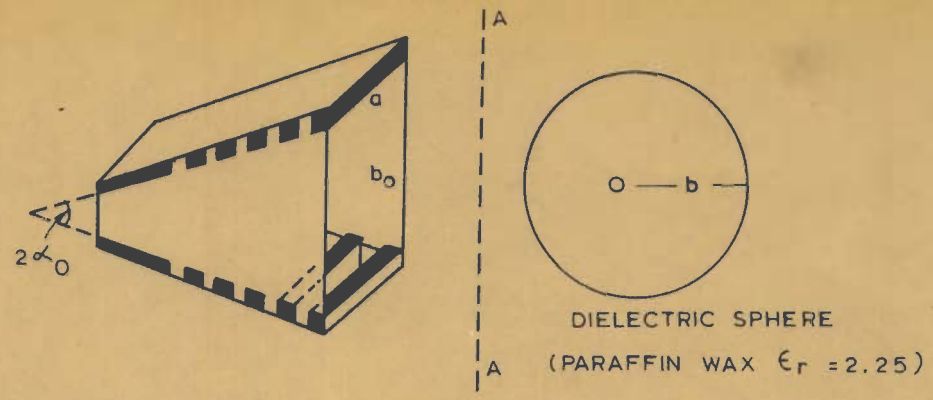
The horn flare angle is designed using relation $\alpha_0 = \cos^{-1} \frac{L}{r_0}$ where L is the axial length and r_0 the flare length of the horn. Now choosing $k_0 r_0 = 18$, the flare angle and H -plane aperture dimension of the horn respectively are found to be

$$\alpha_0 = 15^\circ, \text{ and } b_0 = 5.2 \text{ cm}$$

The corrugated E -plane sectoral horn was fabricated as per the above design specifications. Corrugations were introduced only after a certain distance (≈ 1.5 cm) from the horn throat so as to obtain a low input VSWR.

5.2.3 EXPERIMENTAL RESULTS

Experiments were performed with paraffin wax ($\epsilon_r = 2.25$) spheres of diameter 9 cm, 6cm and 4 cm placed off-set in front of the sectoral horn of the above mentioned specifications excited in the balanced HE_{11} mode at an operating frequency of 8.64 GHz. The sphere off-set positions were determined experimentally for minimum input VSWR performance [85] ,and the optimum off-set positions were found to lie between 1.1 cm and 1.4 cm from the horn aperture for the 3 sphere sizes tested. Theoretical results



$2\alpha_0$ - HORN FLARE ANGLE
 A, A - ARBITRARY LOCATION OF THE SPHERE
 a, b_0 - HORN APERTURE DIMENSIONS

FIG. 5.1 - GEOMETRY OF THE SPHERE LOADED CORRUGATED HORN

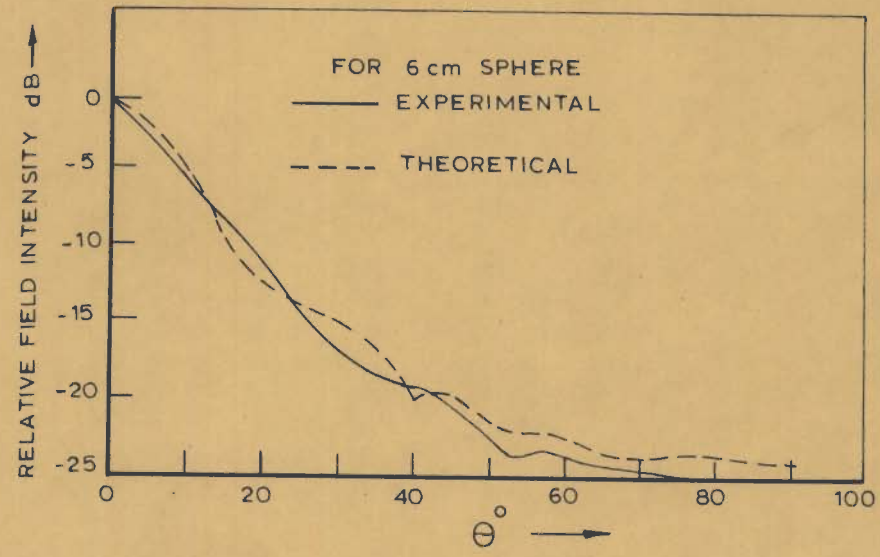


FIG. 5.2 - E-PLANE PATTERNS (THEORETICAL AND EXPERIMENTAL)

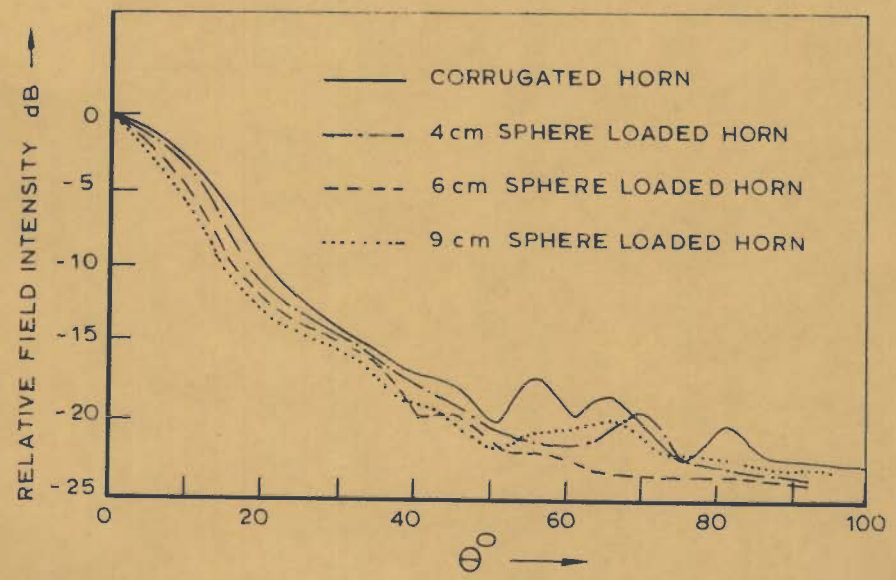


FIG. 5.3 - E-PLANE RADIATION PATTERNS (PATTERNS MEASURED AT $f_0 = 8.64$ GHz)

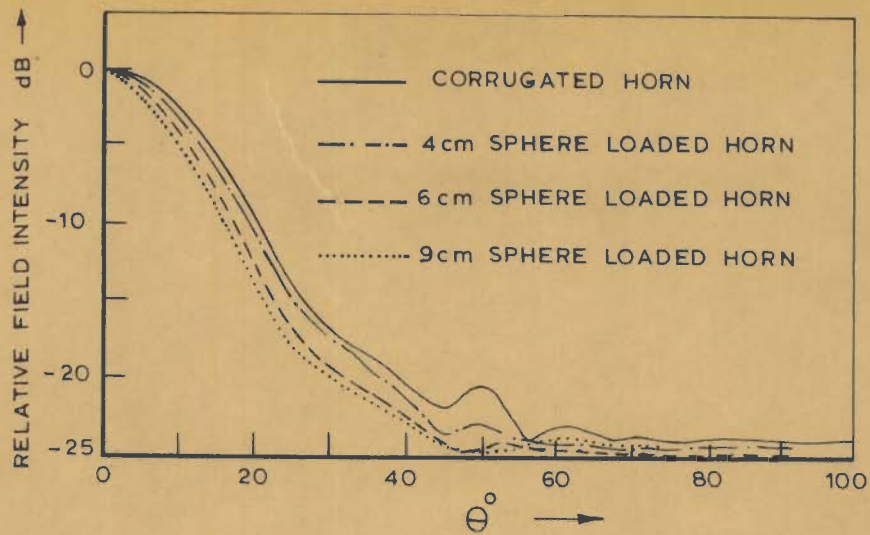


FIG. 5.4 _ H - PLANE RADIATION PATTERNS
(PATTERNS MEASURED AT $f_0 = 8.64$ GHz)

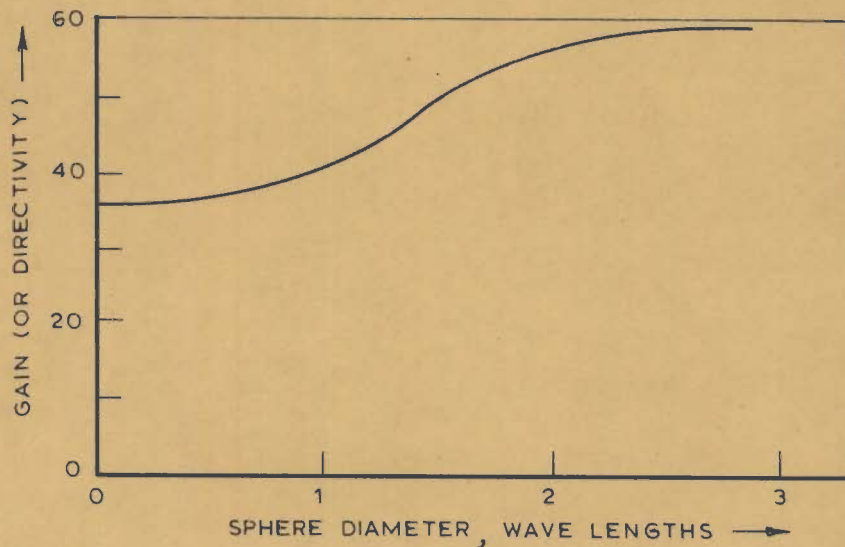


FIG. 5.5 _ GAIN AS A FUNCTION OF THE
SPHERE DIAMETER

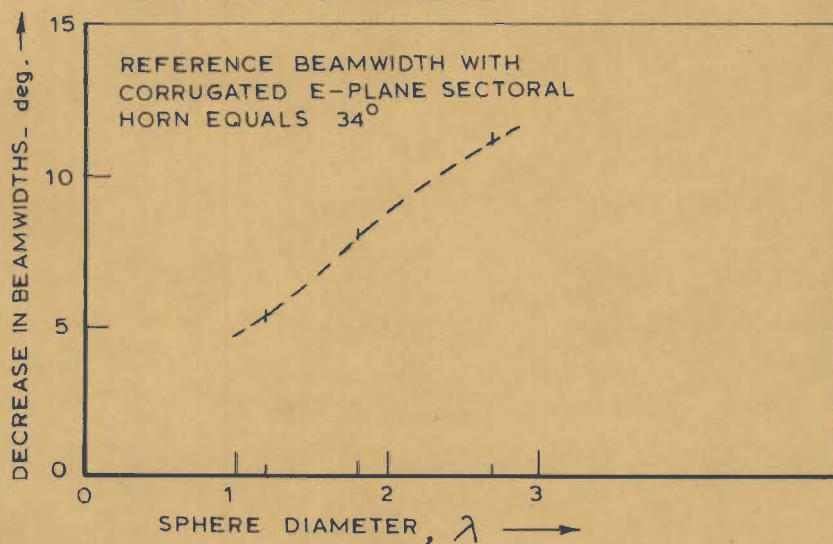


FIG. 5.5a _ DECREASE IN BEAMWIDTH VS SPHERE DIA. FOR
SPHERE LOADED CORRUGATED E-PLANE
SECTORAL HORN

of the E -plane radiation pattern based on Eq. (5.9) are computed for the dielectric sphere of 6 cm dia and are compared with experimental data as in Fig. 5.2. There is reasonable agreement between these two results. The E-plane and H -plane radiation patterns for different sphere diameters were obtained, and are shown in Fig. 5.3 and Fig.5.4 respectively together with those for the corrugated sectoral horn alone. The axial gain of the antenna system was determined experimentally by the substitution method with a standard antenna of known gain (pyramidal horn of gain ≈ 52); and measured values of gain are checked by the approximate formula $G = 41253/\theta_E\theta_H$, where θ_E and θ_H represent -3 dB beamwidth in degrees in E -plane and H -plane respectively. Results of the on-axis gain of the system thus determined are plotted in Fig.5.5 as a function of the dielectric sphere diameter in wavelengths. The corrugated E -plane sectoral horn gain without dielectric sphere loading (experimental) is also included for comparison. It is found that the on-axis gain of the system increases in excess of 2 dB than that available from the corrugated E -plane sectoral horn of the same dimensions. Dielectric sphere loading results in reducing the sidelobe levels. The system also has reduced -3 dB beamwidth, and low input VSWR together with a multiple beam possibility. Decrease in beamwidth due

to dielectric sphere loading is shown in Fig. 5.6 as a function of sphere diameter in wavelengths.

From the observations that the antenna system has radiation patterns with reduced -3 dB beamwidths and sidelobe levels, it can be concluded that the test feed system may be used as a variable beamwidth feed with better directivity and low sidelobes for paraboloidal reflector antennas for special applications in radio astronomy and satellite communication.

5.3 A CORRUGATED CONICAL HORN WITH A DIELECTRIC SPHERE IN FRONT OF ITS APERTURE

The effect of placing a homogeneous dielectric sphere in front of a radiating corrugated conical horn has been investigated. The theoretical treatment of the radiation characteristics of the device is based on the scattering superposition using electric and magnetic vector potentials. Calculations based on this formulation show good overall agreement with experimental results of radiation pattern and directivity measurements. It is seen that dielectric sphere-mounted corrugated conical horn has directivity in excess of that of conventional corrugated conical horn of the same dimension. The system can be used as a highly directive feed with low

sidelobes for paraboloidal reflector antennas. The feed system also possesses a low input VSWR due to the aperture-sphere separation, and a multiple beam possibility depending on the diameters of the off-set spheres in front of the horn aperture.

5.3.1 THEORETICAL FORMULATION

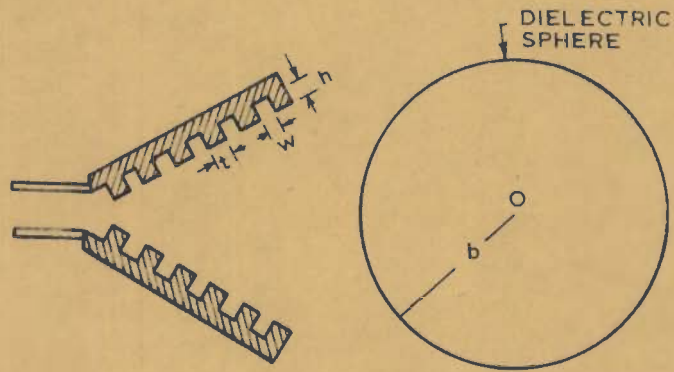
The device under consideration is shown in Fig.5.6. A homogeneous dielectric sphere of radius 'b', and permittivity ϵ_1 is placed in front of, but displaced from, the aperture of the corrugated conical horn. The modal fields in the axial region of the corrugated conical horn can be derived from the magnetic and electric vector potentials \bar{A} and \bar{F} each having a single component only such that $\bar{A} = \bar{i}_r A_r$ and $\bar{F} = \bar{i}_r F_r$. By Eqs. (3.25) the scalar potential functions A_r and F_r are given by

$$A_r = a_{mn} \hat{B}_n(k_0 r) J_m(q\theta) \exp(jm\phi) \quad (5.14)$$

$$F_r = b_{mn} \hat{B}_n(k_0 r) J_m(q\theta) \exp(jm\phi)$$

where, $\hat{B}_n(k_0 r)$ = solution to the modified (spherical) Bessel's equation

and $q = \sqrt{n(n+1)}$, and is obtained from the characteristic equation [94] $J_{\underline{m+1}}(q\theta_0) = 0$, θ_0 being the



HORN FLARE ANGLE $2\alpha_0 = 60^\circ$
HORN AXIAL LENGTH, $L = 9$ cm
CORRUGATION DEPTH, $h = 0.83$ cm
CORRUGATION THICKNESS, $t = 0.254$ cm
CORRUGATION WIDTH, $w = 0.76$ cm

FIG. 5.6_DIELECTRIC SPHERE MOUNTED
CORRUGATED CONICAL HORN

flare angle of the cone ($(m-1)$ for HE modes and $(m+1)$ for EH modes). In Eq. (5.14) m is an integer, and n is real and positive corresponding to ordinal root of the characteristic equation as designated by the mode number.

Substitution of A_r and F_r in Eqs. (3.4) will give interior horn field components E_θ and E_ϕ ; and are given, under balanced conditions, by

$$E_\theta = - \frac{a_{mn}}{r} \left(\frac{\mu_0}{\epsilon_0} \right)^{1/2} \hat{B}_n(k_0 r) J_m(q\theta) \exp(jm\phi)$$

$$E_\phi = - j \frac{a_{mn}}{r} \left(\frac{\mu_0}{\epsilon_0} \right)^{1/2} \hat{B}_n(k_0 r) J_m(q\theta) \exp(jm\phi)$$
(5.15)

The transverse electric field over horn aperture may be obtained by Eq. (3.3); and under balanced condition (i.e. E and H are related by $E/H = \eta_0$, the free space characteristic impedance) the transverse electric field \bar{E}_t over corrugated conical horn aperture for HE_{mn} mode excitation is given by,

$$\bar{E}_t = - \frac{a_{mn}}{r} \left(\frac{\mu_0}{\epsilon_0} \right)^{1/2} B_n(k_0 r) J_{m-1}(q\theta) (\hat{i}_\theta + j\hat{i}_\phi) e^{jm\phi} \quad (5.16)$$

In case of corrugated horns with impedance boundaries, the edge diffraction is negligible; and hence the nature of the field incident on the dielectric sphere

placed slightly displaced from the horn aperture will be similar to that of \bar{E}_t .

Accordingly, restricting the consideration to $m=1$, the proper form of the potential functions for the e.m. waves incident on the sphere mounted in front of the horn aperture may be obtained in the same way [52] as for Eqs. (3.6); and are given by,

$$A_r^i = \sum_{n=1}^{\infty} a_n \hat{B}_n(k_0 r) J_1(q\theta) \cos\theta \quad (5.17)$$

$$F_r^i = \eta_0 \sum_{n=1}^{\infty} a_n \hat{B}_n(k_0 r) J_1(q\theta) \sin\theta$$

where $a_n = j^{-n} \frac{(2n+1)}{n(n+1)}$

$$\eta_0 = \sqrt{\mu_0/\epsilon_0}$$

$\hat{B}_n(k_0 r) = \hat{J}_n(k_0 r)$ for $r \leq b$, b being the radius of the sphere

$= \hat{H}_n^{(2)}(k_0 r)$ for $r > b$, i.e. in the far-zone.

Considering dielectric sphere as a scatterer, the corresponding potential functions for the scattered field becomes,

$$A_r^S = \sum_{n=1}^{\infty} b_n \hat{H}_n^{(2)}(k_0 r) J_1(q\theta) \cos\theta \quad (5.18)$$

$$F_r^S = \eta_0 \sum_{n=1}^{\infty} c_n \hat{H}_n^{(2)}(k_0 r) J_1(q\theta) \sin\theta$$

where b_n and c_n are the coefficients for the potentials of the scattered field, and can be determined from the boundary conditions of tangential E and H being continuous at $r = b$, the radius of the dielectric sphere. As mentioned in Sec. 3.2.2 the constants can be obtained as,

$$b_n = \frac{-\sqrt{\epsilon_1} \hat{J}'_n(k_0 b) \hat{J}_n(k_1 b) + \sqrt{\epsilon_0} \hat{J}_n(k_0 b) \hat{J}'_n(k_1 b)}{\sqrt{\epsilon_1} \hat{H}_n^{(2)'}(k_0 b) \hat{J}_n(k_1 b) - \sqrt{\epsilon_0} \hat{H}_n^{(2)}(k_0 b) \hat{J}'_n(k_1 a)} a_n \quad (5.19)$$

$$c_n = \frac{-\sqrt{\epsilon_1} \hat{J}_n(k_0 b) \hat{J}'_n(k_1 a) + \sqrt{\epsilon_0} \hat{J}'_n(k_0 b) \hat{J}_n(k_1 b)}{\sqrt{\epsilon_1} \hat{H}_n^{(2)}(k_0 b) \hat{J}'_n(k_1 b) - \sqrt{\epsilon_0} \hat{H}_n^{(2)'}(k_0 b) \hat{J}_n(k_1 a)} a_n$$

$$\text{where } k_0 = \omega \sqrt{\mu_0 \epsilon_0}$$

$$k_1 = \omega \sqrt{\mu_0 \epsilon_1}$$

and the prime indicates differentiation with respect to r .

Based on the scattering superposition technique [37] the total radiated field from the device can be obtained by a superposition of the incident and scattered

fields, and hence from Eqs.(5.17) and (5.18) potential functions for the total radiated field at any point in the far-zone are given by

$$A_r^+ = \cos\theta \sum_{n=1}^{\infty} (a_n + b_n) \hat{H}_n^{(2)}(k_0 r) J_1(q\theta)$$

$$F_r^+ = \eta_0 \sin\theta \sum_{n=1}^{\infty} (a_n + c_n) \hat{H}_n^{(2)}(k_0 r) J_1(q\theta)$$
(5.20)

Note that in Eqs. (5.20) the function $\hat{B}_n(k_0 r)$ is taken as $\hat{H}_n^{(2)}(k_0 r)$, the spherical Hankel function representing the outward travelling waves, to account for the field at the far-zone.

As shown in Appendix F-1, the resultant expression for the far-zone field is derived as,

$$E_R(r) = -j \frac{e^{-jk_0 r}}{r} \eta_0 \sum_{n=1}^{\infty} \frac{(2n+1)}{n(n+1)} (\bar{M}\alpha_n + \bar{N}\beta_n) \quad (5.21)$$

where,

$$\bar{M} = \frac{J_1(q\theta)}{\sin\theta} \cos\theta \bar{i}_\theta - qJ_1'(q\theta) \sin\theta \bar{i}_\phi$$

$$\bar{N} = qJ_1'(q\theta) \cos\theta \bar{i}_\theta - \frac{J_1(q\theta)}{\sin\theta} \sin\theta \bar{i}_\phi$$

$$\alpha_n = 1 + \frac{c_n}{a_n}$$

$$\beta_n = 1 + \frac{b_n}{a_n}, \text{ and } \bar{i}_\theta \text{ and } \bar{i}_\phi \text{ are unit-vectors.}$$

Radiation patterns may be computed using Eq.(5.21) by knowing values of α_n and β_n from Eqs.(5.19) for typical values of b and ϵ_1 . Results thus obtained are presented in Fig. 5.7a.

5.3.2 AXIAL GAIN OF THE SYSTEM

The total power W_t radiated by the system may be determined by integrating total power flow across an infinite sphere mounted at the origin. In this case, it is seen in Appendix E-2 that W_t is obtained as

$$W_t = \frac{1}{2} \eta_0 \pi \sum_{n=1}^{\infty} \frac{(2n+1)^2}{n^2(n+1)^2} \left[J_1^2(q\pi) \left\{ 2\alpha_n \beta_n - (\alpha_n^2 + \beta_n^2) \right\} + (\alpha_n^2 + \beta_n^2) I \right] \quad (5.22)$$

where

$$I = \int_0^{\pi} \left[\frac{J_1(q\theta)}{\sin\theta} + q J_1'(q\theta) \right]^2 \sin\theta d\theta$$

An explicit expression for W_t is obtained by an approximate evaluation of the above integral with the assumption $\sin\theta \approx \theta$ (This assumption is a source of error for W_t , but as the integral term is added to the other two terms in Eq. (5.22) to get the total power W_t , the percentage of error in W_t is very small). Accordingly, by Appendix F-2, W_t becomes,

$$W_t = \frac{1}{2} \eta_0 \pi \sum_{n=1}^{\infty} \frac{(2n+1)^2}{n^2(n+1)^2} [J_1^2(q\pi) \{ 2\alpha_n \beta_n - (\alpha_n^2 + \beta_n^2) \} + (\alpha_n^2 + \beta_n^2) \frac{(q\pi)^2}{2} \{ J_0^2(q\pi) + J_1^2(q\pi) \}] \quad (5.23)$$

An expression for on-axis gain of the system is obtained by

$$G(0,0) = \frac{4\pi P(0,0)}{W_t} \quad , \quad \text{where } P(0,0) = \frac{1}{2\eta_0} \left| E_R \right|_{\max}^2$$

Using Eqs. (5.21) and (5.23) the gain is derived in Appendix F-3 as,

$$G(0,0) = \frac{\left| \sum_{n=1}^{\infty} q(\alpha_n + \beta_n) \right|^2}{\sum_{n=1}^{\infty} J_1^2(q\pi) [2\alpha_n \beta_n - (\alpha_n^2 + \beta_n^2)] + \frac{(q\pi)^2}{2} (\alpha_n^2 + \beta_n^2) \cdot [J_0^2(q\pi) + J_1^2(q\pi)]} \quad (5.24)$$

The axial gain based on Eq.(5.2) has been evaluated for the HE_{11} mode using typical values and the results are shown in Fig. 5.8

5.3.3 EXPERIMENTAL RESULTS

In order to investigate the effect of placing a dielectric sphere in front of the aperture of a radiating

corrugated conical horn, experiments were carried out with a corrugated conical horn of the specifications $\alpha_0 = 30^\circ$, $h = 0.83$ cm, $W = 0.76$ cm, $t = 0.254$ cm and of axial length $L = 9$ cm. (the design aspects are the same as discussed in Sec. 5.2.2). The pattern measurements were made for the horn excited in the HE_{11} mode at a frequency of 9.64 GHz with paraffin wax spheres of diameter 4 cm, 6 cm and 9 cm. Spheres were kept in front of, but displaced from, the horn aperture; and the sphere off-set positions were determined experimentally for minimum input VSWR performance [85]. The validity of Eq. (5.21) for the radiation pattern of the sphere mounted corrugated conical horn is verified in Fig.5.7a by establishing a reasonably good agreement between the theoretical pattern based on Eq. (5.21) and the experimental pattern.

Experimental patterns of the dielectric sphere-mounted corrugated conical horn for different sphere diameters are shown in Fig. 5.7b together with the pattern for corrugated conical horn alone. The gain variation due to dielectric sphere mounting is plotted in Fig. 5.8a as a function of the sphere diameter in wavelengths. There is good agreement between experimental values of gain and that based on Eq. (5.24). In Fig.5.8b the

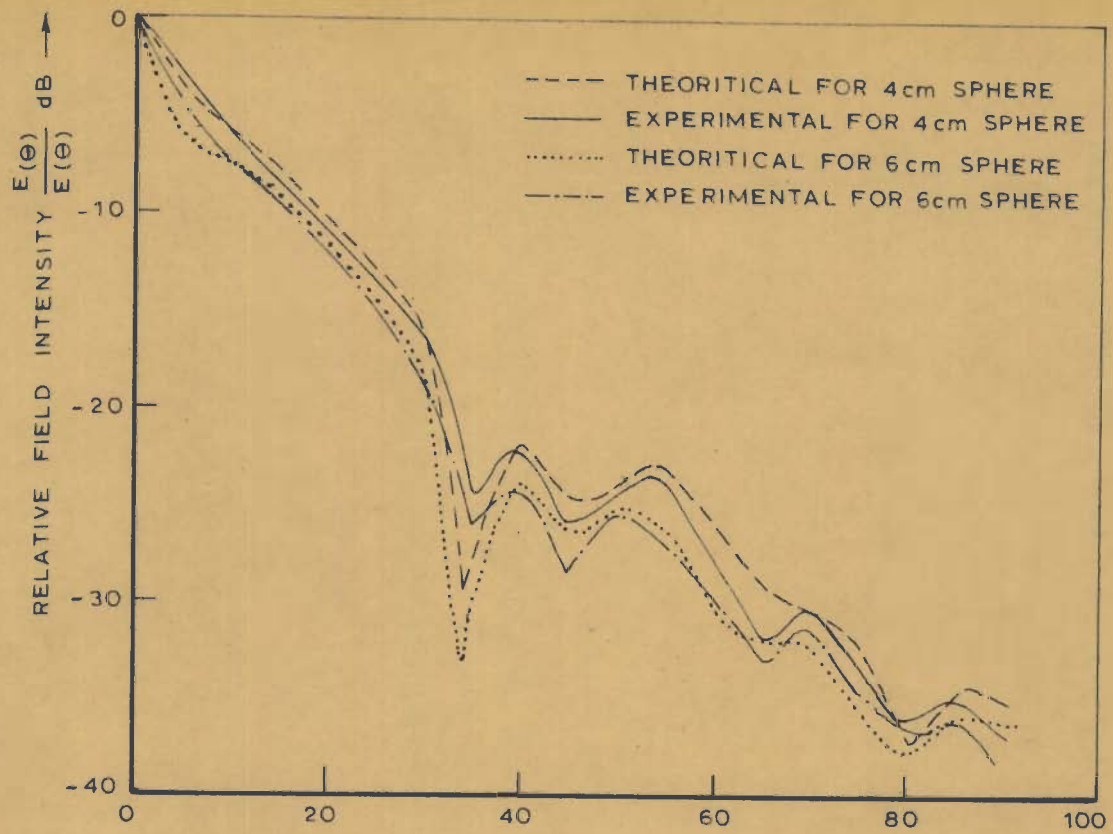


FIG.5.7a_RADIATION PATTERN (THEORITICAL AND EXPERIMENTAL) OF SPHERE LOADED CORRUGATED CONICAL HORN

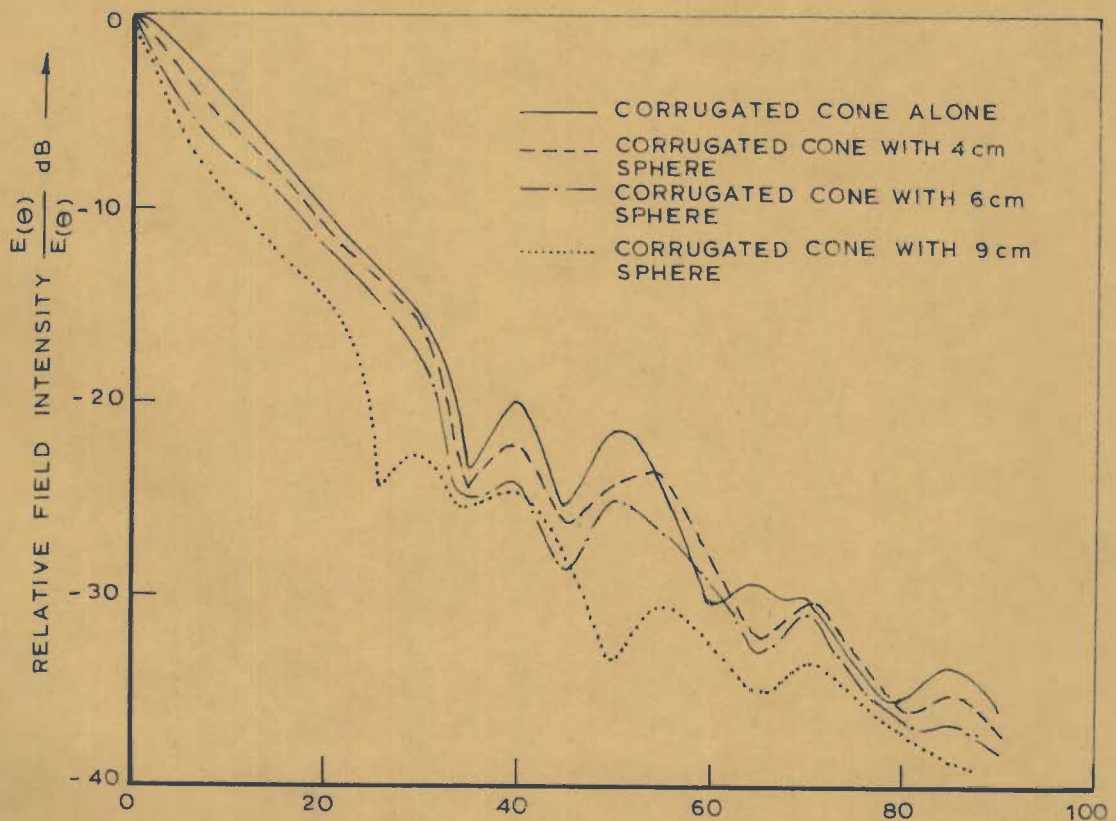


FIG.5.7b_RADIATION PATTERN (EXPERIMENTAL) OF DIELECTRIC SPHERE LOADED CORRUGATED CONICAL HORN

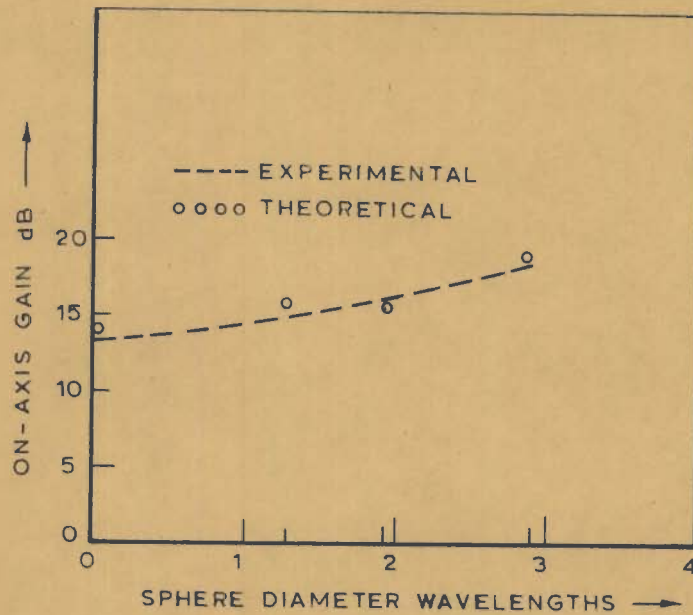


FIG. 5.8a - GAIN VS SPHERE DIAMETER

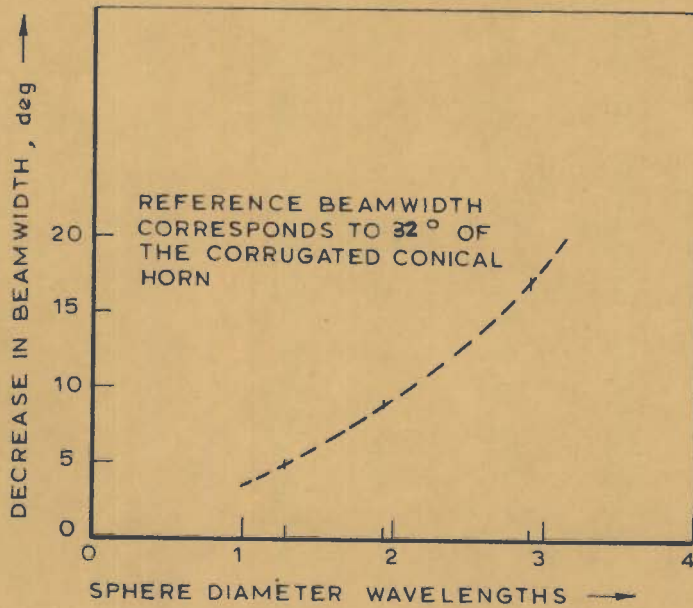


FIG. 5.8 b - DECREASE IN BEAMWIDTH VS SPHERE DIAMETER

reduction in -3 dB beamwidth due to sphere mounting is depicted.

From the results presented it is observed that

- i) the off-set dielectric sphere mounted corrugated conical horn carrying HE_{11} hybrid mode has greater pattern directivity with low sidelobes.
- ii) the -3 dB beamwidth of the pattern decreases as the dielectric sphere diameter in wavelengths is increased.
- iii) there is a significant improvement in the on-axis gain of the corrugated conical horn due to dielectric spheres placed in front of its aperture.
- iv) the test feed system has provision for variable beamwidth, as the -3 dB beamwidth can be controlled by the dielectric sphere diameter.

The test feed system can be used as a low noise variable beamwidth feed with high directivity and on-axis gain for parabolic reflector antennas.

5.4 CONCLUSION

The radiation properties of corrugated conical horn and corrugated E -plane sectoral horn, with dielectric spheres placed in front of, but displaced from apertures of the radiating horns have been studied. Analytical results

obtained on the basis of scattering theory approach are established in good agreement with experimental results of radiation pattern and gain measurements. In both cases the dielectric sphere loading was found to narrow the pattern beamwidth with low sidelobes and greater axial gain. Both the antenna systems can be used as improved variable beamwidth feeds with better directivity, low sidelobes, higher gain and low input VSWR.

CHAPTER VI

DIELECTRIC LOADED SECTORAL HORNS

6.1 INTRODUCTION

Electromagnetic sectoral horns are commonly used as gain standards and as convenient sources of electromagnetic radiations. Moreover there is a class of reflector antennas [33 Part 2, pp 83-84] which incorporate sectoral horns as primary feeds. But conventional sectoral horns with perfectly conducting walls and rectangular aperture have certain limitations due to diffraction at the E -plane edges leading to irregularities in the E -plane pattern. The edge diffraction also causes unequal E- plane and H -plane beamwidths, and raised sidelobe levels. Reflector antennas used in satellite communication and radioastronomy need physically small primary feeds having greater directivity and low sidelobes ; hence the need for improved sectoral horn feeds. Corrugated E -plane sectoral horn was shown [99] to be a suitable improved feed system with reasonable directivity and low sidelobes. In this chapter, results of investigations into the radiation behaviour of two alternative dielectric loaded sectoral horn feeds that will have the additional advantage of ease of construction and light weight are presented. First

the E -plane sectoral horn with a suitable dielectric loading on the E -plane walls is discussed. Analytical results established in reasonable agreement with experiments show that radiation patterns of such antennas have a remarkable increase in directivity, but at the cost of deteriorated sidelobes. Means were explored to improve the pattern with low sidelobes; and dielectric spheres placed in front of the horn aperture were found to be effective in reducing the sidelobe levels and the -3 dB beamwidths significantly. Another horn feed investigated is a dielectric loaded H -plane sectoral horn with a cylindrical aperture. Dielectric loading contributed to the pattern directivity; and the circular aperture resulted in low sidelobes. Accordingly the feed system studied was found to have better directivity at reasonable sidelobe levels.

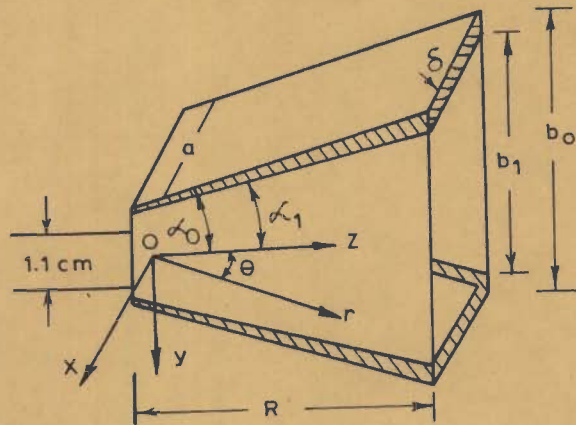
6.2 DIELECTRIC LOADED E-PLANE SECTORAL HORN [71]

The radiation properties of E -plane sectoral horn with dielectric loaded E-plane walls are discussed here. The analytical formulation of the radiation characteristics is made using an electric vector potential on the basis of the vector diffraction formula. The characteristic equation for the eigen values is also derived. The performance of the antenna has been evaluated

theoretically and is found to be in reasonable agreement with experimental values. Results show a remarkable increase in the pattern directivity at the cost of a slight increase in the sidelobe level. Investigations are made to reduce the sidelobes by paraffin wax dielectric spheres placed in front of, but displaced from, the aperture of the dielectric loaded horn. Dielectric sphere loading is found to improve the patterns of this horn with reduced sidelobe levels and -3 dB beam widths. The feed system can be used as a highly directive low noise feed with a variable beamwidth facility for paraboloidal reflector antennas.

6.2.1 THEORY OF OPERATION

The test horn is shown in Fig.6.1. The narrow walls (E -plane walls) of the E -plane sectoral horn are layered with a dielectric material of angular thickness. To satisfy the boundary conditions, hybrid mode (having both E_r and H_r) propagation should exist both in the horn axial region and inside the dielectric coated region. TE_x modes will have both E and H components in the direction of propagation (radial direction). The radial hybrid mode field components of the system can then be derived from an electric vector potential \bar{F} having a single component in the x -direction such that $\bar{F} = \bar{i}_x \psi$. The proper form of the potential function ψ in relation to horn boundary



$\alpha_0 = 19^\circ$, $\alpha_1 = 17^\circ$, $R = 6.7 \text{ cm}$, $b_0 = 5.8 \text{ cm}$, $b_1 = 5.2 \text{ cm}$
 $a = 2.5 \text{ cm}$, $\delta = 3 \text{ mm}$

FIG. 6.1 _ DIELECTRIC COATED E-PLANE SECTORAL HORN

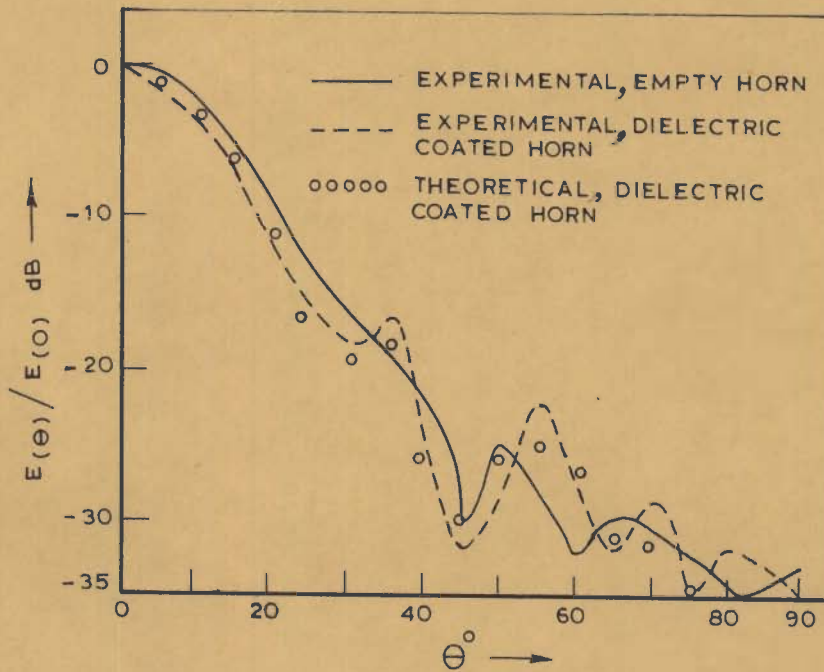


FIG. 6.2 _ RADIATION PATTERN FOR DIELECTRIC COATED E-PLANE SECTORAL HORN

is given by,

$$\psi_{mn}^{TE} = \cos \frac{m\pi}{a} x \cos P\theta B_p(k_r r) \quad (6.1)$$

where m and n are integers, P is positive and real denoting the eigen value of the particular mode designated by m and n,

$$k_r = \sqrt{k_o^2 - \left(\frac{m\pi}{a}\right)^2} \quad (6.2)$$

$$\text{with } k_o = 2\pi/\lambda_o$$

and $B_p(k_r r)$ is solution to the Bessel's equation.

The different field components inside dielectric coated region and in the horn axial region for HE_{mn} mode are determined by substituting ψ_{mn}^{TE} in the appropriate equations [52], and are obtained in Appendix G-1 as,

Inside dielectric coated region

$$E_{rd} = \frac{1}{r} P \cos \frac{m\pi}{a} x \sin p\theta [C J_p(k_{r1} r) + D y_p(k_{r1} r)]$$

$$E_{\theta d} = k_{r1} \cos \frac{m\pi}{a} x \cos p\theta [C J_p'(k_{r1} r) + D y_p'(k_{r1} r)] \quad (6.3)$$

$$E_{xd} = 0$$

$$H_{rd} = \frac{-1}{j\omega\mu_0} \frac{m\pi}{a} k_{r1} \sin \frac{m\pi}{a} x \cos\theta [C J_p'(k_{r1}r) + D y_p'(k_{r1}r)]$$

$$H_{\theta d} = \frac{1}{j\omega\mu_0 r} P \left(\frac{m\pi}{a} \right) \sin \frac{m\pi}{a} x \sin\theta [C J_p(k_{r1}r) + D y_p(k_{r1}r)]$$

$$H_{xd} = \frac{1}{j\omega\mu_0} k_{r1}^2 \cos \frac{m\pi}{a} x \cos\theta [C J_p(k_{r1}r) + D y_p(k_{r1}r)]$$

In the horn axial region

$$E_{r_0} = \frac{F}{r} p \cos \frac{m\pi}{a} x \sin\theta H_p^{(2)}(k_r r)$$

$$E_{\theta_0} = F k_r \cos \frac{m\pi}{a} x \cos\theta H_p^{(2)'}(k_r r) \quad (6.4)$$

$$E_{x_0} = 0$$

$$H_{r_0} = -\frac{1}{j\omega\mu_0} F k_r \frac{m\pi}{a} \sin \frac{m\pi}{a} x \cos\theta H_p^{(2)'}(k_r r)$$

$$H_{\theta_0} = \frac{F}{j\omega\mu_0 r} p \frac{m\pi}{a} \sin \frac{m\pi}{a} x \sin\theta H_p^{(2)}(k_r r)$$

$$H_{x_0} = \frac{F}{j\omega\mu_0} k_r^2 \cos \frac{m\pi}{a} x \cos\theta H_p^{(2)}(k_r r)$$

where C, D and F are constants that depend on the horn excitation,

$$k_{r1} = \sqrt{\epsilon_r k_0^2 - \left(\frac{m\pi}{a}\right)^2} \quad (6.5)$$

ϵ_r being the relative permittivity of the dielectric

material, and the primes on the function indicate differentiation with respect to r . The subscripts 'o' and 'd' are used to denote the fields in the dielectric coated and horn axial regions respectively.

The eigen values of p can be obtained from the characteristic equation formulated on the boundary conditions viz.,

- i) tangential E and H must be continuous at the air-dielectric interface, i.e.

$$\begin{aligned} E_{rd} &= E_{ro} && \text{at } \theta = \alpha_1, \text{ and } r \leq r_o, \text{ the flare} \\ H_{rd} &= H_{ro} && \text{length of the horn.} \end{aligned}$$

- ii) $E_{\theta d} = 0$ at $\theta = \alpha_o$, and $r \leq r_o$.

Applying the above boundary conditions, it is seen in Appendix G-2, that the characteristic equation for p can be obtained as,

$$\frac{J_p(x_1)y_p'(x_2) - J_p'(x_2)y_p(x_1)}{J_p'(x_1)y_p'(x_2) - J_p'(x_2)y_p'(x_1)} = \frac{k_{r1}}{k_r} \frac{H_p^{(2)}\left(k_r \frac{b_1'}{2\sin\alpha_1}\right)}{H_p^{(2)'}\left(k_r \frac{b_1'}{2\sin\alpha_1}\right)} \quad (6.6)$$

$$\text{where } x_1 = k_{r1} \frac{b_1'}{2\sin\alpha_1}$$

$$x_2 = k_{r1} \frac{b_o'}{2\sin\alpha_o}$$

In above expressions for x_1 and x_2 , $b_1' = b_0' - 2\delta'$, denotes the transverse distance (along y -direction) corresponding to any distance $r \leq r_0$ at the angular location $\theta = \alpha_1$, b_0' = the transverse distance corresponding to any radial distance $r \leq r_0$ at the angular location $\theta = \alpha_0$, and δ' = the dielectric coating thickness at that distance for which $r < r_0$.

(It may be noted that $b_1'/2r' = \sin\alpha_1$, and $b_0'/2r' = \sin\alpha_0$ where r' represents any distance $r < r_0$, the horn flare length; and at $r = r_0$, $b_0' = b_0$ and $b_1' = b_1$ and $\delta' = \delta$, the respective quantities at the aperture).

This characteristic equation for the HE_{mn} mode is solved graphically for the eigen value P of any hybrid mode by substituting typical values of x_1 , x_2 ; k_r and k_{r1} (k_r and k_{r1} can be obtained from Eqs. (6.2) and (6.5)) in Eq. (6.6). The eigen value P for HE_{11} mode for the test system was found to be ≈ 0.5 .

6.2.2 RADIATION FROM THE DIELECTRIC LOADED HORN

When the radiating aperture is a horn aperture, the phase of the field in the aperture is not constant, but varies with position in the aperture. From the nature of the aperture, when the flare angle $\alpha_0 \leq 20^\circ$, quadratic field phase variation [44] of the form

$$\psi_y = e^{-j \frac{\pi}{\lambda_g} \frac{y^2}{R}} \quad (6.7)$$

($\lambda_g = 2\pi/k_r$ and $R =$ the horn axial length)

is a reasonable approximation. The radiated far-field from the dielectric-loaded horn can then be obtained by the aperture field method based on the vector diffraction formula. For this, the transverse electric field E_t over the horn aperture is given by,

$$\bar{E}_t = \bar{i}_x E_x + \bar{i}_y E_y \quad (6.8)$$

In obtaining a simplified expression for \bar{E}_t , the following approximations are used

$$\bar{i}_y \approx \bar{i}_\theta, \quad E_y \approx E_\theta$$

(These approximations are true if α_0 is not large i.e. $\alpha_0 < 30^\circ$)
Thus E_t has only a single component E_y (since $E_x = 0$ in this case), and is given, by Eqs. (6.4) and (6.7), as

$$E_t = F \cdot k_r \cos \frac{\pi}{a} x \cos \rho \theta H_p^{(2)'}(k_r R) e^{-j \frac{\pi}{\lambda_g} \frac{y^2}{R}} \quad (6.9)$$

By the vector diffraction formula [44],[66], the radiated far-field in the E-plane ($\phi = \pi/2$) is given by,

$$E_\theta(\theta) = \frac{jk_0}{4\pi} \left(1 + \frac{k_r}{k_0} \cos \theta\right) \frac{e^{-jk_0 r}}{r} \iint_S \bar{E}_t \cdot e^{jk_0 y \sin \theta} ds \quad (6.10)$$

i.e.

$$E_{\theta}(\theta) = \frac{jk_0}{4\pi} \left(1 + \frac{k_r}{k_0} \cos\theta\right) \frac{e^{-jk_0 r}}{r} Fk_r H_p^{(2)'}(k_0 R) \int_{-a/2}^{a/2} \int_{-b_1/2}^{b_1/2} \cos \frac{m\pi}{a} x \cos p\theta e^{-j \frac{\pi}{\lambda_g} \frac{y^2}{R}} e^{jk_0 y \sin\theta} dx dy$$

For the flare angle $10 \leq \alpha_0 \leq 30^\circ$, it can be assumed that

$$\frac{\theta}{2\alpha_1} \approx \frac{y}{b_1}, \text{ and with this approximation,}$$

$$E_{\theta}(\theta) = \frac{jk_0}{4\pi} \left(1 + \frac{k_r}{k_0} \cos\theta\right) \frac{e^{-jk_0 r}}{r} FH_p^{(2)'}(k_0 R) \int_{-a/2}^{a/2} \cos \frac{m\pi}{a} x dx \int_{-b_1/2}^{b_1/2} \cos p \frac{2\alpha_1}{b_1} y e^{-j \frac{\pi}{\lambda_g} \frac{y^2}{R}} e^{jk_0 y \sin\theta} dy$$

It is shown in Appendix G-3 that E_{θ} for HE_{mn} mode can be derived as,

$$E_{\theta}(\theta) = F' k_r \frac{e^{-jk_0 r}}{r} \left(1 + \frac{k_r}{k_0} \cos\theta\right) \frac{a}{m\pi} \cdot \sqrt{\lambda_g R/2} \sin \frac{m\pi}{2} \cdot$$

$$\left[M \left\{ C(v_1) - C(v_2) - j [S(v_1) - S(v_2)] \right\} + N \left\{ C(v_3) - C(v_4) - j [S(v_3) - S(v_4)] \right\} \right]$$

where,

$$F' = jF H_p^{(2)'}(k_r R)$$

$$\begin{pmatrix} M \\ N \end{pmatrix} = e^{j \frac{\pi}{4} \lambda_g R} \left(\frac{2p\alpha_1}{\pi b_1} \pm \frac{2}{\lambda_0} \sin\theta \right)^2$$

(6.11)

$$\begin{pmatrix} v_1 \\ v_2 \end{pmatrix} = \sqrt{\frac{1}{2}} \left[\frac{b_1}{\sqrt{\lambda_g R}} \pm \sqrt{\lambda_g R} \left(\frac{2P\alpha_1}{\pi b_1} + \frac{2}{\lambda_0} \sin\theta \right) \right]$$

$$\begin{pmatrix} v_3 \\ v_4 \end{pmatrix} = \sqrt{\frac{1}{2}} \left[\frac{b_1}{\sqrt{\lambda_g R}} \pm \sqrt{\lambda_g R} \left(\frac{2P\alpha_1}{\pi b_1} - \frac{2}{\lambda_0} \sin\theta \right) \right]$$

The radiation pattern based on Eq (6.11) has been computed for the typical values of the test horn for HE₁₁ mode excitation, and the results are presented in Fig. 6.2.

6.2.3 THE AXIAL GAIN OF THE HORN

The total power P_t transmitted through the aperture of the horn can be obtained as,

$$\begin{aligned} P_t &= \frac{1}{2} \operatorname{Re} \left[\iint_S (\mathbf{E}_t \times \mathbf{H}_t^*) \cdot d\mathbf{s} \right] \\ &= \frac{1}{2} \operatorname{Re} \left[\iint_S E_\theta H_x^* dx dy \right], \text{ and from} \end{aligned}$$

Eqs. (6.4), P_t becomes,

$$P_t = \frac{1}{2} \frac{F'^2 k_r^3}{\omega \mu_0} \int_{-a/2}^{a/2} \cos^2 \frac{\pi x}{a} dx \int_{-b_1/2}^{b_1/2} \cos^2 \frac{2P\alpha_1}{b_1} y dy,$$

and can be derived by Appendix G-4 as,

$$P_t = \frac{1}{8} F'^2 k_r^3 \frac{ab_1}{\omega \mu_0} \left(\frac{2P\alpha_1 + \sin 2P\alpha_1}{2P\alpha_1} \right) \quad (6.12)$$

The on-axis gain (axial gain) is defined as,

$$G(0,0) = \frac{1}{2} \left| E_{\theta} \right|_{\max}^2 \frac{4\pi r^2}{\eta_0 P_t} \quad (6.13)$$

Using Eqs. (6.11) and (6.12), it is seen in Appendix G-4, that the on-axis gain can be obtained as,

$$G(0,0) = \frac{32aR \lambda_g^2 \left(1 + \frac{\lambda_0}{\lambda_g}\right)^2 2P\alpha_1}{m^2 \pi b_1 \lambda_0^3 (2P\alpha_1 + \sin 2P\alpha_1)} \cdot \left\{ [C(v_{o1}) - C(v_{o2})]^2 + [S(v_{o1}) - S(v_{o2})]^2 \right\} \quad (6.14)$$

where

$$\begin{pmatrix} v_{o1} \\ v_{o2} \end{pmatrix} = \sqrt{\frac{1}{2}} \left[\sqrt{\frac{b_1}{\lambda_g R}} + \sqrt{\lambda_g R} \left(\frac{2P\alpha_1}{\pi b_1} \right) \right]$$

The on-axis gain for the dominant HE_{11} mode is obtained as,

$$G(0,0) = \frac{32aR \lambda_g^2 \left(1 + \frac{\lambda_0}{\lambda_g}\right)^2}{\pi b_1 \lambda_0^3} \frac{2P_1 \alpha_1}{(2P_1 \alpha_1 + \sin 2P_1 \alpha_1)} \cdot \left\{ [C(v_{o1}) - C(v_{o2})]^2 + [S(v_{o1}) - S(v_{o2})]^2 \right\} \quad (6.15)$$

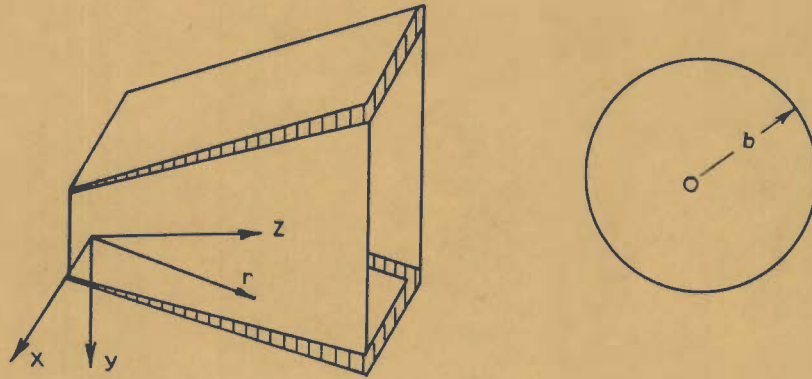
where P_1 = the value of P for the HE_{11} mode, and hence

$$\begin{pmatrix} v_{o1} \\ v_{o2} \end{pmatrix} = \frac{1}{\sqrt{2}} \left[\frac{b_1}{\sqrt{\lambda_g^R}} \pm \sqrt{\lambda_g^R} \left(\frac{2P_1 \alpha_1}{\pi b_1} \right) \right]$$

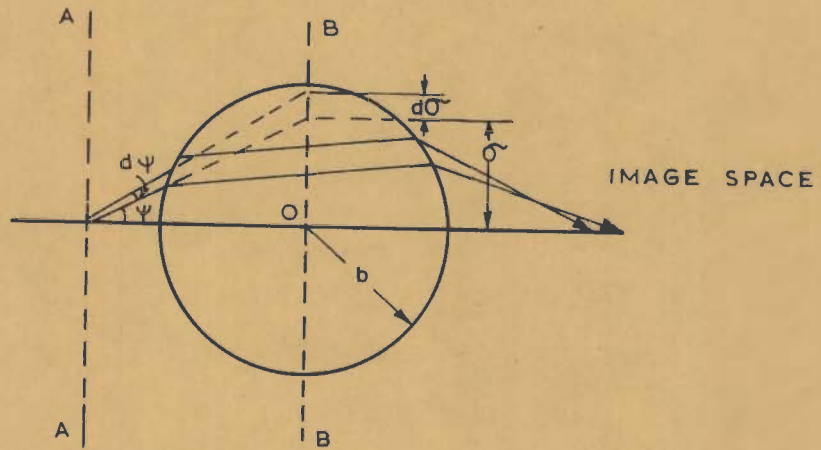
The gain based on Eq. (6.15) has been computed, and the result is shown in Fig.6.5.

6.2.4 DIELECTRIC SPHERE MOUNTED DIELECTRIC COATED E -PLANE SECTORAL HORN [72]

The radiation patterns of the dielectric loaded E -plane sectoral horn have been found to possess better directivity as compared to that of an empty horn of the same dimensions, but at the cost of a slight deterioration in the sidelobe levels. In order to reduce the sidelobe levels, and to increase the directivity of the horn further, the technique of placing dielectric spheres in front of, but displaced from, the aperture of the dielectric loaded E -plane sectoral horn was utilised. The radiation characteristics of the feed system (Fig. 6.3) with dielectric sphere of radius 'b' in front of the horn aperture, are derived by treating the system as a microwave lens illuminated by an aperture source. Accordingly, following the method due to Bakefi and Farnel[9] the approximate expressions for the far-field components of the feed system can be obtained, with assumed azimuthal symmetry, as



a_ Off-set dielectric sphere in front of coated horn aperture



- AA - AN ARBITRARY PLANE IN FRONT OF THE HORN APERTURE
- BB - AN EQUIVALENT PLANE THROUGH THE CENTRE OF THE SPHERE

b_ Equivalent optical system for Fig.6.3 a

FIG. 6.3 - DIELECTRIC SPHERE LOADED DIELECTRIC COATED E-PLANE SECTORAL HORN

$$\begin{aligned} \square_{\theta}(\theta) = j(k_0 b)^2 \frac{e^{-jk_0 r}}{k_0 r} \int_0^{\pi} u_i^{\theta}(\sigma) J_0(k_0 b \sigma \sin\theta) \\ e^{-jk_0 v(\sigma)} \sigma d\sigma \end{aligned} \quad (6.16)$$

for vertical plane, and

$$\begin{aligned} \square_{\phi}(\theta) = j(k_0 b)^2 \frac{e^{-jk_0 r}}{k_0 r} \int_0^{\pi} u_i^{\phi}(\sigma) J_0(k_0 b \sigma \sin\theta) \\ e^{-jk_0 v(\sigma)} \sigma d\sigma \end{aligned} \quad (6.17)$$

for horizontal plane,

where $u_i^{\theta}(\sigma)$ and $u_i^{\phi}(\sigma)$ are as specified in Sec. 3.4.1. It is to be noted that in the case of dielectric coated E-plane sectoral horn, the edge diffraction will be minimum; and hence field patterns at the sphere location that is slightly displaced from the horn aperture is the same as that at the horn aperture [72]. Thus the field incident on the sphere can be taken as the same as the transverse E-field $E_t (\approx E_0)$ over the horn aperture given by Eq. (6.9). On this assumption the radiation patterns are evaluated, and are presented in Fig. 6.3b.

6.2.5 EXPERIMENTAL RESULTS AND COMPARISON WITH THEORY

In order to evaluate the performance of the dielectric loaded E-plane sectoral horn; and to establish

the validity of equations derived, experiments were carried out with a horn of the specifications detailed in Fig. 6.1. The narrow (E-plane) walls of the horn were loaded with bakelite ($\epsilon_r = 3.55$) for an angular thickness of 2° ($\alpha_1 = 17^\circ$, $\delta = 3\text{mm}$). Observations were made for the horn excited in the HE_{11} mode at a frequency of 8.86 GHz. Analytical results of the radiation pattern based Eq. (6.11) are established in reasonable agreement with the experimental pattern in Fig. 6.2. (The experimental pattern for the empty E-plane sectoral horn is also included for comparison). There is a considerable improvement in the pattern directivity, but with raised sidelobe levels. In an effort to reduce the sidelobe levels, experiments were repeated with paraffin wax ($\epsilon_r = 2.25$) spheres of diameter 4 cm, 6 cm and 9 cm placed offset at the minimum [68], [85] input VSWR position in front of the dielectric coated horn aperture. (The sphere off-set positions were found to lie between 1 cm and 1.4 cm from the horn aperture for the 3 sphere sizes tested, and the input VSWR for the off-set spheres were found to be 1.2, 1.15 and 1.1). The experimental radiation patterns with off-set placed dielectric spheres are presented in Fig. 6.4a and in Fig. 6.4b the theoretical pattern based on Eq. (6.16) is established in good agreement with experimental results on pattern measurements. In Fig. 6.5a is depicted the gain (experimental) of the system as a function of the off-set placed dielectric

sphere diameter in wave length. The gain level based on Eq. (6.15) is also shown in Fig. 6.5a. The decrease in -3 dB beamwidth due to the sphere mounting is plotted in Fig. 6.5b as a function of sphere diameter in wave length.

From the results it is concluded that the dielectric loaded E -plane sectoral horns have significantly increased directivity at the cost of slightly increased sidelobe levels. The radiation characteristics of the dielectric loaded E -plane sectoral horn can be improved with reduced sidelobes and further increased directivity and axial gain by dielectric spheres mounted at, but displaced from, the horn aperture. The test feed system with off-set placed spheres provides a variable beamwidth facility and hence indicates the applicability of this system as an adaptive beam parabolic antenna feed. The system also possesses low input VSWR.

6.3 DIELECTRIC LOADED H-PLANE SECTORAL HORN WITH CYLINDRICAL APERTURE

In this section radiation properties of a H -plane sectoral horn with cylindrical aperture having dielectric loading on the parallel walls of the horn are described. The concept of this improved sectoral horn feed is based on the facts that horns with dielectric loaded walls [50]

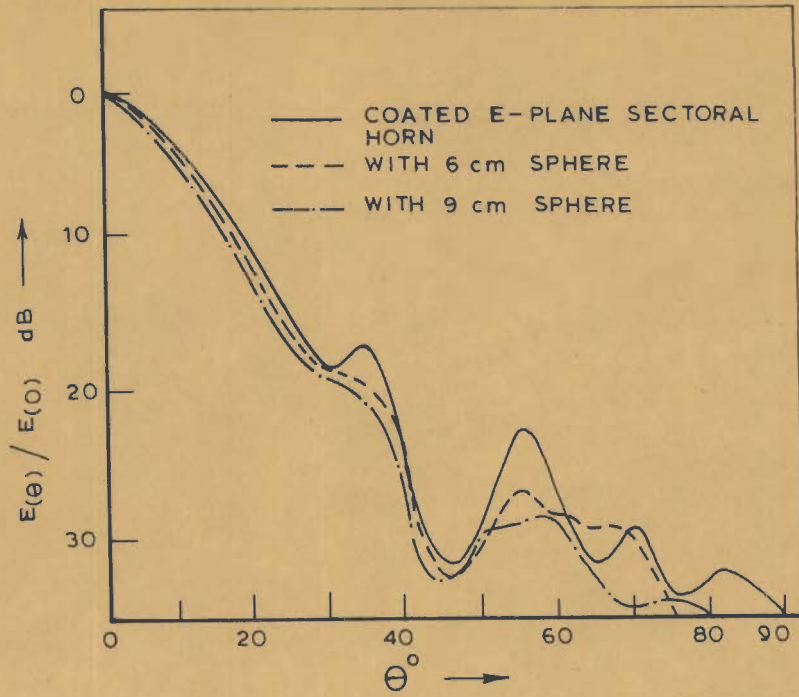


FIG. 6.4a_RADIATION PATTERN FOR DIELECTRIC SPHERE LOADED DIELECTRIC COATED E-PLANE SECTORAL HORN

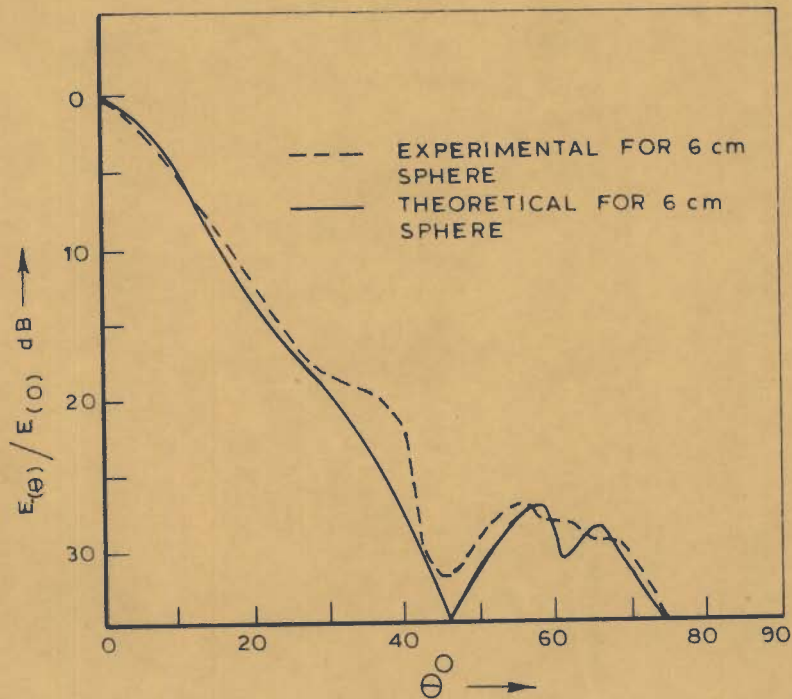


FIG.6.4b_RADIATION PATTERNS (DIELECTRIC SPHERE LOADED DIELECTRIC COATED E-PLANE SECTORAL HORN)

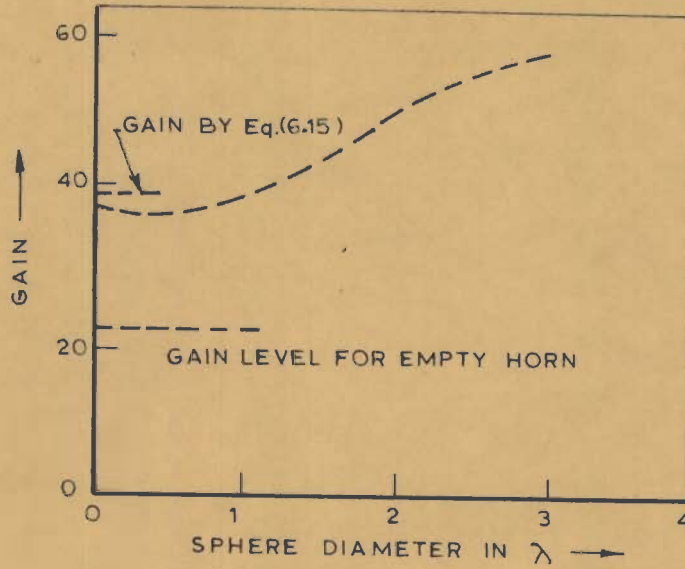


FIG.6.5a_GAIN VS SPHERE DIAMETER FOR SPHERE LOADED DIELECTRIC COATED E-PLANE SECTORAL HORN

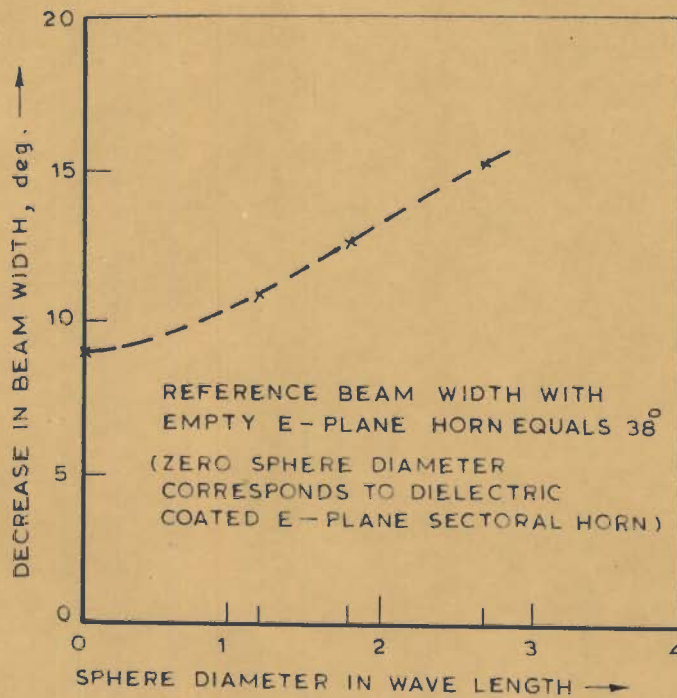


FIG.6.5b_DECREASE IN BEAM WIDTH VS SPHERE DIAMETER FOR DIELECTRIC SPHERE LOADED DIELECTRIC COATED E-PLANE SECTORAL HORN

have increased directivity; and that horns with cylindrical apertures [133] have narrower beamwidths and lower sidelobes than identical horns with rectangular apertures. Here the horn aperture field is determined in terms of cylindrical wave functions. The aperture field method based on the vector diffraction formula is used to obtain the far-field radiation patterns. The characteristic equation for the propagation phase constant k_r , and the on-axis gain of the antenna device are also included. The performance of this antenna has been evaluated experimentally to establish good agreement with theoretical results. It is found that the dielectric loaded H -plane sectoral horn with cylindrical aperture has radiation patterns with significantly increased directivity, and reduced sidelobe levels that are otherwise raised with dielectric coated conventional horns. The improved radiation patterns of this sectoral horn ensure its applicability as a desirable effective feed for parabolic reflector antennas. The analytical treatment for the case of wide flare angle sectoral horns has also been discussed.

6.3.1 MODAL FIELDS IN DIELECTRIC LOADED SMALL FLARE ANGLE H-PLANE SECTORAL HORN

The geometry of the H-plane sectoral horn with circular edges centered along the apex is shown in Fig.6.6.

The parallel walls of the horn are loaded with a dielectric material of permittivity ϵ_1 . Hybrid modes (having both E and H components in the direction of propagation) are to exist, in order to satisfy the boundary conditions. TE to θ modes will have both E_r and H_r components, and such hybrid mode fields can be given by an electric vector potential \bar{F} having a single component in the θ -direction such that $\bar{F} = \bar{i}_\theta \Psi$. The proper forms of Ψ for the horn axial and dielectric loaded regions respectively are given by

$$\Psi_o = A_n \cos k_{yo} y \cos p\theta H_p^{(2)}(k_r r) \quad (6.18)$$

$$\Psi_d = B_n \cos k_{yd} \left(\frac{a}{2} - y \right) \cos p\theta H_p^{(2)}(k_r r)$$

where p is positive and real, and A_n and B_n are mode coefficients to be determined from the boundary conditions. The subscripts 'o' and 'd' refer to the air (horn axial region) and the dielectric layered regions respectively. In selecting Ψ_o and Ψ_d , it is anticipated that the r and θ variations in both the regions must be the same (designated by p). The 'k' in each region must, of course, satisfy the separation relationships,

$$\begin{aligned} k_r^2 + k_{yo}^2 &= k_o^2 = \omega^2 \mu_o \epsilon_o \\ k_r^2 + k_{yd}^2 &= k_1^2 = \omega^2 \mu_o \epsilon_1 \end{aligned} \quad (6.19)$$

Different field components of the hybrid mode in the dielectric coated region are obtained as

$$\begin{aligned}
 E_{rd} &= B_n k_{yd} \sin k_{yd} \left(\frac{a}{2} - y \right) \cos p \theta H_p^{(2)}(k_r r) \\
 E_{yd} &= -B_n k_r \cos k_{yd} \left(\frac{a}{2} - y \right) \cos p \theta H_p^{(2)'}(k_r r) \\
 E_{\theta d} &= 0 \\
 H_{rd} &= - \frac{p k_r B_n}{j \omega \mu_0} \cos k_{yd} \left(\frac{a}{2} - y \right) \sin p \theta H_p^{(2)'}(k_r r) \\
 H_{yd} &= -p \frac{k_{yd} B_n}{j \omega \mu_0} \sin k_{yd} \left(\frac{a}{2} - y \right) \sin p \theta H_p^{(2)}(k_r r) \\
 H_{\theta d} &= \frac{k_1^2 - p^2}{j \omega \mu_0} B_n \cos k_{yd} \left(\frac{a}{2} - y \right) \cos p \theta H_p^{(2)}(k_r r)
 \end{aligned} \tag{6.20}$$

The corresponding field components in axial region of the horn are obtained as

$$\begin{aligned}
 E_{r_0} &= -k_{y_0} A_n \sin k_{y_0} y \cos p \theta H_p^{(2)}(k_r r) \\
 E_{y_0} &= -k_r A_n \cos k_{y_0} y \cos p \theta H_p^{(2)'}(k_r r) \\
 E_{\theta_0} &= 0 \\
 H_{r_0} &= - \frac{p k_r}{j \omega \mu_0} A_n \cos k_{y_0} y \sin p \theta H_p^{(2)'}(k_r r)
 \end{aligned} \tag{6.21}$$

$$H_{y_0} = \frac{pk_{y_0}}{j\omega\mu_0} \Lambda_n \sin k_{y_0} y \cos p\theta H_p^{(2)}(k_r r)$$

$$H_{\theta_0} = \frac{1}{j\omega\mu_0} (k_0^2 - p^2) \Lambda_n \cos k_{y_0} y \cos p\theta H_p^{(2)}(k_r r)$$

where the primes indicate differentiation with respect to r .

The eigen values can be determined from the boundary condition

$$E_{rd} = E_{yd} = 0 \text{ at } \theta = \pm \alpha_0, \text{ the half flare angle of the horn, i.e. } \cos p\alpha_0 = 0; P = \frac{n\pi}{2\alpha_0} \quad (n = 1, 3, 5, \dots)$$

For the dominant HE_{11} mode, P becomes

$$P = \frac{\pi}{2\alpha_0} \quad (6.22)$$

To evaluate the constants Λ_n and B_n , and the mode propagation constant k_r , continuity of tangential E - and H -fields at the air-dielectric interface has been used.

Accordingly

$$i) \quad E_{r_0} = E_{rd} \text{ at } y = \frac{a}{2} - s \quad (s \text{ being the thickness of the dielectric layer})$$

gives,

$$k_{y_0} \Lambda_n \sin k_{y_0} \left(\frac{a}{2} - s \right) = B_n k_{y_d} \sin k_{y_d} s \quad (6.23)$$

$$ii) \quad H_{r_0} = H_{rd} \quad , \text{ and}$$

$$H_{\theta_0} = H_{\theta d} \text{ at } y = \frac{a}{2} - s \text{ give}$$

$$A_n \cos k_{y0} \left(\frac{a}{2} - s \right) = B_n \cos k_{yd} s \quad (6.24)$$

From Eqs. (6.23) and (6.24) it is obtained as,

$$k_{y0} \tan k_{y0} \left(\frac{a}{2} - s \right) = - k_{yd} \tan k_{yd} s \quad (6.25)$$

But both k_{y0} and k_{yd} are functions of k_r by Eqs. (6.19). So the above equation [Eqs.(6.25)] is a transcendental equation for determining possible k_r 's (mode propagation constants). Once k_r is evaluated, k_{y0} and k_{yd} are given by Eq. (6.19), and the ratio A_n/B_n may be obtained either from Eq. (6.23) or from Eq. (6.24).

An explicit relationship between k_{y0} and k_{yd} can be obtained by considering the case of thin layer of dielectric coating with low permittivity dielectric material. In such case, k_0 is not very different from k_1 ($= \omega \sqrt{\mu_0 \epsilon_1}$); and k_{y0} and k_{yd} should be small. If this is so, then Eq. (6.25) can be approximated by

$$k_{y0}^2 \left(\frac{a}{2} - s \right) = - k_{yd}^2 s \quad (6.26)$$

With this explicit relationship between k_{y0} and k_{yd} , Eqs. (6.19) can be solved simultaneously for k_{y0} and k_r for given values of frequency (or ω). Note that when k_{y0} is real, k_{yd} is imaginary and vice versa.

An explicit solution for k_{y0} can be obtained by

using Eqs. (6.19) and (6.26), and is derived as, (see Appendix H-1)

$$k_{y_0}^2 = -k_0^2 (\epsilon_r - 1) \frac{2s}{a} \quad (6.27)$$

where s = the thickness of the dielectric layer

a = the E -plane dimension of the horn

6.3.2 RADIATION FIELD

The radiated far-field by the device can be computed by the aperture field method based on the vector diffraction formula [44] ; and accordingly the radiation pattern in the H -plane ($\phi=0$) for the dielectric loaded horn under study is given by,

$$\begin{aligned} E_{\phi}(\theta) &= j \frac{e^{-jk_0 r}}{2\lambda_0 r} \left(1 + \frac{k_r}{k_0} \cos\theta\right) \iint_S \bar{E}_t e^{jk_0 R \cos(\theta_s - \theta)} ds \\ &= j \frac{e^{-jk_0 r}}{2\lambda_0 r} \left(1 + \frac{k_r}{k_0} \cos\theta\right) \int_{-a/2}^{a/2} \int_{-\alpha_0}^{\alpha_0} \bar{E}_t e^{jk_0 R \cos(\theta_s - \theta)} dy_s R d\theta_s \end{aligned} \quad (6.28)$$

Where \bar{E}_t = the transverse electric field over the horn aperture $\approx \hat{i}_y E_y$ since $E_{\theta} \approx E_x = 0$ over the horn aperture and R = the horn axial length (for small angle horn, the horn flare length $r_0 \approx R$). θ_s is indicated in Fig. 6.6.

It is shown in Appendix H-2 that the radiation pattern in the H-plane ($\phi = 0$) for the horn under study when excited in the dominant HE_{11} mode is derived as,

$$E_{\phi}(\theta) = jE_1 \frac{e^{-jk_0 r}}{\lambda_0 r} \left(1 + \frac{k_r}{k_0} \cos\theta\right) R \sqrt{\lambda_0/2R} \frac{\text{sinc}_{y_0} \frac{a}{2}}{k_{y_0}} \cdot$$

$$\left[e^{j \frac{\pi}{2\alpha_0} \theta} \left\{ C(u_1) - C(u_2) - j [S(u_1) - S(u_2)] \right\} + e^{-j \frac{\pi}{2\alpha_0} \theta} \left\{ C(v_1) - C(v_2) - j [S(v_1) - S(v_2)] \right\} \right] \quad (6.29)$$

where $E_1 = A_1 k_r \frac{H^{(2)'}}{2\alpha_0} (k_r R) e^{j(k_0 R + \frac{\pi}{4} \frac{\lambda_0}{R} \frac{1}{4\alpha_0^2})}$

$C(w)$ and $S(w)$ are the cosine and sine Fresnel integrals,

$$u_1 = \left(\alpha_0 - \theta - \frac{\lambda_0}{4\alpha_0 R} \right) \sqrt{2R/\lambda_0}$$

$$u_2 = \left(-\alpha_0 - \theta - \frac{\lambda_0}{4\alpha_0 R} \right) \sqrt{2R/\lambda_0}$$

$$v_1 = \left(\alpha_0 - \theta + \frac{\lambda_0}{4\alpha_0 R} \right) \sqrt{2R/\lambda_0}$$

$$v_2 = \left(-\alpha_0 - \theta + \frac{\lambda_0}{4\alpha_0 R} \right) \sqrt{2R/\lambda_0}$$

($P = \frac{\pi}{2\alpha_0}$ has been used for HE_{11} mode)

The H -plane pattern based on Eq. (6.29) has been computed for typical test values; and the results are illustrated in Fig. 6.7 b .

6.3.3 AXIAL GAIN OF THE HORN

The total power P_t transmitted through the cylindrical aperture of the horn is obtained as

$$P_t = \frac{1}{2} \operatorname{Re} \int_{-a/2}^{a/2} \int_{-\alpha_0}^{\alpha_0} \frac{E_t^2}{\eta_0} dy R d\theta_s \quad (6.30)$$

For HE_{11} mode of excitation P_t is derived (see Appendix H-3) as,

$$P_t = \frac{1}{4\eta_0} R \alpha_0 \left[A_1 k_r \frac{H^{(2)'}}{2\alpha_0} (k_r R) \right]^2 \left(a + \frac{\operatorname{sinc} k_{y_0} a}{k_{y_0}} \right) \quad (6.31)$$

$$= \frac{E_2^2}{4\eta_0} R \alpha_0 \frac{(k_{y_0} a + \operatorname{sinc} k_{y_0} a)}{k_{y_0}} \quad (6.32)$$

where $E_2 = A_1 k_r \frac{H^{(2)'}}{2\alpha_0} (k_r R) = |E_1|$

The on-axis gain associated with the radiating horn is defined as

$$G(0,0) = \frac{1}{2\eta_0} \left| E_{\theta} \right|_{\max}^2 \frac{4\pi r^2}{P_t}$$

Using Eqs. (6.29) and (6.32) it is seen in Appendix H-3 that the gain for the HE_{11} mode is derived as,

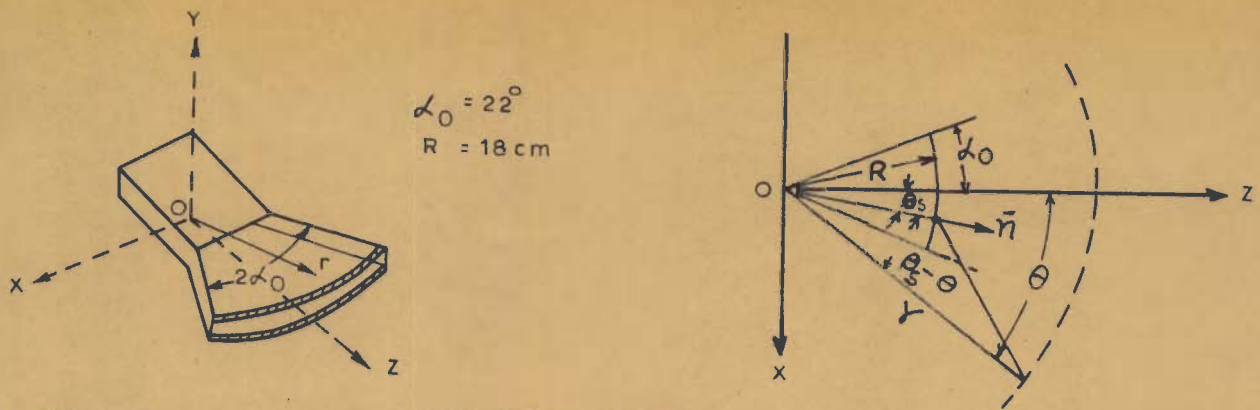


FIG. 6.6 GEOMETRY OF DIELECTRIC LOADED SECTORAL HORN WITH CYLINDRICAL APERTURE

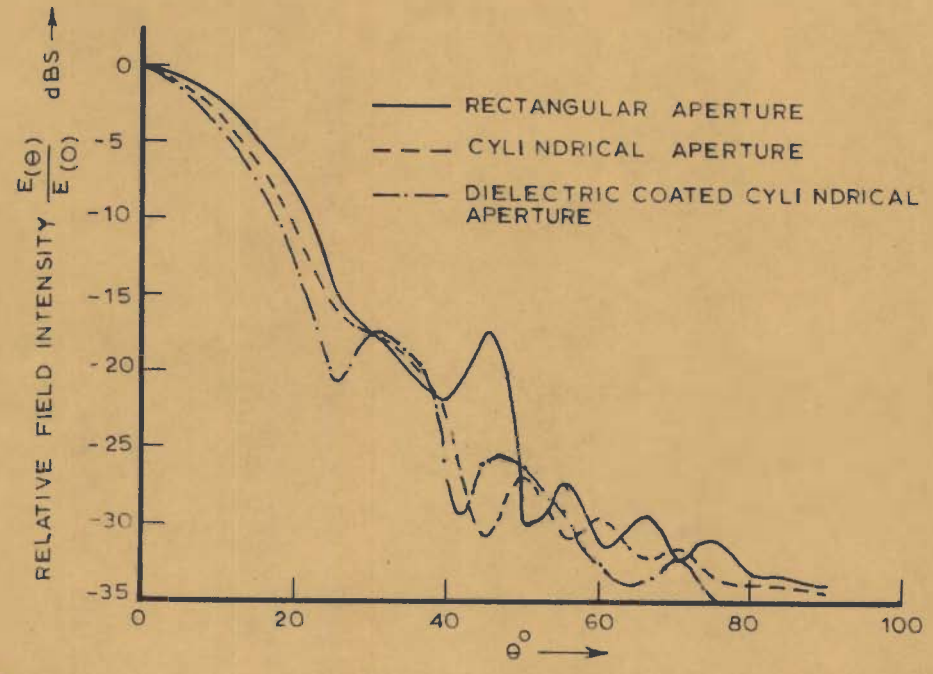


FIG. 6.7a E-PLANE PATTERN OF DIELECTRIC COATED H-PLANE SECTORAL HORN

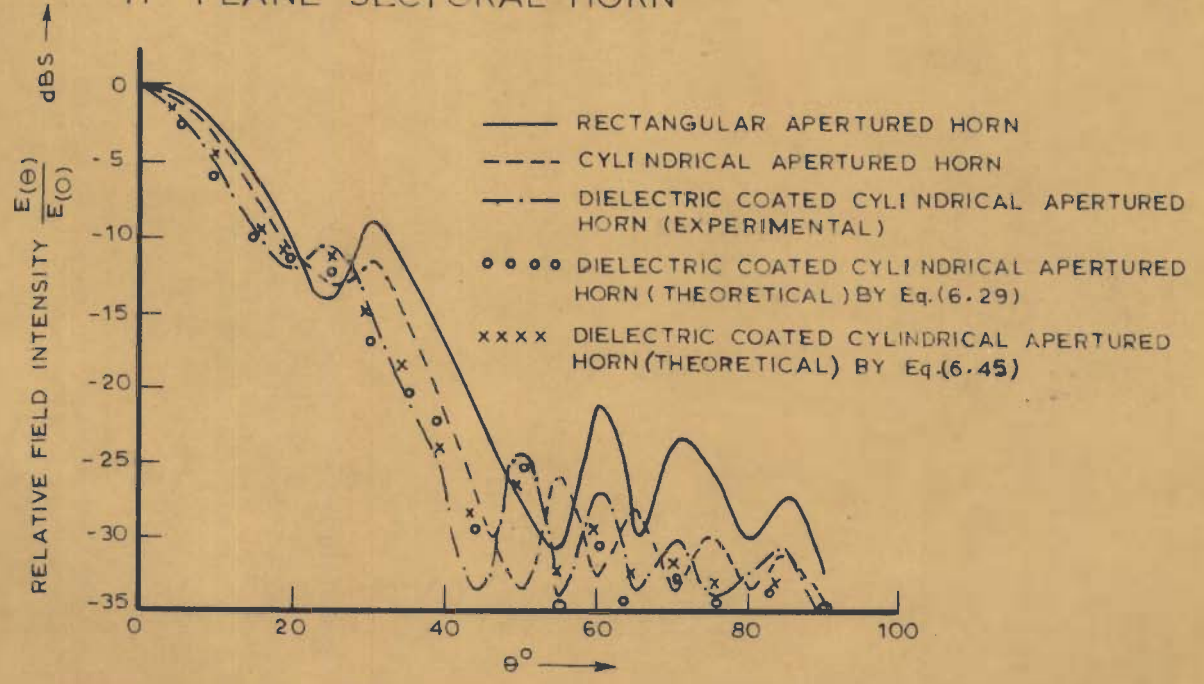


FIG. 6.7b H-PLANE PATTERN OF DIELECTRIC COATED H-PLANE SECTORAL HORN

$$G(0,0) = \frac{16\pi \left(1 + \frac{k_r}{k_o}\right)^2 \sin^2 k_{yo} \frac{a}{2}}{\alpha_o \lambda_o k_{yo} (k_{yo} a + \sin k_{yo} a)} \cdot \left\{ [c(v_{o1}) - c(v_{o2})]^2 + [s(v_{o1}) - s(v_{o2})]^2 \right\} \quad (6.33)$$

where

$$\begin{pmatrix} v_{o1} \\ v_{o2} \end{pmatrix} = \left(\frac{\lambda_o}{4\alpha_o R} \pm \alpha_o \right) \sqrt{2R/\lambda_o}$$

The computed value of the gain based on this Eq. (6.33) is found to be in agreement with the experimental value.

6.3.4 RADIATION FROM A WIDE FLARE ANGLE DIELECTRIC LOADED H-PLANE SECTORAL HORN

The radiation formula given by Eq. (6.29), employing the vector diffraction formula with the assumption of no phase variation of the aperture field is true only for narrow flare angle horns with $\alpha_o < 20^\circ$. Thus the above referred radiation pattern expression is not accurate for wide flare horns with $\alpha_o > 30^\circ$. Analysis of the radiation from such wide flare horns ($\alpha_o > 30^\circ$) has been carried out in this section using a different technique. The technique consists in expressing the far-field pattern of the wide angle horn in terms of a spectrum of cylindrical waves, or in other words free space cylindrical TE and TM

modes [52], the mode coefficients being determined from the known aperture fields.

The co-ordinate system employed for the analysis is shown in Fig. 6.6 The aperture E -field over a constant phase cylindrical surface at the mouth of the horn is represented by

$$\begin{aligned} E_y &= E_y(R, \theta, y) && \text{for } -\frac{a}{2} \leq y \leq \frac{a}{2} \text{ and} \\ E_\theta \quad (\quad E_x) &= E_\theta(R, \theta, y) && -\alpha_0 \leq \theta \leq \alpha_0 \end{aligned} \quad (6.34)$$

$E_y, E_\theta = 0$ every where else.

Expression for the far-field is derived in terms of the tangential components of E over the horn aperture. Anticipating the use of transforms of the fields, cylindrical transforms of the tangential components of E over the horn aperture are defined [52] as

$$\begin{aligned} \bar{E}_y(n, w) &= \frac{1}{2\pi} \int_0^\pi d\theta \int_{-\infty}^\infty dy E_y(R, \theta, y) e^{-jn\theta} e^{-jwy} \\ \bar{E}_\theta(n, w) &= \frac{1}{2\pi} \int_0^\pi d\theta \int_{-\infty}^\infty dy E_\theta(R, \theta, y) e^{-jn\theta} e^{-jwy} \end{aligned} \quad (6.35)$$

The inverse transformation is

$$E_y(R, \theta, y) = \frac{1}{2\pi} \sum_{n=-\infty}^{\infty} e^{jn\theta} \int_{-\infty}^{\infty} \bar{E}_y(n, w) e^{jwy} dw \quad (6.36)$$

$$E_\theta(R, \theta, y) = \frac{1}{2\pi} \sum_{n=-\infty}^{\infty} e^{jn\theta} \int_{-\infty}^{\infty} \bar{E}_\theta(n, w) e^{jwy} dw$$

Note that these are Fourier series on θ and Fourier integrals on y . The field external to the horn aperture can be expressed as the sum of TE and TM components, and the diffracted far-field corresponding to the aperture fields [Eqs.(6.34)] may be expressed in terms of vector potentials $\bar{A} = \bar{i}_\theta A_\theta$, and $\bar{F} = \bar{i}_\theta F_\theta$. The proper forms of A_θ and F_θ for the Fourier expansion [52, p.247]

$$A_\theta = \frac{1}{2\pi} \sum_{n=-\infty}^{\infty} e^{jn\theta} \int_{-\infty}^{\infty} f_n(w) H_n^{(2)}(r \sqrt{k_0^2 - w^2}) e^{jwy} dw \quad (6.37)$$

$$F_\theta = \frac{1}{2\pi} \sum_{n=-\infty}^{\infty} e^{jn\theta} \int_{-\infty}^{\infty} g_n(w) H_n^{(2)}(r \sqrt{k_0^2 - w^2}) e^{jwy} dw$$

In Eqs. (6.37) $H_n^{(2)}(x)$ is chosen to represent the outward travelling waves, and the θ - and y - functions are so chosen that the field will be of the same form as in Eqs. (6.36).

Using the identities [52, pp.244-45]

$$\int_{-\infty}^{\infty} H_0^{(2)}(r \sqrt{k_0^2 - w^2}) e^{jwy} dw \xrightarrow{r \rightarrow \infty} 2j \frac{e^{-jk_0 r}}{r}$$

and

$$H_0^{(2)}(x) \xrightarrow{x \rightarrow \infty} j^n H_0^{(2)}(x), \text{ for the far-zone region}$$

A_θ and F_θ can also be expressed as,

$$A_\theta = \frac{e^{-jk_0 r}}{\pi r} \sum_{n=-\infty}^{\infty} e^{jn\theta} j^{n+1} f_n(w) \quad (6.38)$$

$$F_\theta = \frac{e^{-jk_0 r}}{\pi r} \sum_{n=-\infty}^{\infty} e^{jn\theta} j^{n+1} g_n(w)$$

where $f_n(w)$ and $g_n(w)$ are the mode coefficients and can be determined from the known aperture fields. $f_n(w)$ and $g_n(w)$ can be determined by calculating the fields E_y and E_θ [Eqs.(6.34)] using the relationships,

$$E = -\nabla \times F - j\omega \mu_0 A + \frac{1}{j\omega \epsilon_0} \nabla (\nabla \cdot A) \quad (6.39)$$

$$H = \nabla \times A - j\omega \epsilon_0 F + \frac{1}{j\omega \mu_0} \nabla (\nabla \cdot F)$$

It is seen in Appendix H-4 that $f_n(w)$ and $g_n(w)$ are obtained as,

$$f_n(w) = \frac{j\omega \epsilon_0 \bar{E}_\theta(n,w)}{(k_0^2 - w^2) H_n^{(2)}(R \sqrt{k_0^2 - w^2})}$$

$$g_n(w) = \frac{[\bar{E}_y(n,w) + \frac{nw}{R(k_0^2 - w^2)} \bar{E}_\theta(n,w)]}{\sqrt{k_0^2 - w^2} H_n^{(2)'}(R \sqrt{k_0^2 - w^2})} \quad (6.40)$$

Here $\bar{E}_y(n,w)$ and $\bar{E}_\theta(n,w)$ are the cylindrical transforms of the aperture field components E_y and E_θ respectively, and $w = -k_y = -k_o \sin\theta \sin\phi$ (6.41)

For the evaluation of the radiation pattern of the dielectric loaded test horn in the H -plane, it is observed that in the H -plane ($\phi = 0$) $w = 0$, and by Eq. (6.21), $E_\theta(R,\theta,y) = 0$,

$$E_y(R,\theta,y) = -k_r A_n \cos k_{y0} y \cos \theta H_p^{(2)}(k_r R) ; \quad (6.42)$$

and by Eq. (6.40)

$$f_n(w) = 0 \quad \text{and}$$

$$g_n(w) = \frac{\bar{E}_y(n,w)}{k_o H_n^{(2)'}(k_o R)} \quad (6.43)$$

The required radiation pattern in the H-plane is obtained by using the formula [52, p -133]

$$E_\theta(\theta) = + j k_o F_\theta \quad (6.44)$$

It is seen in Appendix H-4 that, using Eqs. (6.35), (6.42) and (6.44), the H -plane radiation pattern of the dielectric loaded H -plane sectoral horn with cylindrical aperture supporting the HE_{11} mode can be derived as,

$$E_{\phi}(\theta) = \frac{e^{-jk_0 r}}{\pi r} \frac{2E_2}{\pi p} \frac{\text{sinc}_{y_0} \frac{a}{2}}{k_{y_0}} \sum_{n=-\infty}^{\infty} j^n e^{jn\theta} \cdot \frac{\cos n\alpha_0}{(1 - \frac{n^2}{p^2})} \frac{1}{H_n^{(2)'}(k_0 R)} \quad (6.45)$$

where

$$E_2 = \frac{k_r A_1 H_n^{(2)'}(k_r R)}{\pi/2\alpha_0}$$

and

$$p = \frac{\pi}{2\alpha_0}$$

Knowing all the quantities involved, Eq.(6.45) can be used for the accurate evaluation of the H- plane radiation pattern of the dielectric coated H -plane sectoral horn of wide flare angle. The computed results based on Eq. (6.45) is shown in Fig. 6.7a.

6.3.5 EXPERIMENTAL RESULTS AND VERIFICATION WITH THEORY

The validity of the theoretical results derived above is established by experimental investigations using a H -plane sectoral horn of half flare angle $\alpha_0 = 22^\circ$ and axial length $R = 18$ cm, having a circular aperture centered along the horn apex. The parallel walls of the horn was loaded with 0.1 mm thick mica ($\epsilon_r = 7.1$) sheets; and experiments

were carried out with the horn excited in the HE_{11} mode at an operating frequency of 9.64 GHz. Analytical results of the H-plane pattern of the device based on Eq. (6.29) and Eq. (6.45) are compared with the experimental results in Fig. 6.7b (Patterns for circular apertured horn and conventional horn with rectangular aperture are also included for comparison). Reasonable agreement was noticed between calculated and measured patterns. The agreement is more close with calculations based on Eq. (6.29) since the experimental horn was of $\alpha_0 = 22^\circ$. Excellent agreement with results based on Eq. (6.45) would be noticed with test horns of $\alpha_0 > 30^\circ$.

In Fig. 6.7a the E-plane pattern of the dielectric coated horn with circular aperture is depicted together with those for circular apertured and rectangular apertured horns without dielectric loading. It is obvious that the pattern directivity of the dielectric coated horn has significantly increased, and the sidelobe level, though slightly higher than that with circular apertured horn, is reduced considerably as compared with that available in the case of an empty and dielectric loaded conventional sectoral horn with rectangular aperture. Thus the circular aperture has contributed to bring down the probable sidelobe levels. The theoretical value of gain based on Eq. (6.33)

and the experimental value of gain are found approximately equal being 30.5 and 31 respectively.

From the results presented, it may be concluded that dielectric loaded H -plane sectoral horns with cylindrical apertures have patterns with significantly increased directivity and reduced probable sidelobe levels. Since the theory is in satisfactory agreement with experiments, the dielectric loaded sectoral horn with circular aperture can either be used as a desirable improved primary feed for parabolic reflector antennas or as an effective and convenient high directivity source of microwave radiation.

6.4 CONCLUSION

The radiation behaviour of two types of dielectric loaded sectoral horns has been discussed in detail. The radiation patterns of the dielectric loaded E -plane sectoral horn are seen to have more directivity and axial gain at the cost of slightly increased sidelobe levels as compared to those of conventional horns of the same dimensions. The effect of dielectric sphere mounting at a displaced position in front of the aperture of the dielectric loaded E -plane sectoral horn has been investigated to establish that sphere loading resulted

in reducing sidelobe levels as well as narrowing the main beam. The H -plane sectoral horn with a cylindrical aperture having suitable dielectric loading on the parallel walls has been found to possess more directivity, and reduced sidelobes that are generally high with dielectric loading, due to the circular aperture. The analytical treatment has been carried out for both narrow flare angle as well as wide flare angle H -plane sectoral horns. Analytical results obtained for both the dielectric loaded E -plane sectoral horn, and H -plane sectoral horn with cylindrical aperture have been established in good agreement with experimental results.

CHAPTER VII

DIELECTRIC LOADED MULTIMODE HORNS

7.1 INTRODUCTION

The technique of combining higher order modes for improving the radiation patterns of dielectric loaded horn antennas has been discussed in this chapter. Two types of dielectric loaded multimode horn antennas are considered. A multimode dielectric loaded rectangular horn antenna operating in two orthogonal $TE_{10}+TE/TM_{12}$ and $TE_{01}+TE/TM_{21}$ mode sets is analysed first. Due to the presence of the higher order TE/TM modes generated by a symmetric step discontinuity in an oversized waveguide the aperture E -field distribution is tapered to result in a low polarization axial ratio, and a pattern with low sidelobes. Thus the dielectric loaded multimode rectangular horn antenna analysed is found to generate a circularly polarized elliptical shaped beam with better directivity and low sidelobes, and can be used as a satellite antenna to efficiently illuminate an elliptical zone on the earth's surface. Then a dielectric loaded rectangular horn that possesses the facility of shaping its

radiation pattern by suitably combining a controlled amount of higher order modes with the dominant mode has been studied. The wanted hybrid modes are generated by a suitable symmetric horn throat excitation, and the amplitudes of higher order mode content are controlled by the throat dimensions. The significance of higher order mode contents in shaping the pattern of dielectric loaded horn is theoretically demonstrated, and the device has been suggested for applications in monopulse radar antenna systems. The performances of both these dielectric loaded multimode horn antennas have been evaluated experimentally and have been established in good agreement with theoretical results.

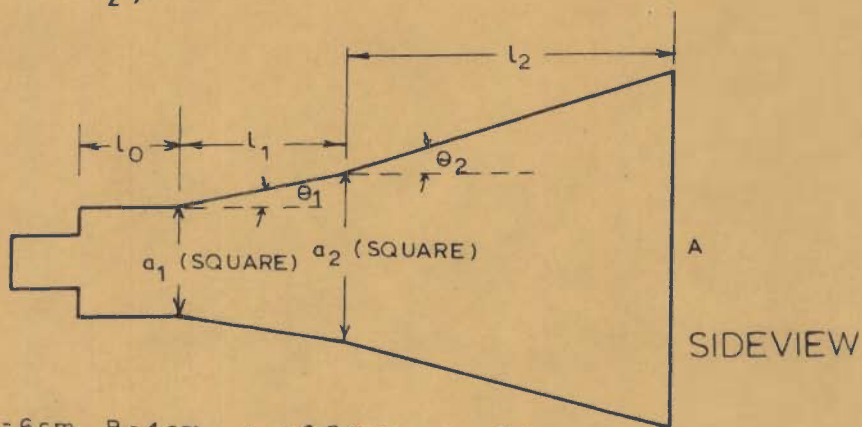
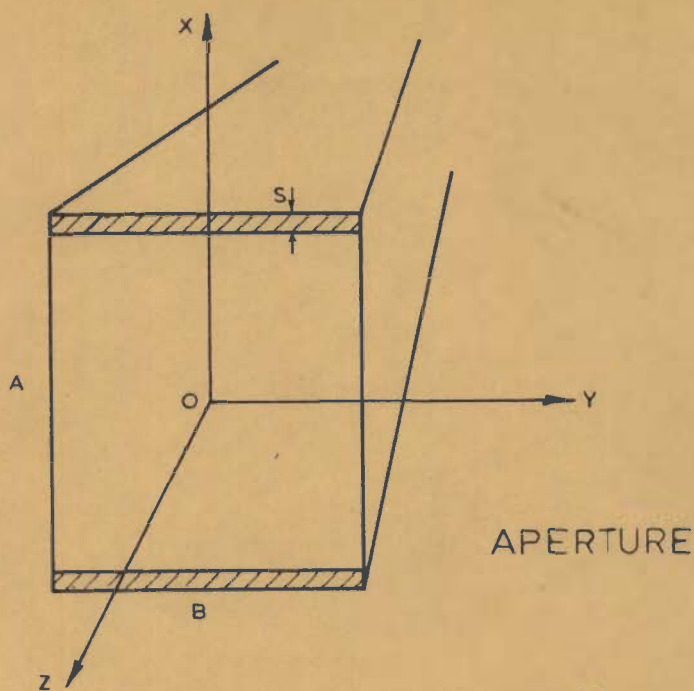
7.2 MULTIMODE DIELECTRIC LOADED RECTANGULAR HORN ANTENNA

A high gain multimode dielectric coated rectangular horn antenna operating in two orthogonal $TE_{10}+TE/TM_{12}$ and $TE_{01}+TE/TM_{21}$ mode sets to generate circularly polarized elliptical beam is described in this section. The presence of higher order TE/TM modes will cause a tapered aperture E -field distribution and this in turn will make the far-field E -plane beamwidth approximately equal to the H -plane beamwidth to result in a nearly unity polarization axial ratio. Consequent of the tapered aperture field

distribution the radiation patterns will also have low sidelobes. The wanted higher order modes are generated by a symmetric step discontinuity in an oversized waveguide. The radiation characteristics together with the on-axis gain of the antenna are derived from an electric vector potential by the aperture field method based on the vector diffraction formula. Analytical results are shown to be in good agreement with the experimental results of radiation pattern and gain measurements. This antenna which generates an elliptical shaped beam, by virtue of its rectangular shaped aperture, with a nearly unity polarization axial ratio would offer better directivity, high on-axis gain, low sidelobes and low cost, and can be used as a satellite antenna to efficiently illuminate an elliptical zone on the earth's surface. The performance of the antenna has been found satisfactory over a broad bandwidth.

7.2.1 ANALYSIS OF MODAL FIELDS

The multimode horn under study is shown in Fig.7.1. The E -plane walls of the double-flare multimode horn are coated with a dielectric material of relative permittivity ϵ_r . The desired higher order modes will be generated by the symmetric step discontinuity in the oversized square waveguide.



$A = 6 \text{ cm}$, $B = 4 \text{ cm}$, $a_1 = 2.54 \text{ cm}$, $a_2 = 3.2 \text{ cm}$
 $l_0 = 3.06 \text{ cm}$, $l_1 = 6.1 \text{ cm}$, $l_2 = 12 \text{ cm}$ $\theta_1 = 3^\circ$
 $\theta_2 = 6^\circ$, $S = \text{THICKNESS OF DIELECTRIC COATING} = 3 \text{ mm}$

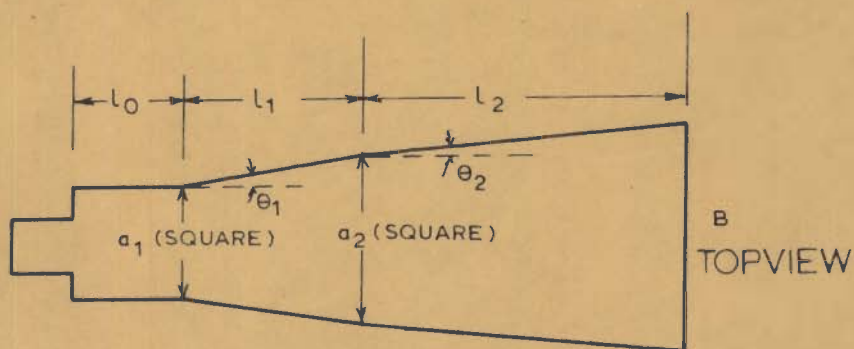


FIG.7.1 _DOUBLE- FLARE MULTI MODE DIELECTRIC COATED HORN

Hybrid modes are to exist to satisfy the boundary conditions; and the TE_x hybrid modes [52] propagating in the Z -direction can be derived from an electric vector potential \bar{F} such that $\bar{F} = \bar{i}_x \psi$. The proper forms of the potential function ψ for the air and dielectric coated regions inside the horn respectively are given by,

$$\begin{aligned} \psi_o^{TE_x} &= C \cos \alpha_o x \cos \frac{n\pi}{b} y e^{-jk_z z} \\ \psi_d^{TE_x} &= D \cos \alpha_d \left(\frac{a}{2} - x \right) \cos \frac{n\pi}{b} y e^{-jk_z z} \end{aligned} \quad (7.1)$$

where α_o and α_d satisfy the relationships

$$\begin{aligned} \left(\frac{n\pi}{b} \right)^2 + k_z^2 + \alpha_o^2 &= k_o^2 \\ \left(\frac{n\pi}{b} \right)^2 + k_z^2 + \alpha_d^2 &= \epsilon_r k_o^2 \end{aligned} \quad (7.2)$$

The subscripts 'o' and 'd' indicate the air and dielectric coated regions respectively; C and D are the coefficients of the potential functions, and 'a' and 'b' are the guide dimensions (at the first portion of the double-flare horn).

The horn dimensions upto the symmetric step discontinuity in the oversized waveguide are chosen ($a/h = 1$, i.e. the first flare section of the double-flare

section of the double-flare horn has a square cross-section) for the propagation of the dominant TE_{10} mode only. The different non-vanishing field components for the dominant TE_{10} mode in the horn axial and dielectric coated regions are obtained (by Appendix I-1) as :

In the horn axial region

$$\begin{aligned} E_{y0} &= jCk_z \cos\alpha_0 x e^{-jk_z z} \\ H_{z0} &= \frac{C}{\omega\mu_0} k_z \alpha_0 \sin\alpha_0 x e^{-jk_z z} \\ H_{x0} &= \frac{C}{j\omega\mu_0} k_z^2 \cos\alpha_0 e^{-jk_z z} \end{aligned} \quad (7.3)$$

In the dielectric coated region

$$\begin{aligned} E_{yd} &= jDk_z \cos\alpha_d \left(\frac{a}{2} - x\right) e^{-jk_z z} \\ H_{zd} &= -\frac{D}{\omega\mu_0} k_z \alpha_d \sin\alpha_d \left(\frac{a}{2} - x\right) e^{-jk_z z} \\ H_{xd} &= \frac{D}{j\omega\mu_0} k_z^2 \cos\alpha_d \left(\frac{a}{2} - x\right) e^{-jk_z z} \end{aligned} \quad (7.4)$$

The characteristic equation relating α_0 and α_d can be obtained by matching the tangential components of the fields at the air-dielectric interface i.e. at

$x = \pm \frac{a}{2} - s$, where s is the thickness of the dielectric coating. It is seen (Appendix I-1) that the characteristic equation can be derived as,

$$\alpha_0 \tan \alpha_0 \left(\frac{a}{2} - s \right) = -\alpha_d \tan \alpha_d s \quad (7.5)$$

But the Eqs.(7.2) both α_0 and α_d are functions of k_z ; so the above equation is a transcendental equation for determining the possible value of k_z . Assuming the same propagation constant k_z for both the regions, an explicit solution for α_0 can be derived for the case of dielectric slabs with low permittivity, and is obtained (Appendix I-1) as,

$$\alpha_0^2 = -k_0^2 (\epsilon_r - 1) \frac{2s}{a} \quad (7.6)$$

It is known that higher order modes will be excited at any discontinuity in an oversized waveguide by an incident dominant mode. The discontinuity used in the double-flare horn considered is a symmetric step; and the unwanted TE_{02} and TE_{11} modes will not be excited because of the even symmetry of the step discontinuity [128]. Moreover the size of the oversized waveguide is chosen ($A/B = 1.5$) to permit the propagation of TE_{12} and TM_{12} higher order modes only. Thus only TE_{12} and TM_{12} modes need be considered to be excited by the dominant TE_{10} mode incident on the symmetric step discontinuity. Assuming that the

transverse E -field at the discontinuity plane is the same as the TE₁₀ incident field which has a single y - component given by Eqs. (7.3) as

$$E_{y_0} = j C k_z \cos \alpha_0 x e^{-jk_z z} = E_0 \cos \alpha_0 e^{-jk_z z} \quad (7.7)$$

only, the boundary conditions require that the total E -field (contributed by the dominant as well as the higher order modes) over any cross section of the oversized waveguide should also have a y-component only. As it has been discussed that only TE₁₂ and TM₁₂ higher order modes can propagate along the oversized waveguide, the transverse E -field E_t^0 over the radiating aperture of the oversized waveguide for TE₁₀ incident field at the step discontinuity can be written as

$$\begin{aligned} E_t^0 &= E_t^{TE_{10}} + E_t^{TE/TM_{12}} \\ &= E (\cos \alpha_0 x + C_y \cos \alpha_0 x \cos \frac{2\pi}{B} y) \quad (7.8) \end{aligned}$$

where E is a constant that depends on the horn excitation and its aperture dimensions, C_y is the amplitude of the mode conversion factor (a complex amplitude ratio of higher order mode to dominant mode) and B is the aperture dimensions of the oversized waveguide (the terms e^{-jk_zz}

and $e^{j(2\pi - \xi_y)}$ is omitted where $(2\pi - \xi_y)$ is the phase difference between the TE_{10} and TE/TM_{12} modes with ξ_y as the phase of the mode conversion factor)

7.2.2 RADIATION FROM MULTIMODE DIELECTRIC LOADED HORN

As the transverse E -field over the aperture is given by Eq. (7.8), the radiated far-field can be determined by the aperture field method based on the vector diffraction formula. But it is to be noted that when the radiating aperture is a horn aperture, the phase of the field in the aperture will vary with position in the aperture. For the test horn under consideration, the proper phase variation of the aperture field appears to be a quadratic phase variation of the form [44, p -127] given by

$$\psi_M = \frac{\pi}{\lambda_0} \left(\frac{x^2}{R} + \frac{y^2}{R} \right) \quad (7.9)$$

where R is the axial length of the horn.

Knowing the aperture field the radiated far field is derived on the basis of the vector diffraction formula [44], [66], and as seen in Appendix I-2, the radiated far-field component in the E -plane ($\phi = \pi/2$) is obtained as,

$$E_{\theta}(\theta) = \frac{j E_0}{4r} e^{-jk_0 r} R \left(1 + \frac{k_z}{k_0} \cos\theta\right) e^{j \frac{\lambda_0 R \alpha_0^2}{4\pi}} \cdot$$

$$\left\{ C(u_1) - C(u_2) - j [S(u_1) - S(u_2)] \right\} [F_i^I + C_y F_i^{II}] \quad (7.10)$$

where

$$F_i^I = e^{j \frac{\lambda_0 R k_0^2}{4\pi} \sin^2\theta} \left\{ C(\eta) - C(\xi) - j [S(\eta) - S(\xi)] \right\}$$

$$F_i^{II} = M \left\{ C(v_1) - C(v_2) - j [S(v_1) - S(v_2)] \right\} +$$

$$N \left\{ C(v_3) - C(v_4) - j [S(v_3) - S(v_4)] \right\}$$

$C(w)$ and $S(w)$ are the Fresnel cosine and sine integrals defined by

$$C(w) = \int_0^w \cos\left(\frac{\pi t^2}{2}\right) dt$$

$$S(w) = \int_0^w \sin\left(\frac{\pi t^2}{2}\right) dt$$

$$\begin{pmatrix} u_1 \\ u_2 \end{pmatrix} = \frac{1}{\sqrt{2}} \left[\frac{\sqrt{\lambda_0 R}}{\pi} \alpha_0 \pm \frac{A'}{\sqrt{\lambda_0 R}} \right]$$

$$\begin{pmatrix} \eta \\ \xi \end{pmatrix} = \frac{1}{\sqrt{2}} \left[\sqrt{\lambda_0 R} \frac{k_0 \sin\theta}{\pi} \pm \frac{B}{\sqrt{\lambda_0 R}} \right]$$

$$\begin{pmatrix} M \\ N \end{pmatrix} = e^{j \frac{\pi}{4} \lambda_0 R \left(\frac{2}{B} \pm \frac{2}{\lambda_0} \sin\theta \right)^2}$$

$$\begin{pmatrix} v_1 \\ v_2 \end{pmatrix} = \frac{1}{\sqrt{2}} \left[\frac{B}{\sqrt{\lambda_0 R}} \pm \sqrt{\lambda_0 R} \left(\frac{2}{B} + \frac{2}{\lambda_0} \sin\theta \right) \right]$$

and

$$\begin{pmatrix} v_3 \\ v_4 \end{pmatrix} = \frac{1}{\sqrt{2}} \left[\frac{B}{\sqrt{\lambda_0 R}} \pm \sqrt{\lambda_0 R} \left(\frac{2}{B} - \frac{2}{\lambda_0} \sin\theta \right) \right]$$

The quantities E and C_y in Eq.(7.10) can be determined by following the method of mode conversion in a rectangular waveguide by a step discontinuity [51] and is seen in Appendix I-2 that the quantities can be derived, in terms of the guide dimensions, as

$$E = E_0 \frac{b}{B} \frac{(\alpha_0 a' + \sin\alpha_0 a')}{(\alpha_0 A' + \sin\alpha_0 A')} \quad (7.11)$$

and

$$C_y = \frac{2\sin\pi \frac{b}{B}}{\pi \frac{b}{B}} \quad (7.12)$$

where E_0 denotes the constant that depends on the dominant mode excitation (TE_{10} mode) of the horn,

$$a' = a - 2s$$

$$\text{and } A' = A - 2s$$

Here a and b are the guide dimensions at the step discontinuity junction; A and B are the aperture dimensions of the oversized waveguide and s is the thickness of the

dielectric layer. Substitution of all the quantities in Eq (7.10) enables the evaluation of the E -plane radiation pattern of the test horn. The pattern in the H -plane ($\phi=0$) could also be derived in the same manner and the final expression is given in Appendix I-2.

7.2.3 ON-AXIS GAIN OF THE MULTIMODE DIELECTRIC LOADED HORN

The total power P_t passing through the horn aperture is determined by,

$$P_t = \frac{1}{2} \iint_s E_t^0 H_t^0 dx dy \quad (7.13)$$

But from Eqs. (7.3) , (7.7) and (7.8)

$$\begin{aligned} H_t^0 &= \frac{k_z}{\omega \mu_0} E (\cos \alpha_0 x + C_y \cos \alpha_0 x \cos \frac{2\pi}{B} y) \\ &= \frac{E_t^0 k_z}{\omega \mu_0} \end{aligned} \quad (7.14)$$

It is seen in Appendix I-3 that P_t can be obtained as

$$P_t = \frac{1}{8} \frac{k_z}{\omega \mu_0} B E^2 \frac{(\alpha_0 A' + \sin \alpha_0 A')}{\alpha_0} (2+C_y^2) \quad (7.15)$$

The on-axis gain of the test horn is given by

$$G(0,0) = \frac{4\pi P(0,0)}{P_t} \quad (7.16)$$

where $P(0,0) = \frac{1}{\eta_0} |E_\theta|_{\max}^2 r^2$ (7.17)

Using Eqs.(7.10) and (7.15), the on-axis gain is derived in Appendix I-3 as,

$$G(0,0) = \frac{4\pi\alpha_0 k_0 R^2 (1 + \frac{k_z}{k_0})^2}{k_z (\alpha_0 A' + \sin\alpha_0 A')} \cdot \left\{ \frac{[C(u_1) - C(u_2)]^2 + [S(u_1) - S(u_2)]^2}{2 + c_y^2} \right\} \left[\sqrt{[C(\xi_1)]^2 + [S(\xi_1)]^2} + c_y \sqrt{[C(v_{o1}) - C(v_{o2})]^2 + [S(v_{o1}) - S(v_{o2})]^2} \right]^2$$

(7.18)

where $\xi_1 = \frac{B}{\sqrt{2}\lambda_0 R}$

$$\begin{pmatrix} v_{o1} \\ v_{o2} \end{pmatrix} = \frac{1}{\sqrt{2}} \left[\frac{B}{\sqrt{\lambda_0 R}} \pm \frac{2}{B} \sqrt{\lambda_0 R} \right]$$

7.2.4 DESIGN CONSIDERATION OF THE DOUBLE-FLARE MULTIMODE DIELECTRIC LOADED HORN

The multimode horn chosen is a double-flare horn shown in Fig.7.1. The first flare section has a square cross-section for the propagation of TE_{10} mode only. The second flare section ends at a rectangular aperture whose dimensions may be determined by the requirement for the propagation of TE/TM_{12} higher order modes.

The wanted higher order modes are generated at the step discontinuity in the oversized square guide in which odd modes (mode number $m+n$ is an odd number) above the TE/TM_{12} and TE/TM_{21} modes cannot propagate. It is noted that other higher order modes are also generated where the flare angle changes, but since the amplitudes of the higher order modes generated are proportional to the changes in the flare [33,part-1, p- 72] and as the flare angle change is kept small other higher order modes are prevented from being strongly excited.

The most important and significant differential phase shifts are those between the dominant mode and beam shaping mode of each set and between the two sets. Usually the former is kept as small as possible to enable the wanted higher order modes to efficiently shape the beam.

This phase slip can be adjusted to a certain degree by adjusting the length of both the oversized guide section and the horn flare section. The latter differential phase is principally chosen to obtain circular polarization.

Thus the overall length of the horn is primarily governed by the differential phase difference between TE_{10} and TE/TM_{12} modes, $\Delta\phi^{(10-12)}$, and between TE_{01} and TE/TM_{21} modes, $\Delta\phi^{(01-21)}$, which are given by

$$\begin{aligned} \Delta\phi^{(10-12)} &= \Delta\phi_{l_0}^{(10-12)} + \Delta\phi_{l_1}^{(10-12)} + \Delta\phi_{l_2}^{(10-12)} + \\ &\quad + \text{contribution from discontinuity.} \\ \Delta\phi^{(01-21)} &= \Delta\phi_{l_0}^{(01-21)} + \Delta\phi_{l_1}^{(01-21)} + \Delta\phi_{l_2}^{(01-21)} + \\ &\quad + \text{contribution from discontinuity.} \end{aligned}$$

where subscripts l_0, l_1 and l_2 denote contributions from different horn sections. The phase of each mode ϕ^{mn} can be calculated by

$$\begin{aligned} \phi^{mn} &= \frac{2\pi}{\lambda_0} \int_0^l \beta_{mn}(z) dz + \frac{2\pi}{\lambda_0} . \\ &\int_0^l \left[1 - \frac{z^2}{4} \left[\left(\frac{m}{a(z)} \right)^2 + \left(\frac{n}{b(z)} \right)^2 \right] \right]^{1/2} dz \end{aligned} \tag{7.9}$$

where β_{mn} = phase constant of TE_{mn} (or TM_{mn}) mode
 $= k_{zmn}$

Using Eqs. (7.19), $\phi_{l_0}, \phi_{l_1}, \phi_{l_2}$ for TE_{10} and TE/TM_{12} modes

can be determined. It is noted that $\phi_{\ell_0}^{12} = \phi_{\ell_1}^{12} = 0$, since TE/TM₁₂ modes are excited only at the discontinuity junction in the oversized waveguide. Thus,

$$\begin{aligned}\Delta\phi^{(10-12)} &= \Delta\phi_{\ell_0}^{(10-12)} + \Delta\phi_{\ell_1}^{(10-12)} + \Delta\phi_{\ell_2}^{(10-12)} \\ &= \Delta\phi_{\ell_0}^{10} + \Delta\phi_{\ell_1}^{10} + \Delta\phi_{\ell_2}^{(10-12)}\end{aligned}\tag{7.20}$$

This phase difference $\Delta\phi^{(10-12)}$ is kept as small as possible to enable the wanted higher order modes to efficiently shape the beam. As per these considerations and the consideration for the propagation of only dominant mode in the first flare section, and for the propagation of TE/TM₁₂ higher order modes in the oversized waveguide, the double-flare horn was designed to have the following specifications

$$\begin{aligned}\ell_0 &= 3.06 \text{ cm} \\ \ell_1 &= 6.1 \text{ cm} \\ \ell_2 &= 12 \text{ cm}\end{aligned}$$

The first flare section was designed to have a square cross section (2.54 cm x 2.54 cm at the throat end, and 3.2 cm x 3.2 cm at the discontinuity junction) and a flare-angle of 3 degrees, and the second flare section (i.e. the oversized guide) with a flare-angle of 6 degrees and of rectangular

cross section. The aperture dimensions of the oversized waveguide were, $A = 6$ cm and $B = 4$ cm.

7.2.5 EXPERIMENTAL RESULTS

To evaluate the performance of the multimode dielectric coated horn experimentally, a X-band double-flare multimode rectangular horn antenna was fabricated for the design specifications detailed in Sec. 7.2.4 (see Fig. 7.1). The E-plane walls of the horn were loaded with 3 mm thick polyethylene ($\epsilon_r = 2.3$) sheets. Experiments were carried out with the horn excited with TE_{10} mode at a frequency of 9.64 GHz. The E-plane and H-plane radiation patterns (experimental) are depicted in Fig. 7.2a and Fig. 7.2b respectively together with those for multimode horn of the same dimensions without dielectric loading. It is noted that the pattern directivity has increased significantly, but at the cost of a slight deterioration (particularly in the E-plane pattern) in the sidelobe level. But, eventhough there is a little increase in the sidelobe level as compared to that for the multimode horn without dielectric coating, the sidelobe level is well below that of empty and dielectric loaded conventional horns of the same dimensions. The validity of the expression for the radiation pattern [Eq.(7.10)] is upheld, by establishing

the theoretical results in good agreement with the experimental results, in Fig. 7.3.

In an effort to explore the possibility of attaining highly directive patterns with low sidelobes from the test horn, experiments were repeated with paraffin wax ($\epsilon_r = 2.25$) spheres of diameter 4 cm, 6 cm and 9 cm placed in front of, but displaced from, the aperture of the dielectric coated multimode horn for the minimum input VSWR performance [85]. The sphere off-set positions were determined experimentally [68], [69] and the positions were found to lie between 1.6 cm to 2.2 cm from the horn aperture for the 3 sphere sizes tested, with VSWR values of 1.41, 1.3 and 1.1 for the respective spheres. The spheres were held in position by cotton tapes that did not interfere with the microwave radiation. The results of the pattern measurements are presented in Fig. 7.2a and Fig. 7.2b together with those for multimode horns with and without dielectric loading. It is seen that the dielectric spheres placed at the horn aperture have improved the radiation patterns of the dielectric coated multimode horn with significantly reduced sidelobe levels, and increased directivity. The dielectric sphere loading also increases the on-axis gain of the horn. The gain variation of the antenna system as a function of the dielectric sphere diameter in wavelength is plotted in Fig. 7.4a (The gain

level of the empty multimode horn, and that based on Eq.(7.18) are also included). The decrease in the -3 dB beamwidth of the patterns due to dielectric sphere loading is depicted in Fig. 7.4b as a function of the sphere diameter.

In order to ascertain the applicability of this class of antennas over a wide frequency band, the effect of varying the operating frequency on the performance of the test antenna was observed over a frequency band extending from 8 GHz to 12 GHz . The radiation pattern was found to be free from degradation over at least 1.5 : 1 frequency bandwidth. The bandwidth properties of the horn are depicted in Fig. 7.5a and Fig. 7.5b. Between 8 GHz and 12 GHz, the half power beamwidth ranges only from about 40 to 36 degrees. Because of the presence of beam shaping higher order modes, the effective E -plane beamwidth is approximately equal to the H -plane beamwidth to result in a off-axis polarization axial ratio near unity. The polarization axial ratio for every 20° pattern plane was found to be less than 1.6 dB. The variation of polarization axial ratio as a function of frequency is shown in Fig. 7.5c. For the frequency band extending from 8 GHz to 12 GHz, the axial ratio varies from 1.2 to 1.1; and from a practical stand point this represents a relatively small deviation from circular polarization.

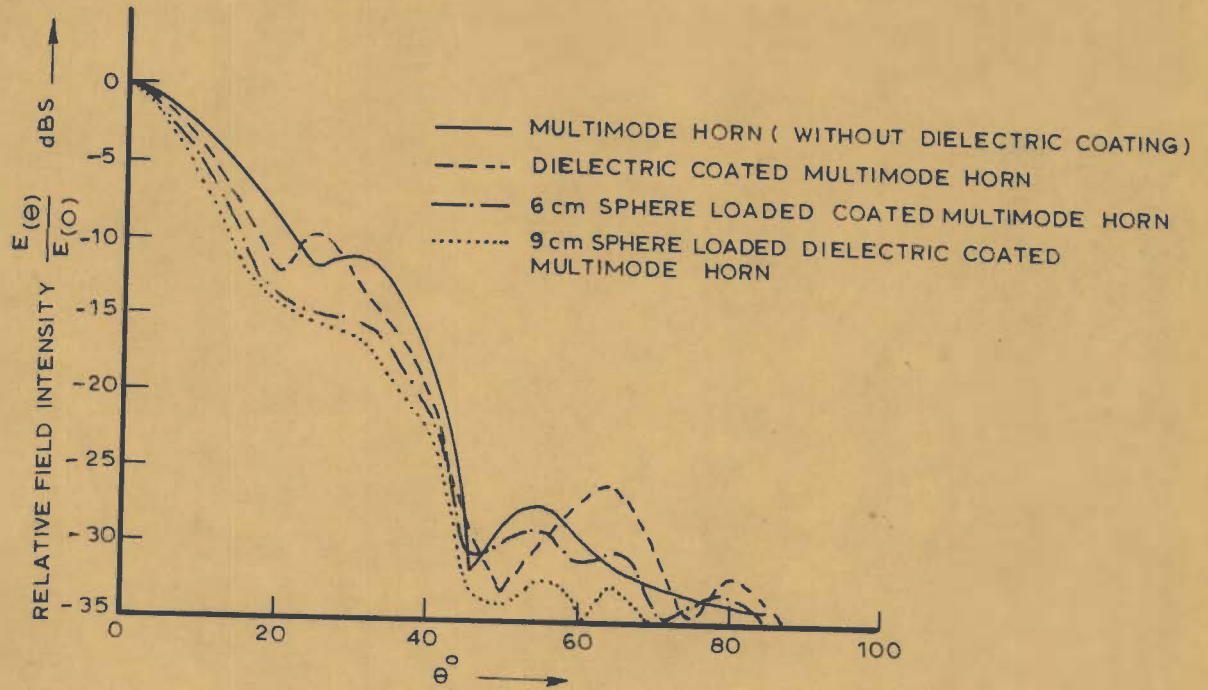


FIG.7.2a_ E - PLANE PATTERN OF DIELECTRIC SPHERE LOADED DIELECTRIC COATED MULTIMODE HORN

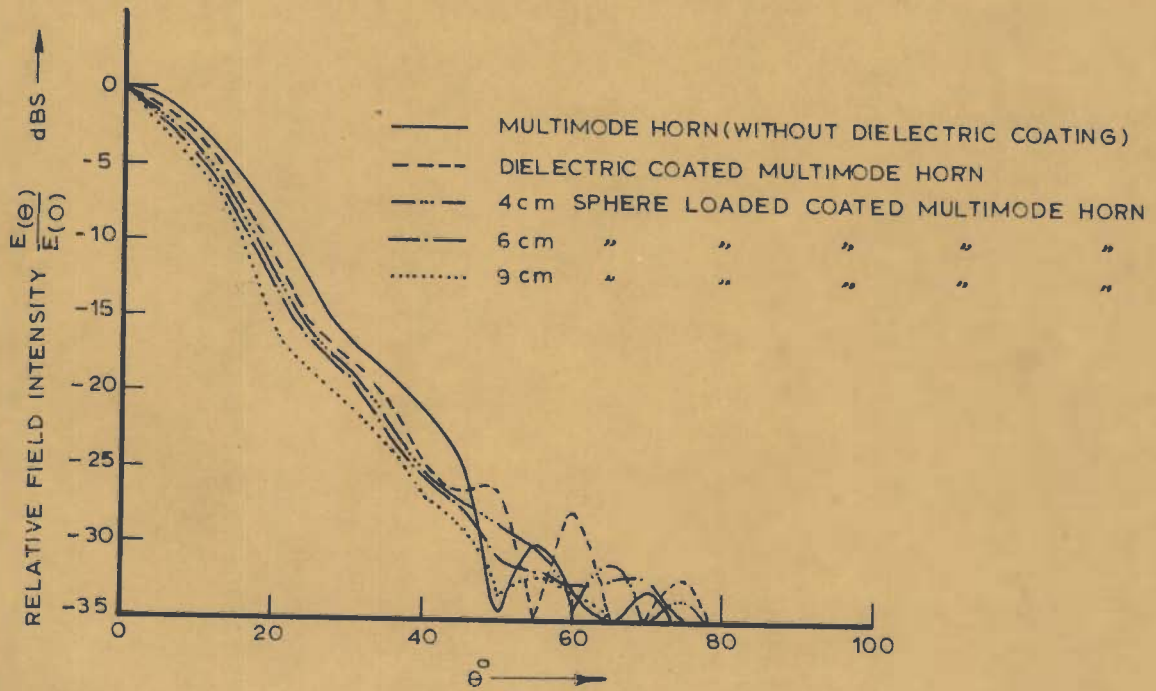


FIG.7.2b_ H - PLANE PATTERN OF DIELECTRIC SPHERE LOADED DIELECTRIC COATED MULTIMODE HORN

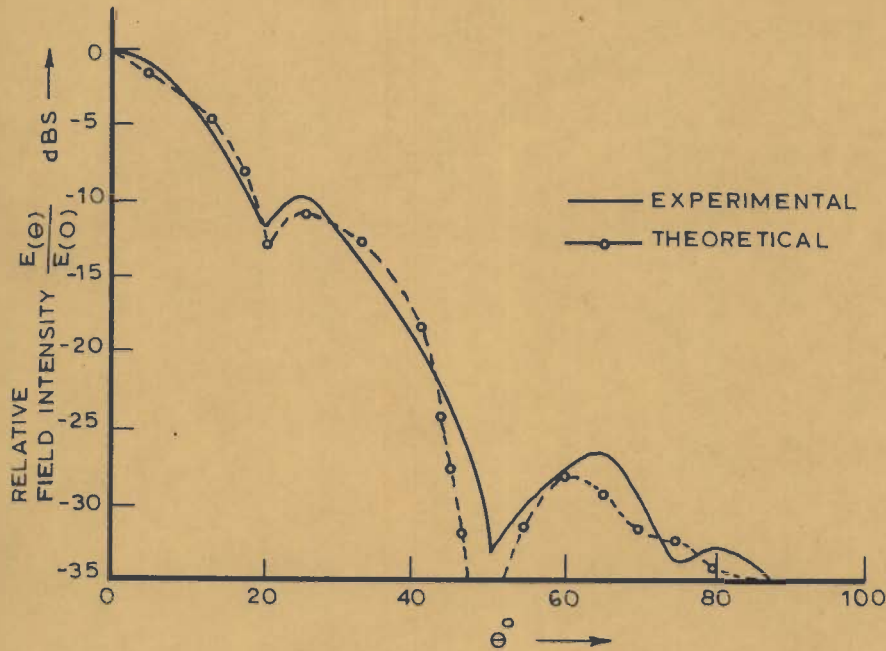


FIG.7.3_ E - PLANE PATTERN OF DIELECTRIC COATED MULTI MODE HORN

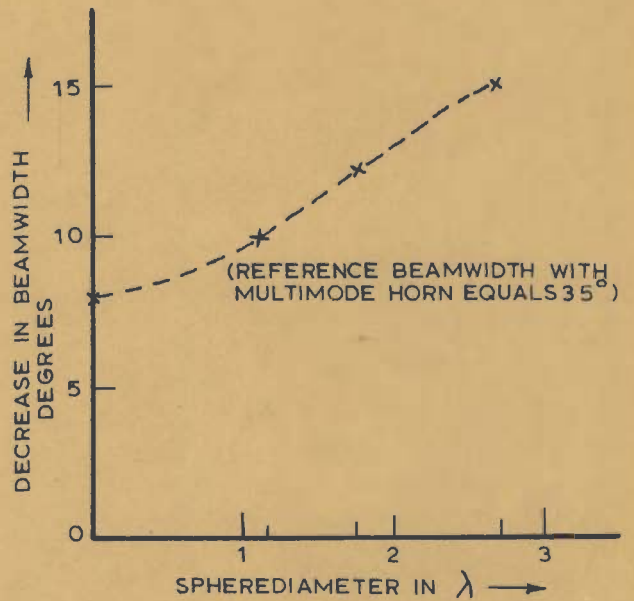
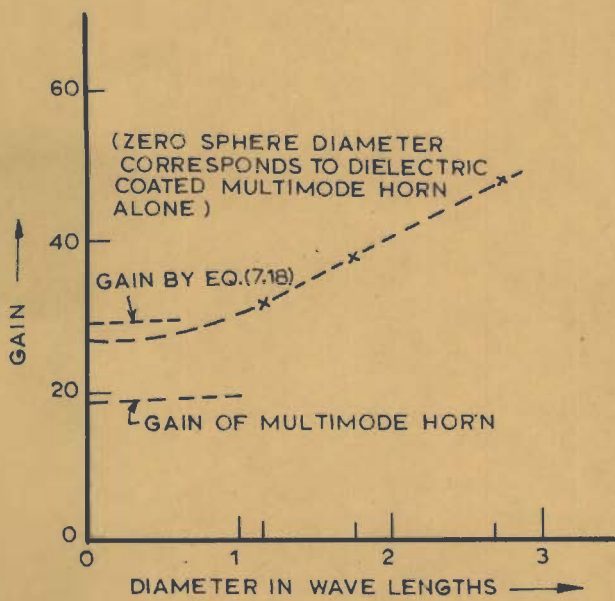


FIG.7.4a_ GAIN VS SPHERE DIAMETER OF DIELECTRIC SPHERE LOADED DIELECTRIC COATED MULTI-MODE HORN

FIG.7.4b_ DECREASE IN BEAMWIDTH VS SPHERE DIAMETER OF DIELECTRIC SPHERE LOADED DIELECTRIC COATED MULTIMODE HORN

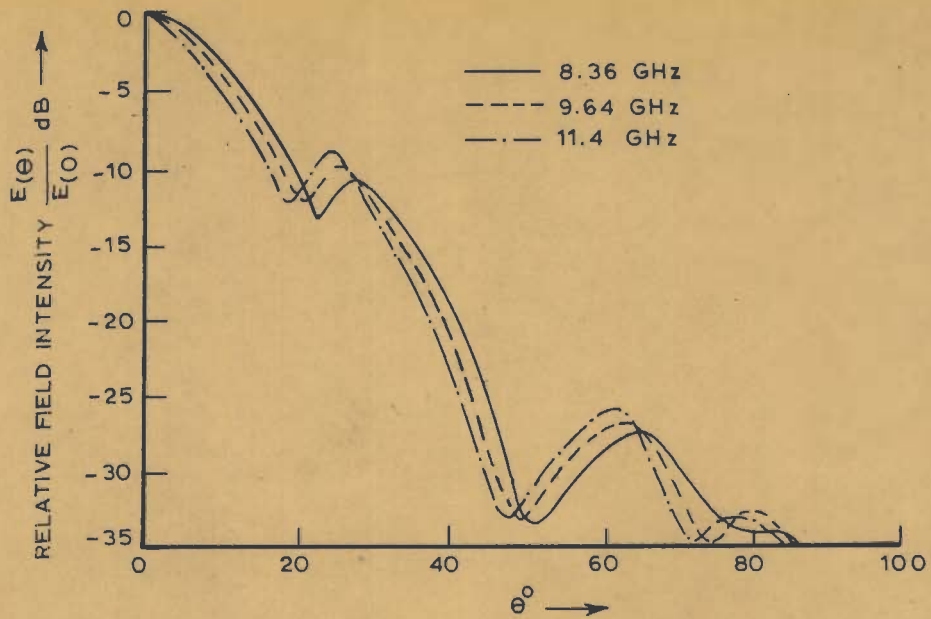


FIG. 7.5 a - PLANE PATTERN OF DIELECTRIC COATED MULTI-MODE HORN FOR DIFFERENT FREQUENCIES

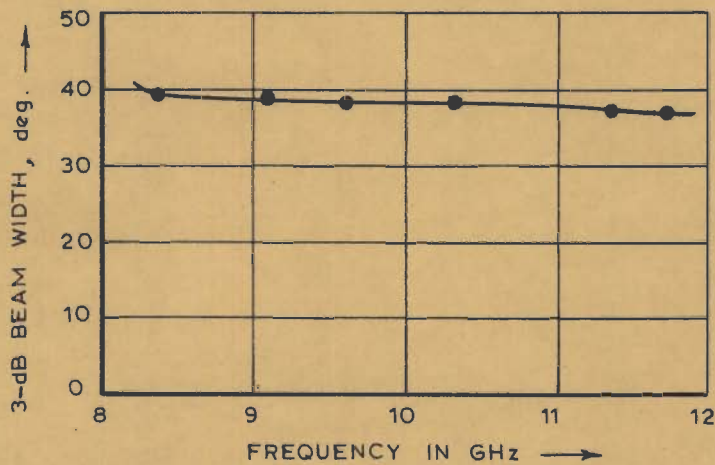


FIG. 7.5 b - BEAM WIDTH VS FREQUENCY

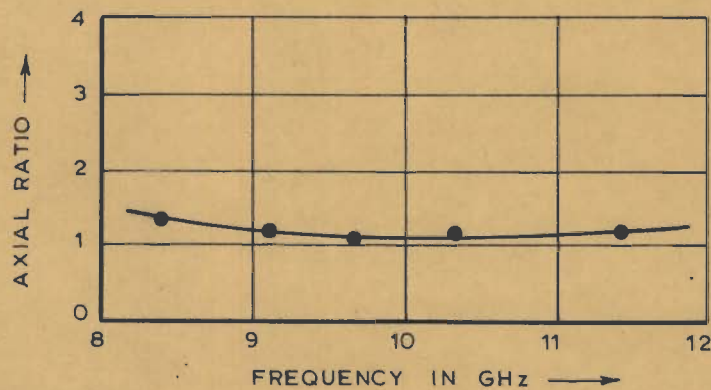


FIG. 7.5 c - AXIAL RATIO AS A FUNCTION OF FREQUENCY

From the results it has been concluded that

- i) Multimode dielectric coated rectangular horn antennas have desirable radiation characteristics with increased directivity and on-axis gain. Due to the presence of beam shaping higher order modes the sidelobe levels of this particular horn antennas are considerably low as compared to the sidelobe levels associated with dielectric loaded conventional horns.
- ii) The radiation characteristics of dielectric coated multimode horn antennas can be improved further with significantly reduced sidelobe levels, greater directivity and increased on-axis gain with off-set placed dielectric spheres in front of the horn aperture.
- iii) As the multimode dielectric coated horn is seen to radiate circularly polarized elliptical beam (the elliptical cross section beam is a direct result of the rectangular shaped aperture) with good off-axis polarization axial ratio, the antenna system with dielectric sphere loading will offer a desirable antenna device with greater directivity and low sidelobe levels for applications in satellite communication systems to efficiently illuminate an elliptical shaped zone on the surface of the earth.

iv) As the -3 dB beamwidth of the antenna can be controlled by the off-set placed dielectric sphere dimension, the system also offers a variable beamwidth facility.

7.3 BEAM SHAPING HYBRID MODE DIELECTRIC LOADED HORN

In this section a highly directive, variable beam hybrid mode dielectric loaded rectangular horn that utilises the technique of combining several higher order modes for beam shaping has been analysed. For a known symmetrical throat excitation the amplitudes of the various modes in the horn have been determined by means of modal expansion of fields, and the mode amplitudes thus obtained are used to evaluate the radiation patterns derived by the aperture field method on the basis of the vector diffraction formula. The characteristic equation as well as the expression for the on-axis gain of the hybrid mode horn has also been derived. The significance of higher order mode content in shaping the pattern of dielectric loaded horn is theoretically demonstrated, and the theoretical results of the hybrid mode horn with symmetrically loaded H-plane walls are established in good agreement with experimental results. Experimental results of the horn with symmetrical dielectric

loading on E -plane walls, as well as E -plane and H -plane walls for considerable control over the E -plane and H-plane patterns by an appropriate change in the higher order mode content are also included.

7.3.1 HYBRID MODE HORN WITH SYMMETRICAL DIELECTRIC LOADING ON THE H-PLANE WALLS OF THE HORN

Modal fields in the horn;

The horn with symmetrical dielectric loading on its H -plane walls is shown in Fig. 7.6 . The boundary conditions are satisfied by assuming the modes to be TE to y, and the fields of these hybrid modes can be derived from an electric vector potential \bar{F} [52] such that $\bar{F} = \bar{i}_y \Psi$, where \bar{i}_y is the unit vector in the y -direction. The proper forms of the potential function Ψ for the horn axial region and the dielectric loaded region respectively are given by

$$\begin{aligned} \Psi_o &= C_n \cos \alpha_o y \cos \frac{n\pi}{A} x e^{-jk_z z} \\ \Psi_d &= D_n \cos \alpha_d \left(\frac{B}{2} - y \right) \cos \frac{n\pi}{A} x e^{-jk_z z} \end{aligned} \quad (7.21)$$

(n = 1, 3, 5, ...)

where C_n and D_n are constants. The separation parameter equations in the two regions are

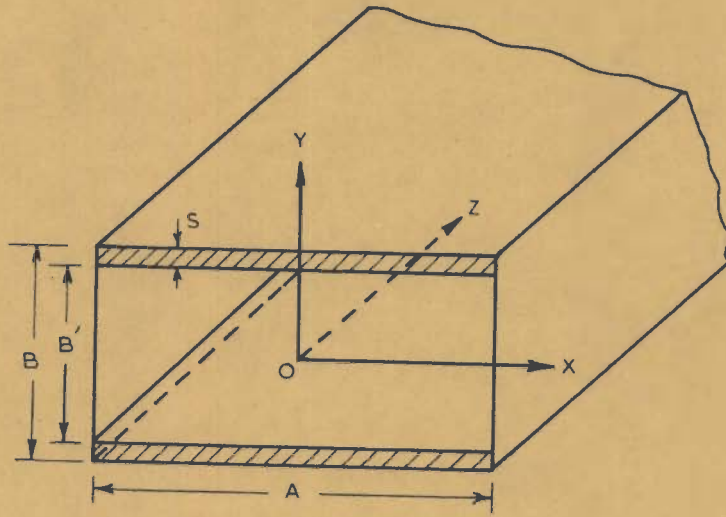


FIG. 7.6_ CO-ORDINATE SYSTEM FOR DIELECTRIC LOADED (H-PLANE WALLS) HORN

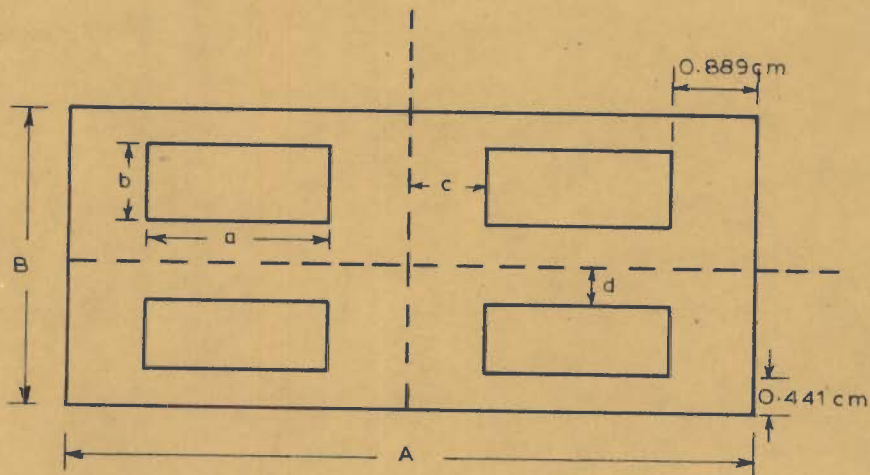


FIG. 7.7_ THE HORN THROAT STRUCTURE

A = 7.62 cm, B = 3.81 cm, a = 2.286 cm,
b = 1.016 cm, c = 0.635 cm, d = 0.448 cm

$$\alpha_o^2 + \left(\frac{n\pi}{A}\right)^2 + k_z^2 = k_o^2$$

$$\alpha_d^2 + \left(\frac{n\pi}{A}\right)^2 + k_z^2 = k_1^2 (= \epsilon_r k_o^2)$$
(7.22)

The subscripts 'o' and 'd' denote the horn axial region and the dielectric loaded region respectively.

The different field components in the horn axial region are derived by substitution of Ψ_o in the appropriate field relations [52] and are obtained (see Appendix J-1) as,

$$E_{x_o} = jC_n k_z \cos\alpha_o y \cos \frac{n\pi}{A} x e^{-jk_z z}$$

$$E_{z_o} = -\frac{n\pi}{A} C_n \cos\alpha_o y \sin \frac{n\pi}{A} x e^{-jk_z z}$$

$$E_{y_o} = 0$$
(7.23)

$$H_{x_o} = \frac{C_n}{j\omega\mu_o} \frac{n\pi}{A} \alpha_o \sin\alpha_o y \sin \frac{n\pi}{A} x e^{-jk_z z}$$

$$H_{z_o} = \frac{C_n k_z \alpha_o}{j\omega\mu_o} \sin\alpha_o y \cos \frac{n\pi}{A} x e^{-jk_z z}$$

$$H_{y_o} = \frac{C_n}{j\omega\mu_o} (k_o^2 - \alpha_o^2) \cos\alpha_o y \cos \frac{n\pi}{A} x e^{-jk_z z}$$

Similar field components can be derived for the dielectric coated region by using Ψ_d in the field relations, and are

obtained as,

$$\begin{aligned}
 E_{xd} &= j D_n k_z \cos \alpha_d \left(\frac{B}{2} - y \right) \cos \frac{n\pi}{A} x e^{-jk_z z} \\
 E_{zd} &= - D_n \frac{n\pi}{A} \cos \alpha_d \left(\frac{B}{2} - y \right) \sin \frac{n\pi}{A} x e^{-jk_z z} \\
 E_{yd} &= 0 \\
 H_{xd} &= - \frac{1}{j\omega\mu_0} D_n \alpha_d \frac{n\pi}{A} \sin \alpha_d \left(\frac{B}{2} - y \right) \sin \frac{n\pi}{A} x e^{-jk_z z} \\
 H_{zd} &= - \frac{D_n k_z \alpha_0}{j\omega\mu_0} \sin \alpha_d \left(\frac{B}{2} - y \right) \cos \frac{n\pi}{A} x e^{-jk_z z} \\
 H_{yd} &= \frac{D_n}{j\omega\mu_0} (k_1^2 - \alpha_d^2) \cos \alpha_d \left(\frac{B}{2} - y \right) \cos \frac{n\pi}{A} x e^{-jk_z z}
 \end{aligned} \tag{7.24}$$

A transcendental equation relating to α_0 and α_d is obtained by matching the tangential E - and H - field components at the air-dielectric interface (i.e. at $y = \frac{B}{2} - s$) and is given by

$$\alpha_0 \tan \alpha_0 \left(\frac{B}{2} - s \right) = - \alpha_d \tan \alpha_d s \tag{7.25}$$

where s = the thickness of the dielectric layer.

With the assumption of dielectric loading by thin slabs of low permittivity, and of the same value of propagation constant k_z for both the regions, an explicit solution for α_0 can be derived from Eq.(7.22) and (7.25);

and is obtained as

$$\alpha_0^2 = -k_0^2 (\epsilon_r - 1) \frac{2s}{B} \quad (7.26)$$

Far field patterns of the hybrid mode dielectric loaded horn:

The radiated far-field components of the hybrid mode horn with dielectric loaded H -plane walls may be derived by the aperture field method based on the vector diffraction formula [44]. Here, it is assumed that reflections occur from the open end of the waveguide, and the field in the aperture is the superposition of the direct and reflected waves [44, p-147]. Accordingly the transverse E - and H -fields over the horn aperture are given by

$$E_s = (1 + \Gamma) E_{ti} \quad (7.27)$$

where E_{ti} = the incident field in the aperture

$$= \bar{i}_x E_{x0} = j C_n k_z \cos \alpha_0 y \cos \frac{n\pi}{A} x e^{-jk_z z} \quad (7.28)$$

$$\text{and } H_s = -(1 - \Gamma) H_{ti} \quad (7.29)$$

where Γ = the reflection coefficient given by the approximate formula

$$\Gamma = \frac{1 - \frac{k_z}{k_0}}{1 + \frac{k_z}{k_0}}$$

Now the radiation patterns in the E -plane and H -plane respectively, by the vector diffraction formula [44,pp -147-148] are given by

$$E_{\theta}(\theta) = \frac{j}{2\lambda_0} \frac{e^{-jk_0 r}}{r} \left(1 + \frac{k_z}{k_0} \frac{1-\Gamma}{1+\Gamma} \cos\theta\right) \iint_S E_{xs} e^{jk_0 y_s \sin\theta} dx_s dy_s \quad (7.30)$$

$$E_{\phi}(\theta) = \frac{j}{2\lambda_0} \frac{e^{-jk_0 r}}{r} \left(\cos\theta + \frac{k_z}{k_0} \frac{1-\Gamma}{1+\Gamma}\right) \iint_S E_{xs} e^{jk_0 x_s \sin\theta} dx_s dy_s$$

It is seen in Appendix J-2 that, by inserting Eqs. (7.27) and (7.28) in Eqs. (7.30) the respective radiated far-fields are derived as,

$$E_{\theta}(\theta) = 2 C_n k_z (1 + \Gamma) \frac{A}{n\pi} \frac{e^{-jk_0 r}}{r} \left(1 + \frac{k_z}{k_0} \frac{1 - \Gamma}{1 + \Gamma} \cos\theta\right) \sin \frac{n\pi}{2} .$$

$$\alpha_0^2 \frac{1}{-(k_0 \sin\theta)^2} \left[\begin{array}{l} k_0 \sin\theta \cos\left(\alpha_0 \frac{B'}{2}\right) \sin\left(k_0 \frac{B'}{2} \sin\theta\right) \\ -\alpha_0 \sin\left(\alpha_0 \frac{B'}{2}\right) \cos\left(k_0 \frac{B'}{2} \sin\theta\right) \end{array} \right] \quad (7.31)$$

$$E_{\phi}(\theta) = 2 C_n k_n (1 + \Gamma) \frac{n\pi}{A} \frac{e^{-jk_0 r}}{\lambda_0 r} \left(\cos\theta + \frac{k_z}{k_0} \frac{1 - \Gamma}{1 + \Gamma}\right) \sin \frac{n\pi}{2} .$$

$$\frac{\cos\left(k_0 \frac{A}{2} \sin\theta\right) \sin\alpha_0 \frac{B'}{2}}{\alpha_0 \left[(k_0 \sin\theta)^2 - \left(\frac{n\pi}{A}\right)^2 \right]} \quad (7.32)$$

(Expression for $E_{\theta}(\theta)$ and $E_{\phi}(\theta)$ show that for non-zero radiation fields, $n = 1, 3, 5, \dots$)

where $B' = B - 2s$, s being the thickness of the dielectric layer.

The radiation patterns are found to depend on the modal amplitudes C_n , there by giving a facility for pattern shaping by controlled amount of higher order mode contents. The patterns based on Eqs. (7.31) and (7.32) have been computed for typical test values; and the results are plotted in Figs. 7.9a and 7.9b together with the respective experimental

patterns.

The on-axis gain of the horn:

The total power radiated from the horn aperture is given by

$$\begin{aligned}
 P_t &= \frac{1}{2} \operatorname{Re} \left[\iint_e (\mathbf{E}_s \times \mathbf{H}_s^*) \cdot d\mathbf{s} \right] \\
 &= \frac{1}{2} \operatorname{Re} \left[\int_{-B/2}^{B/2} \int_{-A/2}^{A/2} E_{xs} H_{ys}^* dx dy \right] \quad (7.33)
 \end{aligned}$$

From Eqs.(7.23) and (7.29)

$$\begin{aligned}
 H_{ys} &= - (1 - \Gamma) H_{yo} \\
 &= -(1 - \Gamma) \frac{C_n}{j\omega\mu_0} (k_o^2 - \alpha_o^2) \cos\alpha_o y \cos\frac{n\pi}{A} x e^{-jk_z z} \quad (7.34)
 \end{aligned}$$

Thus from Eqs. (7.27), (7.28) and (7.34)

$$\frac{E_{xs}}{H_{ys}} = \frac{(1 + \Gamma)}{(1 - \Gamma)} \frac{\omega\mu_0 k_z}{(k_o^2 - \alpha_o^2)} \quad (7.35)$$

Inserting the values of E_{xs} from Eqs. (7.27) and (7.28), and H_{ys} from Eq.(7.35) in Eq.(7.33), the total power radiated by the horn (Appendix J-3) is obtained as,

$$P_t = \frac{1}{8} C_n^2 \left(\frac{1-\Gamma}{1+\Gamma} \right) \frac{(k_o^2 - \alpha_o^2)}{k_o \eta_o} k_z (1+\Gamma)^2 \cdot A \frac{(\alpha_o B' + \sin \alpha_o B')}{\alpha_o} \quad (7.36)$$

The on-axis gain of the horn is defined as

$$G(0,0) = \frac{4\pi P(0,0)}{P_t} \quad \text{where } P(0,0) = \frac{1}{2} \eta_o |E_{\max}|^2 r^2$$

Using Eqs. (7.31) and (7.36), the on-axis gain is obtained as,

$$G(0,0) = \frac{64k_o k_z A \left(1 + \frac{k_z}{k_o} \frac{1-\Gamma}{1+\Gamma}\right)^2 (1+\Gamma)}{n^2 \pi \lambda_o^2 (1-\Gamma) (k_o^2 - \alpha_o^2)} \frac{\sin^2 \alpha_o \frac{B'}{2}}{\alpha_o (\alpha_o B' + \sin \alpha_o B')} \quad (7.37)$$

Substitution of the quantities in Eq. (7.37) enables the evaluation of the on-axis gain. The gain due to higher order modes are found to be inversely proportional to the square of the mode number n , where as the higher order mode contribution to the total power P_t depends on the square of the modal amplitude C_n (see Eq. (7.36))

The gain for the dominant HE_{11} mode becomes

$$G(0,0) = \frac{64k_z k_o A \left(1 + \frac{k_z}{k_o} \frac{1-\Gamma}{1+\Gamma}\right)^2 (1+\Gamma) \sin^2 \alpha_o \frac{B'}{2}}{\pi \lambda_o^2 (1-\Gamma) (k_o^2 - \alpha_o^2) \alpha_o (\alpha_o B' + \sin \alpha_o B')} \quad (7.38)$$

The value of the gain computed on the basis of Eqs.(7.37) has been found in satisfactory agreement with the experimental results.

7.3.2 HYBRID MODE HORN WITH SYMMETRICAL DIELECTRIC LOADING ON E-PLANE WALLS OF THE HORN

In this case the modal fields in the two regions are derived from the potential functions

$$\Psi_o = C_n \cos \alpha_o x \cos \frac{n\pi}{B} y e^{-jk_z z} \quad (7.39)$$

$$\Psi_d = D_n \cos \alpha_d x \cos \frac{n\pi}{B} y e^{-jk_z z}$$

with $n = 1, 3, 5, \dots$

As in Sec 7.3.2, the separation parameter equation in the two regions are

$$\alpha_o^2 + \left(\frac{n\pi}{B} \right)^2 + k_z^2 = k_o^2 \quad (7.40)$$

$$\alpha_d^2 + \left(\frac{n\pi}{B} \right)^2 + k_z^2 = \epsilon_r k_o^2 \quad (=k_1^2)$$

The different field components in the two regions may be determined by using Ψ_o and Ψ_d given by Eqs. (7.39), in the same manner as in Sec. 7.3.1, and are given for the respective regions by

$$E_{xo} = jA_n k_z \cos \alpha_o x \cos \frac{n\pi}{B} y e^{-jk_z z}$$

$$E_{zo} = -\alpha_o C_n \sin \alpha_o x \cos \frac{n\pi}{B} y e^{-jk_z z}$$

$$E_{yo} = 0$$

$$H_{xo} = \frac{C_n}{j\omega\mu_o} \alpha_o \frac{n\pi}{B} \sin \alpha_o x \sin \frac{n\pi}{B} y e^{-jk_z z} \quad (7.41)$$

$$H_{zo} = \frac{C_n k_z}{\omega\mu_o} \frac{n\pi}{B} \cos \alpha_o x \sin \frac{n\pi}{B} y e^{-jk_z z}$$

$$H_{yo} = \frac{C_n}{j\omega\mu_o} [k_o^2 - (\frac{n\pi}{B})^2] \cos \alpha_o x \cos \frac{n\pi}{B} y e^{-jk_z z}$$

and

$$E_{xd} = j D_n k_z \cos \alpha_d (\frac{A}{2} - x) \cos \frac{n\pi}{B} y e^{-jk_z z}$$

$$E_{zd} = D_n \alpha_d \sin \alpha_o (\frac{A}{2} - x) \cos \frac{n\pi}{B} y e^{-jk_z z}$$

$$E_{yd} = 0$$

$$H_{xd} = \frac{-D_n}{j\omega\mu_o} \alpha_d (\frac{n\pi}{B}) \sin \alpha_d (\frac{A}{2} - x) \sin \frac{n\pi}{B} y e^{-jk_z z} \quad (7.42)$$

$$H_{zd} = \frac{D_n k_z}{\omega\mu_o} (\frac{n\pi}{B}) \cos \alpha_d (\frac{A}{2} - x) \sin \frac{n\pi}{B} y e^{-jk_z z}$$

$$H_{yd} = \frac{1}{j\omega\mu_o} [k_1^2 - (\frac{n\pi}{B})^2] \cos \alpha_o (\frac{A}{2} - x) \cos \frac{n\pi}{B} y e^{-jk_z z}$$

Here also the transcendental equation and the explicit solution for α_0 are obtained by the same procedure used in Sec. 7.3.1, and are given respectively by

$$\alpha_0 \tan \alpha_0 \left(\frac{A}{2} - s \right) = - \alpha_d \tan \alpha_d s \quad (7.43)$$

and

$$\alpha_0^2 = - k_0^2 (\epsilon_r - 1) \frac{2s}{A} \quad (7.44)$$

Following the procedure in Sec. 7.3.1, the radiation patterns in the E -plane and H -plane for this case of dielectric loading on the E -plane walls of the horn are obtained as,

$$E_\theta(\theta) = 2C_n k_n \frac{n\pi}{B} \left(1 + \frac{k_z}{k_0} \frac{1-\Gamma}{1+\Gamma} \cos\theta \right) (1+\Gamma) \frac{e^{-jk_0 r}}{\lambda_0^r} \sin \frac{n\pi}{2} \cdot \frac{\sin(\alpha_0 \frac{A'}{2}) \cos(k_0 \frac{B}{2} \sin\theta)}{\alpha_0 \left[(k_0 \sin\theta)^2 - \left(\frac{n\pi}{B} \right)^2 \right]} \quad (7.45)$$

and

$$E_\phi(\theta) = 2C_n k_z \frac{B}{n\pi} \frac{e^{-jk_0 r}}{\lambda_0^r} \left(\cos\theta + \frac{k_z}{k_0} \frac{1-\Gamma}{1+\Gamma} \right) (1+\Gamma) \sin \frac{n\pi}{2} \cdot$$

$$\frac{1}{\alpha_0^2 - (k_0 \sin\theta)^2} \left[\cos(\alpha_0 \frac{A'}{2}) \sin(k_0 \frac{A'}{2} \sin\theta) k_0 \sin\theta - \alpha_0 \sin(\alpha_0 \frac{A'}{2}) \cos(k_0 \frac{A'}{2} \sin\theta) \right] \quad (7.46)$$

Here also it is seen that the radiation patterns are found to depend on the modal amplitudes C_n so that the patterns can be shaped by suitably combining the higher order modes.

The total power transmitted through the horn aperture and the on-axis gain of the hybrid mode dielectric loaded horn in this case can also be obtained in the same manner as in Sec. 7.3.1., and are derived respectively as

$$P_t = \frac{C_n^2}{8} \frac{(1-\Gamma)}{(1+\Gamma)} \left[k_o^2 - \left(\frac{n\pi}{B} \right)^2 \right] \frac{(1+\Gamma)^2}{k_o \eta_o} k_z B \frac{(\alpha_o \Lambda' + \sin \alpha_o \Lambda')}{\alpha_o} \quad (7.47)$$

$$G(0,0) = \frac{64k_o k_z B \left(1 + \frac{k_z}{k_o} \frac{1-\Gamma}{1+\Gamma}\right)^2}{n^2 \pi \lambda_o^2} \frac{(1+\Gamma)}{(1-\Gamma)} \cdot \frac{\sin(\alpha_o \frac{\Lambda'}{2})}{\left[k_o^2 - \left(\frac{n\pi}{B} \right)^2 \right] \alpha_o (\alpha_o \Lambda' + \sin \alpha_o \Lambda')} \quad (7.48)$$

The dependence of P_t and $G(0,0)$ on the higher order modes are found to have the same nature as for the H-plane walls loaded case.

7.3.3 EVALUATION OF MODAL AMPLITUDES OF HYBRID MODE DIELECTRIC LOADED HORN BY MODAL EXPANSION OF FIELDS

Generally the modes existing in a waveguide depend upon the excitation of the guide, and the amplitudes of the various waveguide modes can be determined from the known tangential components of E (or of H) over a guide cross-section.

The horn throat structure of the hybrid mode dielectric coated horn under consideration is shown in Fig.7.7. The horn throat is excited symmetrically by four identical X -band waveguides carrying TE_{10} mode. The mode amplitudes are computed using modal expansion of fields with the assumption that the guide is matched at the junction where the four X -band waveguides join with the dielectric loaded horn (i.e. there is no reflection and only outward travelling waves exist). The method shall be illustrated for hybrid mode horn with dielectric loading on H -plane walls as follows :

Consider the guide junction of Fig.7.7. It is desired to determine the fields for $z > 0$ from the known values of the tangential fields at $z = 0$ under the assumption that the guide is matched. For $TE_{y_{mn}}$ modes, let these modes can be determined by the superposition of the mode

potential functions given as

$$\psi = \sum_{n=1}^{\infty} C_{1n} \cos \alpha_{1n} y \cos \frac{n\pi}{A} x e^{-jk_z z} \quad (7.49)$$

where α_{1n} is the value of α_0 in Eq.(7.22) for $m = 1$,
 $n =$ any integer, and $C_{1n} =$ mode amplitude.

(In fact $\psi = \sum_{m=1}^{\infty} \sum_{n=1}^{\infty} C_{mn} \cos \alpha_{mn} y \cos \frac{n\pi}{A} x e^{-jk_z z}$; but

here consideration is restricted to $m = 1$, having a dependence of E_x on y such that $E_x = 0$ only at $y = \pm \frac{B}{2}$.)

In terms of ψ , the tangential fields E_x for the $TE_{y_{mn}}$ mode ($E_y = 0$) at $Z = 0$ is given by,

$$E_x \Big|_{z=0} = - \frac{\partial \psi}{\partial z} \Big|_{z=0} = k_z \sum_{n=1}^{\infty} C_{1n} \cos \alpha_{1n} y \cos \frac{n\pi}{A} x \quad (7.50)$$

Now let there be a wave incident on the junction from the smaller guide (X-band waveguide) and let the larger guide (the dielectric loaded horn) be matched. The smaller guide is carrying a TE_{10} mode and hence at the junction ($z=c$), $E_x \Big|_{z=0}$ is the incident wave due to the TE_{10} wave in the smaller waveguide, and is given by

$$E_x \Big|_{z=0} = \cos \frac{\pi}{a} x, \quad y < b$$

$$= 0, \quad y > b$$

Thus by Eq. (7.50), it becomes

$$\cos \frac{\pi}{a} x = k_z \sum_{n=1}^{\infty} C_{1n} \cos \alpha_{1n} y \cos \frac{n\pi}{A} x \quad (7.51)$$

It is seen in Appendix J-4 that the modal amplitude C_n is obtained as

$$C_{1n} = \frac{8 \sin \frac{\pi}{a} c \cos n\pi \left(\frac{a+2c}{2A} \right) \cos \frac{n\pi a}{2A} [\sin \alpha_{1n} (d+e) - \sin \alpha_{1n} e]}{\pi a A k_z \left[\left(\frac{n}{A} \right)^2 - \left(\frac{1}{a} \right)^2 \right] (\alpha_{1n} B + \sin \alpha_{1n} B)} \quad (7.52)$$

where the constants, A, B, a, b, c, d, and e are the dimensions of the throat structure and are given in Fig. 7.2. From Eq.(7.52) it is seen that the amplitudes of the higher order modes can be varied by a suitable choice of the throat structure, and can be used for shaping the patterns by a controlled amount of higher order mode content.

The modal amplitudes for the horn with dielectric loaded E -plane walls can also be computed in the same manner.

7.3.4 COMPUTED RESULTS

Assuming that HE_{11} and HE_{13} are the possible significant hybrid modes in the horn, from Eq.(7.52), the ratio of the amplitudes of modes with $n=3$ to the fundamental mode with $n = 1$, becomes,

$$\frac{C_{13}}{C_{11}} = \frac{\left(\frac{1}{A}\right)^2 - \left(\frac{1}{a}\right)^2 \cos \frac{3\pi(a+2c)}{2A} \cos \frac{3\pi a}{2A}}{\left(\frac{3}{A}\right)^2 - \left(\frac{1}{a}\right)^2 \cos \frac{\pi(a+2c)}{2A} \cos \frac{\pi a}{2A}} \cdot \frac{\sin \alpha_{13}(b+d) - \sin \alpha_{13}d}{\sin \alpha_{11}(b+d) - \sin \alpha_{11}d} \cdot \frac{(\alpha_{11}B + \sin \alpha_{11}B)}{(\alpha_{13}B + \sin \alpha_{13}B)} \quad (7.53)$$

where α_{11} and α_{13} are the values of α_0 for the HE_{11} and HE_{13} modes, and are found from Eqs. (7.26) and (7.22). (In obtaining the modal amplitude ratio, it is assumed that the modes are having the same propagation constant k_z). Inserting the values of the throat details and α_{11} and α_{13} for the particular case of the horn given in Fig. 7.7, the relative modal amplitude is found to be

$$\frac{C_{13}}{C_{11}} = 0.25 \quad (7.54)$$

Thus it is seen that with proper choice of the throat specifications, the higher order mode content relative to the fundamental mode can be controlled; and these controlled amount of higher order modes can be combined with the fundamental mode to get the desired beam shape. To establish the effectiveness of this technique for the dielectric loaded horn, patterns based on Eqs. (7.31) and

and (7.32) were computed for various ratios of modal amplitudes C_{13}/C_{11} . The results of the E -plane and H -plane patterns are plotted in Fig. 7.8a and Fig. 7.8b respectively and are seen that the higher order mode contents play a significant role in determining the beam shapes (-3 dB beamwidths) in both the planes.

7.3.5 EXPERIMENTAL RESULTS AND COMPARISON WITH THEORY

In order to test the validity of the expressions derived, experiments were conducted with a rectangular horn of length 9.906 cm ($A = 7.62$ cm and $B = 3.8$ cm) loaded with bakelite ($\epsilon_r = 3.5$) sheets of thickness 2 mm on the H -plane walls. Four X -band waveguides are inserted symmetrically into the horn throat for the specifications detailed in Fig. 7.7. The horn was excited simultaneously by these four X -band identical waveguides carrying TE_{10} mode at a frequency of 9.64 GHz. Theoretical patterns based on Eqs(7.31) and (7.32) are compared with the respective experimental patterns in Fig. 7.9a and Fig. 7.9b, and are found to have reasonable overall agreement. The slight discrepancies may be interpreted as due to the presence of a small amount of surfacewave propagation along the dielectric loaded walls.

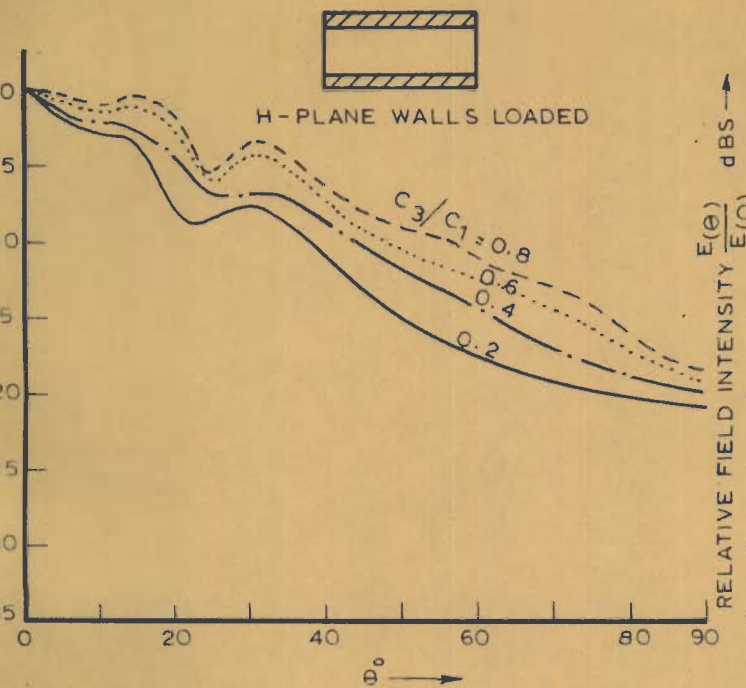


FIG. 7.8 a _E-PLANE PATTERN OF HYBRID MODE DIELECTRIC LOADED HORN (THEORETICAL)

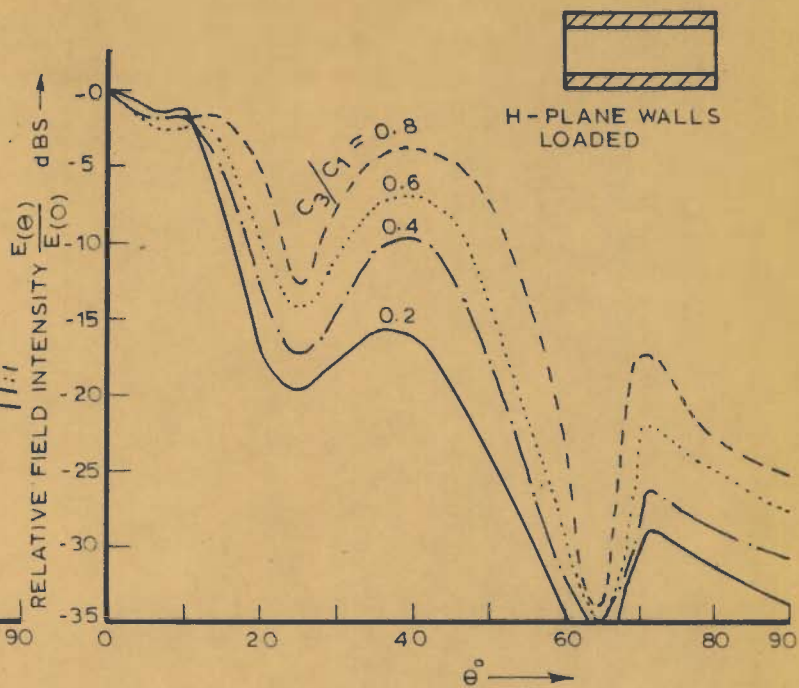


FIG. 7.8 b _H-PLANE PATTERN OF HYBRID MODE DIELECTRIC LOADED HORN (THEORETICAL)

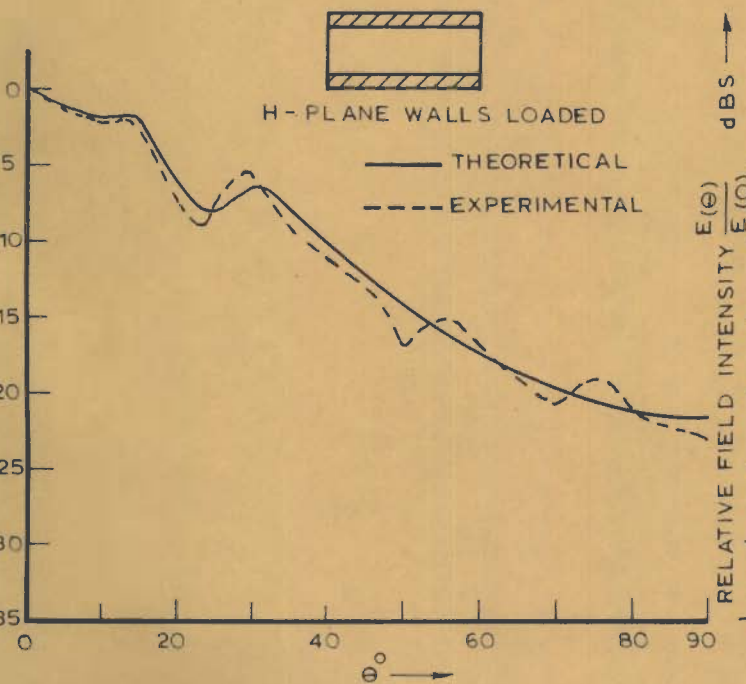


FIG. 7.9 a _E-PLANE PATTERN

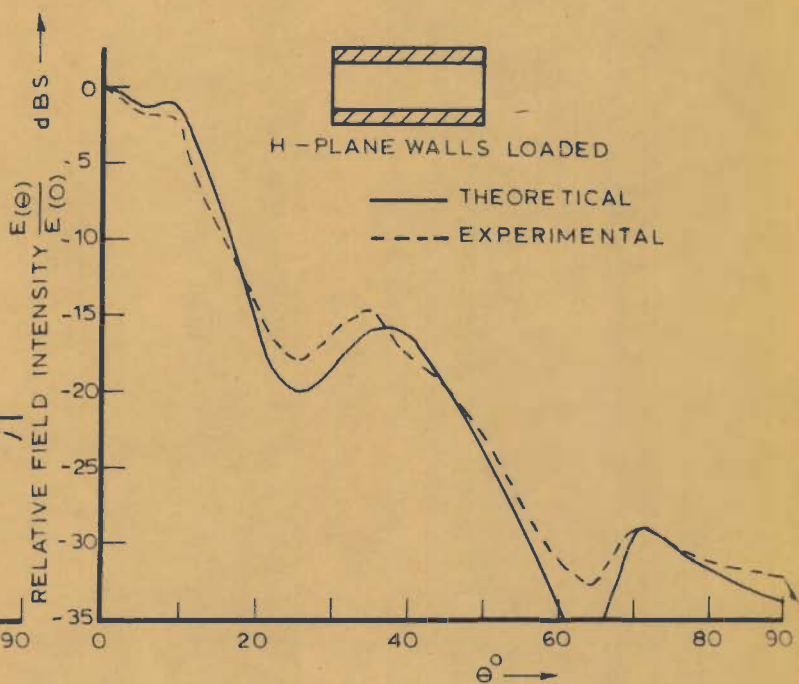


FIG. 7.9 b _H-PLANE PATTERN

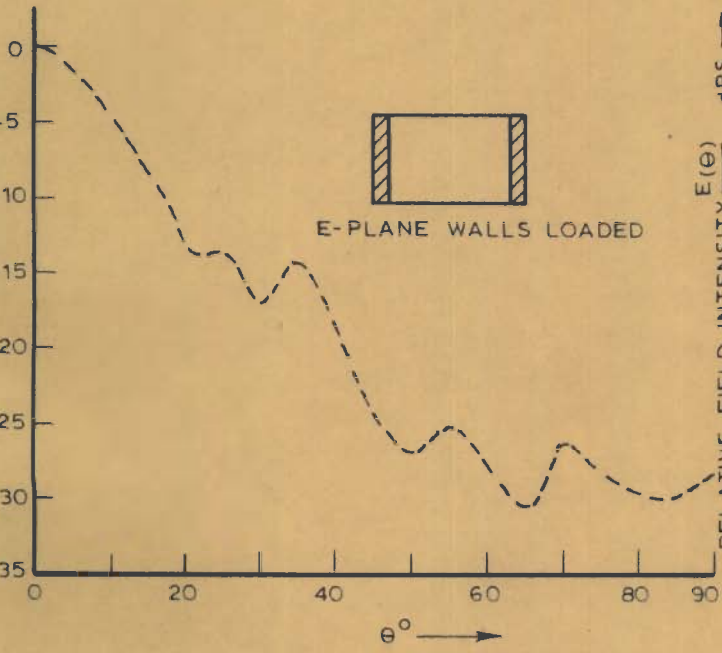


FIG. 7.10 a - E-PLANE PATTERN (EXPERIMENTAL)

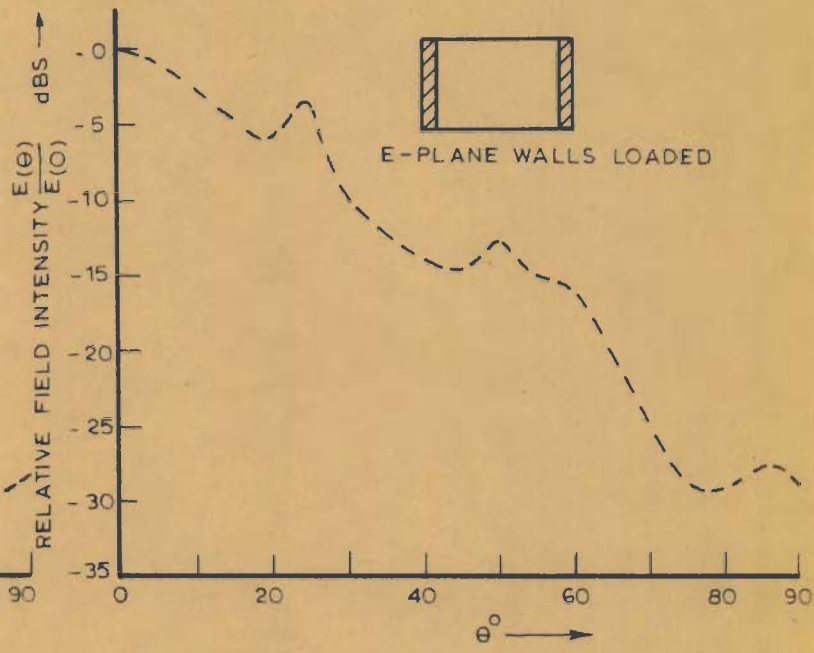


FIG. 7.10 b - H-PLANE PATTERN (EXPERIMENTAL)

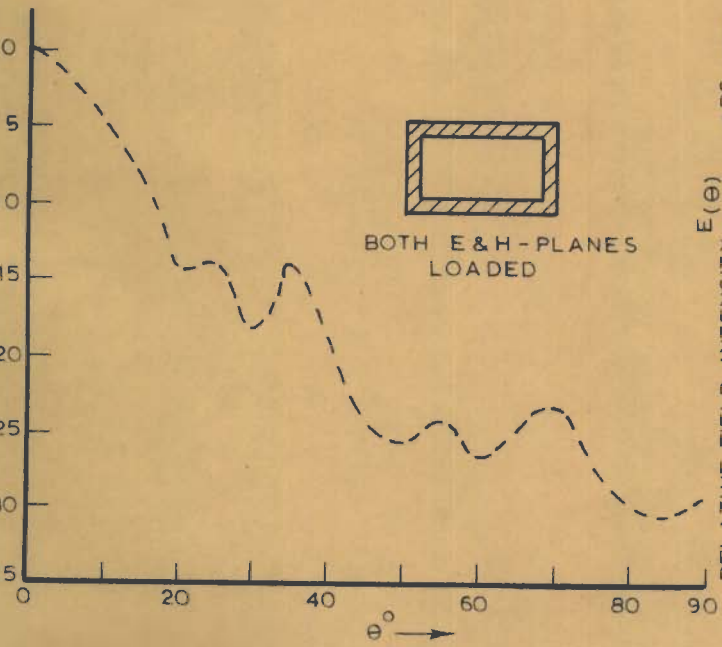


FIG. 7.11 a - E-PLANE PATTERN (EXPERIMENTAL)

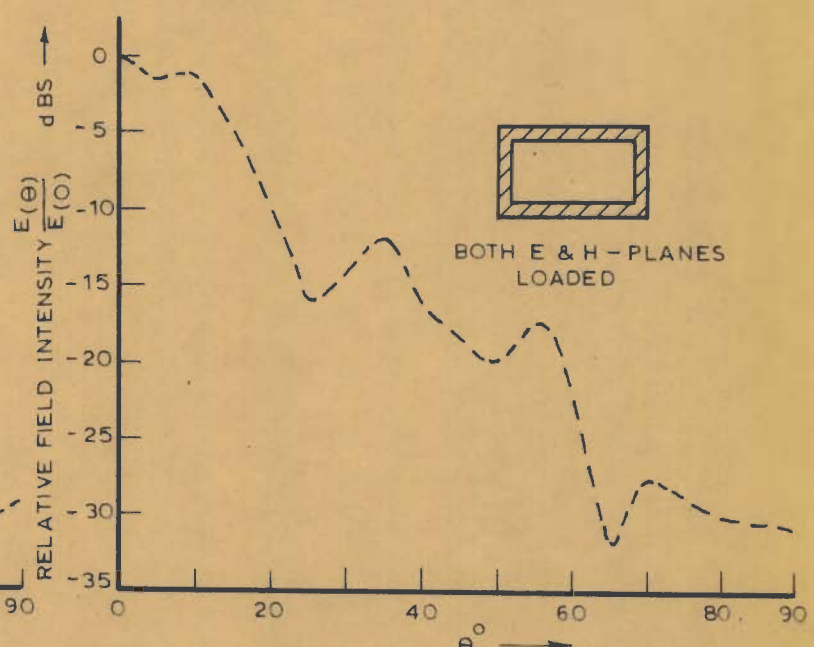


FIG. 7.11 b - H-PLANE PATTERN (EXPERIMENTAL)

The on-axis gain determined by Eq.(7.37) and its experimental value are found to be almost equal, being 18.5 and 19.2 respectively. The experimental results with the E- plane walls of the horn loaded with the same dielectric material are shown in Fig.7.10. The patterns of the horn with both E - and H - plane walls loaded with the dielectric material have also been observed, and are depicted in Fig. 7.11 to show the feasibility of using all the four walls of the rectangular horn with a dielectric material to have a dual polarised horn with considerable control over the E -plane and H -plane patterns.

From the results, it may be concluded that the technique described can be used for shaping the patterns of hybrid mode dielectric loaded horns by combining higher order mode amplitudes. The cross-section of the beam will be elliptical as a direct result of the rectangular shaped aperture, and hence this hybrid mode horn generating an elliptical shaped beam with a variable beamwidth (beam shaping) facility can be used either as a monopulse radar antenna or as a multiple beam parabolic antenna feed for applications in satellite communication systems to efficiently illuminate an elliptical shaped zone on the earth's surface. Hybrid mode dielectric loaded horns will have more pattern directivity than the corrugated horn used

by Manwarren and Farrar [84] . Hybrid mode dielectric loaded horns will also have the additional attractive advantages of its light weight and ease of construction

7.4 CONCLUSION

The radiation characteristics of two types of multimode dielectric loaded horn antennas have been investigated. A double-flare multimode horn with dielectric loading on its E-plane walls have been found to possess desirable radiation characteristics with increased directivity and on-axis gain. The sidelobe levels, that are generally higher with dielectric loading, are also reduced in this case due to the presence of beam shaping higher order modes. Investigations have proved that dielectric sphere mounting at the aperture of the dielectric loaded double-flare horn is effective in further lowering the sidelobe levels, and narrowing the -3 dB beamwidth. The antenna that generates elliptical shaped beam with a nearly unity polarization axial ratio can find its applications in satellite communication systems to efficiently illuminate an elliptical earth zone.

The possibility of beamshaping with dielectric loaded hybrid mode horns has also been established. The

importance of higher order mode amplitudes in shaping the patterns of the hybrid mode horn has been illustrated both theoretically and experimentally. The dielectric loaded hybrid mode horn may be used as a monopulse radar antenna by virtue of its beam shaping facility, light weight and ease of construction.

CHAPTER VIII

SUMMARY OF RESULTS AND CONCLUSIONS

8.1 SUMMARY OF RESULTS

The present work provides a comprehensive study of certain dielectric loaded improved feed systems. The improvement of performance of conical horns with dielectric loading is investigated in chapter III. First the effect of placing a homogeneous dielectric sphere in front of the aperture of a radiating wide angle conical horn is analysed and results are compared with experiments to show that dielectric sphere loading has increased the directivity of conical horn. It is also observed that the directivity is dependent on the sphere diameter and its distance from the horn aperture, thereby giving a means of multiple beam facility. Then the performance of conical horn with dielectric coated walls has been analysed, and results showed a remarkable improvement in the directivity at the cost of slightly increased sidelobe levels. The dielectric coated horn is investigated with off-set placed dielectric spheres at the horn aperture based on the method due to Bakefi and Farnel [9] and is found to produce patterns with narrow beamwidth, higher on-axis gain and low sidelobe

levels. In the same chapter the radiation behaviour of a conical horn with a helical boundary has also been studied using spherical hybrid modes; and the technique of dielectric sphere loading is successfully utilized to improve its radiation patterns with greater gain, reduced -3 dB beamwidth and low sidelobes.

The radiation properties of biconical horn with appropriate dielectric loading are investigated in chapter IV. Results show that dielectric loading has resulted in a considerable increase in the directivity of its vertical pattern, and less variation from uniformity in its omnidirectional horizontal pattern.

In chapter V, the radiation behaviour of corrugated horns in the presence of dielectric spheres in front of their apertures has been studied by the scattering theory approach [15]. The performance of corrugated conical horn as well as corrugated E -plane sectoral horn is found to improve considerably in respect of directivity, gain and sidelobes. These corrugated horns with off-set placed dielectric spheres at their apertures are seen to be efficient antenna feeds with variable beamwidth facility for paraboloidal reflectors for many space applications.

An extensive study of the radiation properties of

dielectric loaded sectoral horns has been made in chapter VI . Analytical results established in good agreement with experiments show that the axial directivity of dielectric loaded E -plane sectoral horn is significantly increased at the cost of slightly deteriorated sidelobe level. The dielectric sphere mounting over the radiating horn aperture is found effective in reducing the sidelobes as well as narrowing the beamwidths. Accordingly a dielectric sphere loaded dielectric coated E -plane sectoral horn is suggested as an effective multiple beam feed for large paraboloidal reflectors for possible applications in satellite communication and radio astronomy. The other sectoral horn considered in this chapter is a H -plane sectoral horn with a cylindrical aperture that inherently will have reduced sidelobes. Dielectric loading on the H -plane walls is found to increase remarkably the axial directivity of its radiation patterns. The sidelobe level is satisfactorily low, as the raise in sidelobe level probable with dielectric loading is rendered ineffective by virtue of its cylindrical aperture. Analytical treatment is extended to wide angle horns as well. Dielectric loaded H -plane horns can conveniently be used as efficient sources of microwave energy for antenna range applications.

The development of two improved feed systems on the

concept of multimode operation is discussed in chapter VII. A high gain dielectric loaded X -band double-flare multimode rectangular horn antenna operating in two orthogonal $TE_{10}+TE/TM_{12}$ and $TE_{01}+TE/TM_{21}$ mode sets is found to generate circularly polarised elliptically shaped beam. The antenna is found to have greater directivity, approximately equal beamwidths in E - and H -planes, and reduced sidelobes as a result of multimode operation.

The radiation characteristics of dielectric coated multimode horn antennas are improved further with significantly reduced sidelobe levels, greater directivity and higher on-axis gain by dielectric spheres mounted over the horn aperture at an off-set position. This high gain antenna system generating circularly polarised elliptical beam with good directivity, low sidelobe levels, equal E - and H -plane beamwidths and an approximately unity polarization axial ratio can be used as an effective antenna feed for satellite communication systems to efficiently illuminate an elliptical shaped zone on the earth's surface. In the same chapter, a highly directive multiple beam hybrid mode dielectric loaded horn that utilises the technique of combining several higher order modes for beam shaping has also been discussed. The importance of higher order mode contents in shaping the antenna pattern is illustrated

both analytically and experimentally. The technique of appropriate dielectric loading for considerable control over the E - and H -plane patterns are established. Such antennas with multiple beam shaping facility is important for several space applications that require simultaneous change in the concentration of energy toward different directions.

The performance details of the various antennas discussed are enlisted in Table I . The importance of dielectric loading in improving the radiation properties of the antennas for specific applications are evident from this table.

8.2 SUGGESTIONS FOR FURTHER WORK

The development of some improved dielectric loaded efficient feed systems for large paraboloidal reflectors for many space applications has been outlined. Still there are many dielectric loaded antenna systems that deserve further investigation. The radiation characteristic of the dielectric coated conical horn analyzed is for small flare angle cones ($\theta_0 \leq 30^\circ$) only with no phase variation of the aperture field. A ready extension would be to consider wideflare angle (i.e. $\theta_0 > 30^\circ$) conical horns. To calculate the radiation patterns of such wide angle horns accurately the transverse electric field over the horn aperture should

be used without any approximations in Silver's formula [125] for the diffracted far fields.

Recently considerable attention has been directed to the broad banding of horn feeds with ring loaded corrugated circular waveguide (RCWG) structures. The broad banding of high directivity dielectric coated conical horns can be investigated with corrugated flanges.

As the elevation beamwidth of an arc or a ring array can be narrowed by stacking several such arrays one above the other with a proper spacing, it is worth while to extend research on dielectric coated conical horns with several identical slots cut on the conical surface of the cone so that equispaced slot ring arrays are placed one above the other in a conical configuration (i.e. a conical array of slot rings). The radiation pattern of such a conical array can be computed by means of the space factor method suggested by Govert and Yang [45] for antenna array conformal to surfaces of revolution from a knowledge of the pattern for a slot on the dielectric coated cone (i.e. element pattern). Such a study is particularly important in view of the need for communication through plasma sheath for spacecraft during re-entry.

Further investigation is also suggested on the

directivity characteristics of a uniformly excited $N \times N$ array of conical helix horn (conical horn with a helical boundary) in the presence of off-set placed dielectric spheres at the horn aperture. Once the element pattern is expressed the field pattern and directivity of the array are computed in the usual way. The improvement of the corrugated horn performance was done by dielectric sphere mounting at the horn aperture. The behaviour of radiating corrugated horns with dielectric cylinder in front of the horn aperture is an interesting subject of further investigation on the basis of scattering theory approach.

The dielectric loaded E -plane sectoral horn that is seen to possess increased directivity can be investigated for applications as a feed for the short backfire type of antenna. Perhaps optimum performance may be obtained by a backfire aperture consisting of a large reflector trough and a small reflector strip as suggested by Large [79] . The short backfire antenna can also be tried with a dielectric loaded rectangular waveguide as its feed.

Currently the technique of multimode operation for pattern improvement has gained considerable attention, and hence the multimode operation discussed for a dielectric loaded double flare rectangular horn can be extended to a

double-flare conical geometry in view of the inherent symmetrical pattern property of conical horns.

It is strongly felt that investigations are to be taken up in the case of reflector antenna with dielectric coated inside surface. The dielectric coated reflector antenna is expected to give better performance (with reduced spillover) in view of the total internal reflection (TIR) property of the boundary between dielectric media.

Further it will be useful to assess the relative performance of the improved feed systems discussed in this thesis report. For this each feed system is to be designed for optimum performance, and then the relative performance may be accurately judged for the choice of the most efficient feed system.

In conclusion it may be said that eventhough some dielectric loaded improved horn antennas have been investigated in this thesis, and further works suggested herein, more efforts are essential in this field in view of the ever-increasing demand for physically small efficient antenna feed systems for many space applications. But it is hoped that this investigation report together with the suggestions for further works would prove to be a worthwhile contribution to the class of improved microwave antennas.

Horn Type	Empty Horn			Dielectric Coated Horn			Dielectric Sphere in front of the Horn Aperture								
	Gain in dB	Beam width	1st side-lobe levels	Gain in dB	Beam width	1st side-lobe level	4 cm dia. sphere			6 cm dia. sphere			9 cm dia. sphere		
							Gain in dB	Beam width	1st side-lobe level	Gain in dB	Beam width	1st side-lobe level	Gain in dB	Beam width	1st side-lobe levels
Conical Horn	14.5	34°	-12dB 23°	17.5	26°	-11.5dB at 26.5°	15.5	-	-	16.4	-	-	18.1	-	-
Dielectric coated conical horn	-	-	-	-	-	-	19	22°	-13.5dB at 25°	21	19.5°	-16 dB at 24.5°	22.5	15.25°	<-20 dB
Conical horn with helical boundary	15.4	30°	-9.5dB at 30°	-	-	-	16.4	23°	-11 dB at at 29.5°	17	20°	-12 dB at 29.5°	17.8	16°	<-15 dB
Biconical Horn	10.4	30°	-17 dB at 35°	13.3	20°	-6 dB at 25°	-	-	-	-	-	-	-	-	-
Corrugated E-plane sectoral Horn	15.8	34°	-16 dB at 55°	-	-	-	16.5	29.5°	-19.5dB at 70°	17.2	26°	<-22.5dB	17.6	22.5°	-20 dB at 68°
Corrugated conical Horn	13.5	32°	-20 dB at 40°	-	-	-	15	27°	-22 dB at 39.5°	16.5	23°	-24.5 dB at 39°	19	15°	-23.5dB at 31°
E-plane sectoral Horn	13.4	38°	-24 dB at 32°	15.8	30°	-18 dB at 35°	-	-	-	-	-	-	-	-	-
Dielectric coated E-plane sectoral Horn	-	-	-	-	-	-	16.2	27°	-21 dB at 40°	17	25°	<-22.5dB	17.6	22.5°	<-25dB
H-plane sectoral horn with cylindrical aperture	12.1	30°	-11.5dB at 32°	14.8	23°	-10 dB at 27.5°	-	-	-	-	-	-	-	-	-
Multimode Horn	12.4	35°	-30 dB at 55°	14.7	26°	-26 dB at 50°	-	-	-	-	-	-	-	-	-
Dielectric coated Multimode Horn	-	-	-	-	-	-	15.2	24°	-31 dB at 65°	16	22°	-32 dB at 70°	16.8	19°	-32.5dB at 55°

TABLE - I PERFORMANCE DETAILS OF THE VARIOUS TEST ANTENNAS DISCUSSED.

LIST OF PUBLICATIONS

1. Radiation from a Wide-angle Conical Horn with a Homogeneous Dielectric Sphere in front of its Aperture. IEEE Trans. Antenna and Propagation, March/May 1978 (to be published).
2. Radiation Characteristics of a Dielectric Sphere Loaded Corrugated E -plane Sectoral Horn, IEEE Trans. Antenna and Propagation (to be published).
3. Dielectric Sphere Loaded Radial Surfacewave Horn, International Journal of Electronics (London), 1978 (to be published).
4. Radiation Characteristics of a Dielectric Sphere Loaded Surfacewave Horn Antenna, Journal of the Institution of Electronics and Telecommunication, New Delhi, India, January 1978.
5. Radiation from a Wide-angle Conical Horn with a Homogeneous Dielectric Sphere in front of its Aperture, International IEEE/AP-S Symposium and USNC/URSI meeting, University of Massachusetts, Amherst, U.S.A. Oct. 11-15, 1976.
6. Radiation Characteristics of Dielectric Sphere Loaded Dielectric Coated E-plane Sectoral Horn. International IEEE AP-S Symposium, USNC/URSI Meeting and URSI International Electromagnetic Symposium, Stanford University, U.S.A. June 20-24, 1977.
7. Propagation and Radiation behaviour of Dielectric Coated E -plane Sectoral Horn. International Microwave Symposium sponsored by IEEE MTT-S, San Diego, California, June 21-23, 1977.
8. A Broad Band High Gain Antenna for Satellite Communications. IEEE sponsored National Telecommunications Conference NTC '77 Los Angles U.S.A., Dec.5-7,1977.
9. Diffraction by a Dielectric Loaded H -plane Sectoral Horn with a Cylindrical Aperture. U.S. National Radio Science Meeting, University of Colorado, Boulder, U.S.A. Jan. 9-13. 1978.

10. An Electromagnetic Approach to Nerve Fiber International Symposium and Workshop on Biomedical Engineering, New Delhi, India, Feb. 15-22, 1978.
11. Radiation Characteristics of a Dielectric Sphere Loaded Dielectric Coated Conical Horn. 20th Technical Convention, Institution of Electronics and Telecommunication Engineers, New Delhi, India, Dec. 11-12, 1976.
12. Radiation Characteristics of a Dielectric Sphere Loaded Surfacewave Horn Antenna 20th Technical Convention, Institution of Electronics and Telecommunication Engineers, New Delhi, India, Dec. 11-12, 1976.
13. Improving Radiation Characteristics of Corrugated Conical Horn using Dielectric Sphere 20th Technical Convention, Institution of Electronics and Telecommunication, Engrs. Delhi, India, Dec. 11-12, 1976.
14. Radiation properties of a High Gain Broad Band Multimode Horn Antenna for Satellite Communication System IEEE-MTT-S and Aerospace and Electronic Systems (India Section) sponsored technical Conference on Microwave Systems, New Delhi, India, October 27-29, 1977.
15. Short Backfire Antennas with Dielectric Coated Horn Feeds 21st Technical Convention, Institution of Electronics and Telecommunication Engineers, New Delhi, India, Dec. 10-11, 1977.
16. A Multiple Beam Hybrid Mode Dielectric Loaded Rectangular Horn. 21st Technical Convention, Institution of Electronics and Telecommunication Engineers, New Delhi, India, Dec. 10-11, 1977.
17. Radiation from a Dielectric Sphere Mounted at the Aperture of a plane Surfacewave Horn 21st Technical Convention, Institution of Electronics and Telecommunication Engrs., New Delhi, India, Dec. 10-11, 1977.
18. Radiation Characteristics of a High Gain Broad Band Conical Helix Antenna 21st Technical Convention, Institution of Electronics and Telecommunication Engrs., New Delhi, India, Dec. 10-11, 1977.
19. A Vector Potential Approach to Nerve Fiber Modelling 7th All India Symposium on Biomedical Engineering, Osmania University, Hyderabad, India, June 1978 (to be held).

BIBLIOGRAPHY

1. Ajioka J.A and Harry Jr. H.E. 'Shaped Beam Antenna for Earth Coverage from a Stabilised Satellite', IEEE Trans. Ant. and Prop., Vol. AP-18, May 1970, pp. 323-327.
2. Al-Hakkak M.J. 'Dielectric Loading of Corrugated Waveguide', Electronics letters, Vol. 8;7, April 6, 1972, pp. 179-180.
3. Allen P.A .and Tampkins R.D. 'An Instantaneous Microwave Polariser', Pro. IRE, 47, July 1959, pp. 1231-1237.
4. Ancona C 'Wide-angle Horns using Leaky Wave Wall Structures', IEEE Trans. Ant. and Prop., Vol. AP -23, May 1975, pp. 475-477.
5. Anderson J.B. 'Radiation from Surfacewave Antennas', Electronics letters , Vol. 3;7, July 1967, p.344.
6. Arora R.K. 'Unsymmetrical Radial Surfacewaves', IEEE Trans. Ant. and Prop. Vol. AP-14, Nov. 1966, pp. 797-798.
7. Ashton R.W. 'The Spiral Horn Antenna' 4th European Microwave Conference Proceedings, Sept. 10-13, 1974, pp. 499-503.
8. Attwood S.S. 'Surfacewave Propagation over a Coated Plane Conductor', Jou. Appl. Phy. Vol. 22, April 1951, pp. 504-509.
9. Bakefi G. and Farnel G.W. ' A Homogeneous Dielectric Sphere as a Microwave Lens' Can. Jou.Phy. Vol. 34, 1956, pp. 790-803.
10. Baldwin R. and McInnes P.A. 'Radiation Patterns of Dielectric Loaded Rectangular Horns', IEEE Trans. Ant. and Prop. vol. AP-21, May 1973, pp. 375-376.
11. Barlow H.M. and Cullen A.L. ' Surfacewaves' Pro.IEE Vol. 100, Nov. 1953, Part III Radio and Communication Engg., pp. 100-120.
12. Barrow W.L., Chu L.J. and Tansen J.J. 'Biconical Electromagnetic Horns' Pro. IRE Vol.27, Dec.1939, pp. 769-779.

13. Barrow W.L. and Chu L.J. 'Theory of Electromagnetic Horns', Pro. IRE, Vol. 27, 1939, pp. 5-9.
14. Bartlett H.E. and Moseley R.E. 'Dielectric-Highly Efficient Low Noise Antenna Feeds', Microwave Journal Vol.9, Dec. 1966, pp. 53-58.
15. Blakey J.R. 'A Scattering Theory Approach to the Prediction of Dielectric Rod Antenna Radiation Patterns: TM_{01} Mode', IEEE Trans. Ant. and Prop. Vol. AP-23, July 1975, pp. 577-579.
16. Born M. and Wolf E. 'Principles of Optics', (Pergamon Press) 1964.
17. Boulanger R.J. and Hamid M.A.K. 'A New Type of Dielectric Loaded Waveguide Antenna', Microwave Journal, Vol. 13, Dec. 1970, pp. 67-68.
18. Braun E.H. 'Some Data for Design of Electromagnetic Horns', IRE Trans. Ant. and Prop. Vol. AP-4, Jan 1956, pp. 29-31.
19. Brooking N, Clarricoats P.J.B. and Olver A.D. 'Radiation Patterns of Pyramidal Dielectric Waveguides', Electronics Letters Vol. 10;3, Feb.7,1974, pp. 33-34.
20. Bryant. G.H. 'Propagation in Corrugated Waveguides', Pro. IEE, Vol. 116, Feb.1969, pp. 203-213.
21. Caldecott R, Mentzer C.A. and Peters Jr. L 'Corrugated Horn as an Antenna Range Standard', IEEE Trans. Ant. and Prop., Vol. AP-21, July 1973, pp. 562-564.
22. Chatterjee J.S. 'Radiation Characteristics of a Conical Helix of Low Pitch Angle', Jou. Appl. Phy. Vol.26, March 1955, pp. 331-335.
23. Chatterjee J.S. and Crosswell W.F. 'Waveguide Excited Dielectric Sphere as Feeds', IEEE Trans. Ant. and Prop. Vol. AP-20, March 1972, pp. 206-208.
24. Chu T.S. and Sumbeck R.A. 'Gain of Electromagnetic Horns', Bell System Tech. Jou. Vol.44, March 1965, pp. 527-537.
25. Clarricoats P.J.B. 'Analysis of Spherical Hybrid Modes

- in a Corrugated Conical Horn', Electronics letters
Vol.5;9, May, 1969, pp. 189-190.
26. Clarricoats P.J.B. and Saha P.K. 'Radiation from
Wideflare Angle Scalar Horns', Electronics letters
Vol.5;16, Aug 7, 1969, pp. 376-378.
 27. Clarricoats P.J.B. and Saha P.K. 'Radiation Pattern
of a Lens Corrected Conical Scalar Feed', Electronics
letters Vol.5;23, Nov. 1969, pp. 592-593.
 28. Clarricoats P.J.B. and Saha P.K. 'Propagation and
Radiation Behaviour of Corrugated Feeds', Part I and
Part II, Pro. IEE ,Vol. 118, Sept. 1971, pp. 1167-1186.
 29. Clarricoats, P.J.B. , Salema C.E.R.C. and Lim S.H.
'Design of Cassegrain Antennas Employing Dielectric
Cone Feeds', Electronics letters, Vol.8;15, 27th July
1972, pp. 384-385.
 30. Clarricoats P.J.B. and Salema C.E.R.C.' Antennas
Employing Conical Dielectric Horns' - Part-2 the
Cassegrain Antenna Pro. IEE Vol. 120, July 1973,
pp. 750-756.
 31. Clarricoats P.J.B. and Salema C.E.R.C. 'Antennas
Employing Conical Dielectric Horns Pt I - Propagation
and Radiation Characteristics of Dielectric Cones',
Pro. IEE Vol.120, July 1973, pp. 741-749.
 32. Cohn S.B. 'Flare-angle Changes in a Horn as a means
of Pattern Control', Microwave Jou. Vol. 13 , Oct.1970
pp. 41,42,44,46.
 33. Collin R.E. and Zucker, Z.J.'Antenna Theory Part-1 and
Part -2, (McGraw Hill). 1960.
 34. Cook J.S., Elam E.M. and Zucker H 'The Open Cassegrain
Antenna - Part I Electromagnetic Design and Analysis',
Bell System Tech. Jou. Vol.44, Sept. 1965, pp.1255-1300.
 35. Cowles P.R. and Parker, E.A. 'Reflector Surface Error
Compensation in Cassegrain Antennas', IEEE Trans.
Ant. and Prop. Vol. AP-23, May 1975, pp. 323-327.
 36. Crawford A.B., Hogg D.C. and Hunt L.E. ' A Horn
Reflector Antenna for Space Communication', Bell Syst.
Tech. Jou. vol.40, July 1961, pp. 1045-1116.

37. Crosswell W.F., Chatterjee J.S. Mason V.B. and Tai C.T. 'Radiation from a Homogeneous Sphere Mounted on a Waveguide Aperture', IEEE Trans. Ant. and Prop. Vol. AP-23, Sept. 1975, pp. 647-656.
38. Cummins J.A 'Two Methods of Improving the Performance of Lens Connected H -plane Horns', IRE Canadian Convention Record 1958, pp. 232-239.
39. Cutler C.C. 'Parabolic Antenna Design for Microwaves', Pro. IRE Vol. 35, Nov. 1947, pp. 1284-1294.
40. Davies D.E.N. and Rudge A.W. 'Some Results of Electronic Compensation for Surface Profile Errors in Parabolic Reflectors', Electronics letters vol. 4;20, 4th Oct. 1968, pp. 433-434.
41. Davis, D. 'Corrugations Improve Monopulse Feed Horns', Microwaves, vol. 11, April 1972, pp. 58-63.
42. Drabowitz S 'Multimode Antennas', Microwave Jou. vol.9, Jan. 1966, pp. 41-51.
43. Elliot R.S. 'Spherical Surfacewave Antennas', IRE Trans. Ant. and Prop. Vol. AP-4 , July 1956, pp. 422-428.
44. Fradin A.Z 'Microwave Antennas', (Pergamon Press).
45. Gobert J.F. and Yang R.F. 'A Theory of Antenna Array Conformal to Surfaces of Revolution' IEEE Trans. Ant. and Prop. Vol. AP-22, January 1974, pp.87-91.
46. Goubau G. 'Surfacewaves and their Applications', Jo . Appl. Phy. Vol. 21, Nov. 1950, pp.1119-1128.
47. Hamid M.A.K 'Diffraction by a Conical Horn', IEEE Trans. Ant. and Prop. Vol. AP-16, Sept. 1968, pp.520-528.
48. Hamid M.A.K, Bhartia P., Mohsen A., Boerner W.M. and Boulanger R.J. 'Diffraction by Dielectric Loaded Conical Horn' Ist European Microwave Conf. (London 1969), IEEE Conf. Publication, No. 58, Sept. 1969, pp. 363-366.
49. Hamid M.A.K and Mohsen, A. 'Diffraction by Dielectric Loaded Horns and Corner Reflectors', IEEE Trans. Ant. and Prop. Vol. AP-17, Sept. 1969, pp. 660-662.

50. Hamid M.A.K., Boulanger R.J., Mostowy N.J. and Mohsen A 'Radiation Characteristics of Dielectric Loaded Horn Antennas', Electronics letters, Vol.6;1, 8th January 1970, pp. 20-21.
51. Han C.C. and Wickert A.N. 'A new Multimode Rectangular Horn Antenna Generating a Circularly Polarized Elliptical Beam', IEEE Trans. Ant. and Prop., Vol. AP-22 Nov. 1974, pp. 746-751.
52. Harrington R.F. 'Time Harmonic Electromagnetic Fields' (McGraw Hill Book Co.) 1961.
53. Herbison- Evans D 'Optimum Paraboloidal Aerial and Feed Design', Pro. IEE Vol. 115, Jan 1968, pp.87-90.
54. Horton C.W. 'On the Theory of the Radiation Patterns of Electromagnetic Horns of Moderate Flare-angles', Pro. IRE Vol. 37, July 1949, pp. 747-749.
55. Ingerson, P.G. and Rusch, W.V.T. 'Radiation from a Paraboloid with an Axially Defocussed Feed', IEEE Trans. Ant. and Prop., Vol. AP-21, Jan. 1973, pp. 104-106.
56. James, J.R. 'Engineering Approach to the Design of Tapered Dielectric Rod and Horn Antennas', Radio Electro. Engg. Vol. 42, June 1972, pp. 251-259.
57. James G.L., and Kerdelmidis 'Reflector Antenna Radiation Pattern Analysis by Equivalent Edge Currents', IEEE Trans. Ant. and Prop. Vol. AP-21, Jan.1973, pp. 19-24.
58. Jansen J.K.M. and Jeuken, M.E.J.' Surfacewaves in the Corrugated Conical Horn', Electronics letters, vol. 8;13, June 29, 1972, pp. 342-344.
59. Jeuken, M.E.J. and Kikkert, J.S. 'A Broad Band Aperture Antenna with a Narrow Beam', Alta Frequenza, vol. 38, March 1969, pp. 270-276.
60. Jeuken, M.E.J. and Lambrechtse, C.W. 'Small Corrugated Conical Horn Antenna with Wideflare Angle' Ele.lett. Vol. 5;20, Oct. 2, 1969, pp. 489-490.
61. Jeuken M.E.J. 'Experimental Radiation Pattern of the Corrugated Conical Horn Antenna with Small Flare-angle' Electronics letters Vol.5;20, Oct.2,1969, pp.484-485.

62. Jones E.M.T. 'Paraboloid Reflector and Hyperboloid Lens Antenna', IRE Trans. Ant. and Prop. Vol. AP-4, July 1956, pp. 119-127.
63. Jull E.V. 'Finite Range Gain of Sectoral and Pyramidal Horns', Electronics letters vol. 6;21, 15th Oct. 1970, pp. 680-681.
64. Jull E.V. 'Errors in the Predicted Gain of Pyramidal Horns', IEEE Trans. Ant. and Prop. Vol. AP-21, Jan.1973, pp. 25-31.
65. Jull E.V. 'Aperture Field and Gain of a Open Endèd Parallel Plate Waveguide', IEEE Trans. Ant. and Prop. vol. AP-21, Jan. 1973, pp. 14-18.
66. Jull E.V. and Allan L.E. 'Gain of an E -plane Sectoral Horn - A Failure of Kirchoff's Theory and a new proposal' IEEE Trans. Ant.and Prop. Vol. AP-22, March 1974, pp. 221-226.
67. Kamal A.K., Agarwal N. 'Gain of a Surfacewave Horn Antenna' IEEE Trans Ant.and Prop. Vol. AP-23, Sept.1975, pp 739-740
68. Kamal A.K., Nair R.A. and Gupta S.C. 'Radiation Characteristics of Dielectric Sphere Loaded Corrugated E -plane Sectoral Horn', IEEE Trans. Ant. and Prop. (to be published).
69. Kamal A.K., Gupta S.C. and Nair R.A 'Dielectric Sphere Loaded Radial Surfacewave Horn Antenna', Int. Journal of Electronics, London (to be published).
70. Kamal A.K. Gupta S.C. and Nair R.A. 'Radiation Characteristics of a wide-angle Conical Horn with a Homogeneous Dielectric Sphere at its Aperture', IEEE-A-P-S/URSI Int. Symposium, University of Massachussets,U.S.A. Oct. 10-14, 1976.
71. Kamal A.K., Nair R.A,Gupta S.C.' Propagation and Radiation behaviour of Dielectric Coated E -plane Sectoral Horn', Int. Microwave Symposium (MIT-S) San Diego, California, 21-23 June, 1977.
72. Kamal A.K., Nair R.A, and Gupta S.C. 'Radiation Characteristics of a Dielectric Sphere Loaded Dielectric Coated E-plane Sectoral Horn, URSI, Int. Electromagnetic Symposium, Stanford University, June 20-24, 1977.

73. Kamal A.K., Gupta S.C., Nair R.A. 'Radiation from a Wide-angle Conical Horn with a Homogeneous Dielectric Sphere at its Aperture', IEEE Trans. Ant and Prop. March 1978 (To be published)
74. Kamal A.K., Nair R.A. and Gupta S.C. ' A Broad Band High Gain Antenna for Satellite Communication', IEEE National Telecomn. Conference, Los Angles, U.S.A. Dec.5-7, 1977.
75. Katagi T and Takeichi 'Shaped Beam Horn Reflector Antennas', IEEE Trans. Ant. and Prop., Vol. AP-23 Nov. 1975, pp. 757-763.
76. King A.P. 'Radiation Characteristics of Conical Horn Antennas', Pro. IRE Vol. 38, March 1950, pp. 249-251.
77. Kraus J.D. 'Helical Beam Antennas for Wideband Applications' Pro. IRE, Vol. 36, Oct. 1948 pp. 1236-1242.
- 77a Kraus J.D. 'Antennas', (McGraw Hill Book Co.) New York, 1961.
78. Lawrie R.E. and Peters Jr. L 'Modification of Horn Antennas for Low Sidelobe Levels', IEEE Trans. Ant. and Prop. Vol. AP-14, Sept. 1966, pp. 605-610.
79. Large A.C. 'Short Backfire Antennas with Waveguide Linear Feeds', Microwave Journal Vol. 19, August 1976, pp. 49-52.
80. Love A.W. 'The Diagonal Horn Antenna', Microwave Journal Vol. 5, March 1962, pp. 117-122.
81. Ludwig A.C. 'Nearfield-Farfield Transformations using Spherical Expansion', IEEE Trans. Ant. and Prop. Vol. AP-19, March 1971, pp.214-218.
82. MacA T.B. Minnett, H.C. and Bao V.T. 'Fields in the Focal Region of a Spherical Reflector', IEEE Trans. Ant. and Prop. Vol. AP-17, March 1969, pp. 229-232.
83. MacA T.B. 'Bandwidth Properties of Corrugated Conical Horns', Electronics letters, Vol.5, 22; Oct. 30, 1969, pp. 561-563.
84. Manwarren, T. and Farrar, A. 'Pattern Shaping with Hybrid Mode Corrugated Horns' , IEEE Trans. Ant. and Prop. Vol. AP-22, May 1974, pp. 484-487.

85. Martin A.G. and Oxtoby A.J.A. 'Waveguide Fed Spherical Dielectric Antennas', IEEE Trans Ant. and Prop. Vol. AP-22, March 1974, pp. 338-340.
86. McKee, K.E., Holtum, A.J. and Charlton T, 'Optimising Gain of Parabolic Antennas', Microwaves, Vol. 6, No.3, March 1967, pp. 34-39.
87. M. de Vecchis, Aubin, M., Guigue, P.L. and Reymond, P. 'A Biconical Horn for Circular Polarisation', Microwave Jou. Vol. 13, May 1970, pp. 20B, 42-44.
88. Mentzer C.A. and Peters Jr. L. 'Properties of cut-off Corrugated Surfaces for Corrugated Horn Design', IEEE Trans. Ant. and Prop. Vol. AP-22, March 1974, pp. 191-196.
89. Minnett H.C. and MacA, T.B. 'A Method of Synthesizing Radiation Patterns with Axial Symmetry', IEEE Trans. Ant. and Prop. Vol. AP-14, Sept. 1966, pp. 654-656.
90. Minnett H.C. and MacA, T.B. 'Fields in the Image Space of Symmetrical Focussing Reflectors', Pro. IEE Vol.115, Oct. 1968, pp.1419-1430.
91. Minnett H.C. and MacA T.B. 'Propagation and Radiation behaviour of Corrugated Feeds', Pro. IEE Vol. 119, Sept. 1972, p.1280.
92. Mizusawa, M and Takeda, F 'Radiation Characteristics of Corrugated Conical Horn', The transaction of the Int. of Elect. and Commn. Engrs. of Japan, Vol. 56, No.1, June 1973, pp 11-13.
93. Nagelberg, E and Shefer, J. 'Mode Conversion in Circular Waveguides ' Bell System Tech. Jou. Vol.44, Sept.1965, pp. 1321-1328.
94. Narasimhan M.S. and Rao B.V. 'Hybrid Modes in Corrugated Conical Horns', Electronics letters Vol. 2; 22 Jan.1970, pp. 32-34.
95. Narasimhan M.S. and Rao B.V. 'Diffraction by Wideflare angle Corrugated Conical Horns', Electronics letters, Vol. 5;15, 23 July 1970, pp. 469-471.
96. Narasimhan M.S. and Rao B.V. 'Modes in a Conical Horn : New Approach', Pro. IEE Vol. 118, Feb. 1971, pp.287-292.

97. Narasimhan M.S. and Rao. B.V. 'Radiation from Conical Horns with large Flare-angles', IEEE Trans. Ant. and Prop. Vol. AP-19, Sept. 1971..pp.678-681.
98. Narasimhan M.S. and Mella Y.B. 'Paraboloidal Reflector Illumination with Conical Scalar Horns', Electronics letters vol.8;5, 9th March, 1972, pp. 111.-112.
99. Narasimhan M.S. and Rao B.V. 'Radiation Characteristics of Corrugated E -plane Sectoral Horns', IEEE Trans. Ant. and Prop. Vol. AP-21, May 1973, pp. 320-327.
100. Narasimhan M.S. and Rao B.V. 'A Correction to the available Radiation Formula for E -plane Sectoral Horn', IEEE Trans. Ant. and Prop. Vol. AP-21, Nov. 1973, pp. 878-879.
101. Narasimhan M.S. and Rao B.V. 'Radiation from Wide-flare Corrugated E -plane Sectoral Horn', IEEE Trans. Ant. and Prop. Vol. AP-22, July 1974, pp.603-607.
102. Neelakantaswamy P.S. and Banerjee D.K. 'Radiation Characteristics of Waveguide Excited Dielectric Spheres with matched Sphere-air Boundary', Electronics letters Vol. 9;2, 25th January 1973, pp. 40-41.
103. Neelakantaswamy P.S. and Banerjee D.K. 'Radiation Characteristics of a Waveguide Excited Dielectric Sphere Backed by a Metallic Hemispheres', IEEE Trans. Ant. and Prop. Vol. AP-21, May 1973, pp. 384-385.
104. Neelkantaswamy P.S. and Banerjee D.K.'Radiation Characteristics of a Dielectric Sphere Loaded Corrugated Pipe', IEE Trans. Ant. and Prop. Vol. AP-22, Sept. 1975, pp. 728-730.
105. Papas C.H. and King R. 'Radiation from a Wideangle Conical Antenna Fed by a Coaxial Line', Pro. IRE Vol.39 Jan 1951, pp. 49-51.
106. Phillips C.J.E. and Clarricoats P.J.B.' Optimum Design of a Gregorian Corrected Spherical Reflector Antenna', Pro . IEE Vol. 117, April 1970, pp.718-738.
107. Pritchard W.L. 'Satellite Communication - An overview of the problems and programs', Pro. IEEE Vol. 65, March 1977, pp. 294-307.

108. Potter P.D. 'A New Horn Antenna with Suppressed Sidelobes and equal Beamwidths', Microwave Journal Vol. 6, June 1963, pp. 71-78.
109. Potter P.D. and Ludwig A.C. 'Beam Shaping by use of Higher order Modes in Conical Horns', North-East Electron : Res. and Engineering Nov. 1963, pp.92-93.
110. Rhodes D.R. 'An Experimental Investigation of the Radiation Patterns of Electromagnetic Horn Antennas', Pro. IRE Vol.36, Sept. 1948, pp.1101-1105.
111. Rudge A.W. and Withers M.J. 'Design of Flared Horn Primary Feeds for Parabolic Reflector Antennas', Pro. IEE Vol. 108, Part -D , 1961, pp. 1741-1749.
112. Rudge A.W. 'Focal Plane Field Distribution of Parabolic Reflectors', Electronics letters Vol.5; 21, Oct. 1969, pp. 510-512.
113. Rudge A.W. and Davies D.E.N. 'Electronically Controllable Primary feed for Profile Error Compensation for Large Paraboloid Reflectors', Pro. IEE Vol. 117 (2), February 1970, pp. 351-358.
114. Rudge A.W. 'Multiple Beam Antennas : Off-set Reflectors with Off-set Feeds.' IEEE Trans. Ant. and Prop., Vol. AP-23, May 1975, pp. 317-322.
115. Rumsey V.H. 'Horn Antennas with Uniform Power Patterns around their Axes' IEEE Trans. Ant and Prop. Vol.AP-14, Sept. 1966, pp. 656-658.
116. Rusch W.V.T. 'Scattering from a Hyperboloidal Reflector in a Cassegrainian Feed System', IEEE Trans. Ant. and Prop. Vol. AP-11, July 1963, pp. 414-421.
117. Ruze J. 'Lateral Feed Displacement in a Paraboloid' IEEE Trans. Ant. and Prop. Vol. AP-13, Sept. 1965, pp. 660-665.
118. Sadler S.S. 'Paraboloidal Reflector Patterns for Off-axis Feed', IRE Trans. Ant. and Prop. Vol. AP-18, July 1970, pp. 368-379.
119. Satoh T. 'Dielectric Loaded Horn Antennas' IEEE Trans. Ant. and Prop. Vol. AP-20, March 1972, pp.199-201.

120. Schelknoff S.A. 'On Diffraction and Radiation of Electromagnetic waves', Phy. Rev. Vol. 56, July 1939, pp. 308-316.
121. Schelknoff S.A and Friss 'Antenna Theory and Practice (Wiley Publication) 1952,
122. Schell A.C. 'Diffraction Theory of Large Aperture Spherical Reflector Antennas', IEEE Trans. Ant. and Prop. Vol. AP-11, July 1963, pp. 428-432.
123. Schorr M.G. and Beck F.J. 'Electromagnetic Field of a Conical Horn', Journal of Applied Phy. Vol. 21, Aug. 1950, pp. 795-801.
124. Shimizu J.K. ' Octave Bandwidth Feed Horn for Paraboloid', IRE Trans. Ant. and Prop. Vol. AP-9, March 1961, pp. 223-224.
125. Silver S 'Microwave Antenna Theory and Design', Dover Publications N.Y. 1965.
126. Simmons A.J. and Kay A.F. 'The Scalar Feed - A High - performance Feed for Large Paraboloidal Reflectors, IEE Conference Pub. 21, 1966, pp. 213-217.
127. Southworth G.C. 'Hyper Frequency Waveguides - General Considerations and Experimental Results', Bell System Tech. Jou. Vol. 15, April 1936, pp. 284-309.
128. Southworth G.C. 'Principles and Applications of Waveguide Transmission' (Canada , Van Nostrand) 1950, p.356.
129. Stratton J.A. 'Electromagnetic Theory' (McGraw Hill Book Co.), N.Y., 1941.
130. Takeda F. and Hashimoto T 'Broad Banding of Corrugated Conical Horns by means of the Ring Loaded Corrugated Waveguide Structure' IEEE Trans. Ant. and Prop. Vol. AP-24, Nov. 1976, pp. 786-791.
131. Takeichi, Y, Hoshimoto T and Takeda F' A Ring Loaded Corrugated Waveguide' IEEE Trans. Microwave Theory and Tech. Vol. MTT-19, Dec. 1971, pp. 947-950.
132. Tomiyasu K 'Conversion of TE_{11} Mode by a Large Diameter Conical Junction', IEEE Trans. Microwave Theory and Tech. Vol. MTT-17, May 1969, pp. 277-279.

133. Towaij, S.J. Bhartia P, and Hamid M.A.K. 'Diffraction by a Sectoral Horn with Cylindrical Aperture', Int. Journal of Electronics Vol. 34, 3rd March 1973, pp. 381-383.
134. Tsandoulas G.N. and Fitzgerald W.D. 'Aperture Efficiency Enhancement in Dielectric Loaded Horns', IEEE Trans. Ant. and Prop. Vol. AP-21, Jan 1972, pp. 69-74.
135. Truman W.M. and Balanis C.A. 'Optimum Design of Horn Feed for Reflector Antennas', IEEE Trans. Ant. and Prop. Vol. AP-22, July 1974, pp. 585-586.
136. Turrin R.H. 'Dual Mode Small Aperture Antennas', IEEE Trans. Ant. and Prop. Vol. AP-15, March 1967, pp. 307-308.
137. Vu T.B. 'Optimisation of Efficiency of Deep Reflectors' IEEE Trans. Ant and Prop. Vol. AP -17, November 1969, pp. 811-813.
138. Vu T.B 'Optimization of Efficiency of Reflector Antennas Approximate Method', Pro. IEE Vol. 117, 1970, pp. 30-34.
139. Vu T.B. and Hien N.V. 'A New Type of High Performance Monopulse Feed', IEEE Trans. Ant. and Prop. Vol. AP-21, Nov. 1973, pp. 855-857.
140. Wood P.J. 'Reflector Profiles for the Pencil Beam Cassegrain Antennas', Marconi Rev. Vol. 35, no. 118, 1972, pp. 121-138.
141. Woonton G.A ., Hay D.R. and Vogan E.L.' An Experimental Investigation of Formulae for the Prediction of Horn Radiation Patterns', Jou Appl. Phy. Vol.20, Jan 1949, pp. 71-78.
142. Yu, J.S. Rudduck, R.C. and Peters Jr. L. 'Comprehensive Analysis for E -plane Pattern of Horn Antennas by Edge Diffraction Theory', IEEE Trans. Ant. and Prop. Vol. AP-14, March 1969, pp. 138-149.

APPENDIX A

EQUATION FOR DIELECTRIC SPHERE MOUNTED CONICAL HORN

A-1 THE CONSTANTS OF THE SCATTERED FIELD POTENTIALS

The boundary conditions to be met with are that the tangential components of E and H must be continuous at $r = b$

$$\begin{aligned} \text{i.e. } E_{\theta}^{+} &= E_{\theta}^{-} & H_{\theta}^{+} &= H_{\theta}^{-} \\ E_{\phi}^{+} &= E_{\phi}^{-} & H_{\phi}^{+} &= H_{\phi}^{-} \end{aligned} \quad \text{at } r = b.$$

The superscripts - denote the region $r < b$, and the superscripts + denote the region $r > b$. The total field external to the sphere is the sum of the incident and scattered fields, and hence by Eqs.(3.4),(3.6),(3.7) and (3.8), matching E_{θ} at $r = b$, it becomes,

$$\begin{aligned} & - \frac{1}{r \sin \theta} \eta_0 \cos \phi P_n^1(\cos \theta) [a_n \hat{J}_n(k_0 b) + c_n \hat{H}_n^{(2)}(k_0 b)] + \\ & \quad \frac{1 k_0}{j \omega \epsilon_0 r} \cos \phi [a_n \hat{J}_n'(k_0 b) + b_n \hat{H}_n^{(2)'}(k_0 b)] . \\ & \quad \frac{\partial}{\partial \theta} P_n^1(\cos \theta) \\ = & - \frac{1}{r \sin \theta} \eta_1 \cos \phi e_n P_n^1(\cos \theta) \hat{J}_n(k_1 b) + \frac{1}{j \omega \epsilon_1 r} k_1 \cos \phi d_n . \\ & \quad \hat{J}_n'(k_1 b) \frac{\partial}{\partial \theta} P_n^1(\cos \theta) \end{aligned}$$

Equating the coefficients of $P_n^1(\cos \theta)$ in the above equation,

it becomes,

$$\eta_0 [a_n \hat{J}_n(k_0 b) + c_n \hat{H}_n^{(2)}(k_0 b)] = \eta_1 e_n J_n(k_1 b) \quad (A-1)$$

and equating the coefficients of $\frac{\partial}{\partial \theta} P_n^1(\cos \theta)$,

$$\frac{k_0}{\epsilon_0} [a_n \hat{J}'_n(k_0 b) + b_n \hat{H}'_n^{(2)}(k_0 b)] = \frac{k_1}{\epsilon_1} d_n \hat{J}'_n(k_1 b) \quad (A-2)$$

Similarly,

$$H_\theta^+ = H_\theta^- \quad \text{at } r = b \quad \text{gives the relation,}$$

$$\begin{aligned} & - \frac{1}{r \sin \theta} \sin \theta P_n^1(\cos \theta) [a_n \hat{J}_n(k_0 b) + b_n \hat{H}_n^{(2)}(k_0 b)] + \\ & \frac{1 \eta_0}{j \omega \mu_0 r} \sin \theta k_0 [a_n \hat{J}'_n(k_0 a) + c_n \hat{H}'_n^{(2)}(k_0 b)] \frac{\partial}{\partial \theta} P_n^1(\cos \theta) \\ & = - \frac{1 d_n}{r \sin \theta} \sin \theta P_n^1(\cos \theta) \hat{J}_n(k_1 b) + \frac{1 \eta_1 k_1 e_n}{j \omega \mu_0 r} \sin \theta \hat{J}'_n(k_1 b) \cdot \\ & \qquad \qquad \qquad \frac{\partial}{\partial \theta} P_n^1(\cos \theta) \end{aligned}$$

Equating coefficients of $P_n^1(\cos \theta)$ in this relation it is obtained,

$$a_n \hat{J}_n(k_0 b) + b_n \hat{H}_n^{(2)}(k_0 b) = d_n \hat{J}_n(k_1 b) \quad (A-3)$$

and equating coefficients of $\frac{\partial}{\partial \theta} P_n^1(\cos \theta)$,

$$k_0 \eta_0 [a_n \hat{J}'_n(k_0 a) + c_n \hat{H}'_n^{(2)}(k_0 b)] = k_1 \eta_1 e_n \hat{J}'_n(k_1 b) \quad (A-4)$$

Multiplying Eq. (A-2) by $\hat{J}_n(k_1 b)$ and Eq. (A-3) by $\frac{k_1}{\epsilon_1} \hat{J}'_n(k_1 b)$ it becomes,

$$\begin{aligned} \frac{k_1}{\epsilon_1} d_n \hat{J}'_n(k_1 b) \hat{J}_n(k_1 b) - \frac{k_0}{\epsilon_0} b_n \hat{H}_n^{(2)'}(k_0 b) \hat{J}_n(k_1 b) \\ = \frac{k_0}{\epsilon_1} a_n \hat{J}'_n(k_0 b) \hat{J}_n(k_1 b) \end{aligned} \quad (A-5)$$

and

$$\begin{aligned} \frac{k_1}{\epsilon_1} d_n \hat{J}_n(k_1 b) \hat{J}'_n(k_1 b) - \frac{k_1}{\epsilon_1} b_n \hat{H}_n^{(2)}(k_0 b) \hat{J}'_n(k_1 b) \\ = \frac{k_1}{\epsilon_1} a_n \hat{J}_n(k_0 b) \hat{J}'_n(k_1 b) \end{aligned} \quad (A-6)$$

(A-6) - (A-5) gives

$$\begin{aligned} b_n \left[\frac{k_0}{\epsilon_0} \hat{H}_n^{(2)'}(k_0 b) \hat{J}_n(k_1 b) - \frac{k_1}{\epsilon_1} \hat{H}_n^{(2)}(k_0 b) \hat{J}'_n(k_1 b) \right] \\ = \left[\frac{k_1}{\epsilon_1} \hat{J}_n(k_0 b) \hat{J}'_n(k_1 b) - \frac{k_0}{\epsilon_0} \hat{J}'_n(k_0 b) \hat{J}_n(k_1 b) \right] a_n \end{aligned} \quad (A-7)$$

Multiplying Eq. (A-7) throughout by $\sqrt{\epsilon_1 \epsilon_0}$

$$\begin{aligned} b_n (\sqrt{\epsilon_1} \hat{H}_n^{(2)'}(k_0 b) \hat{J}_n(k_1 b) - \sqrt{\epsilon_0} \hat{H}_n^{(2)}(k_0 b) \hat{J}'_n(k_1 b)) \\ = [-\sqrt{\epsilon_1} \hat{J}'_n(k_1 b) \hat{J}_n(k_1 b) + \sqrt{\epsilon_0} \hat{J}_n(k_0 b) \hat{J}'_n(k_1 b)] a_n \end{aligned}$$

$$\text{i.e. } b_n = \frac{-\sqrt{\epsilon_1} \hat{J}'_n(k_0 b) \hat{J}_n(k_1 b) + \sqrt{\epsilon_0} \hat{J}_n(k_0 b) \hat{J}'_n(k_1 b)}{\sqrt{\epsilon_1} \hat{H}_n^{(2)'}(k_0 b) \hat{J}_n(k_1 b) - \sqrt{\epsilon_0} \hat{H}_n^{(2)}(k_0 b) \hat{J}'_n(k_1 b)} \cdot a_n \quad (\text{A-8})$$

Similar operations on Eqs. (A-1) and (A-4) would give,

$$c_n = \frac{-\sqrt{\epsilon_1} \hat{J}_n(k_0 b) \hat{J}'_n(k_1 b) + \sqrt{\epsilon_0} \hat{J}'_n(k_0 b) \hat{J}_n(k_1 b)}{\sqrt{\epsilon_0} \hat{H}_n^{(2)}(k_0 b) \hat{J}'_n(k_1 b) - \sqrt{\epsilon_1} \hat{H}_n^{(2)'}(k_0 b) \hat{J}_n(k_1 b)} \cdot a_n \quad (\text{A-9})$$

Substitution of typical test values of the sphere diameter 'b', permittivity ϵ_1 and the operating frequency f_0 in Eqs. (A-8) and (A-9) will give the values of b_n and c_n respectively, in terms of a_n whose value is defined by the relation,

$$a_n = j^{-n} \frac{(2n+1)}{n(n+1)}$$

A-2 RADIATED FAR-FIELD

The total field at any point in the far-zone region is the sum of the incident and scattered fields. Thus by Eq. (3.4) the total field components at the far-zone point become

$$E_{\theta}^{+} = E_{\theta}^{i} + E_{\theta}^{s} = \frac{1}{r \sin \theta} \frac{\partial}{\partial \theta} F_r^{+} + \frac{1}{j \omega \epsilon_0 r} \frac{\partial^2 A_r^{+}}{\partial r \partial \theta} \quad (\text{A-10})$$

$$E_{\phi}^{+} = E_{\phi}^{i} + E_{\phi}^{s} = \frac{1}{r} \frac{\partial}{\partial \theta} F_r^{+} + \frac{1}{j \omega \epsilon_0 r \sin \theta} \frac{\partial^2 A_r^{+}}{\partial r \partial \theta}$$

The values of A_r^{+} and F_r^{+} are given by the Eqs. (3.6) and (3.7) as,

$$A_r^{+} = A_r^i + A_r^s = \cos \theta \sum_{n=1}^{\infty} \hat{H}_n^{(2)}(k_0 r) P_n^1(\cos \theta) (a_n + b_n) \quad (\text{A-11})$$

$$F_r^{+} = F_r^i + F_r^s = \eta_0 \sin \theta \sum_{n=1}^{\infty} \hat{H}_n^{(2)}(k_0 r) P_n^1(\cos \theta) (a_n + c_n)$$

From the above Eqs (A-10) and (A-11), the field components are obtained as

$$E_{\theta}^{+} = - \frac{1}{r \sin \theta} \eta_0 \cos \theta \sum_{n=1}^{\infty} \hat{H}_n^{(2)}(k_0 r) P_n^1(\cos \theta) (a_n + c_n) + \frac{1}{j \omega \epsilon_0 r} k_0 \cos \theta \sum_{n=1}^{\infty} \hat{H}_n^{(2)'}(k_0 r) (a_n + b_n) \frac{\partial}{\partial \theta} P_n^1(\cos \theta)$$

and

$$E_{\theta}^+ = \frac{1}{r} \eta_0 \sin\theta \sum_{n=1}^{\infty} \hat{H}_n^{(2)}(k_0 r) \frac{\partial}{\partial \theta} P_n^1(\cos\theta) (a_n + c_n) +$$

$$\frac{1}{j\omega \epsilon_0 r \sin\theta} (-) \sin\theta k_0 \sum_{n=1}^{\infty} \hat{H}_n^{(2)'}(k_0 r) P_n^1(\cos\theta) (a_n + b_n)$$

Using far-field approximations (i.e. for $k_0 r \gg 1$,

$$\hat{H}_n^{(2)}(k_0 r) = j^{n+1} e^{-jk_0 r} \quad \text{and} \quad \frac{H'}{H} = -j, \quad E_{\theta}^+ \quad \text{and} \quad E_{\phi}^+$$

$$E_{\theta}^+ = -\eta_0 \cos\theta \frac{\exp(-jk_0 r)}{r} \sum_{n=1}^{\infty} j^{n+1} .$$

$$\left[P_n^1(\cos\theta) (a_n + c_n) + \frac{\partial}{\partial \theta} P_n^1(\cos\theta) (a_n + b_n) \right] \quad (\text{A-12})$$

and

$$E_{\phi}^+ = \eta_0 \sin\theta \frac{\exp(-jk_0 r)}{r} \sum_{n=1}^{\infty} j^{n+1} .$$

$$\left[\frac{\partial}{\partial \theta} P_n^1(\cos\theta) (a_n + c_n) + \frac{P_n^1(\cos\theta)}{\sin\theta} (a_n + b_n) \right]$$

$$(\text{A-13})$$

Hence the resultant field at any point in the far-zone becomes,

$$E_R(r) = \bar{i}_{\theta} E_{\theta} + \bar{i}_{\phi} E_{\phi}$$

$$= -\eta_0 \frac{\exp(-jk_0 r)}{r} \sum_{n=1}^{\infty} j^{n+1} a_n .$$

$$\left[\left\{ \left(1 + \frac{c_n}{a_n} \right) P_n^1(\cos\theta) + \left(1 + \frac{b_n}{a_n} \right) \frac{\partial}{\partial \theta} P_n^1(\cos\theta) \right\} \cos\theta \bar{i}_{\theta} \right.$$

$$\left. - \left\{ \left(1 + \frac{c_n}{a_n} \right) \frac{\partial}{\partial \theta} P_n^1(\cos\theta) + \left(1 + \frac{b_n}{a_n} \right) \frac{P_n^1(\cos\theta)}{\sin\theta} \right\} \sin\theta \bar{i}_{\phi} \right]$$

$$(\text{A-14})$$

$$\begin{aligned}
 E_R(r) &= -\eta_0 \frac{\exp(-jk_0 r)}{r} \sum_{n=1}^{\infty} j^{n+1} a_n \left[\left(1 + \frac{c_n}{a_n}\right) \cdot \right. \\
 &\quad \left. \left\{ P_n^1(\cos\theta) \cos\theta \bar{i}_\theta - \frac{\partial}{\partial\theta} P_n^1(\cos\theta) \sin\theta \bar{i}_\phi \right\} + \right. \\
 &\quad \left. \left(1 + \frac{b_n}{a_n}\right) \cdot \left\{ \frac{\partial}{\partial\theta} P_n^1(\cos\theta) \cos\theta \bar{i}_\theta - \frac{P_n^1 \cos\theta}{\sin\theta} \sin\theta \bar{i}_\phi \right\} \right] \\
 &= -\eta_0 \frac{\exp(-jk_0 r)}{r} \sum_{n=1}^{\infty} j^{n+1} a_n [\alpha_n M_n + \beta_n N_n] \quad (A-15)
 \end{aligned}$$

Inserting $a_n = j^{-n} \frac{(2n+1)}{n(n+1)}$, the resultant expression for the far-zone field becomes,

$$E_R(r) = -j \eta_0 \frac{\exp(-jk_0 r)}{r} \sum_{n=1}^{\infty} \frac{(2n+1)}{n(n+1)} (M_n \alpha_n + N_n \beta_n) \quad (A-16)$$

where $\alpha_n = \left(1 + \frac{c_n}{a_n}\right)$

$$\beta_n = \left(1 + \frac{b_n}{a_n}\right)$$

$$M_n = P_n^1(\cos\theta) \cos\theta \bar{i}_\theta - \frac{\partial}{\partial\theta} P_n^1(\cos\theta) \sin\theta \bar{i}_\phi$$

$$N_n = \frac{\partial}{\partial\theta} P_n^1(\cos\theta) \cos\theta \bar{i}_\theta - \frac{P_n^1(\cos\theta)}{\sin\theta} \sin\theta \bar{i}_\phi$$

A-3 POWER RADIATED AND GAIN

The total power radiated W_t

$$= \frac{1}{2} \operatorname{Re} \left[\int_{\phi=0}^{2\pi} \int_{\theta=0}^{\pi} r^2 (E_R \times H_R^*) \sin\theta d\theta d\phi \right]$$

Noting that for free space $E_R(r) = \eta_0 H_R(r)$, by Eq. (A-15)

W_t becomes,

$$W_t = \frac{1}{2} \eta_0 \int_0^{2\pi} \int_0^{\pi} [a_n (M_n \alpha_n + N_n \beta_n)]^2 \sin\theta d\theta d\phi$$

where M_n, N_n, α_n and β_n are given by Eq. (3.16)

Inserting the expression for M_n and N_n ,

$$\begin{aligned} W_t = \frac{1}{2} \eta_0 a_n^2 & \left[\int_0^{2\pi} \int_0^{\pi} \alpha_n^2 \left\{ \left[\frac{P_n^1(\cos\theta)}{\sin\theta} \right]^2 \sin^2\phi + \right. \right. \\ & + \left. \left[\frac{\partial}{\partial\theta} P_n^1(\cos\theta) \right]^2 \cos^2\phi \right\} + \beta_n^2 \left[\frac{\partial}{\partial\theta} P_n^1(\cos\theta) \right]^2 \sin^2\phi + \\ & + \left. \left[\frac{P_n^1(\cos\theta)}{\sin\theta} \right]^2 \cos^2\phi \right\} + \\ & + 2\alpha_n \beta_n \left\{ \frac{P_n^1(\cos\theta)}{\sin\theta} \frac{\partial}{\partial\theta} P_n^1(\cos\theta) \left[\cos^2\phi + \sin^2\phi \right] \right\} \right] \sin\theta d\theta d\phi \end{aligned}$$

Using the orthogonal relationships

$$\begin{aligned} \int_0^{\pi} \left[\frac{\partial}{\partial\theta} P_n^1(\cos\theta) \right]^2 + \left[\frac{P_n^1(\cos\theta)}{\sin\theta} \right]^2 \sin\theta d\theta & = \\ & = \frac{2}{(2n+1)} \frac{(n+1)!}{(n-1)!} n(n+1) \end{aligned}$$

$$\text{and } \int_0^\pi \frac{P_n^1(\cos\theta)}{\sin\theta} \frac{\partial}{\partial\theta} P_n^1(\cos\theta) + \frac{P_n^1(\cos\theta)}{\sin\theta} \frac{\partial}{\partial\theta} P_n^1(\cos\theta) \sin\theta d\theta = 0,$$

the above integral for W_t is determined as,

$$W_t = \eta_0 \pi \sum_{n=1}^{\infty} \frac{a_n^2 n^2 (n+1)^2}{(2n+1)} (|\alpha_n|^2 + |\beta_n|^2),$$

and replacing a_n , W_t becomes,

$$W_t = \eta_0 \pi \sum_{n=1}^{\infty} (2n+1) (|\alpha_n|^2 + |\beta_n|^2)$$

The forward directivity is defined as

$$D_0 = \frac{1}{2} \left| E_R(r) \right|_{\theta=\pi}^2 \frac{4\pi r^2}{\eta_0 W_t}$$

Making use of the relationships

$$\frac{P_n^1(\cos\theta)}{\sin\theta} \xrightarrow{\theta \rightarrow \pi} \frac{(-1)^n}{2} n(n+1)$$

and $-\frac{\partial}{\partial\theta} P_n^1(\cos\theta) \xrightarrow{\theta \rightarrow \pi} \frac{(-1)^n}{2} n(n+1)$ in the expression for $E_R(r)$, and inserting the value of a_n , D_0 becomes

$$D_0 = \frac{\left| \sum_{n=1}^{\infty} \frac{(2n+1)}{2} (-1)^n (\alpha_n + \beta_n) \right|^2}{\sum_{n=1}^{\infty} \frac{2n+1}{2} (|\alpha_n|^2 + |\beta_n|^2)}$$

APPENDIX B

EQUATIONS FOR DIELECTRIC COATED CONICAL HORN

B - 1 CHARACTERISTIC EQUATION FOR DIELECTRIC COATED CONICAL HORN

The fields in the axial region of the horn are given by the potential functions,

$$\begin{aligned} A_r &= a_{mn} \hat{H}_n^{(2)}(k_0 r) J_m(q\theta) \exp(jm\phi) \\ F_r &= b_{mn} \hat{H}_n^{(2)}(k_0 r) J_m(q\theta) \exp(jm\phi) \end{aligned} \quad (B-1)$$

and those in the dielectric loaded region, to account for the standing waves, are given by

$$\begin{aligned} A_r^d &= [c_{mn} J_m(q\theta) + d_{mn} Y_m(q\theta)] \hat{H}_n^{(2)}(k_1 r) \exp(jm\phi) \\ F_r^d &= [e_{mn} J_m(q\theta) + f_{mn} Y_m(q\theta)] \hat{H}_n^{(2)}(k_1 r) \exp(jm\phi) \end{aligned} \quad (B-2)$$

where

$$\frac{b_{mn}}{a_{mn}} = -j \eta_0 B_0, \quad \frac{e_{mn}}{c_{mn}} = -j \eta_1 B_0$$

and

$$\frac{f_{mn}}{d_{mn}} = -j \eta_1 B_0, \quad \text{with } \eta_0 = \sqrt{\mu_0 / \epsilon_0}$$

$$\eta_1 = \sqrt{\mu_0 / \epsilon_1}, \quad B_0 = \text{a coefficient depending on}$$

the horn excitation, $m = \text{an integer}$ and n is real and positive.

The eigen values 'n' can be obtained from the characteristic equation formulated on the boundary conditions viz.,

1. the tangential component of $E = 0$ at $\theta = \theta_0$

$$\text{i.e. } E_r^d = \frac{1}{j\omega\epsilon_0} \left(\frac{\partial^2}{\partial r^2} + k_1^2 \right) A_r^d = 0 \text{ at } \theta = \theta_0$$

$$\text{Thus } d_{mn} = -c_{mn} \frac{J_m(q\theta_0)}{y_m(q\theta_0)} \quad (\text{B-3})$$

2. the E -field is continuous at $\theta = \theta_1$,

$$\text{Thus } E_r = E_r^d \text{ at } \theta = \theta_1$$

$$\text{i.e. } a_{mn} \frac{n(n+1)}{j\omega\epsilon_0 r^2} \hat{H}_n^{(2)}(k_0 r) J_m(q\theta_1)$$

$$= \frac{n(n+1)}{j\omega\epsilon_1 r^2} [c_{mn} J_m(q\theta_1) + d_{mn} y_m(q\theta_1)] \hat{H}_n(k_1 r)$$

$$\therefore a_{mn} \hat{H}_n^{(2)}(k_0 r) J_m(q\theta_1) = \frac{\epsilon_0}{\epsilon_1} [c_{mn} J_m(q\theta_1) + d_{mn} y_m(q\theta_1)] \cdot$$

$$\hat{H}_n^{(2)}(k_1 r) \quad (\text{B-4})$$

3. the H -field is continuous at $\theta = \theta_1$.

$$\text{Thus , } H_\phi = H_\phi^d$$

$$\begin{aligned}
 \text{i.e. } & - \frac{a_{mn}}{r} \hat{H}_n^{(2)}(k_0 r) q J_m'(q\theta_1) + \\
 & + \frac{jmk_0}{j\omega \mu_0 r \sin\theta} \frac{b_{mn}}{\sin\theta} \hat{H}_n^{(2)'}(k_0 r) J_m(q\theta_1) \\
 = & \frac{1}{r} \left\{ q [c_{mn} J_m'(q\theta_1) + d_{mn} y_m'(q\theta_1)] \hat{H}_n^{(2)}(k_1 r) \right\} + \\
 & + \frac{jmk_1}{j\omega \mu_0 r \sin\theta} \hat{H}_n^{(2)'}(k_1 r) [e_{mn} J_m(q\theta_1) + f_{mn} y_m(q\theta_1)]
 \end{aligned}$$

Now inserting the relationships between b_{mn} and a_{mn} ;
 e_{mn} and c_{mn} ; f_{mn} and d_{mn} and also using Eq. (B-3) the above
relation becomes,

$$\begin{aligned}
 a_{mn} & \left[\hat{H}_n^{(2)}(k_0 r) q J_m'(q\theta_1) + \right. \\
 & \left. \frac{j m \omega \sqrt{\mu_0 \epsilon_0}}{j \omega \mu_0 \sin\theta_1} j \eta_0 B_0 \hat{H}_n^{(2)'}(k_0 r) J_m(q\theta_1) \right] \\
 = & c_{mn} \left[\frac{q \{ J_m'(q\theta_1) y_m(q\theta_0) - y_m'(q\theta_1) J_m(q\theta_0) \}}{y_m(q\theta_0)} \hat{H}_n^{(2)}(k_1 r) \right. \\
 & \left. + \frac{B_0 j m k_1 j \eta_1}{j \omega \mu_0 \sin\theta_1} \hat{H}_n^{(2)'}(k_1 r) \left\{ \frac{J_m(q\theta_1) y_m(q\theta_0) - J_m(q\theta_0) y_m(q\theta_1)}{y_m(q\theta_0)} \right\} \right]
 \end{aligned}$$

(B-5)

Using Eq. (B-3), Eq. (B-4) becomes,

$$\begin{aligned}
 & a_{mn} \hat{H}_n^{(2)}(k_o r) J_m(q\theta_1) \\
 &= \frac{\epsilon_o}{\epsilon_1} c_{mn} \left[\frac{J_m(q\theta_1)y_m(q\theta_o) - J_m(q\theta_o)y_m(q\theta_1)}{y_m(q\theta_o)} \right] \hat{H}_n^{(2)}(k_1 r)
 \end{aligned}
 \tag{B-6}$$

Dividing (B-5) by (B-6), and remembering the relationship

$$\begin{aligned}
 & k_o \eta_o = \omega \mu_o, \quad k_1 \eta_1 = \omega \mu_o, \text{ it becomes,} \\
 & q \frac{J_m'(q\theta_1)}{J_m(q\theta_1)} + \frac{j m B_o}{\sin \theta_1} \frac{\hat{H}_n^{(2)'}(k_o r)}{\hat{H}_n^{(2)}(k_o r)} \\
 &= \frac{\epsilon_1}{\epsilon_o} \left[q \frac{J_m'(q\theta_1)y_m(q\theta_o) - y_m'(q\theta_1)J_m(q\theta_o)}{J_m(q\theta_1)y_m(q\theta_o) - J_m(q\theta_o)y_m(q\theta_1)} \right. \\
 & \quad \left. + \frac{j B_o}{\sin \theta_1} \frac{\hat{H}_n^{(2)'}(k_1 r)}{\hat{H}_n^{(2)}(k_1 r)} \right]
 \end{aligned}
 \tag{B-7}$$

With the far-field approximation (i.e. $\frac{H'}{H} = -j$), and multiplying throughout by $\sin \theta$ the above Eq.(B-7) becomes,

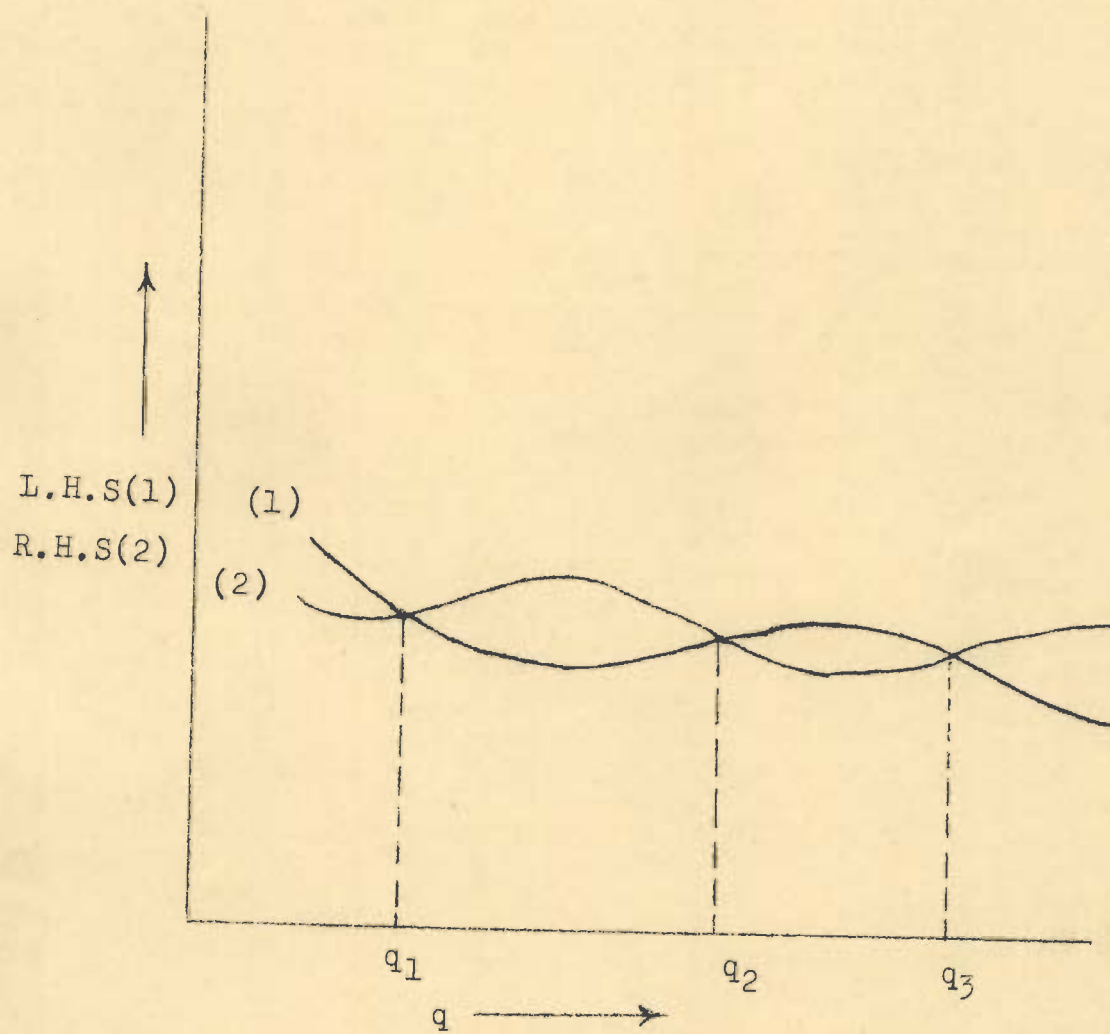
$$\begin{aligned}
 & q \frac{J_m'(q\theta_1)}{J_m(q\theta_1)} \sin \theta_1 + m B_o = \\
 &= \frac{\epsilon_1}{\epsilon_o} \left[q \sin \theta_1 \frac{J_m'(q\theta_1)y_m(q\theta_o) - J_m(q\theta_o)y_m'(q\theta_1)}{J_m(q\theta_1)y_m(q\theta_o) - J_m(q\theta_o)y_m(q\theta_1)} + B_o \right]
 \end{aligned}
 \tag{B-8}$$

Now restricting the consideration to the case with $m = 1$, and the excitation coefficient $B_0 = +1$, the characteristic equation for the HE_{1n} mode becomes,

$$\begin{aligned} & \frac{J'_m(q\theta_1)}{q J_m(q\theta_1)} \sin\theta_1 + 1 = \\ & = \frac{\epsilon_1}{\epsilon_0} \left[q \frac{J'_m(q\theta_1)y_m(q\theta_0) - J_m(q\theta_0)y'_m(q\theta_1)}{J_m(q\theta_1)y_m(q\theta_0) - J_m(q\theta_0)y_m(q\theta_1)} \sin\theta_1 + 1 \right] \end{aligned} \tag{B-9}$$

Eq. (B-9) is the characteristic equation for the eigen values 'n'.

This equation is solved graphically for a dielectric coating thickness of 2° with a dielectric material of permittivity $\epsilon_1 = 2.25$. The graphical method of solution is illustrated in Fig. B-1. The eigen value n for the hybrid $HE_{1,1}$ mode is obtained by obtaining the first ordinal root of the characteristic equation. The values thus obtained are shown in Fig. 3.6 for different values of the coated cone flare angle θ_1 together with those for conventional and corrugated conical horns.



q_1 , q_2 , and q_3 correspond to the values of q for HE_{11} , HE_{12} and HE_{13} mode respectively.

Fig. B-1 Method of Solution of Characteristic Equation.

B - 2 THE RADIATION FROM DIELECTRIC COATED CONICAL HORN

The transverse electric field \bar{E}_t over the horn aperture for HE_{11} mode is given by

$$\bar{E}_t = -(j)^{n+1} a_{11} \eta_0 \frac{e^{-jk_0 r}}{r} q J_0(q\theta) (\bar{i}_\theta + j\bar{i}_\phi) \exp j\phi$$

The radiated far-field can be derived using the vector diffraction formula; and thus assuming no phase variation of E_t over the horn aperture, radiated far-field at any point (r, θ, ϕ) is given by

$$E_R(r, \theta, \phi) = j \frac{e^{-jk_0 r}}{2\lambda_0 r} (1 + \cos\theta) \int_0^{a_0} \int_0^{2\pi} E_t \cdot e^{jk_0 \rho \cos\phi \sin\theta} \rho d\rho d\phi \quad (B-10)$$

And inserting the value of \bar{E}_t for HE_{11} mode

$$E_R(r, \theta, \phi) = j \frac{e^{-jk_0 r}}{2\lambda_0 r} (1 + \cos\theta) (\bar{i}_\theta + j\bar{i}_\phi) e^{j\phi} \frac{a_{11} \eta_0}{L} \int_0^{a_0} \int_0^{2\pi} q J_0(q\theta) e^{jk_0 \rho \cos\phi \sin\theta} \rho d\rho d\phi \quad (B-11)$$

But $\int_0^{2\pi} e^{jk_0 \rho \cos\phi \sin\theta} d\phi = 2\pi J_0(k_0 \rho \sin\theta)$

Thus

$$E_R(r, \theta, \phi) = j \frac{e^{-jk_0 r}}{2\lambda_0 r} (1 + \cos\theta) \frac{a_{11} \eta_0}{L} 2\pi q (\bar{i}_\theta + j\bar{i}_\phi) e^{j\phi} \int_0^a J_0\left(\frac{q}{L} \rho\right) J_0(k \sin\theta \rho) d\rho$$

$$\left(\theta \approx \frac{S}{L} \right)$$

Horn Type	Empty Horn			Dielectric Coated Horn			Dielectric Sphere in front of the Horn Aperture								
	Gain in dB	Beam width	1st side-lobe levels	Gain in dB	Beam width	1st side-lobe level	4 cm dia. sphere			6 cm dia. sphere			9 cm dia. sphere		
							Gain in dB	Beam width	1st side-lobe level	Gain in dB	Beam width	1st side-lobe level	Gain in dB	Beam width	1st side-lobe levels
Conical Horn	14.5	34°	-12dB 23°	17.5	26°	-11.5dB at 26.5°	15.5	-	-	16.4	-	-	18.1	-	-
Dielectric coated conical horn	-	-	-	-	-	-	19	22°	-13.5dB at 25°	21	19.5°	-16 dB at 24.5°	22.5	15.25°	<-20 dB
Conical horn with helical boundary	15.4	30°	-9.5dB at 30°	-	-	-	16.4	23°	-11 dB at at 29.5°	17	20°	-12 dB at 29.5°	17.8	16°	<-15 dB
Biconical Horn	10.4	30°	-17 dB at 35°	13.3	20°	-6 dB at 25°	-	-	-	-	-	-	-	-	-
Corrugated E-plane sectoral Horn	15.8	34°	-16 dB at 55°	-	-	-	16.5	29.5°	-19.5dB at 70°	17.2	26°	<-22.5dB	17.6	22.5°	-20 dB at 68°
Corrugated conical Horn	13.5	32°	-20 dB at 40°	-	-	-	15	27°	-22 dB at 39.5°	16.5	23°	-24.5 dB at 39°	19	15°	-23.5dB at 31°
E-plane sectoral Horn	13.4	38°	-24 dB at 32°	15.8	30°	-18 dB at 35°	-	-	-	-	-	-	-	-	-
Dielectric coated E-plane sectoral Horn	-	-	-	-	-	-	16.2	27°	-21 dB at 40°	17	25°	<-22.5dB	17.6	22.5°	<-25dB
H-plane sectoral horn with cylindrical aperture	12.1	30°	-11.5dB at 32°	14.8	23°	-10 dB at 27.5°	-	-	-	-	-	-	-	-	-
Multimode Horn	12.4	35°	-30 dB at 55°	14.7	26°	-26 dB at 50°	-	-	-	-	-	-	-	-	-
Dielectric coated Multimode Horn	-	-	-	-	-	-	15.2	24°	-31 dB at 65°	16	22°	-32 dB at 70°	16.8	19°	-32.5dB at 55°

TABLE - I PERFORMANCE DETAILS OF THE VARIOUS TEST ANTENNAS DISCUSSED.

$$= j \frac{e^{-jk_0 r}}{2\lambda_0 r} (1+\cos\theta) \frac{a_{11} \eta_0}{L} 2\pi q a_0 (\bar{i}_\theta + j\bar{i}_\phi) \cdot$$

$$\left[\frac{k \sin\theta J_0\left(\frac{q}{L} a_0\right) J_{-1} k_0 a_0 \sin\theta - \frac{q}{L} J_{-1}\left(\frac{q}{L} a_0\right) J_0 k a_0 \sin\theta}{\left(\frac{q}{L}\right)^2 - (k \sin\theta)^2} \right]$$

(B-12)

Now $J_0\left(q \frac{a_0}{L}\right) = J_0(q\theta_0) = 0$ Since,

$$E_\theta = E_\phi = 0 \text{ at } \theta = \theta_0. \quad \left(\frac{a_0}{L} \approx \theta_0\right)$$

Thus

$$E_R(r, \theta, \phi) = j \frac{e^{-jk_0 r}}{2\lambda_0 r} (1+\cos\theta) \frac{a_{11} \eta_0}{L} 2\pi q a_0 (\bar{i}_\theta + j\bar{i}_\phi) e^{j\phi} \cdot$$

$$\frac{q}{L} \left[\frac{J_1(q\theta_0) J_0(k a_0 \sin\theta)}{\left(\frac{q}{L}\right)^2 - (k_0 \sin\theta)^2} \right] \quad \text{(B-13)}$$

Dividing and multiplying Eq. (B-13) by a_0^2 , E_R is obtained as,

$$E_R(r, \theta, \phi) = j \frac{e^{-jk_0 r}}{r} (1+\cos\theta) a_{11} \eta_0 \pi q^2 a_0 \theta_0^2 \cdot$$

$$\frac{J_1(q\theta_0) J_0(k a_0 \sin\theta)}{(q\theta_0)^2 - (k_0 a_0 \sin\theta)^2} (\bar{i}_\theta + j\bar{i}_\phi) e^{j\phi}$$

$$= B_{11} j \frac{e^{-jk_0 r}}{r} (1+\cos\theta) \frac{J_0(k_0 a_0 \sin\theta)}{(q\theta_0)^2 - (k_0 a_0 \sin\theta)^2} (\bar{i}_\theta + j\bar{i}_\phi) e^{j\phi}$$

(B-14)

where $B_{11} = a_{11} \eta_0 \frac{\pi}{\lambda_0} q^2 a_0 \theta_0^2 J_1(q\theta_0)$

B - 3 THE ON-AXIS GAIN

The total power radiated through a spherical cap of radius L in the cone region is given by

$$\begin{aligned}
 P_t &= \frac{1}{2} \int \int (E_t \times H_t^*) ds. \\
 &= \frac{1}{2} \int_0^{2\pi} \int_0^{\theta_1} \eta_0 \frac{a_{11}^2}{L^2} q^2 J_0^2(q\theta) \cdot L^2 d\phi \sin\theta d\theta \\
 &= \frac{1}{2} \eta_0 a_{11}^2 q^2 2\pi \int_0^{\theta_1} J_0^2(q\theta) \sin\theta d\theta \quad (B-15)
 \end{aligned}$$

This integral is evaluated by assuming that for small angle cones, $\sin\theta \approx \theta$. Thus P_t becomes,

$$\begin{aligned}
 P_t &= \pi \eta_0 a_{11}^2 q^2 \int_0^{\theta_1} J_0^2(q\theta) \theta d\theta \\
 &= \pi \eta_0 a_{11}^2 q^2 \frac{\theta_1^2}{2} [J_0^2(q\theta_1) - J_{-1}(q\theta_1)J_1'(q\theta_1)] \\
 &= \frac{1}{2} \pi \eta_0 a_{11}^2 q^2 \theta_1^2 [J_0^2(q\theta_1) + J_1^2(q\theta_1)] \quad (B-16)
 \end{aligned}$$

The on-axis gain (the axial gain) is defined as

$$G(0,0) = \frac{4\pi P(0,0)}{P_t} = \frac{1}{2} \left| E_R \right|_{\max}^2 \frac{4\pi r^2}{\eta_0 P_t} ; \quad \text{and}$$

from Eq B.(B-14) and (B-16), the on-axis gain becomes,

$$G(0,0) = \frac{16\pi^2 \frac{a_0^2}{\lambda^2} J_1^2(q\theta_0)}{(q\theta_1)^2 [J_0^2(q\theta_1) + J_1^2(q\theta_1)]} \quad (B-17)$$

APPENDIX C

EQUATIONS FOR CONICAL HORN WITH HELICAL BOUNDARY

C-1 CHARACTERISTIC EQUATIONS

The potential functions for modal fields inside the horn region are given by

$$\bar{A}_r = A_n \hat{J}_n(k_o r) J_m(q\theta) e^{jm\theta} \quad (C-1)$$

$$\bar{F}_r = B_n \hat{J}_n(k_o r) J_m(q\theta) e^{jm\theta}$$

and the corresponding potential functions for fields outside the horn are given by,

$$A_r^o = C_n \hat{H}_n^{(2)}(k_o r) J_m(q\theta) e^{jm\theta} \quad (C-2)$$

$$F_r^o = D_n \hat{H}_n^{(2)}(k_o r) J_m(q\theta) e^{jm\theta}$$

with $q = \sqrt{n(n+1)}$

The characteristic equation for the eigen values 'n' may be formed by the application of the following boundary conditions :

- i) $E_r(\text{inside}) = E_r(\text{outside})$ at the horn boundary
i.e. at $r = a_o$, $\theta = \theta_o$.
- ii) $H_r(\text{inside}) = H_r(\text{outside})$ at the horn boundary
- iii) $E_\theta = E_\phi = 0$ at $r = a_o$, $\theta = \theta_o$.

iv) The functions $\hat{J}_n(k_0 r)$ and $\hat{H}_n^{(2)}(k_0 r)$ are taken in Eqs. (C-1) and (C-2) respectively, as at the horn radius = 0, the field is finite and at $r = \infty$, the field is infinite.

Modal fields inside and outside the horn regions may be obtained by the following formulae [52]

$$\begin{aligned}
 E_r &= \frac{1}{j\omega\epsilon_0} \left(\frac{\partial^2}{\partial r^2} + k_0^2 \right) \Lambda_r \\
 E_\theta &= -\frac{1}{r \sin\theta} \frac{\partial F_r}{\partial \phi} + \frac{1}{j\omega\epsilon_0} \frac{\partial^2 \Lambda_r}{\partial r \partial \theta} \\
 E_\phi &= \frac{1}{r} \frac{\partial F_r}{\partial \theta} + \frac{1}{j\omega\epsilon_0 r \sin\theta} \frac{\partial^2 \Lambda_r}{\partial r \partial \phi} \\
 H_r &= \frac{1}{j\omega\mu_0} \left(\frac{\partial^2}{\partial r^2} + k_0^2 \right) F_r \\
 H_\theta &= \frac{1}{r \sin\theta} \frac{\partial \Lambda_r}{\partial \phi} + \frac{1}{j\omega\mu_0 r} \frac{\partial^2 F_r}{\partial r \partial \theta} \\
 H_\phi &= -\frac{1}{r} \frac{\partial \Lambda_r}{\partial \theta} + \frac{1}{j\omega\mu_0 r \sin\theta} \frac{\partial^2 F_r}{\partial r \partial \phi}
 \end{aligned} \tag{C-3}$$

Thus from Eqs. (C-1), (C-2) and (C-3) respective fields become,

inside the horn

$$E_r = \frac{1}{j\omega\epsilon_0} \frac{n(n+1)}{r^2} A_n \hat{J}_n(k_0 r) J_m(q\theta) e^{jm\phi}$$

$$E_{\theta} = \left[\frac{-1}{r \sin \theta} \frac{j m}{B_n} \hat{J}_n(k_0 r) J_m(q\theta) + \frac{1}{j \omega \epsilon_0 r} \frac{A_n k_0 q}{\hat{J}'_n(k_0 r) J'_m(q\theta)} \right] e^{j m \phi}$$

$$E_{\phi} = \left[\frac{1}{r} B_n q \hat{J}_n(k_0 r) J'_m(q\theta) + \frac{1}{j \omega \epsilon_0 r \sin \theta} \frac{j m A_n k_0}{\hat{J}'_n(k_0 r) J_m(q\theta)} \right] e^{j m \phi} \quad (C-4)$$

$$H_r = B_n \frac{n(n+1)}{j \omega \mu_0 r^2} \hat{J}_n(k_0 r) J_m(q\theta) e^{j m \phi}$$

$$H_{\theta} = \left[\frac{1}{r \sin \theta} \frac{j m A_n}{\hat{J}_n(k_0 r) J_m(q\theta)} + \frac{1}{j \omega \mu_0 r} \frac{B_n k_0 q}{\hat{J}'_n(k_0 r) J'_m(q\theta)} \right] e^{j m \phi}$$

$$H_{\phi} = \left[-\frac{1}{r} A_n q \hat{J}_n(k_0 r) J'_m(q\theta) + \frac{1}{j \omega \mu_0 r \sin \theta} \frac{j m B_n k_0}{\hat{J}'_n(k_0 r) J_m(q\theta)} \right] e^{j m \phi}$$

outside the horn

$$E_r = \frac{1}{j \omega \epsilon_0} \frac{n(n+1)}{r^2} C_n \hat{H}_n^{(2)}(k_0 r) J_m(q\theta) e^{j m \phi}$$

$$E_{\theta} = \left[\frac{-1 j m}{r \sin \theta} D_n \hat{H}_n^{(2)}(k_o r) J_m(q\theta) + \frac{1 C_n k_o q}{j \omega \epsilon_o r} \hat{H}_n^{(2)'}(k_o r) J_m'(q\theta) \right] e^{j m \theta}$$

$$E_{\phi} = \left[\frac{1}{r} D_n q \hat{H}_n^{(2)}(k_o r) J_m'(q\theta) + \frac{1}{j \omega \epsilon_o r \sin \theta} j m C_n k_o \hat{H}_n^{(2)'}(k_o r) J_m(q\theta) \right] e^{j m \theta}$$

$$H_r = \frac{1}{j \omega \mu_o} \frac{n(n+1)}{r^2} D_n \hat{H}_n^{(2)}(k_o r) J_m(q\theta) e^{j m \theta} \quad (C-5)$$

$$H_{\theta} = \left[-\frac{1}{r \sin \theta} j m C_n \hat{H}_n^{(2)}(k_o r) J_m(q\theta) + \frac{1}{j \omega \mu_o r} D_n k_o q \hat{H}_n^{(2)'}(k_o r) J_m'(q\theta) \right] e^{j m \theta}$$

$$H_{\phi} = \left[-\frac{1}{r} C_n q \hat{H}_n^{(2)}(k_o r) J_m'(q\theta) + \frac{1}{j \omega \mu_o r \sin \theta} j m D_n k_o \hat{H}_n^{(2)'}(k_o r) J_m(q\theta) \right] e^{j m \theta}$$

Now by applying boundary conditions,

i) $E_r(\text{inside}) = E_r(\text{outside})$ at $r = a_o$, $\theta = \theta_o$ gives

$$C_n = A_n \frac{\hat{J}_n(k_o a)}{\hat{H}_n^{(2)}(k_o a)} \quad (C-6)$$

ii) $H_r(\text{inside}) = H_r(\text{outside})$ at $r = a_0$ $\theta = \theta_0$, gives

$$D_n = B_n \frac{\hat{J}_n(k_0 a)}{\hat{H}_n^{(2)}(k_0 a)} \quad (C-7)$$

iii) By Eqs. (C-4) and (C-5) $E_\theta = 0$ at $r = a_0$, $\theta = \theta_0$, gives

$$B_n = - \frac{A_n k_0 q}{m \omega \epsilon_0} \frac{\hat{J}_n'(k_0 a)}{\hat{J}_n(k_0 a)} \frac{J_m'(q\theta_0)}{J_m(q\theta_0)} \sin\theta_0 \quad (C-8)$$

and

$$D_n = - \frac{C_n k_0 q}{m \omega \epsilon_0} \frac{\hat{H}_n^{(2)'}(k_0 a)}{\hat{H}_n^{(2)}(k_0 a)} \frac{J_m'(q\theta_0)}{J_m(q\theta_0)} \sin\theta_0 \quad (C-9)$$

Using Eq. (C-6), Eq. (C-9) becomes

$$D_n = - A_n \frac{\hat{J}_n(k_0 a)}{\hat{H}_n^{(2)}(k_0 a)} \frac{k_0 q}{m \omega \epsilon_0} \frac{\hat{H}_n^{(2)'}(k_0 a)}{\hat{H}_n^{(2)}(k_0 a)} \frac{J_m'(q\theta_0)}{J_m(q\theta_0)} \sin\theta_0 \quad (C-10)$$

Similarly by Eq. (C-4)

iv) $E_\theta = 0$ at $r = a_0$, $\theta = \theta_0$ gives,

$$B_n = - \frac{A_n^m k_0}{\omega \epsilon_0 q \sin\theta_0} \frac{\hat{J}_n'(k_0 a_0)}{\hat{J}_n(k_0 a_0)} \frac{J_m(q\theta_0)}{J_m'(q\theta_0)}, \quad (C-11)$$

and by (C-7), (C-11) becomes,

$$D_n = \frac{A_n m k_o}{\omega \epsilon_o q \sin \theta_o} \frac{\hat{J}_n(k_o a_o) \hat{J}'_n(k_o a_o)}{\hat{H}_n^{(2)}(k_o a_o) \hat{J}_n(k_o a_o)} \frac{J_m(q\theta_o)}{J'_m(q\theta_o)} \quad (C-12)$$

From Eqs. (C-10) and (C-12), it is obtained

$$\begin{aligned} & \frac{m k_o}{\omega \epsilon_o q \sin \theta_o} \frac{\hat{J}'_n(k_o a_o)}{\hat{J}_n(k_o a_o)} \frac{J_m(q\theta_o)}{J'_m(q\theta_o)} \\ &= \frac{k_o q}{m \omega \epsilon_o} \frac{\hat{H}_n^{(2)'}(k_o a_o)}{\hat{H}_n^{(2)}(k_o a_o)} \frac{J'_m(q\theta_o)}{J_m(q\theta_o)} \sin \theta_o \quad (C-13) \end{aligned}$$

i.e.

$$\frac{\hat{J}'_n(k_o a_o) J_m(q\theta_o)}{\hat{J}_n(k_o a_o) J'_m(q\theta_o)} = \frac{q^2}{m} \sin^2 \theta_o \cdot \frac{\hat{H}_n^{(2)'}(k_o a_o) J'_m(q\theta_o)}{\hat{H}_n^{(2)}(k_o a_o) J_m(q\theta_o)} \quad (C-14)$$

where the prime indicates differentiation with respect to the argument.

This is the characteristic equation for the HE_{mn} mode.

Now restricting the consideration to $m = 1$, the characteristic equation becomes,

$$\frac{\hat{J}'_n(k_o a_o) J_1(q\theta_o)}{\hat{J}_n(k_o a_o) J'_1(q\theta_o)} = q^2 \sin^2 \theta_o \frac{\hat{H}_n^{(2)'}(k_o a_o) J'_1(q\theta_o)}{\hat{H}_n^{(2)}(k_o a_o) J_1(q\theta_o)} \quad (C-15)$$

This characteristic equation is solved graphically as

illustrated in Fig. B-1 for $a_o = 3.5$ cm and $f_o = 9.58$ GHz; and the eigen values thus obtained for the HE_{11} mode, by taking the first root of Eq. (C-15), for different horn angles θ_o are plotted in Fig. 3.12

It can also be seen that by using Eq. (C-11) in Eqs. (C-4), the E -fields inside the horn may be obtained, in terms of A_n only as,

inside the horn

$$E_r = \frac{1}{j\omega\epsilon_o} \frac{n(n+1)}{r^2} A_n \hat{J}_n(k_o r) J_m(q\theta) e^{jm\phi}$$

$$E_\theta = \frac{jA_n k_o q}{\omega\epsilon_o r} \hat{J}'_n(k_o a_o) J'_m(q\theta_o) .$$

$$\left[\frac{\hat{J}'_n(k_o r) J_m(q\theta)}{\hat{J}_n(k_o a_o) J_m(q\theta_o)} - \frac{\hat{J}'_n(k_o r) J'_m(q\theta)}{\hat{J}'_n(k_o a_o) J'_m(q\theta_o)} \right] e^{jm\phi} \quad (C-16)$$

$$E_\phi = \frac{A_n k_o}{\omega\epsilon_o r} \hat{J}'_n(k_o a_o) J'_m(q\theta_o) .$$

$$\left[\frac{-q^2 \hat{J}_n(k_o r) J'_m(q\theta)}{m \hat{J}_n(k_o a_o) J_m(q\theta_o)} \sin\theta_o + \frac{m}{\sin\theta} \frac{\hat{J}'_n(k_o r) J_m(q\theta)}{\hat{J}'_n(k_o a_o) J'_m(q\theta_o)} \right] e^{jm\phi}$$

Similarly by substituting Eqs. (C-6) and (C-10) in Eqs. (C-5) the E -fields outside the horn, in terms of A_n , become,

outside the horn

$$E_r = \frac{1}{j\omega\epsilon_0} \frac{A_n}{r^2} \frac{\hat{H}_n^{(2)}(k_0 r)}{\hat{H}_n^{(2)}(k_0 a_0)} \hat{J}_n(k_0 a_0) J_m(q\theta) e^{jm\phi}$$

$$E_\theta = \frac{j A_n k_0 q}{\omega\epsilon_0 r} \frac{\hat{J}'_n(k_0 a_0)}{\hat{H}_n^{(2)}(k_0 a_0)} \hat{H}_n^{(2)'}(k_0 a_0) J'_m(q\theta_0)$$

$$\left[\frac{\hat{H}_n^{(2)}(k_0 r) J'_m(q\theta) \sin\theta_0}{\hat{H}_n^{(2)}(k_0 a_0) J_m(q\theta_0) \sin\theta} - \frac{\hat{H}_n^{(2)'}(k_0 r) J'_m(q\theta)}{\hat{H}_n^{(2)'}(k_0 a_0) J_m(q\theta_0)} \right] e^{jm\phi}$$

(C-17)

$$E_\phi = \frac{A_n k_0}{\omega\epsilon_0 r} \frac{\hat{J}_n(k_0 a_0)}{\hat{H}_n^{(2)}(k_0 a_0)} \hat{H}_n^{(2)'}(k_0 a_0) J'_m(q\theta_0)$$

$$\left[-\frac{q^2}{m} \sin\theta_0 \frac{\hat{H}_n^{(2)}(k_0 r) J'_m(q\theta)}{\hat{H}_n^{(2)}(k_0 a_0) J_m(q\theta_0)} + \frac{m}{\sin\theta} \frac{\hat{H}_n^{(2)'}(k_0 r) J_m(q\theta)}{\hat{H}_n^{(2)'}(k_0 a_0) J'_m(q\theta_0)} \right] e^{jm\phi}$$

C - 2 RADIATED FAR FIELD FROM A CONICAL HORN WITH HELICAL BOUNDARY

The transverse electric field over the horn aperture for HE₁₁ mode excitation is obtained as, [Eq. (3.48)]

$$E_t = D_1 \frac{e^{-jk_0 r}}{r} (j)^n q J_0(q\theta) (\bar{i}_\theta + j\bar{i}_\phi) e^{j\phi} \quad (C-18)$$

The phase variation of the field over the circular horn aperture is assumed as [44, pp -134]

$$\Psi_{\rho} = e^{-j \frac{\pi}{\lambda_0} \frac{\rho^2}{L}} \quad (C-19)$$

(L is the axial length of the horn)

Now the radiation field at a far point (r, θ, φ) may be obtained by the diffraction formula for a circular opening [44], and thus the radiated far-field in the H-plane (φ = 0) for the horn excited in HE₁₁ mode becomes,

$$E_{\phi}(r, \theta) = j \frac{e^{-jk_0 r}}{2\lambda_0 r} (1+\cos\theta) \iint_S \bar{E}_t e^{jk_0 \rho \cos\phi \sin\theta} e^{-j \frac{\pi}{\lambda_0} \frac{\rho^2}{L}} \rho d\rho d\phi \quad (C-20)$$

Using (C-18), Eq. (C-20) becomes,

$$\begin{aligned} E_{\phi}(r, \theta) &= j \frac{e^{-jk_0 r}}{2\lambda_0 r} (1+\cos\theta) D_1 \frac{e^{-jk_0 r_0}}{r_0 (\approx L)} j^n q J_0(q\theta) \cdot \\ &\int_0^{a_0} \int_0^{2\pi} e^{jk_0 \rho \cos\phi \sin\theta} e^{-j \frac{\pi}{\lambda_0} \frac{\rho^2}{L}} \rho d\rho d\phi \quad (r_0 \approx L) \\ &= j^{n+1} \frac{e^{-jk_0 r'}}{2\lambda_0 r L} (1+\cos\theta) D_1 q J_0(q\theta) \cdot \\ &\int_0^{a_0} 2\pi J_0(k_0 \rho \sin\theta) e^{-j \frac{\pi}{\lambda_0} \frac{\rho^2}{L}} \rho d\rho \quad (C-21) \end{aligned}$$

where $r' = r + r_0$, r_0 being the horn flare length.

Setting $y = k_0 \rho \sin\theta$, Eqn. (C-21) is reduced to

$$E_{\phi}(r, \theta) = j^{n+1} \frac{e^{-jk_0 r'}}{\lambda_0 r L} (1 + \cos \theta) \frac{\pi D_1 q J_0(q\theta)}{k_0^2 \sin^2 \theta} \int_0^{a_0} J_0(y) e^{-jBy^2} y dy$$

(C-22)

where $B = \frac{\pi}{\lambda_0 L k_0^2 \sin^2 \theta}$

Carrying out the transformation as in [44, pp-110] the integral in Eq(C-22) may be represented in the form of a component containing the Bessel function without integral and an integral of the same form but with a higher order integrand. Repeating similar operations further it is possible to expand the integral in a series of Bessel functions and finally substituting the Λ -function (Lamda function) for the Bessel functions, $E_{\phi}(r, \theta)$ can be obtained as,

$$E_{\phi}(r, \theta) = j^{n+1} \frac{e^{-jk_0 r'}}{\lambda_0 r L} (1 + \cos \theta) \frac{\pi D_1 q J_0(q\theta)}{k_0^2 \sin^2 \theta} S_k .$$

$$e^{-j \frac{\pi a_0^2}{\lambda_0 L}} \sum_{n=1}^{\infty} \left(\frac{\pi a_0^2}{\lambda_0 L} \right)^{n-1} \frac{j^{n-1}}{n!} \Lambda_n \left(\frac{\xi}{\eta} \right)$$

(C-23)

Replacing k_0 by $\frac{2\pi}{\lambda_0}$, $E_{\phi}(r, \theta)$ becomes,

$$E_{\theta}(r, \theta) = \frac{\lambda_0 D_1 q}{2\pi L \sin^2 \theta} \cdot J_0(q\theta) \cdot \cos^2 \frac{\theta}{2} \frac{e^{-jk_0 r'}}{r} \cdot e^{-j \frac{\pi}{\lambda_0} \frac{a_0^2}{L}} S_k \sum_{n=1}^{\infty} \left(\frac{\pi}{\lambda_0} \frac{a_0^2}{L} \right)^{n-1} \frac{j^{2n}}{n!} \Lambda_n(\xi) \quad (C-24)$$

where

$S_k = \pi a_0^2$, the area of the horn aperture

$\xi = k_0 a_0 \sin \theta$, a_0 being the radius of the conical horn aperture.

$\Lambda_n(x) = \frac{n!}{(x/2)^2} J_n(x)$, is the Lamda function

and L = axial length of the cone,

The E -plane pattern can also be obtained in the same way by the relation

$$E_{\theta}(r, \theta) = j \frac{e^{-jk_0 r}}{2 \lambda_0 r} (1 + \cos \theta) \iint_S \bar{E}_t \cdot e^{jk_0 \rho \sin \theta \sin \phi} e^{-j \frac{\pi \rho^2}{\lambda_0 L}} \rho d\rho d\phi$$

(C-25)

C - 3 GAIN OF THE CONICAL HORN WITH HELICAL BOUNDARY

By Eq. (C-21), $E_{\phi}(r, \theta) = \frac{j^{n+1} e^{-jk_0 r'} (1 + \cos \theta) D_1 q J_0(q\theta)}{2 \lambda_0 r L}$

$$\int_0^{a_0} 2\pi J_0(k_0 \rho \sin \theta) e^{-j\pi \frac{\rho^2}{L}} \rho d\rho$$

Therefore, since $J_0(0) = 1$,

$$|E_{\phi}|_{\max} = E_{\phi}|_{\theta=0} = \frac{2\pi D_1 q}{\lambda_0 r L} \int_0^{a_0} e^{-j\pi \frac{\rho^2}{L}} \rho d\rho \quad (C-26)$$

Letting $\frac{\pi}{\lambda_0} \frac{\rho^2}{L} = \theta$, the integral in (C-26) is solved to result as,

$$\begin{aligned} |E_{\phi}|_{\max} &= \frac{D_1 q}{r} \left[j \left(\cos \frac{\pi}{\lambda_0} \frac{a_0^2}{L} - 1 \right) + \sin \frac{\pi}{\lambda_0} \frac{a_0^2}{L} \right] \\ &= \frac{D_1 q}{r} \sqrt{\left[\cos \frac{\pi}{\lambda_0} \frac{a_0^2}{L} - 1 \right]^2 + \sin^2 \frac{\pi}{\lambda_0} \frac{a_0^2}{L}} \end{aligned} \quad (C-27)$$

Therefore,

$$\begin{aligned} r^2 |E_{\phi}|_{\max}^2 &= D_1^2 q^2 \left[\left(\cos \frac{\pi}{\lambda_0} \frac{a_0^2}{L} - 1 \right)^2 + \sin^2 \frac{\pi}{\lambda_0} \frac{a_0^2}{L} \right] \\ &= D_1^2 q^2 \left(2 - 2 \cos \frac{\pi}{\lambda_0} \frac{a_0^2}{L} \right) \end{aligned}$$

$$= 4 D_1^2 q^2 \sin^2 \left(\frac{\pi a_o^2}{2 \lambda_o L} \right) \quad (C-28)$$

The total power P_t crossing a spherical cap of radius L in the cone region is given by

$$P_t = \frac{1}{2} R_e \left[\iint_s E_t \times H_t^* L^2 ds \right], \text{ and from Eq. (C-18),}$$

P_t becomes,

$$P_t = \frac{1}{L^2 2 \eta_o} \int_0^{2\pi} \int_0^{\theta_o} (D_1 q)^2 L^2 J_o^2(q\theta) d\phi \sin\theta d\theta$$

$$= \frac{1}{2 \eta_o} D_1^2 q^2 2\pi \int_0^{\theta_o} J_o^2(q\theta) \theta d\theta$$

($\sin \theta \approx \theta$ since small angle cone)

$$= \frac{D_1^2 q^2}{\eta_o} \frac{\pi \theta_o^2}{2} [J_o^2(q\theta_o) + J_1^2(q\theta_o)] \quad (C-29)$$

Now the axial gain of the horn is defined as,

$$G(0,0) = \frac{\frac{1}{2} |E_\phi|_{\max}^2 4\pi r^2}{\eta_o P_t}, \text{ and by Eqs. (C-28) and (C-29)}$$

the gain becomes,

$$G(0,0) = \frac{16 \sin^2 \frac{\pi a_o^2}{2 \lambda_o L}}{\theta_o^2 [J_o^2(q\theta_o) + J_1^2(q\theta_o)]} \quad (C-30)$$

APPENDIX D

EQUATIONS FOR DIELECTRIC LOADED BICONICAL HORN

D-1 FIELDS IN A DIELECTRIC COATED BICONICAL HORN

The proper forms of the potential function ψ for the dielectric coated and the horn apex angle regions respectively are given as,

$$\psi_d = \hat{J}_n(k_1 r) [C_n P_n^m(\cos\theta) + D_n Q_n^m(\cos\theta)] e^{jm\phi} \quad (D-1)$$

$$\psi_o = F_n \hat{H}_n^{(2)}(k_o r) P_n^m(\cos\theta) e^{jm\phi}$$

where $k_1 = \omega \sqrt{\mu_o \epsilon_1}$ and $k_o = \omega \sqrt{\mu_o \epsilon_o}$

The E- and H - field intensities are found by the relations,

$$\vec{E} = -\nabla \times \vec{F} \quad (D-2)$$

$$H = \frac{1}{j\omega \mu_o} \nabla \times \nabla \times \vec{F}$$

Now noting that $\vec{F} = \vec{r}_\theta \psi$, by Eq.(D-2), the different field components are given by the relation

$$E_r = \frac{1}{r \sin\theta} \frac{\partial \psi}{\partial \phi}$$

$$E_{\phi} = - \frac{1}{r} \left[\frac{\partial}{\partial r} (r \psi) \right]$$

$$E_{\theta} = 0$$

$$H_r = \frac{1}{j \omega \mu_0} \left[\frac{\partial^2 \psi}{\partial \theta \partial r} + \frac{1}{r} \frac{\partial \psi}{\partial \theta} \right] \quad (D-3)$$

$$H_{\phi} = \frac{1}{j \omega \mu_0} \frac{1}{r \sin \theta} \frac{\partial^2 \psi}{\partial \theta \partial \phi}$$

$$H_{\theta} \approx \frac{1}{j \omega \mu_0} k^2 \psi$$

Using Eqs.(D-1) in Eqs.(D-3), the different field components in the two regions are obtained as,

In the dielectric coated region

$$E_{rd} = \frac{j m}{r \sin \theta} \hat{J}_n(k_1 r) L_n^m(\cos \theta) e^{j m \phi}$$

$$E_{\phi d} = \left[\hat{J}_n(k_1 r) + k_1 \hat{J}'_n(k_1 r) \right] L_n^m(\cos \theta) e^{j m \phi}$$

$$E_{\theta d} = 0$$

$$H_{rd} = \frac{1}{j \omega \mu_0} \left[k_1 \hat{J}'_n(k_1 r) \frac{\partial}{\partial \theta} L_n^m(\cos \theta) + \frac{1}{r} \hat{J}_n(k_1 r) \frac{\partial}{\partial \theta} L_n^m(\cos \theta) \right] e^{j m \phi}$$

$$H_{\phi d} = \frac{m}{\omega \mu_0 r \sin \theta} \hat{J}_n(k_1 r) \frac{\partial}{\partial \theta} L_n^m(\cos \theta) e^{j m \phi}$$

$$H_{\theta d} \approx \frac{1}{j \omega \mu_0} k_1^2 \hat{J}_n(k_1 r) L_n^m(\cos \theta) e^{j m \phi} \quad (D-4)$$

where $L_n^m(\cos\theta) = C_n P_n^m(\cos\theta) + D_n Q_n^m(\cos\theta)$

and the prime indicates differentiation with respect to r .

In the horn apex angle region

$$E_{r_0} = \frac{j m F_n}{r \sin\theta} \hat{H}_n^{(2)}(k_0 r) P_n^m(\cos\theta) e^{j m \phi}$$

$$E_{\phi_0} = - \left[\frac{\hat{H}_n^{(2)}(k_0 r)}{r} + k_0 \hat{H}_n^{(2)'}(k_0 r) \right] F_n P_n^m(\cos\theta) e^{j m \phi}$$

$$E_{\theta_0} = 0 \tag{D-5}$$

$$H_{r_0} = \frac{F_n}{j \omega \mu_0} \left[k_0 \hat{H}_n^{(2)'}(k_0 r) \frac{\partial}{\partial \theta} P_n^m(\cos\theta) + \frac{1}{r} \hat{H}_n^{(2)}(k_0 r) \frac{\partial}{\partial \theta} P_n^m(\cos\theta) \right] e^{j m \phi}$$

$$H_{\phi_0} = \frac{m F_n}{\omega \mu_0 r \sin\theta} \hat{H}_n^{(2)}(k_0 r) \frac{\partial}{\partial \theta} P_n^m(\cos\theta) e^{j m \phi}$$

$$H_{\theta_0} \approx \frac{F_n}{j \omega \mu_0} k_0^2 \hat{H}_n^{(2)}(k_0 r) P_n^m(\cos\theta) e^{j m \phi}$$

D-2 CHARACTERISTIC EQUATION

The value of the separation constant n can be

obtained from the characteristic equation derived by applying appropriate boundary condition, and by matching the fields at $\theta = \theta_1$.

The boundary condition that $E_{\theta d} = 0$ at $\theta = \theta_0$ gives

$$C_n = -D_n \frac{Q_n^m(\cos\theta_0)}{P_n^m(\cos\theta_0)} \quad (D-6)$$

Matching the fields at $\theta = \theta_1$,

(i) $E_{rd} = E_{ro}$ at $\theta = \theta_1$ gives

$$\begin{aligned} \hat{J}_n(k_1 r) [C_n P_n^m(\cos\theta_1) + D_n Q_n^m(\cos\theta_1)] \\ = F_n \hat{H}_n^{(2)}(k_0 r) P_n^m(\cos\theta_1) \end{aligned} \quad (D-7)$$

Using Eq. (D-6), Eq.(D-7) becomes,

$$\begin{aligned} D_n \hat{J}_n(k_1 r) [P_n^m(\cos\theta_0) Q_n^m(\cos\theta_1) - P_n^m(\cos\theta_1) Q_n^m(\cos\theta_0)] \\ = F_n \hat{H}_n^{(2)}(k_0 r) P_n^m(\cos\theta_1) \end{aligned} \quad (D-8)$$

(ii) $H_{rd} = H_{ro}$ at $\theta = \theta_1$ gives,

$$\begin{aligned}
 & [k_1 \hat{J}'_n(k_1 r) + \frac{1}{r} \hat{J}_n(k_1 r)] [C_n \frac{\partial}{\partial \theta} P_n^m(\cos \theta_1) + D_n \frac{\partial}{\partial \theta} Q_n^m(\cos \theta_1)] \\
 & = F_n [k_0 \hat{H}_n^{(2)'}(k_0 r) + \frac{1}{r} \hat{H}_n^{(2)}(k_0 r)] \frac{\partial}{\partial \theta} P_n^m(\cos \theta_1)
 \end{aligned}
 \tag{D-9}$$

Using Eq.(D-8), the above equation becomes,

$$\begin{aligned}
 & D_n [k_1 \hat{J}'_n(k_1 r) + \frac{1}{r} \hat{J}_n(k_1 r)] \cdot \\
 & [P_n^m(\cos \theta_0) \frac{\partial}{\partial \theta} Q_n^m(\cos \theta_1) - Q_n^m(\cos \theta_0) \frac{\partial}{\partial \theta} P_n^m(\cos \theta_1)] \\
 & = F_n [k_0 \hat{H}_n^{(2)'}(k_0 r) + \frac{1}{r} \hat{H}_n^{(2)}(k_0 r)] \frac{\partial}{\partial \theta} P_n^m(\cos \theta_1)
 \end{aligned}
 \tag{D-10}$$

Dividing Eq.(D-8) by Eq.(D-10), it becomes,

$$\begin{aligned}
 & \frac{P_n^m(\cos \theta_0) Q_n^m(\cos \theta_1) - P_n^m(\cos \theta_1) Q_n^m(\cos \theta_0)}{P_n^m(\cos \theta_0) \frac{\partial}{\partial \theta} Q_n^m(\cos \theta_1) - Q_n^m(\cos \theta_0) \frac{\partial}{\partial \theta} P_n^m(\cos \theta_1)} \\
 & = \frac{[k_1 \hat{J}'_n(k_1 r) + \frac{1}{r} \hat{J}_n(k_1 r)] \hat{H}_n^{(2)}(k_0 r)}{[k_0 \hat{H}_n^{(2)'}(k_0 r) + \frac{1}{r} \hat{H}_n^{(2)}(k_0 r)] \hat{J}_n(k_1 r)} \cdot \frac{P_n^m(\cos \theta_1)}{\frac{\partial}{\partial \theta} P_n^m(\cos \theta_1)}
 \end{aligned}
 \tag{D-11}$$

The above equation is the characteristic equation for

the HE_{mn} mode that can be solved for the value of the separation constant for any mode. Now restricting the consideration to the case with $m = 1$, the characteristic equation for HE_{1n} mode becomes,

$$\left[P_n^1(\cos\theta_0) Q_n^1(\cos\theta_1) - P_n^1(\cos\theta_1) Q_n^1(\cos\theta_0) \right] \frac{\partial}{\partial \theta} P_n^1(\cos\theta_1)$$

$$\left[P_n^1(\cos\theta_0) \frac{\partial}{\partial \theta} P_n^1(\cos\theta_1) - Q_n^1(\cos\theta_0) \frac{\partial}{\partial \theta} P_n^1(\cos\theta_1) \right] P_n^1(\cos\theta_1)$$

$$= \frac{(1 + k_1 r) \frac{\hat{J}'_n(k_1 r)}{\hat{J}_n(k_1 r)}}{(1 + k_0 r) \frac{\hat{H}_n^{(2)'}(k_0 r)}{\hat{H}_n^{(2)}(k_0 r)}} \quad (D-12)$$

The characteristic equation is valid for any value of r within the horn region i.e. for values of $r \leq L$, where L is the flare length of the horn. The characteristic equation for the HE_{1n} mode (Eq (D-12)) can be solved graphically for typical values of $\theta_0, \theta_1, \epsilon_1$ and f_0 , and the value of the separation constant for HE_{11} mode can be determined by taking the first root of the above equation.

D-3 RADIATION FROM DIELECTRIC COATED
BICONICAL HORN

Using the vector diffraction formula, the radiation pattern of the HE_{11} mode in the vertical plane (i.e. E -plane with $\phi = \pi/2$) is given by

$$E_{\theta}(\theta) = \frac{jk_0 e^{-jk_0 r}}{4\pi r} (1+\cos\theta) \iint_s \bar{E}_t e^{jk_0 r_0 \cos(\theta_s - \theta)} ds \quad (D-13)$$

where

$$\bar{E}_t \approx \bar{i}_{\theta} E_{\theta_0} + \bar{i}_{\phi} E_{\phi_0} \Big|_{r=r_0}$$

By Eq. (D-5) $\approx \bar{i}_{\phi} E_{\phi_0} \Big|_{r=r_0}$ since $E_{\theta} = 0$

$$E_t = E_0 \left[\frac{\hat{H}_v^{(2)}(k_0 r_0)}{r_0} + k_0 \hat{H}_v^{(2)'}(k_0 r_0) \right] P_v^1(\cos\theta) \quad (D-14)$$

where E_0 = a constant that depends on the horn excitation

and v = the separation constant for HE_{11} mode.

Thus the radiation pattern in the E -plane for HE_{11} mode excitation of horn becomes,

$$\begin{aligned}
 E_{\theta}(\theta) &= jE_0 \frac{e^{-jk_0 r}}{2\lambda_0 r} (1+\cos\theta) \int_0^{2\pi} \int_{-\theta_1}^{+\theta_1} \\
 & \left[(k_0 \hat{H}_v^{(2)})'(k_0 r_0) + \frac{\hat{H}_v^{(2)}(k_0 r_0)}{r_0} \right] P_v^1(\cos\theta_s) \cdot \\
 & e^{jk_0 r_0 \cos(\theta_s - \theta)} r_0^2 \sin\theta_s d\theta_s d\phi_s \\
 &= jE_0 \frac{e^{-jk_0 r}}{2\lambda_0 r} (1+\cos\theta) 2\pi r_0^2 \left[k_0 \hat{H}_v^{(2)}'(k_0 r) + \frac{\hat{H}_v^{(2)}(k_0 r_0)}{r_0} \right] \\
 & \int_{-\theta_1}^{+\theta_1} P_v^1(\cos\theta_s) e^{jk_0 r_0 \cos(\theta_s - \theta)} \sin\theta_s d\theta_s \quad (D-15)
 \end{aligned}$$

The evaluation of the integral in the above expression is made by the following approximations :

(i) $P_v^1(\cos\theta)$ is replaced by its asymptotic approximation.

$$\begin{aligned}
 \text{i.e.} \quad P_v^1(\cos\theta_s) &= -v \sqrt{\frac{2}{v\pi \sin\theta}} \sin \left[\left(v + \frac{1}{2}\right)\theta + \frac{\pi}{4} + \frac{\pi}{2} \right] \\
 &= -\sqrt{\frac{2v}{\pi}} \frac{\cos \left[\left(v + \frac{1}{2}\right)\theta + \frac{\pi}{4} \right]}{\sqrt{\sin\theta}} \\
 &= -\sqrt{\frac{2v}{\pi}} \left(\frac{1}{2} \right) \left\{ \frac{e^{j \left[\left(v + \frac{1}{2}\right)\theta + \frac{\pi}{4} \right]} + e^{-j \left[\left(v + \frac{1}{2}\right)\theta + \frac{\pi}{4} \right]}}{\sqrt{\sin\theta}} \right\} \\
 & \hspace{15em} (D-16)
 \end{aligned}$$

(ii)

$$\begin{aligned} \sqrt{\sin\theta} &= \left[\frac{e^{j\theta} - e^{-j\theta}}{2j} \right]^{\frac{1}{2}} = \left[\frac{e^{j\theta}(1 - e^{-j2\theta})}{2j} \right]^{\frac{1}{2}} \\ &= \left[\frac{e^{j\theta}(1 - e^{-j2\theta})}{2e^{j\frac{\pi}{2}}} \right]^{\frac{1}{2}} \quad \text{Since } j = e^{j\frac{\pi}{2}} \\ &= \frac{e^{j\frac{\theta}{2}}}{\sqrt{2} e^{j\frac{\pi}{4}}} \left[1 - \frac{1}{2} e^{-j2\theta} + \frac{1.3}{2.4} e^{-j4\theta} + \dots \right] \end{aligned}$$

As a first approximation, the first term in the Binomial Series expression is taken and hence

$$\sqrt{\sin\theta} \approx \frac{e^{j\frac{\theta}{2}}}{\sqrt{2} e^{j\frac{\pi}{4}}} \quad \text{(D-17)}$$

$$(iii) \quad \cos x = 1 - \frac{x^2}{2!} + \frac{x^4}{4!} + \dots$$

As a first approximation let $\cos x \approx 1 - \frac{x^2}{2!}$ so that

$$\cos(\theta_s - \theta) \approx 1 - \frac{(\theta_s - \theta)^2}{2} \quad \text{(D-18)}$$

$$\text{and } e^{jk_o r_o} \cos(\theta_s - \theta) = e^{jk_o r_o} e^{-jk_o r_o} \frac{(\theta_s - \theta)^2}{2} \quad \text{(D-19)}$$

Inserting the above approximations

$$\int_{-\theta_1}^{+\theta_1} P_v^1(\cos\theta_s) e^{jk_0 r_0 \cos(\theta_s - \theta)} d\theta_s$$

$$= -\frac{1}{2} e^{jk_0 r_0} \sqrt{v/\pi} I_1 I_2 \dots \quad (D-20)$$

where $I_1 = \int_{-\theta_1}^{+\theta} e^{j(v+1)\theta_s} \cdot e^{-j \frac{\pi}{\lambda_0} r_0 (\theta_s - \theta)^2} d\theta_s$

$$= \int_{-\theta_1}^{+\theta_1} e^{-j \frac{\pi}{2} \left\{ \left[\sqrt{\frac{2r_0}{\lambda_0}} (\theta_s - \theta) - \sqrt{\frac{\lambda_0}{2r_0}} \left(\frac{v+1}{\pi} \right)^2 \right]^2 - \frac{\lambda_0}{2r_0} \left(\frac{v+1}{\pi} \right)^2 - \frac{2(v+1)}{\pi} \theta_s \right\}} d\theta_s$$

$$= e^{j \frac{\pi}{4} \frac{\lambda_0}{r_0} \left(\frac{v+1}{\pi} \right)^2} e^{j(v+1)\theta} \sqrt{\frac{\lambda_0}{2r_0}}$$

$$\cdot [C(u_1) - C(u_2) - j[S(u_1) - S(u_2)]] \quad (D-21)$$

$$u_1 = \left[\theta_1 - \theta - \frac{\lambda_0}{2r_0} \left(\frac{v+1}{\pi} \right)^2 \right] \sqrt{\frac{2r_0}{\lambda_0}}$$

$$u_2 = \left[-\theta_1 - \theta - \frac{\lambda_0}{2r_0} \left(\frac{v+1}{\pi} \right)^2 \right] \sqrt{\frac{2r_0}{\lambda_0}}$$

and $I_2 = e^{-j \frac{\pi}{2}} \int_{-\theta_1}^{+\theta_1} e^{-jv\theta} e^{-j \frac{\pi}{\lambda_0} r_0 (\theta_s - \theta)^2} d\theta_s$

$$\begin{aligned}
 I_2 &= e^{-j\frac{\pi}{2}} e^{j\frac{\pi}{4}} \frac{\lambda_0}{r_0} \left(\frac{v}{\pi}\right)^2 e^{-jv\theta} \\
 &= e^{-j\frac{\pi}{2}} e^{j\frac{\pi}{4}} \frac{\lambda_0}{r_0} \left(\frac{v}{\pi}\right)^2 e^{-jv\theta} \int_{-\theta_1}^{+\theta_1} \left[\sqrt{\frac{2r_0}{\lambda_0}} (\theta_s - \theta) + \sqrt{\frac{\lambda_0}{2r_0}} \frac{v}{\pi} \right]^2 d\theta_s \\
 &= e^{-j\frac{\pi}{2}} e^{j\frac{\pi}{4}} \frac{\lambda_0}{r_0} \left(\frac{v}{\pi}\right)^2 e^{-jv\theta} \sqrt{\frac{\lambda_0}{2r_0}} \cdot \\
 &\quad \left\{ C(v_1) - C(v_2) - j [S(v_1) - S(v_2)] \right\} \quad (D-22)
 \end{aligned}$$

where

$$\begin{aligned}
 v_1 &= \left[\theta_1 - \theta + \frac{\lambda_0}{2r_0} \frac{v}{\pi} \right] \sqrt{\frac{2r_0}{\lambda_0}} \\
 v_2 &= \left[-\theta_1 - \theta + \frac{\lambda_0}{2r_0} \frac{v}{\pi} \right] \sqrt{\frac{2r_0}{\lambda_0}}
 \end{aligned}$$

Inserting Eqs. (D-19), (D-21) and (D-22) in Eq. (D-15), $E_\theta(\theta)$ becomes,

$$\begin{aligned}
 E_\theta(\theta) &= -j E_1 \pi \frac{e^{-jk_0 r}}{2\lambda_0 r} (1 + \cos\theta) r_0^2 \sqrt{\frac{v}{\pi} \frac{\lambda_0}{2r_0}} \cdot \\
 &\quad \left[M \left\{ C(u_1) - C(u_2) - j [S(u_1) - S(u_2)] \right\} + \right. \\
 &\quad \left. N \left\{ C(v_1) - C(v_2) - j [S(v_1) - S(v_2)] \right\} \right] \quad (D-23)
 \end{aligned}$$

where

$$E_1 = E_0 \left[k_0 \hat{H}_v^{(2)}(k_0 r_0) + \frac{\hat{H}_v^{(2)}(k_0 r_0)}{r_0} \right] e^{jk_0 r_0}$$

$$M = e^{j \frac{\lambda_0}{4r_0} \frac{(v+1)^2}{\pi}} e^{j(v+1)\theta}$$

$$N = e^{j \frac{\lambda_0}{4r_0} \frac{v^2}{\pi}} e^{-j(v\theta + \frac{\pi}{2})}$$

D-4 POWER GAIN OF DIELECTRIC COATED
BICONICAL HORN

The total power 'P_t' transmitted through the horn region may be calculated by integrating the power density flowing in the radial direction over a closed surface of $r = r_0$, a constant, between the cones. Thus for the HE_{11} mode P_t becomes,

$$P_t = \iint \frac{E_t^2}{\eta_0} ds$$

Using Eq.(D-14) P_t is given by

$$P_t = \frac{E_0^2}{\eta_0} (k_0 \hat{H}_v^{(2)})' (k_0 r_0) + \frac{\hat{H}_v^{(2)} (k_0 r_0)}{r_0})^2 .$$

$$\int_0^{2\pi} \int_{-\theta_1}^{+\theta_1} [P_v^1(\cos\theta)]^2 r_0^2 \sin\theta d\theta d\phi \quad (D-24)$$

Now using the asymptotic approximation for $P_v^1(\cos\theta)$

as $P_v^1(\cos\theta) = -\sqrt{\frac{2v}{\pi \sin\theta}} \cdot \cos [(v + \frac{1}{2})\theta + \frac{\pi}{4}]$, P_t is obtained as

$$\begin{aligned}
 P_t &= \left[(k_o \hat{H}_v^{(2)})'(k_o r_o) + \frac{\hat{H}_v^{(2)}(k_o r_o)}{r_o} \right]^2 \frac{E_o^2}{\eta_o} \\
 &\quad \frac{2v}{\pi} \int_0^{2\pi} \int_{-\theta_1}^{+\theta_1} \cos^2 \left[(v + \frac{1}{2})\theta + \frac{\pi}{4} \right] r_o^2 d\theta d\phi \\
 &= \frac{4}{\eta_o} |E_1|^2 v r_o^2 \theta_1 \tag{D-25}
 \end{aligned}$$

where $|E_1| = E_o \left(k_o \hat{H}_v^{(2)}(k_o r_o) + \frac{\hat{H}_v^{(2)}(k_o r_o)}{r_o} \right)$

Now the gain of the horn may be obtained by the relation

$$G = \frac{4\pi r^2 |E_\theta|_{\max}^2}{\eta_o P_t} \tag{D-26}$$

Using the Eqs.(D-23) and (D-25) in Eq.(D-26), the gain is obtained as,

$$\begin{aligned}
 G &= \frac{\pi^2 r_o^2}{2 \lambda_o \theta_1} \left[\sqrt{[C(u_{o1}) - C(u_{o2})]^2 + [S(u_{o1}) - S(u_{o2})]^2} \right. \\
 &\quad \left. + \sqrt{[C(v_{o1}) - C(v_{o2})]^2 + [S(v_{o1}) - S(v_{o2})]^2} \right]^2 \tag{D-27}
 \end{aligned}$$

where,

$$\begin{pmatrix} u_{o1} \\ u_{o2} \end{pmatrix} = \left[-\frac{\lambda_o}{2r_o} \frac{(v+1)}{\pi} \pm \theta_1 \right] \sqrt{\frac{2r_o}{\lambda_o}}$$

and

$$\begin{pmatrix} v_{o1} \\ v_{o2} \end{pmatrix} = \left[\frac{\lambda_o}{2r_o} \frac{v}{\pi} \pm \theta_1 \right] \sqrt{\frac{2r_o}{\lambda_o}}$$

APPENDIX E

EVALUATION OF THE SCATTERED FIELD FOR DIELECTRIC SPHERE LOADED CORRUGATED E-PLANE SECTORAL HORN

From Eq. (5.5)

$$E_{\theta}^s = \frac{k_o^2(\epsilon_r - 1)}{4\pi} A_o b^2 \int_0^{\pi} e^{jn\theta'} \sin\theta' d\theta' \cdot \int_0^{2\pi} e^{jk_o b \sin\theta \cos(\phi - \phi')} d\phi' \quad (E-1)$$

But $J_n(x) = \frac{j^{-n}}{2\pi} \int_0^{2\pi} e^{j[x \cos(\phi - \phi') + n\phi']} d\phi'$, and

hence E_{θ}^s can be written as,

$$E_{\theta}^s = \frac{k_o^2(\epsilon_r - 1)}{4\pi} A_o b^2 2\pi J_o(k_o b \sin\theta) \int_0^{\pi} e^{jn\theta'} \sin\theta' d\theta' \quad (E-2)$$

Let $I = \int_0^{\pi} e^{jn\theta'} \sin\theta' d\theta'$, and can be evaluated as

$$I = \frac{1 + e^{jn\pi}}{1 - n^2} = \frac{1 + \cos n\pi}{(1 - n^2)}$$

since $\sin n\pi = 0$ for $n = 0, 1, 2, 3, \dots$

$$\text{Thus } E_{\theta}^s = \frac{k_o^2(\epsilon_r - 1)}{4\pi} A_o b^2 2\pi J_o(k_o b \sin\theta) \cdot \frac{1 + \cos n\pi}{(1 - n^2)} \quad (E-3)$$

APPENDIX F

DERIVATION OF EXPRESSIONS FOR DIELECTRIC SPHERE LOADED
CORRUGATED CONICAL HORN

F-1 RADIATION PATTERN OF DIELECTRIC SPHERE LOADED
CORRUGATED CONICAL HORN

By Eqs. (5.20) potential functions for the total radiated far-field are given by,

$$\begin{aligned} \Delta_r^+ &= \cos\phi \sum_{n=1}^{\infty} \hat{H}_n^{(2)}(k_0 r) J_1(q\theta) (a_n + b_n) \\ F_r^+ &= \eta_0 \sin\phi \sum_{n=1}^{\infty} \hat{H}_n^{(2)}(k_0 r) J_1(q\theta) (a_n + c_n) \end{aligned} \quad (F-1)$$

The radiated far-field component E_θ^+ is obtained as,

$$\begin{aligned} E_\theta^+ &= -\frac{1}{r \sin\theta} \frac{\partial}{\partial \phi} F_r^+ + \frac{1}{j\omega\epsilon_0 r} \frac{\partial^2 \Delta_r^+}{\partial r \partial \theta} \\ &= \cos\phi \eta_0 \frac{\hat{H}_n^{(2)}(k_0 r)}{r} a_n \cdot \\ &\quad \left[-\frac{J_1(q\theta)}{\sin\theta} \alpha_n + q J_1'(q\theta) \frac{\hat{H}_n^{(2)'}(k_0 r)}{j \hat{H}_n^{(2)}(k_0 r)} \beta_n \right], \end{aligned}$$

and under far-field approximation, E_θ^+ becomes,

$$E_{\theta}^{+} = -(j)^{n+1} \frac{e^{-jk_0 r}}{r} \eta_0 a_n \cos \phi \left[\frac{J_1(q\theta)}{\sin \theta} \alpha_n + q J_1'(q\theta) \beta_n \right] \quad (F-2)$$

with α_n and β_n as defined in Eq. (5.21)

Similarly,

$$\begin{aligned} E_{\phi} &= \frac{1}{r} \frac{\partial}{\partial \theta} F_r^{+} + \frac{1}{j\omega \epsilon_0 r \sin \theta} \frac{\partial^2 A_r^{+}}{\partial r \partial \phi} \\ &= (j)^{n+1} \frac{e^{-jk_0 r}}{r} \eta_0 \sin \phi a_n \left[\frac{J_1(q\theta)}{\sin \theta} \beta_n + q \frac{J_1'(q\theta)}{1} \alpha_n \right] \end{aligned} \quad (F-3)$$

The resultant radiated far-field E_R is given by

$$E_R(r) = \bar{i}_{\theta} E_{\theta}^{+} + \bar{i}_{\phi} E_{\phi}^{+}; \text{ and by Eqs. (F-2) and (F-3),}$$

$E_R(r)$ becomes,

$$\begin{aligned} E_R(r) &= -(j)^{n+1} \frac{e^{-jk_0 r}}{r} \eta_0 a_n \left[\left\{ \frac{J_1(q\theta)}{\sin \theta} \cos \phi \bar{i}_{\theta} - q J_1'(q\theta) \sin \phi \bar{i}_{\phi} \right\} \alpha_n \right. \\ &\quad \left. + \left\{ q J_1'(q\theta) \cos \phi \bar{i}_{\theta} - \frac{J_1(q\theta)}{\sin \theta} \sin \phi \bar{i}_{\phi} \right\} \beta_n \right] \\ &= -(j)^{n+1} \frac{e^{-jk_0 r}}{r} \eta_0 \sum_{n=1}^{\infty} a_n (\bar{M}_n \alpha_n + \bar{N}_n \beta_n) \end{aligned} \quad (F-4)$$

Inserting the value of $a_n = j^{-n} \frac{(2n+1)}{n(n+1)}$

$$E_R(r) = -j \frac{e^{-jk_0 r}}{r} \eta_0 \sum_{n=1}^{\infty} \frac{(2n+1)}{n(n+1)} (\bar{M}_n \alpha_n + \bar{N}_n \beta_n) \quad (F-5)$$

where,

$$\bar{M} = \frac{J_1(q\theta)}{\sin\theta} \cos\phi \bar{i}_\theta - q J_1'(q\theta) \sin\phi \bar{i}_\phi$$

$$\bar{N} = J_1'(q\theta) \cos\phi \bar{i}_\theta - \frac{J_1(q\theta)}{\sin\theta} \sin\phi \bar{i}_\phi$$

$$\alpha_n = 1 + \frac{c_n}{b_n} \quad ; \quad \beta_n = 1 + \frac{b_n}{a_n}$$

F-2 POWER RADIATED FROM SPHERE-MOUNTED
CORRUGATED CONICAL HORN

The total Power W_t radiated from the system may be determined by integrating total power flow across an infinite sphere placed concentric with the diffracting dielectric sphere. Thus W_t becomes,

$$W_t = \frac{1}{2} \operatorname{Re} \left[\int_{\phi=0}^{2\pi} \int_{\theta=0}^{\pi} r^2 S_R \sin\theta d\theta d\phi \right] \quad (F-6)$$

where, $S_R = (E_R \times H_R^*)$

By Eq. (F-4)

$$W_t = \frac{1}{2} \eta_0 a_n^2 \int_0^{2\pi} \int_0^{\pi} (\bar{M} \alpha_n + \bar{N} \beta_n)^2 \sin\theta d\theta d\phi$$

$$\begin{aligned}
 W_t &= \frac{1}{2} \eta_0 a_n^2 \int_0^{2\pi} \int_0^\pi (\bar{M}^2 \alpha_n^2 + \bar{N}^2 \beta_n^2 + 2\bar{M} \bar{N} \alpha_n \beta_n) \sin\theta d\theta d\phi \\
 &= \frac{1}{2} \eta_0 a_n^2 \int_0^{2\pi} \int_0^\pi \left[\alpha_n^2 \left\{ \left[\frac{J_1(q\theta)}{\sin\theta} \right]^2 \cos^2\phi + [qJ_1'(q\theta)]^2 \sin^2\phi \right\} \right. \\
 &\quad \left. + \beta_n^2 \left\{ \left[\frac{J_1(q\theta)}{\sin\theta} \right]^2 \sin^2\phi + [qJ_1'(q\theta)]^2 \cos^2\phi \right\} \right. \\
 &\quad \left. + 2\alpha_n \beta_n \frac{J_1(q\theta)}{\sin\theta} qJ_1'(q\theta) (\cos^2\phi + \sin^2\phi) \right] \sin\theta d\theta d\phi
 \end{aligned}$$

since $\bar{i}_\theta \cdot \bar{i}_\theta = 1$; $i_\phi \cdot i_\phi = 1$; $i_\theta \cdot i_\phi = 0$

Integrating w.r.t. ϕ ,

$$\begin{aligned}
 W_t &= \frac{1}{2} \eta_0 \pi a_n^2 \int_0^\pi \left\{ \left[\frac{J_1(q\theta)}{\sin\theta} \right]^2 + [qJ_1'(q\theta)]^2 \right\} (\alpha_n^2 + \beta_n^2) + \\
 &\quad 4\alpha_n \beta_n \frac{J_1(q\theta)}{\sin\theta} qJ_1'(q\theta) \sin\theta d\theta \\
 &= \frac{1}{2} \eta_0 \pi a_n^2 \int_0^\pi \left\{ \left[\frac{J_1(q\theta)}{\sin\theta} + qJ_1'(q\theta) \right]^2 - \right. \\
 &\quad \left. \frac{2J_1(q\theta)}{\sin\theta} qJ_1'(q\theta) \right\} (\alpha_n^2 + \beta_n^2) + 4\alpha_n \beta_n \frac{J_1(q\theta)}{\sin\theta} qJ_1'(q\theta) \sin\theta d\theta
 \end{aligned}$$

$$\begin{aligned}
 W_t &= \frac{1}{2} \eta_0 \pi a_n^2 \left[\int_0^\pi \left[\frac{J_1(q\theta)}{\sin\theta} + q J_1'(q\theta) \right]^2 (\alpha_n^2 + \beta_n^2) \sin\theta d\theta \right. \\
 &\quad - \int_0^\pi 2J_1(q\theta) q J_1'(q\theta) (\alpha_n^2 + \beta_n^2) d\theta + 4\alpha_n \beta_n \int_0^\pi J_1(q\theta) q J_1'(q\theta) d\theta. \left. \right] \\
 &= \frac{1}{2} \eta_0 \pi a_n^2 \left[\int_0^\pi \left[\frac{J_1(q\theta)}{\sin\theta} + q J_1'(q\theta) \right]^2 (\alpha_n^2 + \beta_n^2) \sin\theta d\theta \right. \\
 &\quad - 2(\alpha_n^2 + \beta_n^2) \int_0^\pi J_1(q\theta) dJ_1(q\theta) + 4\alpha_n \beta_n \int_0^\pi J_1(q\theta) dJ_1(q\theta) \\
 &\quad \left. \text{since } q J_1'(q\theta) = \frac{d}{d\theta} J_1(q\theta) \right] \\
 &= \frac{1}{2} \eta_0 \pi a_n^2 \left[J_1^2(q\theta) \{ 2\alpha_n \beta_n - (\alpha_n^2 + \beta_n^2) \} + (\alpha_n^2 + \beta_n^2) I \right]
 \end{aligned}$$

(F-7)

where,

$$I = \int_0^\pi \left[\frac{J_1(q\theta)}{\sin\theta} + q J_1'(q\theta) \right]^2 \sin\theta d\theta$$

To get an explicit expression for W_t , an approximate evaluation of the integral term is possible by assuming $\sin\theta \approx \theta$. This assumption is a source of error for W_t , but as the integral term is added to the other two terms in Eq. (F-7) to get the total power W_t , the percentage of error in W_t is small.

Thus with $\sin\theta \approx \theta$, I becomes,

$$I = \int_0^\pi \left[\frac{J_1(q\theta)}{\theta} + q J_1'(q\theta) \right]^2 \theta d\theta; \text{ and by using}$$

recurrence formula for Bessel functions,

$$\begin{aligned} I &= \int_0^\pi [qJ_0(q\theta)]^2 \theta d\theta \\ &= \frac{(q\theta)^2}{2} [J_0^2(q\theta) - J_{-1}(q\theta)J_1(q\theta)]_{\theta=0}^\pi \\ &= \frac{(q\theta)^2}{2} [J_0^2(q\theta) + J_1^2(q\theta)]_{\theta=0}^\pi \\ &\quad \text{since } J_{-1}(x) = -J_1(x) \\ &= \frac{(q\pi)^2}{2} [J_0^2(q\pi) + J_1^2(q\pi)] \end{aligned} \tag{F-8}$$

Thus, with the approximate evaluation of the integral assuming $\sin\theta \approx \theta$, the expression for W_t becomes,

$$\begin{aligned} W_t &= \frac{1}{2} \eta_0 \pi \sum_{n=1}^{\infty} a_n^2 [J_1^2(q\pi) \{2\alpha_n \beta_n - (\alpha_n^2 + \beta_n^2)\} + \\ &\quad (\alpha_n^2 + \beta_n^2) \frac{(q\pi)^2}{2} \{J_0^2(q\pi) + J_1^2(q\pi)\}] \end{aligned} \tag{F-9}$$

F-3 GAIN OF THE SYSTEM

The on-axis gain of the system is defined as

$$G(0,0) = \frac{1}{2} \left| E_R \right|_{\max}^2 \frac{4\pi r^2}{\eta_0 W_t} \quad (\text{or } G(0,0) = \frac{4\pi P(0,0)}{W_t})$$

E_R is max at $\theta=0$, $\phi = 0$ and from Eq. (F-4)

$$E_R \Big|_{\substack{\phi=0 \\ =\pi}} = j^{n+1} \left[\frac{J_1(q\theta)}{\sin\theta} \alpha_n + q J_1'(q\theta) \beta_n \right] \alpha_n \frac{e^{-jk_0 r}}{r} \eta_0$$

$$\text{Now } J_1(q\theta) \xrightarrow{\theta \rightarrow 0} \frac{q\theta}{2} \quad \text{as } J_n(x) \xrightarrow{x \rightarrow 0} \frac{1}{n!} \frac{x^n}{2} \quad (n > 0)$$

$$\sin\theta \xrightarrow{\theta \rightarrow 0} \theta \quad \therefore \frac{J_1(q\theta)}{\sin\theta} \Big|_{\theta \rightarrow 0} = \frac{q}{2}$$

$$q J_1'(q\theta) = \frac{d}{d\theta} J_1(q\theta) = q \frac{d}{d(q\theta)} J_1(q\theta)$$

$$= q \left[J_0(q\theta) - \frac{1}{q\theta} J_1(q\theta) \right]$$

$$\text{But } J_0(q\theta) \xrightarrow{\theta \rightarrow 0} 1, \quad J_1(q\theta) \xrightarrow{\theta \rightarrow 0} \frac{q\theta}{2}$$

Therefore, $E_R \Big|_{\substack{\theta=0 \\ \phi=0 \\ =\pi}}$ becomes

$$\begin{aligned} \left| E_R \right|_{\max} &= \frac{\eta_0}{r} a_n \left[\frac{q}{2} \alpha_n + q \left\{ 1 - \frac{1}{q\theta} \cdot \frac{(q\theta)}{2} \right\} \beta_n \right] \\ &= \frac{\eta_0}{r} a_n \frac{q}{2} \left[\alpha_n + \beta_n \right] \end{aligned} \quad (F-10)$$

Using Eqs. (F-9) and (F-10), the axial gain becomes,

$$\begin{aligned} G(0,0) &= \frac{4 \left| \sum_{n=1}^{\infty} a_n \frac{q}{2} (\alpha_n + \beta_n) \right|^2}{\sum_{n=1}^{\infty} a_n^2 \left[J_1^2(q\pi) \left\{ 2\alpha_n \beta_n - (\alpha_n + \beta_n) \right\} + \right.} \\ &\quad \left. (\alpha_n^2 + \beta_n^2) \frac{(q\pi)^2}{2} \left\{ J_0^2(q\pi) + J_1^2(q\pi) \right\} \right]} \end{aligned} \quad (F-11)$$

Inserting the value of a_n the gain is finally obtained as,

$$\begin{aligned} G(0,0) &= \frac{\left| \sum_{n=1}^{\infty} \frac{(2n+1)}{n(n+1)} q (\alpha_n + \beta_n) \right|^2}{\sum_{n=1}^{\infty} \frac{(2n+1)^2}{n^2(n+1)^2} \left[J_1^2(q\pi) \left\{ 2\alpha_n \beta_n - (\alpha_n^2 + \beta_n^2) \right\} + \right.} \\ &\quad \left. \frac{(q\pi)^2}{2} (\alpha_n^2 + \beta_n^2) \left\{ J_0^2(q\pi) + J_1^2(q\pi) \right\} \right]} \end{aligned} \quad (F-12)$$

APPENDIX G

EQUATIONS FOR DIELECTRIC COATED E-PLANE SECTORAL HORN

G-1 THE FIELDS IN DIELECTRIC COATED E-PLANE SECTORAL HORN

The fields can be obtained from the potential function

$$\Psi_{mn}^{TE} = \cos \frac{m\pi}{a} x \cos p\theta B_p(k_r r)$$

where $k_r = \sqrt{k_0^2 - \left(\frac{m\pi}{a}\right)^2}$ (G-1)

$B_p(k_r r)$ = the solution to the Bessel's equation.

For dielectric coated region, as there will be standing waves due to reflections from the air dielectric interface, the proper form of

$$B_p(k_r r) = [CJ_p(k_{r1} r) + Dy_p(k_{r1} r)]$$

where $k_{r1} = \sqrt{\epsilon_r k_0^2 - \left(\frac{m\pi}{a}\right)^2}$ (G-2)

$J_p(k_{r1} r)$ = Bessel function of the first kind

$y_p(k_{r1} r)$ = Bessel function of the second kind

and C and D are constants.

In the horn axial region outward travelling waves will exist; and hence the suitable form of $B_n(k_r r)$ for this region is $H_p^{(2)}(k_r r)$, Hankel function of the second kind.

The different field components in the two regions are obtained by substituting ψ_{mn}^{TE} into the following equations

$$\begin{aligned}
 E_r &= -\frac{1}{r} \frac{\partial \psi}{\partial \theta} & H_r &= \frac{1}{j\omega \mu_0} \frac{\partial^2 \psi}{\partial r \partial x} \\
 E_\theta &= \frac{\partial \psi}{\partial r} & H_\theta &= \frac{1}{j\omega \mu_0} \frac{\partial^2 \psi}{\partial \theta \partial x} \\
 E_y &= 0 & H_x &= \frac{1}{j\omega \mu_0} \left(\frac{\partial^2 \psi}{\partial x^2} + k_0^2 \right) \psi
 \end{aligned} \tag{G-3}$$

Thus by Eqs. (G-1) and (G-3) and taking appropriate forms for $B_n(k_r r)$, field components in the two regions become

In the dielectric coated region

$$E_{rd} = \frac{p}{r} \cos \frac{m\pi}{a} x \sin p\theta [CJ_p(k_{r1}r) + Dy_p(k_{r1}r)]$$

$$E_{\theta d} = k_{r1} \cos \frac{m\pi}{a} x \cos p\theta [CJ_p'(k_{r1}r) + Dy_p'(k_{r1}r)]$$

$$E_{xd} = 0$$

(G-4)

$$H_{rd} = - \frac{1}{j\omega\mu_0} \frac{m\pi}{a} k_{r1} \sin \frac{m\pi}{a} x \cos p\theta [CJ'_p(k_{r1}r) + Dy'_p(k_{r1}r)]$$

$$H_{\theta d} = \frac{1}{j\omega\mu_0} p \frac{m\pi}{a} \sin \frac{m\pi}{a} x \sin p\theta [CJ_p(k_{r1}r) + Dy_p(k_{r1}r)]$$

$$H_{xd} = \frac{1}{j\omega\mu_0} k_{r1}^2 \cos \frac{m\pi}{a} x \cos p\theta H_p^{(2)}(k_{r1}r)$$

In the horn axial region

$$E_{r0} = \frac{F}{r} p \cos \frac{m\pi}{a} x \sin p\theta H_p^{(2)}(k_r r)$$

$$E_{\theta 0} = F k_r \cos \frac{m\pi}{a} x \cos p\theta H_p^{(2)'}(k_r r)$$

$$E_{x0} = 0$$

(G-5)

$$H_{r0}^+ = - \frac{1}{j\omega\mu_0} F k_r \frac{m\pi}{a} \sin \frac{m\pi}{a} x \cos p\theta H_p^{(2)'}(k_r r)$$

$$H_{\theta 0}^+ = \frac{1}{j\omega\mu_0} F \frac{m\pi}{a} \sin \frac{m\pi}{a} x \sin p\theta H_p^{(2)}(k_r r)$$

$$H_{x0}^+ = \frac{1}{j\omega\mu_0} k_r^2 \cos \frac{m\pi}{a} x \cos p\theta H_p^{(2)}(k_r r)$$

where F is a constant that depends on the excitation of the horn. The prime on the functions indicates differentiation with respect to r.

G-2 CHARACTERISTIC EQUATION FOR DIELECTRIC
LOADED E-PLANE SECTORAL HORN

The values of the separation constant 'p' are obtained from the characteristic equation formulated on the boundary conditions viz,

- i) tangential E and H must be continuous at the air-dielectric interface

$$\begin{aligned} \text{i.e. } E_{rd} &= E_{ro} \\ H_{rd} &= H_{ro} \end{aligned} \quad \begin{array}{l} \text{at } \theta = \alpha_1 \\ r \leq r_0 \end{array}$$

- ii) $E_{\theta d} = 0$ at $\theta = \alpha_0$, the flare angle of the empty horn.
Thus $E_{rd} = E_{ro}$ at $\theta = \alpha_1$,

(α_1 is the flare angle of the dielectric coated horn) from Eqs.(G-4) and (G-5), gives

$$[C J_p(k_{r1}r) + D y_p(k_{r1}r)] = F H_p^{(2)}(k_r r) \quad (G-6)$$

for $r \leq r_0$, the flare length of the horn and $H_{rd} = H_{ro}$ at $\theta = \alpha_1$ gives

$$k_{r1} [C J_p'(k_{r1}r) + D y_p'(k_{r1}r)] = k_r F H_p^{(2)'}(k_r r) \quad (G-7)$$

for $r \leq r_0$

Another boundary condition i.e. $E_{\theta d} = 0$ at $\theta = \alpha_0$ gives a relation between C and D

i.e. $E_{\theta d} = 0$ at $\theta = \alpha_0$ gives

$$\cos \alpha_0 [CJ_p'(k_{r1}r) + Dy_p'(k_{r1}r)] = 0 \quad \text{for } r \leq r_0$$

i.e. either $\cos \alpha_0 = 0$ or $[CJ_p'(k_{r1}r) + Dy_p'(k_{r1}r)] = 0$

$\cos \alpha_0 = 0$ gives $\rho = \frac{n\pi}{2\alpha_0}$ and is the case for empty horns.

To differentiate the dielectric coated case from the empty horn case, the other relation

$$CJ_p'(k_{r1}r) + Dy_p'(k_{r1}r) = 0 \quad (\text{for } r \leq r_0)$$

holds good,

$$\text{i.e. } D = -C \frac{J_p'(k_{r1}r)}{y_p'(k_{r1}r)}, \quad \text{for } r \leq r_0 \quad (G-8)$$

Equations (G-6) and (G-7) are true for $\theta = \alpha_1$ and $r \leq r_0$, the flare length of the horn, and Eq. (G-8) is valid at $\theta = \alpha_0$ and $r \leq r_0$. Hence, to make the characteristic equation depend on the dielectric coating specifications, it is better to use the relation $\frac{b_1'}{2r'} = \sin \alpha_1$ in Eqs. (G-6) and (G-7), and the relation $\frac{b_0'}{2r'} = \sin \alpha_0$ in Eq. (G-8) where (see Fig. 6.1) $b_1' = b_0' - 2\delta'$, corresponding to any value of $r \leq r_0$ (δ' = the corresponding dielectric coating thickness), b_0' = the distance along y-direction corresponding to $\theta = \alpha_0$ and $r \leq r_0$. At $r = r_0$, $b_1' = b_1$, $b_0' = b_0$, $\delta' = \delta$; the

respective quantities at the aperture . Introducing these relationships, and the relation by Eqs.(G-8), Eqs.(G-6) and (G-7) respectively become

$$\begin{aligned} & \int \left[J_p \left(k_{r1} \frac{b_1'}{2 \sin \alpha_1} \right) y_p' \left(k_{r1} \frac{b_0'}{2 \sin \alpha_0} \right) - \right. \\ & \quad \left. J_p' \left(k_{r1} \frac{b_0'}{2 \sin \alpha_0} \right) y_p \left(k_{r1} \frac{b_1'}{2 \sin \alpha_1} \right) \right] \\ & = F H_p^{(2)} \left(k_r \frac{b_1'}{2 \sin \alpha_1} \right) \end{aligned} \quad (G-9)$$

and

$$\begin{aligned} & \int \left[J_p' \left(k_{r1} \frac{b_1'}{2 \sin \alpha_1} \right) y_p' \left(k_{r1} \frac{b_0'}{2 \sin \alpha_0} \right) - \right. \\ & \quad \left. J_p' \left(k_{r1} \frac{b_0'}{2 \sin \alpha_0} \right) y_p' \left(k_{r1} \frac{b_1'}{2 \sin \alpha_1} \right) \right] \\ & = \frac{k_r}{k_{r1}} F H_p^{(2)'} \left(k_r \frac{b_1'}{2 \sin \alpha_1} \right) \end{aligned} \quad (G-10)$$

Dividing Eq.(G-9) by Eq.(G-10), it becomes

$$\begin{aligned}
 & \frac{J_p(k_{r1} \frac{b_1'}{2\sin\alpha_1}) y_p'(k_{r1} \frac{b_0'}{2\sin\alpha_0}) - J_p'(k_{r1} \frac{b_0'}{2\sin\alpha_0}) y_p(k_{r1} \frac{b_1'}{2\sin\alpha_1})}{J_p'(k_{r1} \frac{b_1'}{2\sin\alpha_1}) y_p'(k_{r1} \frac{b_0'}{2\sin\alpha_0}) - J_p'(k_{r1} \frac{b_0'}{2\sin\alpha_0}) y_p'(k_{r1} \frac{b_1'}{2\sin\alpha_1})} \\
 & = \frac{k_{r1}}{k_r} \cdot \frac{H_p^{(2)}(k_r \frac{b_1'}{2\sin\alpha_1})}{H_p^{(2)'}(k_r \frac{b_1'}{2\sin\alpha_1})} \quad (G-11)
 \end{aligned}$$

i.e.

$$\frac{J_p(x_1) y_p'(x_2) - J_p'(x_2) y_p(x_1)}{J_p'(x_1) y_p'(x_2) - J_p'(x_2) y_p'(x_1)} = \frac{k_{r1} H_p^{(2)}(k_r \frac{b_1'}{2\sin\alpha_1})}{k_r H_p^{(2)'}(k_r \frac{b_1'}{2\sin\alpha_1})} \quad (G-12)$$

where $x_1 = k_{r1} \frac{b_1'}{2\sin\alpha_1}$; $x_2 = k_{r1} \frac{b_0'}{2\sin\alpha_0}$

and the primes on the functions indicate differentiation with respect to r . This is the characteristic equation for HE_{mn} mode and can be solved graphically for 'p' by substituting the quantities in Eq.(G-11). k_{r1} and k_r are obtained from Eqs.(G-1) and (G-2) respectively for the particular values of m and ϵ_r .

G-3 THE RADIATED FAR FIELD

The radiation field from the dielectric loaded horn can be obtained by the aperture field method employing the vector diffraction formula. The phase of the field over the horn aperture will not be constant, and from the nature of the aperture, a field phase variation of the form

$$\psi = e^{-j \frac{\pi}{\lambda_g} \frac{y^2}{R}}, \text{ (where } \lambda_g = 2\pi/k_r \text{ and R is the horn axial length)}$$

is a reasonable assumption.

The radiated far-field in the E-plane ($\phi = \pi/2$) based on the vector diffraction formula is given by

$$E(\theta) = \frac{jk_0}{4\pi} \frac{e^{-jk_0 r}}{r} \left(1 + \frac{k_r}{k_0} \cos\theta\right) \iint_s \bar{E}_t e^{jk_0 y_s \sin\theta} ds$$

where \bar{E}_t = the transverse electric field over the horn aperture and is given by

$\bar{E}_t = \bar{i}_x E_x + \bar{i}_y E_y^-$. In obtaining a simplified expression for E_t the following approximations are used. (The approximations are true if the apex angle ($2\alpha_0$) of the horn is not very large)

$$E_y \approx E_\theta \quad \text{and} \quad \bar{i}_y \approx \bar{i}_\theta$$

Thus the transverse E -field over the horn aperture from Eqs.(G.5) becomes,

$$E_t = F k_r \cos \frac{m\pi}{a} x \cos p\theta H_p^{(2)'}(k_r R) \quad (\text{since } E_x=0; R \approx r_0)$$

Thus,

$$E_\theta = F' \frac{k_r k_0}{4\pi} \frac{e^{-jk_0 r}}{r} \left(1 + \frac{k_r}{k_0} \cos\theta\right) \int_{-a/2}^{a/2} \cos \frac{m\pi}{a} x \, dx \cdot \int_{-b_1/2}^{b_1/2} \cos p\theta e^{-j\frac{\pi}{\lambda g} \frac{y^2}{R}} e^{jk_0 y \sin\theta} \, dy$$

where $F' = jF H_p^{(2)'}(k_r R)$

Considering that $b_1 < R$ (i.e. if the flare angle is not large)

$$\frac{\theta}{2\alpha_1} \approx \frac{y}{b_1} \quad \text{i.e.} \quad \theta \approx \frac{2\alpha_1}{b_1} y$$

$$\therefore E_\theta = \frac{F' k_r k_0}{4\pi} \frac{e^{-jk_0 r}}{r} \left(1 + \frac{k_r}{k_0} \cos\theta\right) I_1 I_2 \quad (G-13)$$

where,

$$I_1 = \int_{-a/2}^{a/2} \cos \frac{m\pi}{a} x \, dx = 2 \frac{a}{m\pi} \sin \frac{m\pi}{2} \quad (G-14)$$

(I_1 is non zero only for $m = 1, 3, 5, \dots$)

and

$$\begin{aligned}
 I_2 &= \int_{-b_1/2}^{b_1/2} \cos\left(p \frac{2a_1}{b_1} y\right) e^{-\frac{j\pi}{\lambda_g} \frac{y^2}{R}} e^{jk_0 y \sin\theta} dy \\
 &= \int_{-b_1/2}^{b_1/2} \left(e^{\frac{jp2a_1}{b_1} y} + e^{-\frac{j2pa_1}{b_1} y} \right) e^{jk_0 y \sin\theta} e^{-\frac{j\pi}{\lambda_g} \frac{y^2}{R}} dy \\
 &= I_3 I_4
 \end{aligned}$$

$$I_3 = \sqrt{\lambda_g R / 2} \quad M \left\{ C(v_1) - C(v_2) - j [S(v_1) - S(v_2)] \right\}$$

where,

(G-15)

$$M = \frac{j\pi}{4} \lambda_g R \left(\frac{2pa_1}{\pi b_1} + 2 \sin\theta \right)^2$$

$$\begin{pmatrix} v_1 \\ v_2 \end{pmatrix} = \frac{1}{\sqrt{2}} \left[\frac{b_1}{\sqrt{\lambda_g R}} \pm \sqrt{\lambda_g R} \left(2 \frac{pa_1}{\pi b_1} + \frac{2}{\lambda_0} \sin\theta \right) \right]$$

$$I_4 = \sqrt{\lambda_g R / 2} \quad N \left\{ C(v_3) - C(v_4) - j [S(v_3) - S(v_4)] \right\}$$

where

$$N = e^{-\frac{j\pi}{4} \lambda_g R} \left(\frac{2pa_1}{\pi b_1} - \frac{2}{\lambda_0} \sin\theta \right)^2$$

(G-16)

$$\begin{pmatrix} v_3 \\ v_4 \end{pmatrix} = \frac{1}{\sqrt{2}} \left[\frac{b_1}{\sqrt{\lambda_g R}} \pm \sqrt{\lambda_g R} \left(\frac{2pa_1}{\pi b_1} - \frac{2}{\lambda_0} \sin\theta \right) \right]$$

i.e.

$$E_\theta = F' k_r \frac{e^{-jk_0 r}}{\lambda_0 r} \left(1 + \frac{k_r}{k_0} \cos\theta \right) \cdot \frac{a}{m\pi} \sin \frac{m\pi}{2} \sqrt{\lambda_g R / 2}$$

$$\left[M \left\{ C(v_1) - C(v_2) - j [S(v_1) - S(v_2)] \right\} + N \left\{ C(v_3) - C(v_4) - j [S(v_3) - S(v_4)] \right\} \right] \quad (G-17)$$

G-4 ON-AXIS GAIN OF THE SYSTEM

The total power transmitted through the aperture of the horn becomes,

$$P_t = \frac{1}{2} \operatorname{Re} \iint_S E_\theta H_X^* ds$$

Inserting the relation $\theta \approx \frac{2a_1}{b_1} y$, from Eqs. (G-5)

$$\begin{aligned} P_t &= \frac{1 F'^2}{2 \omega \mu_0} \int_{-a/2}^{a/2} \cos^2 \frac{m\pi}{a} x dx \\ &\quad \int_{-b/2}^{b/2} \cos^2 \frac{2p\alpha_1}{b_1} y dy \\ &= \frac{1}{8} F'^2 \frac{k_r^3}{\omega \mu_0} a b_1 \left(1 + \frac{\sin 2p\alpha_1}{2p\alpha_1} \right) \end{aligned}$$

Now on-axis gain is defined as,

$$G(0,0) = 4\pi \frac{P(0,0)}{P_t} \quad \text{where}$$

$$p(0,0) = \frac{1}{2\eta_0} E_{\theta \max}^2 r^2$$

Using Eq.(G-17) and inserting the relation $\omega \mu_0 = k_0 \eta_0$,

$$\begin{aligned} G(0,0) &= \frac{32aR}{m^2 \pi b_1 \lambda_0^3} \frac{2}{g} \left(1 + \frac{\lambda_0}{\lambda g} \right)^2 \frac{2p\alpha_1}{(2p\alpha_1 + \sin 2p\alpha_1)} \\ &\quad \left\{ [C(v_{o1}) - C(v_{o2})]^2 + [S(v_{o1}) - S(v_{o2})]^2 \right\} \end{aligned}$$

APPENDIX H

DERIVING EXPRESSIONS FOR DIELECTRIC LOADED H-PLANE
SECTORAL HORN WITH CYLINDRICAL APERTURE

H-1 FIELDS IN THE DIELECTRIC LOADED SMALL FLARE
H-PLANE SECTORAL HORN

$$\bar{F} = \bar{i}_\theta \psi$$

$$\psi_o = A_n \cos k_{y_o} y \cos p\theta H_p^{(2)}(k_r r) \quad (H-1)$$

$$\psi_d = B_n \cos k_{y_d} \left(\frac{a}{2} - y \right) \cos \theta H_p^{(2)}(k_r r)$$

The different field components are given by

$$\bar{E} = -\nabla \times \bar{F} \quad (H-2)$$

$$\bar{H} = -j\omega \epsilon \bar{F} + \frac{1}{j\omega\mu_o} \nabla (\nabla \cdot \bar{F})$$

Accordingly,

$$E_r = + \frac{\partial \psi}{\partial y} \quad H_r = \frac{1}{j\omega\mu_o} \frac{\partial^2 \psi}{\partial r \partial \theta}$$

$$E_y = - \frac{\partial \psi}{\partial r} \quad H_y = \frac{1}{j\omega\mu_o} \frac{\partial^2 \psi}{\partial y \partial \theta} \quad (H-3)$$

$$E_\theta = 0 \quad H_\theta = \frac{1}{j\omega\mu_o} \left(\frac{\partial^2 \psi}{\partial \theta^2} + k^2 \psi \right)$$

Thus, from Eqs. ((H-1) and (H-2), the fields inside the dielectric layered region and in the horn axial region

respectively are obtained as :

Inside dielectric region

$$E_{rd} = B_n k_{yd} \operatorname{sinc} k_{yd} \left(\frac{a}{2} - y \right) \cos p\theta H_p^{(2)}(k_r r)$$

$$E_{yd} = -B_n k_r \operatorname{cosec} k_{yd} \left(\frac{a}{2} - y \right) \cos p\theta H_p^{(2)'}(k_r r)$$

$$E_{\theta d} = 0 \tag{H-4}$$

$$H_{rd} = -\frac{1}{j\omega\mu_0} P k_r B_n \operatorname{cosec} k_{yd} \left(\frac{a}{2} - y \right) \sin p\theta H_p^{(2)'}(k_r r)$$

$$H_{yd} = -\frac{1}{j\omega\mu_0} k_{yd} B_n \operatorname{sinc} k_{yd} \left(\frac{a}{2} - y \right) \sin p\theta H_p^{(2)}(k_r r)$$

$$H_{\theta d} = \frac{(k_1^2 - p^2)}{j\omega\mu_0} \operatorname{cosec} k_{yd} \left(\frac{a}{2} - y \right) \cos p\theta H_p^{(2)}(k_r r)$$

In the axial region

$$E_{r0} = -k_{y0} A_n \operatorname{sinc} k_{y0} y \cos p\theta H_p^{(2)}(k_r r)$$

$$E_{y0} = -k_r A_n \operatorname{cosec} k_{y0} y \cos p\theta H_p^{(2)'}(k_r r)$$

$$E_{\theta 0} = 0 \tag{H-5}$$

$$H_{r0} = -\frac{P k_r}{j\omega\mu_0} A_n \operatorname{cosec} k_{y0} y \sin p\theta H_p^{(2)'}(k_r r)$$

$$H_{y0} = \frac{p k_{y0}}{j\omega\mu_0} A_n \operatorname{sinc} k_{y0} y \cos p\theta H_p^{(2)}(k_r r)$$

$$H_{\theta 0} = \frac{1}{j\omega\mu_0} (k_0^2 - p^2) A_n \operatorname{cosec} k_{y0} y \cos p\theta H_p^{(2)}(k_r r)$$

where the prime indicates differentiation with respect to r . The constants A_n and B_n , eigen values p and the separation parameters k_{y_0} and k_{y_d} are all obtained from the following boundary conditions :

i) tangential E is zero at $\theta = \pm\alpha_0$ (half flare angle of the horn) i.e. $E_{y_d} = E_{r_d} = 0$, at $\theta = \pm\alpha_0$

Thus $\cos p\alpha_0 = 0$, i.e. $p = \frac{n\pi}{2\alpha_0}$, ($n = 1, 3, 5, \dots$)

For the dominant HE_{11} mode $n = 1$, and $p = \pi/2\alpha_0$.

ii) $E_{r_0} = E_{r_d}$ at $y = \frac{a}{2} - s$ (where s = thickness of the dielectric coating.)

gives,

$$k_{y_0} A_n \sin k_{y_0} \left(\frac{a}{2} - s \right) = -k_{y_d} B_n \sin k_{y_d} s \quad (H-6)$$

iii) $H_{r_0} = H_{r_d}$

at $y = \frac{a}{2} - s$, give
 $H_{\theta_0} = H_{\theta_d}$

$$A_n \cos k_{y_0} \left(\frac{a}{2} - s \right) = B_n \cos k_{y_d} s \quad (H-7)$$

Dividing Eq.(H-6) by Eq.(H-7) it is obtained as,

$$k_{y_0} \tan k_{y_0} \left(\frac{a}{2} - s \right) = -k_{y_d} \tan k_{y_d} s \quad (H-8)$$

If the dielectric loading is by thin dielectric sheets with low permittivity, k_{y_0} and k_{y_d} are small and hence the above Eq.(H-8) can be written as

$$k_{y_0}^2 \left(\frac{a}{2} - s \right) = - k_{y_d}^2 s \quad (\text{H-9})$$

Another set of relationships also exist between the separation parameters as,

$$\begin{aligned} k_{y_0}^2 + k_r^2 &= k_0^2 = \omega^2 \mu_0 \epsilon_0 \\ k_{y_d}^2 + k_r^2 &= k_1^2 = \omega^2 \mu_0 \epsilon_1 \end{aligned} \quad (\text{H-10})$$

(It is assumed that the propagation constant k_r is the same in both regions)

Thus, from Eqs. (H-9) and (H-10), an explicit expression for k_{y_0} can be obtained as

$$k_{y_0}^2 = - k_0^2 (\epsilon_r - 1) \frac{2s}{a} \quad (\text{H-11})$$

Knowing k_{y_0} , possible values of k_r can be obtained from Eq. (H-10); and the ratio A_n/B_n can be obtained either from Eq. (H-6) or from Eq. (H-17) by knowing the values of k_{y_0} and k_{y_d} .

H-2 RADIATION FIELD

The aperture field method based on the vector diffraction formula is employed for the evaluation of radiation field. Thus the radiated far-field in the

XZ -plane ($\phi = 0$) is obtained as,

$$E_{\phi}(\theta) = j \frac{e^{-jk_0 r}}{2\lambda_0 r} \left(1 + \frac{k_r}{k_0} \cos\theta\right) \iint_S \bar{E}_t e^{jk_0 R \cos(\theta_s - \theta)} ds$$

where \bar{E}_t = the transverse E -field over the horn aperture
 R = the horn axial length (\approx horn flare length for small angle horns)

$$\bar{E}_t = \bar{i}_x E_x + \bar{i}_y E_y = -k_r A_n \cos k_{y_0} y_s \cos \theta H_p^{(2)'}(k_r R)$$

Since, $E_x \approx E_\theta = 0$. Thus the radiation pattern in the H -plane for HE_{11} mode becomes,

$$\begin{aligned} E_{\phi}(\theta) &= -j \frac{e^{-jk_0 r}}{2\lambda_0 r} \left(1 + \frac{k_r}{k_0} \cos\theta\right) k_r A_n H_p^{(2)'}(k_r R) \\ &\quad \int_{-a/2}^{a/2} \int_{-a_0}^{a_0} \cos k_{y_0} y_s \cos \theta_s e^{jk_0 R \cos(\theta_s - \theta)} dy_s R d\theta_s \\ &= -j A_n H_p^{(2)'}(k_r R) \frac{e^{-jk_0 r}}{2\lambda_0 r} \left(1 + \frac{k_r}{k_0} \cos\theta\right) k_r R \\ &\quad \int_{-a/2}^{a/2} \cos k_{y_0} y_s dy_s \int_{-a_0}^{a_0} \cos \theta_s e^{jk_0 R \cos(\theta_s - \theta)} d\theta_s \end{aligned}$$

Now $\int_{-a/2}^{a/2} \cos k_y dy_s = \frac{2 \operatorname{sinc} k_{y_0} \frac{a}{2}}{k_{y_0}}$ (H-12)

(H-13)

and

$$\int_{-\alpha_0}^{\alpha_0} \cos p\theta_s e^{jk_0 R \cos(\theta_s - \theta)} d\theta_s$$

$$= \int_{-\alpha_0}^{\alpha_0} \left(\frac{e^{jp\theta_s} + e^{-jp\theta_s}}{2} \right) e^{jk_0 R \cos(\theta_s - \theta)} d\theta_s$$

But $\cos x = 1 - \frac{x^2}{2!} + \dots$

Taking $\cos(\theta_s - \theta) \approx 1 - \frac{(\theta_s - \theta)^2}{2!}$, the above integral becomes,

$$\int_{-\alpha_0}^{\alpha_0} \left(\frac{e^{jp\theta_s} + e^{-jp\theta_s}}{2} \right) e^{jk_0 R \left(1 - \frac{(\theta_s - \theta)^2}{2} \right)} d\theta_s$$

$$= \frac{1}{2} e^{jk_0 R} \int_{-\alpha_0}^{\alpha_0} (e^{jp\theta} + e^{-jp\theta}) e^{-jk_0 R \frac{(\theta_s - \theta)^2}{2}} d\theta_s$$

$$= \frac{1}{2} e^{jk_0 R} \int_{-\alpha_0}^{\alpha_0} e^{jp\theta_s} e^{-jk_0 R \frac{(\theta_s - \theta)^2}{2}} d\theta_s$$

$$+ \int_{-\alpha_0}^{\alpha_0} e^{-jp\theta_s} e^{-jk_0 R \frac{(\theta_s - \theta)^2}{2}} d\theta_s$$

$$\int_{-\alpha_0}^{\alpha_0} e^{jp\theta_s} e^{-jk_0 R \frac{(\theta_s - \theta)^2}{2}} d\theta_s \text{ can be evaluated}$$

as follows

$$I_1 = \int_{-\alpha_0}^{\alpha_0} e^{jp\theta_s} e^{-jk_0 R \frac{(\theta_s - \theta)^2}{2}} d\theta_s$$

$$= \sqrt{\lambda_0/2R} e^{jp\theta} e^{j \frac{\lambda_0}{4R} \frac{p^2}{\pi}} \left\{ C(u_1) - C(u_2) - j [S(u_1) - S(u_2)] \right\}$$

where

$$u_1 = \left(\alpha_0 - \theta - \frac{\lambda_0}{2R} \frac{p}{\pi} \right) \sqrt{2R/\lambda_0}$$

$$u_2 = \left(-\alpha_0 - \theta - \frac{\lambda_0}{2R} \frac{p}{\pi} \right) \sqrt{2R/\lambda_0}$$

Similarly

$$I_2 = \int_{-\alpha_0}^{\alpha_0} e^{-jp\theta_s} e^{-jk_0 R \frac{(\theta_s - \theta)^2}{2}} d\theta_s$$

$$= \sqrt{\lambda_0/2R} e^{-jp\theta} e^{j \frac{\lambda_0}{4R} \frac{p^2}{\pi}} \left\{ C(v_1) - C(v_2) - j [S(v_1) - S(v_2)] \right\}$$

where

$$v_1 = \left(\alpha_0 - \theta + \frac{\lambda_0}{2R} \frac{p}{\pi} \right) \sqrt{2R/\lambda_0}$$

$$v_2 = \left(-\alpha_0 - \theta + \frac{\lambda_0}{2R} \frac{p}{\pi} \right) \sqrt{2R/\lambda_0}$$

Thus it becomes,

$$\int_{-\alpha_0}^{\alpha_0} \cos p\theta_s e^{jk_0 \cos(\theta_s - \theta)} d\theta_s = \sqrt{\lambda_0/2R} e^{jk_0 R} e^{j \frac{\lambda_0}{4R} \frac{p^2}{\pi}} \cdot$$

$$\left[e^{jp\theta} \left\{ C(u_1) - C(u_2) - j [S(u_1) - S(u_2)] \right\} + \right.$$

$$\left. + e^{-jp\theta} \left\{ C(v_1) - C(v_2) - j [S(v_1) - S(v_2)] \right\} \right]$$

(H-14)

Finally from Eqs. (H-12), (H-13) and (H-14), E_{ϕ} is obtained as,

$$E_{\phi} = jE \frac{e^{-jk_0 r}}{\lambda_0 r} \left(1 + \frac{k_r}{k_0} \cos\theta\right) \frac{\sin k_{y0} \frac{a}{2}}{k_{y0}} R \sqrt{\lambda_0 / 2R} \left[e^{jp\theta} \left\{ C(v_1) - C(v_2) - j[S(u_1) - S(u_2)] \right\} + e^{-jp\theta} \left\{ C(v_1) - C(v_2) - j[S(v_1) - S(v_2)] \right\} \right] \quad (H-15)$$

where $E = A_n k_r H_p^{(2)'}(k_r R) e^{j(k_0 R + \frac{\pi}{4} \frac{\lambda_0}{R} \frac{p^2}{\pi^2})}$

$$P = \frac{n\pi}{2\alpha_0}, \quad (\text{for HE}_{11} \text{ mode } P = \frac{\pi}{2\alpha_0})$$

H-3 POWER RADIATED

The total power transmitted through cylindrical aperture may be obtained as

$$\begin{aligned} P_t &= \frac{1}{2} \iint_s \frac{E_t^2}{\eta_0} d_{ys} R d\theta_s \\ &= \frac{1}{2} \frac{R}{\eta_0} [k_r A_n H_{n\pi/2\alpha_0}^{(2)'}(k_r R)]^2 \int_{-a/2}^{a/2} \cos^2 k_{y0} y_s d_{ys} \\ &\quad \cdot \int_{-\infty}^{\infty} \cos^2 p\theta_s d\theta_s \\ &= \frac{1}{8} \frac{R}{\eta_0} |E|^2 \left(a + \frac{\sin k_{y0} a}{k_{y0}} \right) \left(2\alpha_0 + \frac{\sin 2p\alpha_0}{p} \right) \quad (H-16) \end{aligned}$$

where

$$|E| = k_r A_n H_{n\pi/2\alpha_0}^{(2)'}(k_r R)$$

Now the on-axis gain is given by

$$G(0,0) = \frac{4\pi p(0,0)}{P_t}$$

where

$$P(0,0) = \frac{1}{2\eta_0} |E_\phi|_{\max}^2 r^2$$

Using Eqs. (H-15) and (H-16), the gain becomes

$$G(0,0) = \frac{32\pi(1 + \frac{k_r}{k_0})^2 \sin^2 k_{y_0} a \left\{ [C(v_{01}) - C(v_{02})]^2 + [S(v_{01}) - S(v_{02})]^2 \right\}}{\lambda_0 k_{y_0} (k_{y_0} a + \sin k_{y_0} a) (2\alpha_0 + \frac{\sin 2p\alpha_0}{p})}$$

where

$$v_{01} = \left(\alpha_0 + \frac{\lambda_0}{2R} \frac{p}{\pi} \right) \sqrt{2R/\lambda_0}$$

$$v_{02} = \left(-\alpha_0 + \frac{\lambda_0}{2R} \frac{p}{\pi} \right) \sqrt{2R/\lambda_0}$$

H-4 WIDE FLARE HORN : DETERMINATION OF $f_n(w)$ AND $g_n(w)$ AND DERIVATION OF RADIATION PATTERNS

To determine the mode coefficients $f_n(w)$ and $g_n(w)$, the fields E_y and E_θ are calculated by the relations :

$$E = -\nabla \times \bar{F} - j\omega \mu_0 \bar{A} + \frac{1}{j\omega \epsilon_0} \nabla (\nabla \cdot \bar{A})$$

$$H = \nabla \times \bar{A} - j\omega \epsilon_0 \bar{F} + \frac{1}{j\omega \mu_0} \nabla (\nabla \cdot \bar{F})$$

$$\therefore E_y = \frac{\partial}{\partial r} F_\theta + \frac{1}{j\omega\epsilon_0 r} \frac{\partial^2 A_\theta}{\partial \theta^2} \quad (H-18)$$

$$\text{and } E_\theta = -j\omega\mu_0 A_\theta + \frac{1}{j\omega\epsilon_0 r^2} \frac{\partial^2 A_\theta}{\partial \theta^2}$$

Using the values of A_θ and F_θ , as given by Eq. (6.37), in Eq. (H-18)

$$E_y(r, \theta, y) = \frac{1}{2\pi} \sum_{n=-\infty}^{\infty} e^{jn\theta} \left[\int_{-\infty}^{\infty} g_n(w) \sqrt{k_0^2 - w^2} H_n^{(2)'}(r\sqrt{k_0^2 - w^2}) \right. \\ \left. - \frac{nw}{j\omega\epsilon_0 r} \int_{-\infty}^{\infty} f_n(w) H_n^{(2)}(r\sqrt{k_0^2 - w^2}) \right] e^{jwy} dw \quad (H-19)$$

and

$$E_\theta(r, \theta, y) = \frac{1}{2\pi} \frac{(k_0^2 - w^2)}{j\omega\epsilon_0 r^2} \sum_{n=-\infty}^{\infty} e^{jn\theta} \int_{-\infty}^{\infty} f_n(w) H_n^{(2)}(r\sqrt{k_0^2 - w^2}) e^{jwy} dw \quad (H-20)$$

Since these equations for E_y and E_θ at the aperture where $r = R$ should be equal to the transforms given by Eqs. (6.36) it is obtained that,

$$g_n(w) = \frac{\bar{E}_y(n, w) + \frac{nw}{j\omega\epsilon_0 R} f_n(w) H_n^{(2)}(R\sqrt{k_0^2 - w^2})}{\sqrt{k_0^2 - w^2} H_n^{(2)'}(R\sqrt{k_0^2 - w^2})} \quad (H-21)$$

and

$$f_n(w) = \frac{j\omega\epsilon_0 R^2 \bar{E}_\theta(n,w)}{(k_0^2 - w^2) H_n^{(2)}(R\sqrt{k_0^2 - w^2})} \quad (H-22)$$

Inserting the value of $f_n(w)$ by Eq.(H-22) in Eq.(H-21), $g_n(w)$ becomes

$$g_n(w) = \frac{\bar{E}_y(n,w) + \frac{nwR \bar{E}_\theta(n,w)}{k_0^2 - w^2}}{\sqrt{k_0^2 - w^2} H_n^{(2)'}(R\sqrt{k_0^2 - w^2})} \quad (H-23)$$

where $w = k_y = -k_0 \sin\theta \sin\phi$

and $\bar{E}_y(n,w)$ and $\bar{E}_\theta(n,w)$ respectively are the cylindrical transforms of the aperture fields E_y and E_θ .

Now the required radiation pattern in the H-plane ($\phi = 0$) is obtained by observing that in the H-plane, $w = 0$ and that for the dielectric coated H-plane sectoral horn,

$$f_n(w) = 0 \quad (\text{Since by Eqs.(6.21) } E_\theta(R, \theta, y) = 0)$$

$$E_y(R, \theta, y) = -k_r A_r \cos k_{y0} y \cos p\theta H_p^{(2)'}(k_r R) \quad (H-24)$$

and $E_\phi(\theta) = +jk_0 F_\theta$

But by Eqs. (6.38)

$$F_\theta = \frac{e^{-jk_0 r}}{\pi r} \sum_{n=-\infty}^{\infty} e^{jn\theta} j^{n+1} g_n(w)$$

Hence the H -plane radiation pattern becomes,

$$E_{\phi}(\theta) = + j \frac{k_o e^{-jk_o r}}{\pi r} \sum_{n=-\infty}^{\infty} e^{jn\theta} j^{n+1} g_n(w) \quad (H-25)$$

But by Eq.(H-23) for the H -plane

$$g_n(w) = \frac{E_y^-(n,w)}{k_o H_n^{(2)'}(R)} \quad (\text{since } E_{\theta} = 0 \text{ and } w = 0)$$

and by Eqs. (6.35) and (6.21)

$$\bar{E}_y(n,w) = - \frac{|E|}{2\pi} I_1 I_2 \quad (H-26)$$

where $|E| = k_r A_n H_p^{(2)'}(k_r R)$

$$\begin{aligned} I_1 &= \int_{-\alpha_o}^{\alpha_o} \cos p\theta e^{-jn\theta} d\theta \\ &= \frac{2 \cos n\alpha_o}{(1 - \frac{n^2}{p^2})} \left[\frac{\sin p\alpha_o}{p} - \frac{jn}{p^2} \cos p\alpha_o \right] \end{aligned} \quad (H-27)$$

But for HE_{11} mode $p = \frac{\pi}{2\alpha_o}$, and hence

$$I_1 = \frac{2 \cos n\alpha_o}{p(1 - \frac{n^2}{p^2})} \quad (H-28)$$

and

$$I_2 = \int_{-a/2}^{a/2} \cos k_{y0} y \, dy = \frac{2 \operatorname{sinc} k_{y0} \frac{a}{2}}{k_{y0}} \quad (\text{H-29})$$

Thus for HE_{11} mode, from Eqs. (H-26), (H-28) and (H-29) $g_n(w)$ becomes,

$$g_n(w) = \frac{E_2}{\pi} \frac{2 \cos n \alpha_0}{p \left(1 - \frac{n^2}{p^2}\right) k_{y0} k_o} \frac{\operatorname{sinc} k_{y0} \frac{a}{2}}{H_n^{(2)'}(k_o R)} \quad (\text{H-30})$$

By Eqs. (H-25) and (H-30), for HE_{11} mode, E_θ becomes,

$$E_\theta(\theta) = \frac{e^{-jk_o r}}{\pi r} \frac{2E_2}{\pi p} \frac{\operatorname{sinc} k_{y0} \frac{a}{2}}{k_{y0}} \sum_{n=-\infty}^{\infty} \frac{\cos n \alpha_0}{\left(1 - \frac{n^2}{p^2}\right)} \frac{e^{jn\theta} j^n}{H_n^{(2)'}(k_r R)}$$

where $E_2 = k_r A_1 H_p^{(2)'}(k_r R)$ with $p = \frac{\pi}{2\alpha_0}$

APPENDIX I

DERIVING EQUATIONS FOR MULTIMODE DIELECTRIC LOADED RECTANGULAR HORN

I-1 FIELDS IN THE MULTIMODE DIELECTRIC LOADED RECTANGULAR HORN

$$\bar{F} = \bar{i}_x \psi$$

$$\psi_0^{TE_x} = C \cos \alpha_0 x \cos \frac{n\pi}{b} y e^{-jk_z z} \quad (I-1)$$

$$\psi_0^{TE_x} = D \cos \alpha_d \left(\frac{a}{2} - x \right) \cos \frac{n\pi}{b} y e^{-jk_z z}$$

where $\left(\frac{n\pi}{b} \right)^2 + k_z^2 + \alpha_0^2 = k_0^2$

(I-2)

$$\left(\frac{n\pi}{b} \right)^2 + k_z^2 + \alpha_d^2 = k_1^2 = \epsilon_r k_0^2$$

The different field components of TE_x modes are obtained by the relations,

$$\begin{aligned} E_y &= -\frac{\partial \psi}{\partial z}, & H_y &= \frac{1}{j\omega\mu_0} \frac{\partial^2 \psi}{\partial x \partial y} \\ E_z &= \frac{\partial \psi}{\partial y}, & H_z &= \frac{1}{j\omega\mu_0} \frac{\partial^2 \psi}{\partial x \partial z} \\ E_x &= 0, & H_x &= \frac{1}{j\omega\mu_0} \left(\frac{\partial^2 \psi}{\partial x^2} + k_0^2 \psi \right) \end{aligned} \quad (I-3)$$

From Eqs. (I-1) and (I-3), different field components for the dominant TE_{x10} mode ($n=0$) in the horn axial and dielectric coated regions are obtained as,

In the horn axial region

$$E_{y0} = C j k_z \cos \alpha_0 x e^{-j k_z z} \quad (\text{since for } n = 0, \cos \frac{n\pi}{b} y = 1)$$

$$E_{z0} = 0 \quad (\text{Since } \psi^{TE_{x10}} \text{ is independent of } y \text{ with } n = 0)$$

$$E_{x0} = 0$$

$$H_{y0} = 0 \quad (\text{since } \psi^{TE_{x10}} \text{ is independent of } y) \quad (I-4)$$

$$H_{z0} = \frac{C \alpha_0 k_z}{j \omega \mu_0} \cos \alpha_0 x e^{-j k_z z}$$

$$H_{x0} \approx \frac{k_z^2 C}{j \omega \mu_0} \cos \alpha_0 x e^{-j k_z z} \quad (\text{since } k_0^2 - \alpha_0^2 \approx k_z^2)$$

In the dielectric coated region

$$E_{yd} = j k_z D \cos \alpha_d \left(\frac{a}{2} - x \right) e^{j k_z z}$$

$$E_{zd} = 0$$

$$E_{xd} = 0$$

$$H_{yd} = 0$$

$$H_{zd} = \frac{-k_z \alpha_d D}{j \omega \mu_0} \sin \alpha_d \left(\frac{a}{2} - x \right) e^{-j k_z z} \quad (I-5)$$

$$H_{xd} \approx \frac{k_z^2 D}{j \omega \mu_0} \cos \alpha_d x e^{-j k_z z}$$

The evaluation of the constant (C and D) and the propagation constant k_z can be made by matching the E -and H- field components at $x = \pm \frac{a}{2} -s$ (s being the dielectric coating thickness)

Thus i) $E_{y0} = E_{yd}$ at $x = \pm \frac{a}{2} -s$, gives

$$C \cos \alpha_0 \left(\frac{a}{2} -s \right) = D \cos \alpha_d s \quad (I-6)$$

ii) $H_{z0} = H_{zd}$ at $x = \pm \left(\frac{a}{2} -s \right)$, gives

$$C \alpha_0 \sin \alpha_0 \left(\frac{a}{2} -s \right) = -D \alpha_d \sin \alpha_d s \quad (I-7)$$

Dividing Eq.(I-7) by Eq.(I-6), it becomes

$$\alpha_0 \tan \alpha_0 \left(\frac{a}{2} -s \right) = - \alpha_d \tan \alpha_d s \quad (I-8)$$

But by Eq.(I-2) both α_0 and α_d are functions of k_z , so the above Eq.(I-8) is a transcendental equation for determining the value of k_z . Knowing k_z , α_0 and α_d are obtained by Eq.(I-2), and the ratio C/D can be obtained either from Eq.(I-6) or from Eq.(I-7).

Since both the regions will have the same propagation constant k_z , by Eq.(I-2), a single equation relating α_0 and α_d is obtained as

$$k_o^2 - \alpha_o^2 = \epsilon_r k_o^2 - \alpha_d^2$$

(I-9)

$$\text{i.e. } \alpha_d^2 = k_o^2 (\epsilon_r - 1) + \alpha_o^2$$

Now for the case of thin dielectric coating with low permittivity material, k_o is not very different from k_1 , and α_o and α_d will be small. Accordingly

$$\tan \alpha_o \left(\frac{a}{2} - s \right) \approx \sin \alpha_o \left(\frac{a}{2} - s \right) \approx \alpha_o \left(\frac{a}{2} - s \right)$$

$$\text{and } \tan \alpha_d s \approx \alpha_d s,$$

and hence Eq.(I-8) can be written as,

$$\alpha_o^2 \left(\frac{a}{2} - s \right) = - \alpha_d^2 s \quad \text{(I-10)}$$

An explicit relationship for α_o can be obtained, by using Eq.(I-9) in Eq.(I-10) as

$$\alpha_o^2 = -k_o^2 (\epsilon_r - 1) \frac{2s}{a} \quad \text{(I-11)}$$

I-2 THE RADIATED FAR FIELD FROM DIELECTRIC LOADED MULTIMODE HORN

By Eq.(7.8)

$$E_t^o = E_t^{TE_{10}} + E_t^{TE/TM_{12}} = E (\cos \alpha_o x + C_y \cos \alpha_o x \cos \frac{2\pi}{B} y)$$

Knowing the transverse electric field \bar{E}_t over the

horn aperture, by the vector diffraction formula, the radiated far-field at a point 'P' is given by

$$E(P) = jk_0 \frac{e^{-jk_0 r}}{4\pi r} \left(1 + \frac{k_z}{k_0} \cos\theta\right) \iint_S \bar{E}_t e^{jk_0 (x \sin\theta \cos\phi + y \sin\theta \sin\phi)} dx dy$$

Thus the radiated far-field of the test horn in the E-plane ($\phi = \pi/2$) is given by,

$$\begin{aligned} E_\theta(\theta) &= jk_0 \frac{e^{-jk_0 r}}{4\pi r} \left(1 + \frac{k_z}{k_0} \cos\theta\right) \iint_S E_t^0 e^{jk_0 y \sin\theta} dx dy \\ &= jk_0 \frac{e^{-jk_0 r}}{4\pi r} \left(1 + \frac{k_z}{k_0} \cos\theta\right) \cdot \end{aligned}$$

$$\int_{-A'/2}^{A'/2} \int_{-B/2}^{B/2} E_0 (\cos\alpha_0 x + C_y \cos\alpha_0 x \cos \frac{2\pi}{B} y) \cdot$$

$$e^{-j \frac{\pi}{\lambda_0} \left(\frac{x^2}{R} + \frac{y^2}{R} \right)} \cdot e^{jk_0 y \sin\theta} dx dy \quad (I-12)$$

(A phase variation of $\psi = e^{-j \frac{\pi}{\lambda_0} \left(\frac{x^2}{R} + \frac{y^2}{R} \right)}$ over the aperture is assumed, where R = the horn axial length)

$$= jk_0 \frac{e^{-jk_0 r}}{4\pi r R} E_0 [I_2 + C_y I_3] I_1 \quad (I-13)$$

where

$$\begin{aligned} I_1 &= \int_{-A'/2}^{A'/2} \cos\alpha_0 x \cdot e^{-j \frac{\pi}{\lambda_0 R} x^2} dx \\ &= \frac{1}{2} \int_{-A'/2}^{A'/2} (e^{j\alpha_0 x} + e^{-j\alpha_0 x}) e^{-j \frac{\pi}{\lambda_0 R} x^2} dx \end{aligned}$$

$$I_1 = e^{\frac{j\lambda_0}{4\pi} R \alpha_0^2} \sqrt{\frac{(\lambda_0 R)}{2}} \left\{ C(u_1) - C(u_2) - j [S(u_1) - S(u_2)] \right\} \quad (I-14)$$

where

$$\begin{pmatrix} u_1 \\ u_2 \end{pmatrix} = \frac{1}{\sqrt{2}} \left[\sqrt{\lambda_0 R} \frac{\alpha_0}{\pi} \pm \frac{\Delta'}{\sqrt{\lambda_0 R}} \right]$$

$$\begin{aligned} I_2 &= \int_{-B/2}^{B/2} e^{-j\frac{\pi}{\lambda_0} \frac{y^2}{R}} e^{jk_0 y \sin \theta} dy \\ &= \int_0^{B/2} e^{-j\frac{\pi}{\lambda_0} \frac{y^2}{R}} e^{jk_0 y \sin \theta} dy + \\ &\quad + \int_0^{B/2} e^{-j\frac{\pi}{\lambda_0} \frac{y^2}{R}} e^{-jk_0 y \sin \theta} dy \\ &= e^{\frac{j\pi\lambda_0}{4} \frac{Rk_0^2 \sin^2 \theta}{\pi^2}} \sqrt{\frac{\lambda_0 R}{2}} \left\{ C(\eta) - C(\xi) - j [S(\eta) - S(\xi)] \right\} \end{aligned} \quad (I-15)$$

where

$$\begin{pmatrix} \eta \\ \xi \end{pmatrix} = \frac{1}{\sqrt{2}} \left[\sqrt{\lambda_0 R} \frac{k_0 \sin \theta}{\pi} \pm \frac{B}{\sqrt{\lambda_0 R}} \right]$$

$$\begin{aligned} \text{and } I_3 &= \int_{-B/2}^{B/2} \cos \frac{2\pi}{B} y e^{jk_0 y \sin \theta} e^{-j\frac{\pi}{\lambda_0} \frac{y^2}{R}} dy \\ &= \frac{1}{2} \int_{-B/2}^{B/2} \left(e^{j\frac{2\pi}{B} y} + e^{-j\frac{2\pi}{B} y} \right) e^{jk_0 y \sin \theta} e^{-j\frac{\pi}{\lambda_0} \frac{y^2}{R}} dy \end{aligned}$$

$$\begin{aligned}
 I_3 &= \frac{1}{2} \left[\int_{-B/2}^{B/2} e^{\frac{j2\pi}{B} y} e^{jk_0 y \sin\theta} e^{-\frac{j\pi}{\lambda_0 R} y^2} dy \right. \\
 &\quad \left. + \int_{-B/2}^{B/2} e^{-\frac{j2\pi}{B} y} e^{jk_0 y \sin\theta} e^{-\frac{j\pi}{\lambda_0 R} y^2} dy \right] \\
 &= \sqrt{\frac{\lambda_0 R}{2}} \left[e^{\frac{j\pi\lambda_0 R}{4} \left(\frac{2}{B} + \frac{2}{\lambda_0} \sin\theta \right)^2} \left\{ C(v_1) - C(v_2) - j[S(v_1) - S(v_2)] \right\} \right. \\
 &\quad \left. + e^{\frac{j\pi\lambda_0 R}{4} \left(\frac{2}{B} - \frac{2}{\lambda_0} \sin\theta \right)^2} \left\{ C(v_3) - C(v_4) - j[S(v_3) - S(v_4)] \right\} \right]
 \end{aligned}$$

(I-16)

where

$$\begin{pmatrix} v_1 \\ v_2 \end{pmatrix} = \frac{1}{\sqrt{2}} \left[\frac{B}{\sqrt{\lambda_0 R}} \pm \sqrt{\lambda_0 R} \left(\frac{2}{B} + \frac{2}{\lambda_0} \sin\theta \right) \right]$$

$$\begin{pmatrix} v_3 \\ v_4 \end{pmatrix} = \frac{1}{\sqrt{2}} \left[\frac{B}{\sqrt{\lambda_0 R}} \pm \sqrt{\lambda_0 R} \left(\frac{2}{B} - \frac{2}{\lambda_0} \sin\theta \right) \right]$$

Using Eqs. (I-14), (I-15) and (I-16) in Eq. (I-13) $E_\theta(\theta)$ becomes

$$\begin{aligned}
 E_\theta(\theta) &= \frac{jE_0 e^{-jk_0 r}}{4r} R \left(1 + \frac{k_z}{k_0} \cos\theta \right) e^{\frac{j\lambda_0 R \alpha_0^2}{4\pi}} \\
 &\quad \left\{ C(u_1) - C(u_2) - j[S(u_1) - S(u_2)] \right\} [F_i^I + C_y F_i^{II}]
 \end{aligned}$$

(I-17)

where $F_i^I = e^{\frac{j\lambda_0 R k_0^2 \sin^2\theta}{4}} \left\{ C(\eta) - C(\xi) - j[S(\eta) - S(\xi)] \right\}$

$$\text{with } \begin{pmatrix} \eta \\ \xi \end{pmatrix} = \frac{1}{\sqrt{2}} \left[\sqrt{\lambda_0 R} \frac{k_0 \sin \theta}{\pi} \pm \frac{B}{\sqrt{\lambda_0 R}} \right]$$

$$\begin{aligned} \text{and } F_i^{II} &= e^{\frac{j\pi\lambda_0 R}{4}} \left(\frac{2}{B} + \frac{2}{\lambda_0} \sin \theta \right)^2 \left\{ C(v_1) - C(v_2) - j[S(v_1) - S(v_2)] \right\} \\ &+ e^{\frac{j\pi\lambda_0 R}{4}} \left(\frac{2}{B} - \frac{2}{\lambda_0} \sin \theta \right)^2 \left\{ C(v_3) - C(v_4) - j[S(v_1) - S(v_2)] \right\} \end{aligned}$$

And the radiation pattern in the H-plane ($\phi=0$) is given by

$$\begin{aligned} E_{\phi}(\theta) &= \frac{jk_0 e^{-jk_0 r}}{4\pi r} \left(1 + \frac{k_z}{k_0} \cos \theta \right) \cdot \\ &\int \int E_t^0 e^{-\frac{j\pi}{\lambda_0} \left(\frac{x^2}{R} + \frac{y^2}{R} \right)} e^{jk_0 x \sin \theta} dx dy \quad (I-18) \\ &= \frac{jk_0 e^{-jk_0 r}}{4\pi r} \left(1 + \frac{k_z}{k_0} \cos \theta \right) E \int_{-A'/2}^{A'/2} \int_{-B/2}^{B/2} \\ &(\cos \alpha_0 + C_y \cos \alpha_0 x \cos \frac{2\pi y}{B}) e^{-\frac{j\pi}{\lambda_0} \left(\frac{x^2}{R} + \frac{y^2}{R} \right)} e^{jk_0 x \sin \theta} dx dy \end{aligned}$$

Following the above mathematical operations (carried out for $E_{\theta}(\theta)$), $E_{\phi}(\theta)$ can be derived as,

$$E_{\phi}(\theta) = \frac{jE e^{-jk_0 r}}{4r} \left(1 + \frac{k_z}{k_0} \cos \theta \right) R F_i^a [F_i^b + C_y F_i^c] \quad (I-19)$$

where

$$F_i^a = M \left\{ C(u_1') - C(u_2') - j [S(u_1') - S(u_2')] \right\} + \\ N \left\{ C(u_3') - C(u_4') - j [S(u_3') - S(u_4')] \right\}$$

with

$$\begin{pmatrix} M \\ N \end{pmatrix} = e^{j \frac{\pi \lambda_0 R}{4} \left(\frac{\alpha_0}{\pi} \pm \frac{2}{\lambda_0} \sin \theta \right)^2}$$

$$\begin{pmatrix} u_1' \\ u_2' \end{pmatrix} = \frac{1}{\sqrt{2}} \left[\frac{A'}{\sqrt{\lambda_0 R}} \pm \sqrt{\lambda_0 R} \left(\frac{\alpha_0}{\pi} + \frac{2}{\lambda_0} \sin \theta \right) \right]$$

$$\begin{pmatrix} u_3' \\ u_4' \end{pmatrix} = \frac{1}{\sqrt{2}} \left[\frac{A'}{\sqrt{\lambda_0 R}} \pm \sqrt{\lambda_0 R} \left(\frac{\alpha_0}{\pi} - \frac{2}{\lambda_0} \sin \theta \right) \right]$$

$$F_i^b = 2 [C(w) - jS(w)]$$

where

$$w = \frac{B}{\sqrt{2 \lambda_0 R}}$$

$$F_i^c = e^{\frac{j\pi \lambda_0 R}{B^2}} [C(\gamma') - C(\beta) - j [S(\gamma') - S(\beta)]]$$

where

$$\begin{pmatrix} \gamma' \\ \beta \end{pmatrix} = \frac{1}{\sqrt{2}} \left[\frac{B}{\sqrt{\lambda_0 R}} \pm \frac{2\sqrt{\lambda_0 R}}{B} \right]$$

I-3 EVALUATION OF E AND C_y - MODE CONVERSION IN
A RECTANGULAR WAVEGUIDE BY A STEP DISCONTINUITY

The conversion of a portion of the TE_{10} mode energy to TE/TM_{12} mode in the rectangular waveguide is achieved by a symmetric step discontinuity in an oversized guide as shown in Fig.I-1. The oversized square guide is designed to support the propagation of TE/TM_{12} mode; and to be evanescent for other unwanted higher order modes.

Assume that the TE_{10} E -field has a perfect match at the step discontinuity junction, and let the transverse E -field \bar{E}_t at the discontinuity plane ($z = 0$) be the same as for the TE_{10} incident field,

$$\text{i.e. } \bar{E}_t = \bar{i}_y jck_z \cos\alpha_0 x = \bar{i}_y E_0 \cos\alpha_0 x$$

The electric field of the TE_{10} mode $E_t^{TE_{10}}$ in the oversized guide is given by

$$E_t^{TE_{10}} = \bar{i}_y E \cos\alpha_0 x$$

The transverse electric field of the TE/TM_{12} mode, $E_t^{TE/TM_{12}}$ in the oversized guide is given by

$$E_t^{TE/TM_{12}} = \bar{i}_y A_y \cos\alpha_0 x \cos \frac{2\pi}{B} y$$

where A_y = the amplitude of the TE/TM_{12} modes.

At the left side of the junction only TE_{10} mode can propagate. At the junction plane, however, an infinite number of modes are excited, but all higher order modes except TE/TM_{12} modes are evanescent modes for the oversized guide. Thus to match the boundary conditions the transverse field of these modes should satisfy the following relation

$$\bar{E}_t = E_t^{TE_{10}} + E_t^{TE/TM_{12}} + \text{higher order modes}$$

(these higher order mode terms are neglected since they are evanescent modes for the oversized guide)

i.e.

$$\begin{aligned} E_0 \cos \alpha_0 x &= E \cos \alpha_0 x + A_y \cos \alpha_0 x \cos \frac{2\pi}{B} y \\ &= E \left(\cos \alpha_0 x + \frac{A_y}{E} \cos \alpha_0 x \cos \frac{2\pi}{B} y \right) \\ &= E \left(\cos \alpha_0 x + C_y \cos \alpha_0 x \cos \frac{2\pi}{B} y \right) \quad (I-20) \end{aligned}$$

where C_y = the mode conversion factor defined as the complex amplitude ratio of higher order modes to dominant mode.

Multiplying both sides of Eq.(I-20) by $\cos \alpha_0 x$ and integrating within their respective limits,

$$\begin{aligned} \int_{-a'/2}^{a'/2} \int_{-b/2}^{b/2} E_0 \cos^2 \alpha_0 x dx dy &= E \left[\int_{-A'/2}^{A'/2} \int_{-B/2}^{B/2} \cos^2 \alpha_0 x dx dy + \right. \\ &\quad \left. C_y \int_{-A'/2}^{A'/2} \int_{-B/2}^{B/2} \cos^2 \alpha_0 x \cos \frac{2\pi}{B} y dx dy \right] \end{aligned}$$

$$\text{i.e. } E_0 b \left(a' + \frac{\sin \alpha_0 a'}{\alpha_0} \right) = EB \left(A' + \frac{\sin \alpha_0 A'}{\alpha_0} \right) + 0$$

$$\therefore E = E_0 \frac{b}{B} \frac{(\alpha_0 a' + \sin \alpha_0 a')}{(\alpha_0 A' + \sin \alpha_0 A')} \quad (\text{I-21})$$

Now to find C_y multiply both sides of Eq.(I-20) by $\cos \alpha_0 x \cos \frac{2\pi}{B} y$ and integrate within their respective limits, Thus it becomes,

$$\begin{aligned} E_0 \int_{-a'/2}^{a'/2} \cos^2 \alpha_0 x \, dx \int_{-b/2}^{b/2} \cos \frac{2\pi}{B} y \, dy = \\ = E \left[\int_{-A'/2}^{A'/2} \cos^2 \alpha_0 x \, dx \int_{-B/2}^{B/2} \cos \frac{2\pi}{B} y \, dy + \right. \\ \left. C_y \int_{-A'/2}^{A'/2} \cos^2 \alpha_0 x \, dx \int_{B/2}^{B/2} \cos^2 \frac{2\pi}{B} y \, dy \right] \end{aligned}$$

$$\text{i.e. } E_0 \frac{1}{2} \left(a' + \frac{\sin \alpha_0 a'}{\alpha_0} \right) \frac{\sin \frac{\pi}{B} b}{\frac{\pi}{B}} = E \left[0 + C_y \frac{1}{2} \left(A' + \frac{\sin \alpha_0 A'}{\alpha_0} \right) \right] \frac{B}{2}$$

$$\therefore C_y = 2E_0 \frac{(\alpha_0 a' + \sin \alpha_0 a')}{EB(\alpha_0 A' + \sin \alpha_0 A')} \frac{\sin \frac{\pi}{B} b}{\frac{\pi}{B}} \quad (\text{I-22})$$

Inserting the value of E from Eq.(I-21) C_y becomes,

$$C_y = \frac{2 \sin \frac{\pi}{B} b}{\frac{\pi b}{B}} \quad (\text{I-23})$$

I-4 GAIN OF THE MULTIMODE DIELECTRIC LOADED HORN

Transverse E-and H -fields over the radiating aperture of the oversized waveguide are obtained from Eqs (I-4) and (I-20) as,

$$E_t^0 = E_y^0 = E(\cos\alpha_0 x + C_y \cos\alpha_0 x \cos \frac{2\pi}{B} y)$$

$$H_t^0 = H_x^0 = \frac{C}{j\omega\mu_0} k_z^2 (\cos\alpha_0 x + C_y \cos\alpha_0 x \cos \frac{2\pi}{B} y)$$

$$= \frac{k_z E_t^0}{\omega\mu_0}$$
(I-24)

The total power passing through the radiating horn aperture is determined by

$$P_t = \frac{1}{2} \text{Re} \left[\iint_s E_t^0 \cdot H_t^{0*} ds \right]$$

$$= \frac{1}{2} \int_{-A'/2}^{A'/2} \int_{-B/2}^{B/2} \frac{E^2 k_z}{\omega\mu_0} (\cos^2\alpha_0 x + C_y^2 \cos^2\alpha_0 x \cos^2 \frac{2\pi}{B} y + 2C_y \cos^2\alpha_0 x \cos \frac{2\pi}{B} y) dx dy$$

$$= \frac{1}{8} \frac{E^2 k_z B}{\omega\mu_0 \alpha_0} (\alpha_0 A' + \sin\alpha_0 A') (2 + C_y^2)$$
(I-25)

The on-axis gain of the test horn is defined by

$$G(0,0) = 4\pi \frac{P(0,0)}{P_t}$$
(I-26)

where $P(0,0) = \frac{1}{2\eta_0} |E_\theta|_{\max}^2 r^2$

By Eq.(I-17) and knowing that $C(\eta_1) = -C(\xi_1)$ and $S(\eta_1) = -S(\xi_1)$ where η_1 and ξ_1 are the values of η and ξ at $\theta = 0$, and are given by

$$\begin{pmatrix} \eta_1 \\ \xi_1 \end{pmatrix} = \pm \frac{B}{\sqrt{2\lambda_0 R}}, \quad P(0,0) \text{ is obtained as,}$$

$$P(0,0) = \frac{1}{8\eta_0} E^2 R^2 \left(1 + \frac{k_z}{k_0}\right)^2 \left\{ [C(u_1) - C(u_2)]^2 + [S(u_1) - S(u_2)]^2 \right\}.$$

$$\left[\sqrt{[C(\xi_1)]^2 + [S(\xi_1)]^2} + c_y \sqrt{[C(v_{o1}) - C(v_{o2})]^2 + [S(v_{o1}) - S(v_{o2})]^2} \right]^2 \tag{I-27}$$

Using Eqs.(I-25) and (I-27) in Eq.(I-26), the gain becomes

$$G(0,0) = \frac{4\pi}{\eta_0} \frac{\omega\mu_0}{k_z} \frac{\alpha_0}{B} \frac{R^2 \left(1 + \frac{k_z}{k_0}\right)^2}{(\alpha_0 A' + \sin\alpha_0 A')} \cdot \frac{[C(u_1) - C(u_2)]^2 + [S(u_1) - S(u_2)]^2}{(2 + c_y^2)}$$

$$\cdot \left[\sqrt{c^2(\xi_1) + s^2(\xi_1)} + c_y \sqrt{[C(v_{o1}) - C(v_{o2})]^2 + [S(v_{o1}) - S(v_{o2})]^2} \right]^2 \tag{I-28}$$

,and using the relation, $\omega\mu_0 = k_0\eta_0$, the above Eq.(I-28) reduces to

$$G(0,0) = \frac{4\pi R^2 \alpha_o (1 + \frac{k_z}{k_o})^2 k_o}{B(\alpha_o A' + \sin \alpha_o A') k_z} \left\{ \frac{[C(u_1) - C(u_2)]^2 + [S(u_1) - S(u_2)]^2}{(2 + c_y^2)} \right\}$$

$$\left[\sqrt{[C(\xi_1)]^2 + [S(\xi_1)]^2} + c_y \sqrt{[C(v_{o1}) - C(v_{o2})]^2 + [S(v_{o1}) - S(v_{o2})]^2} \right]^2$$

(I-29)

where $\xi_1 = \frac{B}{\sqrt{2\lambda_o R}}$

$$\begin{pmatrix} v_{o1} \\ v_{o2} \end{pmatrix} = \frac{1}{\sqrt{2}} \left[\frac{B}{\sqrt{\lambda_o R}} \pm \frac{2\sqrt{\lambda_o R}}{B} \right]$$

and u_1 and u_2 are as defined earlier.

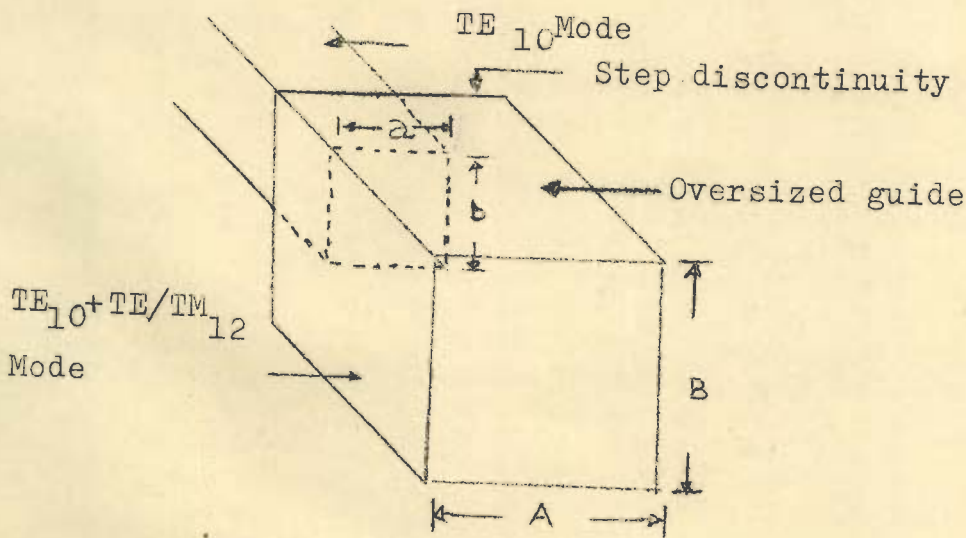


Fig. I-1 Rectangular Step Discontinuity

APPENDIX J

DERIVING EQUATIONS FOR HYBRID MODE DIELECTRIC
LOADED HORNS

J-1 FIELDS IN THE HYBRID MODE HORN WITH DIELECTRIC
LOADING ON H- PLANE WALLS

The electric vector potential \bar{F} for TE to y mode is given by

$$\bar{F} = \bar{i}_y \psi \quad (J-1)$$

The proper forms of the potential function ψ , for the horn axial and dielectric loaded regions respectively, become

$$\psi_o = C_n \cos \alpha_o y \cos \frac{n\pi}{A} x e^{-jk_z z} \quad (J-2)$$

$$\psi_d = D_n \cos \alpha_d \left(\frac{B}{2} - y \right) \cos \frac{n\pi}{A} x e^{-jk_z z}$$

where

$$\alpha_o^2 + k_z^2 + \left(\frac{n\pi}{A} \right)^2 = k_o^2 \quad (J-3)$$

$$\alpha_d^2 + k_z^2 + \left(\frac{n\pi}{A} \right)^2 = k_1^2 \quad (= \epsilon_r k_o^2)$$

The different field components of the hybrid mode are given by

$$\begin{aligned} E_x &= -\frac{\partial \psi}{\partial z} & H_x &= \frac{1}{j\omega \mu_o} \frac{\partial^2 \psi}{\partial x \partial y} \\ E_z &= \frac{\partial \psi}{\partial x} & H_z &= \frac{1}{j\omega \mu_o} \frac{\partial^2 \psi}{\partial y \partial z} \\ E_y &= 0 & H_y &= \frac{1}{j\omega \mu_o} \left(\frac{\partial^2}{\partial y^2} + k_o^2 \right) \psi \end{aligned} \quad (J-4)$$

Substitution of Ψ_o in Eqs.(J-4) gives the different field components in the horn axial region ; and are obtained as

$$\begin{aligned}
 E_{x_o} &= j C_n k_z \cos \alpha_o y \cos \frac{n\pi}{A} x e^{-jk_z z} \\
 E_{z_o} &= -\frac{n\pi}{A} C_n \cos \alpha_o y \sin \frac{n\pi}{A} x e^{-jk_z z} \\
 E_{y_o} &= 0 \\
 H_{x_o} &= \frac{C_n}{j\omega\mu_o} \frac{n\pi}{A} \alpha_o \sin \alpha_o y \sin \frac{n\pi}{A} x e^{-jk_z z} \\
 H_{z_o} &= \frac{C_n}{\omega\mu_o} k_z \alpha_o \sin \alpha_o y \cos \frac{n\pi}{A} x e^{-jk_z z} \\
 H_{y_o} &= \frac{C_n}{j\omega\mu_o} (k_o^2 - \alpha_o^2) \cos \alpha_o y \cos \frac{n\pi}{A} x e^{-jk_z z}
 \end{aligned} \tag{J-5}$$

Similar field components are obtained for the dielectric coated region by substituting Ψ_d in Eqs. (J-4), and are given by,

$$\begin{aligned}
 E_{x_d} &= jD_n k_z \cos \alpha_d \left(\frac{B}{2} - y \right) \cos \frac{n\pi}{A} x e^{-jk_z z} \\
 E_{z_d} &= -D_n \frac{n\pi}{A} \cos \alpha_d \left(\frac{B}{2} - y \right) \sin \frac{n\pi}{A} x e^{-jk_z z} \\
 E_{y_d} &= 0
 \end{aligned}$$

$$H_{xd} = - \frac{1}{j\omega\mu_0} D_n \alpha_d \frac{n\pi}{A} \sin\alpha_d \left(\frac{B}{2} - y \right) \sin \frac{n\pi}{A} x e^{-jk_z z} \quad (J-6)$$

$$H_{zd} = - \frac{D_n k_z \alpha_0}{\omega\mu_0} \sin\alpha_d \left(\frac{B}{2} - y \right) \cos \frac{n\pi}{A} x e^{-jk_z z}$$

$$H_{yd} = \frac{1}{j\omega\mu_0} D_n (k_1^2 - \alpha_d^2) \cos\alpha_d \left(\frac{B}{2} - y \right) \cos \frac{n\pi}{A} x e^{-jk_z z}$$

Now continuity of E_x and E_z at the air-dielectric interface i.e. at $y = \frac{B}{2} - s$, (where s is the thickness of the dielectric coating) gives

$$C_n \cos\alpha_0 \left(\frac{B}{2} - s \right) = D_n \cos\alpha_d s \quad (J-7)$$

Continuity of H_x and H_z at $y = \frac{B}{2} - s$ gives

$$C_n \alpha_0 \sin\alpha_0 \left(\frac{B}{2} - s \right) = -D_n \alpha_d \sin\alpha_d s \quad (J-8)$$

Division of Eq.(K-8) by Eq.(J-7) gives the relation

$$\alpha_0 \tan \alpha_0 \left(\frac{B}{2} - s \right) = -\alpha_d \tan\alpha_d s \quad (J-9)$$

This is the characteristic equation for the possible values of k_z . As in Sec. (7.2.1), considering the case of dielectric coating by very thin dielectric slabs of low permittivity, it is possible to obtain an explicit expression for α_0 . Accordingly, assuming the same k_z for both the regions, from Eqs.(J-2) and (J-8) it is obtained as,

$$\alpha_0^2 = -k_0^2 (\epsilon_r - 1) \frac{2s}{B} \quad (J-10)$$

J -2 FAR-FIELD PATTERNS OF THE HYBRID MODE
DIELECTRIC LOADED HORN

The radiated far-field is determined by the aperture field method based on the vector diffraction formula . It is assumed that reflection occurs at the open end of the waveguide, and the field in the aperture is defined as the superposition of the direct and reflected waves. Thus, denoting the reflection coefficient by Γ , the total aperture field becomes

$$E_{xs} = (1+\Gamma)E_{ti} = (1+\Gamma)j C_n k_z \cos \alpha_o y \cos \frac{n\pi}{A} x e^{-jk_z z} \quad (J-11)$$

where $E_{ti} = \bar{i}_x E_{xo} = j C_n k_z \cos \alpha_o y \cos \frac{n\pi}{A} x e^{-jk_z z}$

and

$$H_{ys} = (1-\Gamma)\bar{i}_y H_{yo} = -(1-\Gamma) \frac{C_n}{j\omega\mu_o} (k_o^2 - \alpha_o^2) \cos \alpha_o y \cos \frac{n\pi}{A} x e^{-jk_z z} \quad (J-12)$$

Therefore

$$\frac{E_{xs}}{H_{ys}} = \frac{(1+\Gamma)\omega\mu_o k_z}{(1-\Gamma)(k_o^2 - \alpha_o^2)} \quad (J-13)$$

Now the radiated far-fields in the E-plane and H-plane respectively are obtained by the vector diffraction formula as

$$E_\theta(\theta) = \frac{j}{2\lambda_o} \left(1 + \frac{k_z}{k_o} \frac{1-\Gamma}{1+\Gamma} \cos\theta \right) \frac{e^{-jk_o r}}{r} \iint_S |E_{xs}| e^{jk_o y \sin\theta} dx dy \quad (J-14)$$

$$E_{\theta}(\theta) = \frac{j}{2\lambda_0} \frac{e^{-jk_0 r}}{r} \left(1 + \frac{k_z}{k_0} \frac{1-\Gamma}{1+\Gamma} \cos\theta\right) (1+\Gamma) jk_z C_n I_1 I_2 \quad (J-15)$$

$$\text{where } I_1 = \int_{-A/2}^{+A/2} \cos \frac{n\pi}{A} x dx = \frac{2A}{n\pi} \sin \left(\frac{n\pi}{2} \right) \quad (J-16)$$

$$\begin{aligned} I_2 &= \int_{-B'/2}^{B'/2} \cos \alpha_0 y e^{jk_0 y \sin\theta} dy \\ &= \frac{2}{(k_0 \sin\theta)^2 - \alpha_0^2} \left[k_0 \sin\theta \cos\left(\alpha_0 \frac{B'}{2}\right) \sin\left(k_0 \frac{B'}{2} \sin\theta\right) \right. \\ &\quad \left. - \alpha_0 \sin\left(\alpha_0 \frac{B'}{2}\right) \cos\left(k_0 \frac{B'}{2} \sin\theta\right) \right] \quad (J-17) \end{aligned}$$

and inserting Eqs.(J-16) and (J-17) in Eq.(J-15), $E_{\theta}(\theta)$ becomes

$$\begin{aligned} E_{\theta}(\theta) &= 2C_n k_z (1+\Gamma) \frac{A}{n\pi} \frac{e^{-jk_0 r}}{\lambda_0 r} \left(1 + \frac{k_z}{k_0} \frac{1-\Gamma}{1+\Gamma} \cos\theta\right) \sin \frac{n\pi}{2} \cdot \\ &\quad \frac{1}{\alpha_0^2 - (k_0 \sin\theta)^2} \left[k_0 \sin\theta \cos\left(\alpha_0 \frac{B'}{2}\right) \sin\left(k_0 \frac{B'}{2} \sin\theta\right) \right. \\ &\quad \left. - \alpha_0 \sin\left(\alpha_0 \frac{B'}{2}\right) \cos\left(k_0 \frac{B'}{2} \sin\theta\right) \right] \quad (J-18) \end{aligned}$$

and

$$\begin{aligned} E_{\phi}(\theta) &= \frac{j}{2\lambda_0} \frac{e^{-jk_0 r}}{r} \left(\cos\theta + \frac{1-\Gamma}{1+\Gamma} \frac{k_z}{k_0}\right) \iint E_{xs} e^{jk_0 x \sin\theta} dx dy \\ &= \frac{j}{2\lambda_0} \frac{e^{-jk_0 r}}{r} \left(\cos\theta + \frac{1-\Gamma}{1+\Gamma} \frac{k_z}{k_0}\right) (1+\Gamma) jC_n k_z I_3 I_4 \quad (J-19) \end{aligned}$$

where

$$I_3 = \int_{-B'/2}^{B'/2} \cos \alpha_0 y \, dy = \frac{2 \sin \alpha_0}{\alpha_0} \frac{B'}{2} \quad (J-20)$$

$$\begin{aligned} I_4 &= \int_{-A/2}^{A/2} \cos \frac{n\pi}{A} x \, dx \cos(k_0 \sin \theta) \\ &= \frac{2 \frac{n\pi}{A} \sin \frac{n\pi}{2} \cos(k_0 \frac{A}{2} \sin \theta)}{\left(\frac{n\pi}{A}\right)^2 - (k_0 \sin \theta)^2} \end{aligned} \quad (J-21)$$

and using Eqs. (J-20) and (J-21) in Eq. (J-19) $E_\theta(\theta)$ becomes,

$$\begin{aligned} E_\theta(\theta) &= 2C_n k_z \frac{n\pi}{A} \frac{e^{-jk_0 r}}{\lambda_0 r} (1 + \Gamma) \left(\cos \theta + \frac{k_z}{k_0} \frac{1 - \Gamma}{1 + \Gamma} \right) \cdot \\ &\quad \frac{\sin \frac{n\pi}{2} \cos(k_0 \frac{A}{2} \sin \theta)}{(k_0 \sin \theta)^2 - \left(\frac{n\pi}{A}\right)^2} \cdot \frac{\sin \alpha_0 \frac{B'}{2}}{\alpha_0} \end{aligned} \quad (J-22)$$

It is seen from Eqs. (J-18) and (J-22) that the radiated far-field is non-zero only for $n = 1, 3, 5, \dots$

J-3 ON-AXIS GAIN OF THE HYBRID MODE HORN WITH DIELECTRIC LOADED H-PLANE WALLS

$$P_t = \frac{1}{2} \operatorname{Re} \left[\int_{-B'/2}^{B'/2} \int_{-A/2}^{A/2} E_{xs} H_{ys}^* \, dx dy \right] \quad (J-23)$$

But by Eq. (J-13)

$$\frac{E_{xs}}{H_{ys}} = \frac{1+\Gamma}{1-\Gamma} \frac{\omega \mu_0 k_z}{k_0^2 - \alpha_0^2}$$

Therefore

$$P_t = \frac{1}{2} \int_{-B'/2}^{B'/2} \int_{-A/2}^{A/2} \frac{(1-\Gamma)}{(1+\Gamma)} \frac{(k_0^2 - \alpha_0^2)}{\omega \mu_0 k_z} |E_{xs}|^2 dx dy$$

Inserting the value of E_{xs} by Eq.(J-11), P_t is obtained as,

$$P_t = \frac{C_n^2}{8} \frac{1-\Gamma}{1+\Gamma} (1+\Gamma)^2 \frac{(k_0^2 - \alpha_0^2)}{k_0 \eta_0} k_z A \frac{(\alpha_0 B' + \sin \alpha_0 B')}{\alpha_0} \quad (J-24)$$

(since $\omega \mu_0 = k_0 \eta_0$)

The on-axis gain is defined as

$$G(0,0) = \frac{1}{2\eta_0} |E_\theta|_{\max}^2 \frac{4\pi r^2}{P_t} \quad (J-25)$$

From (J-18),

$$|E_\theta|_{\max} = 2C_n k_z (1+\Gamma) \frac{A}{n\pi} \frac{1}{\lambda_0 r} \left(1 + \frac{k_z}{k_0} \frac{1-\Gamma}{1+\Gamma}\right) \frac{\sin \alpha_0 \frac{B'}{2}}{\alpha_0} \quad (J-26)$$

Thus by Eqs.(J-24),(J-25) and (J-26), $G(0,0)$ becomes

$$G(0,0) = \frac{64k_0 k_z A \left(1 + \frac{k_z}{k_0} \frac{1-\Gamma}{1+\Gamma}\right)^2 (1+\Gamma) \sin^2 \alpha_0 \frac{B'}{2}}{n^2 \pi \lambda_0^2 (k_0^2 - \alpha_0^2) (1-\Gamma) \alpha_0 (\alpha_0 B' + \sin \alpha_0 B')} \quad (J-27)$$

J-4 EVALUATION OF MODAL AMPLITUDES BY MODAL EXPANSION OF FIELDS

Consider the guide junction of Fig.7.7. It is desired to determine the fields for $z > 0$, from the known values of the tangential fields at $z = 0$, with the assumption that the guide is matched at the junction. Let the $TE_{y,mn}$ modes may be determined by the superposition of the mode functions as

$$\psi_{mn}^{TE_y} = \sum_{m=1}^{\infty} \sum_{n=1}^{\infty} C_{mn} \cos \alpha_{0mn} y \cos \frac{n\pi}{A} x e^{-jk_z z} \quad (J-28)$$

(k_z is assumed to be the same for all the modes)

Limiting the consideration to $m=1$, let the function be given by

$$\psi = \sum_{n=1}^{\infty} C_{1n} \cos \alpha_{1n} y \cos \frac{n\pi}{A} x e^{-jk_z z} \quad (J-29)$$

where α_{1n} is the value of α_0 (in Eq. (J-3)) for the HE_{1n} mode.

Now the tangential field E_x , ($E_y = 0$ for TE_y mode) is given by

$$E_x = - \frac{\partial \psi}{\partial z} \quad ; \text{ and by Eq. (J-29) } E_x \text{ becomes}$$

$$E_x = j k_z \sum_{n=1}^{\infty} C_{1n} \cos \alpha_{1n} y \cos \frac{n\pi}{A} x e^{-jk_z z} \quad (J-30)$$

Thus the tangential field at $z = 0$, by Eq. (J-30), becomes

$$E_x \Big|_{z=0} = k_z \sum_{n=1}^{\infty} C_{1n} \cos \alpha_{1n} y \cos \frac{n\pi}{A} x \quad (J-31)$$

Let there be a wave incident on the junction from the smaller waveguide (X- band) and let the longer guide be matched. Assuming that the smaller guide is carrying a TE_{10} mode, the incident wave at the junction ($z=0$) is due to this TE_{10} mode, and hence it becomes,

$$\begin{aligned} E_x \Big|_{z=0} &= \cos \frac{\pi}{a} x & , y < b \\ &= 0 & , y > b \end{aligned} \quad (J-32)$$

where 'a' and 'b' are dimensions of the smaller (X-band) guide.

From Eqs.(J-31) and (J-32), it is obtained,

$$\cos \frac{\pi}{a} x = k_z \sum_{n=1}^{\infty} C_{1n} \cos \alpha_{1n} y \cos \frac{n\pi}{A} x \quad (J-33)$$

Multiplying both the sides of Eq. (J-33) by $\cos \alpha_{1n} y \cos \frac{n\pi}{A} x$, and integrating over the respective limits for the smaller and longer waveguides at the junction

$$\begin{aligned} & e \int_c^{d+e} \int_a^c \cos \frac{\pi}{a} x \cos \frac{n\pi}{A} x \cos \alpha_{1n} y \, dx \, dy \\ &= k_z C_{1n} \int_{-B/2}^{B/2} \int_{-A/2}^{A/2} \cos^2 \alpha_{1n} y \cos^2 \frac{n\pi}{A} x \, dx \, dy \end{aligned}$$

i.e.

$$\begin{aligned} & \sin \alpha_{1n} (d+e) - \sin \alpha_{1n} e \int_c^{a+c} \cos \frac{\pi}{a} x \cos \frac{n\pi}{A} x dx \\ & = \frac{k_z C_{1n}}{4} A \cdot (\alpha_{1n} B + \sin \alpha_{1n} B) \end{aligned} \quad (J-34)$$

The integral in Eq.(J-34) can be evaluated as,

$$\begin{aligned} & \int_c^{a+c} \cos \frac{\pi}{a} x \cos \frac{n\pi}{A} x dx \\ & = \frac{2 \sin \frac{\pi}{a} c}{\pi a \left[\left(\frac{n}{A} \right)^2 - \left(\frac{1}{a} \right)^2 \right]} \cos \frac{n\pi}{A} \left(\frac{a+2c}{2} \right) \cos \frac{n\pi}{A} \frac{a}{2} \end{aligned} \quad (J-35)$$

(in the evaluation of the integral, a term whose amplitude increases with the mode number n has been neglected)

From Eqs.(J-34) and (J-35), the modal amplitude C_{1n} becomes,

$$C_{1n} = \frac{8 \sin \frac{\pi}{a} c \cos \frac{n\pi}{2A} (a+2c) \cos \frac{n\pi}{2A} a}{\pi a k_z \left[\left(\frac{n}{A} \right)^2 - \left(\frac{1}{a} \right)^2 \right]} \frac{\sin \alpha_{1n} (d+e) - \sin \alpha_{1n} e}{(\alpha_{1n} B + \sin \alpha_{1n} B)} \quad (J-36)$$

Eq.(J-36) can be used to compute the amplitude of any higher order mode corresponding to the values of n.

